Molecular function and regulation of the bacterial injectisome

Dissertation

zur

Erlangung des Doktorgrades

der Naturwissenschaften

(Dr. rer. nat.)

dem Fachbereich Biologie

der Philipps-Universität Marburg

vorgelegt

von

Stephan Immanuel Dieter Wimmi

aus Weil am Rhein

Marburg (Lahn), im März 2021

Die Studien zur vorliegenden Arbeit wurden von März 2017 bis Februar 2021 am Max-Planck-Institut für Terrestrische Mikrobiologie, im Department Ökophysiologie und unter der Leitung von Dr. Andreas Diepold durchgeführt.

Vom Fachbereich Biologie der Philipps-Universität Marburg als Dissertation angenommen am ___.___._____.

Erstgutachter: Dr. Andreas Diepold

Zweitgutachter: Prof. Dr. Martin Thanbichler

Weitere Mitglieder der Prüfungskommission:

Prof. Dr. Lars Oliver Essen

Prof. Dr. Ulrike Endesfelder

Tag der mündlichen Prüfung am: ___.___._____

Während der Promotion erzielten Ergebnisse wurden zum Teil in folgenden Originalpublikationen veröffentlicht:

Die während der Promotion erzielten Ergebnisse wurden zum Teil in folgenden Originalpublikationen veröffentlicht:

Milne-Davies B, Helbig C, Wimmi S, Cheng DWC, Paczia N, Diepold A. Life After Secretion – *Yersinia enterocolitica* Rapidly Toggles Effector Secretion and Can Resume Cell Division in Response to Changing External Conditions. Front Microbiol. 2019 Sep 13;10:2128. doi: 10.3389/fmicb.2019.02128. PMID:31572334; PMCID: PMC6753693.

Wimmi S, Balinovi A, Jeckel H, Selinger L, Lampak D, Eisemann E, Meuskens I, Linke D, Drescher K, Endesfelder U & Diepold A. Dynamic relocalization of the cytosolic type III secretion system components prevents premature protein secretion at low external pH. Nature Communications in print, doi: 10.1038/s41467-021-21863-4

I met a lot of people along the way, this is for all of you

Table of contents

Table of figures

Table of supplementary figures

Table of tables

Abstract

Many bacterial pathogens use a type III secretion system (T3SS) to manipulate host cells by translocating molecular toxins, called effector proteins. It resembles a molecular syringe, which establishes a cytosolic connection between bacteria and host cells. While the structure of the injectisome is well-defined, little is known about its molecular function and regulation. To investigate those, we focused on the adaptation of the injectisome to local pH as well as on the dynamics interactions of the cytosolic components with the effector proteins. Protein secretion by the T3SS injectisome is activated upon contact to any host cell, and it has been unclear how premature secretion is prevented during infection. We found that in the gastrointestinal pathogens *Yersinia enterocolitica* and *Shigella flexneri*, cytosolic injectisome components are temporarily released from the proximal interface of the injectisome at low external pH, preventing protein secretion in acidic environments, such as the stomach. In *Y. enterocolitica*, low external pH is detected in the periplasm and leads to a partial dissociation of the inner membrane injectisome component SctD, which in turn causes the dissociation of the cytosolic injectisome components. This effect is reversed upon restoration of neutral pH, allowing a fast activation of the injectisome at the native target regions within the host. These findings indicate that the cytosolic components form an adaptive regulatory interface, which regulates injectisome activity in response to environmental conditions. In a next step, we study the binding of effector proteins to those dynamics of the cytosolic components, which also exchange between a free diffusing cytoplasmic and a injectisome bound state. An attempt to identify novel interaction partners of SctQ by co-IP did not yield in significantly new candidates and recent publications showed that protein dynamics are linked to the function of the injectisome. We analyzed the diffusion behavior of the cytosolic protein SctQ with single particle tracking photoactivated localization microscopy (sptPALM) in different strain backgrounds. Our data shows that SctQ diffuses in two populations and that the presence of effector proteins slows down that speed. This suggests that the cytosolic components are not only essential for secretion but participate actively in effector shuttling and recruitment to the injectisome.

Zusammenfassung

Viele bakterielle Pathogene nutzen ein Typ-III-Sekretionssystem (T3SS), um ihre Wirtszellen zu manipulieren, indem sie molekulare Toxine, sogenannte Effektor Proteine, translozieren. Es ähnelt einer molekularen Spritze, die eine direkte zytosolische Verbindung zwischen Bakterien und Wirtszellen herstellt. Während die Struktur des Injektisoms gut definiert ist, ist über seine molekulare Funktion und Regulation wenig bekannt. Um diese zu untersuchen, konzentrierten wir uns auf die Anpassung des Injektisoms an den lokalen pH-Wert sowie auf die dynamischen Interaktionen der zytosolischen Komponenten mit den Effektor Proteinen. Die Protein Sekretion durch das T3SS-Injektisom wird bei Kontakt mit einer beliebigen Wirtszelle aktiviert, und es war bisher unklar, wie eine vorzeitige Sekretion von Effektoren während einer Infektion verhindert wird. Wir fanden heraus, dass in den gastrointestinalen Pathogenen *Y. enterocolitica* und *S. flexneri* zytosolische Injektisome Komponenten bei niedrigem externem pH-Wert vorübergehend von der proximalen Schnittstelle des Injektisome dissoziieren, wodurch die Proteinsekretion in sauren Umgebungen, wie dem Magen, verhindert wird. In *Yersinia enterocolitica* führt ein niedriger externer pH-Wert im Periplasma zu einer teilweisen Dissoziation des inneren Membrane Ring des Injectisomes SctD, die wiederum hat die Dissoziation der zytosolischen Injektisom-Komponenten zufolge. Dieser Effekt wird bei der Wiederherstellung des neutralen pH-Wertes rückgängig gemacht, was eine schnelle Aktivierung des Injectisomes an den nativen Zielregionen im Wirt ermöglicht. Diese Ergebnisse deuten darauf hin, dass die zytosolischen Komponenten eine adaptive regulatorische Schnittstelle bilden, welche die Injectisome Aktivität in Abhängigkeit von den Umweltbedingungen reguliert. In einem nächsten Schritt untersuchen wir die Bindung von Effektorproteinen an die Dynamik der zytosolischen Komponenten. Diese wechseln zwischen einem frei diffundierenden zytoplasmatischen und einem an das Injektisom gebundenen Zustand. Der Versuch, neue Interaktionspartner von SctQ durch Co-IP zu identifizieren, ergab keine signifikant neuen Kandidaten, und neuere Publikationen zeigten, dass die Dynamik des Proteins mit der Funktion des Injektisoms verknüpft ist. Wir analysierten das Diffusionsverhalten des zytosolischen Proteins SctQ haben könnten, haben wir das Diffusionsverhalten des zytosolischen Proteins SctQ mit Single Particle Tracking Photoactivated Localization Microscopy (sptPALM) in verschiedenen Stammhintergründen analysiert. Unsere Daten zeigen, dass SctQ in zwei Populationen diffundiert und dass die Anwesenheit von Effektorproteinen diese Geschwindigkeit verlangsamt. Dies deutet darauf hin, dass die zytosolischen Komponenten nicht nur für die Sekretion essentiell sind, sondern auch aktiv am Effektor Transport und der Rekrutierung zum Injectisome teilnehmen. Insgesamt tragen unsere gesammelten Daten zum Wissen darüber bei, wie der

Effektor Transport zum Injectisome und in die Wirtszelle reguliert wird und wie dieser überhaupt erst ermöglicht werden kann.

Introduction

1.1 Bacterial secretion systems

Once, bacteria were believed to just be a bag of enzymes, held together by a cell wall and a membrane. This assumption has been outdated for several years now. Bacteria have complex life cycles, they establish polarity, organize their DNA and even confine whole metabolic pathways within one cluster (Cheng *et al.*, 2008; Treuner-Lange and Søgaard-Andersen, 2014; Kerfeld and Erbilgin, 2015; Surovtsev and Jacobs-wagner, 2018; Greening and Lithgow, 2020). All of this is done, while maintaining cell wall integrity, turgor pressure and concentration gradients in sometimes harsh environmental and host conditions. To interact with, effect, or combat the environment as well as other bacteria, or eukaryotic cells, bacterial secretion systems are utilized (Green and Mecsas, 2016). Since bacteria, as well as the secretion application, are diverse, there is not only one molecular machine to do the job, but actually a variety. The general secretion pathway (Sec) and the twin arginine translocation pathway (Tat) are the simplest way to transport proteins. They are mostly used to facilitate protein translocation within the cell into the periplasm or into a membrane (Natale *et al.*, 2008). Those systems are not limited to bacteria, but have been identified in all branches of life (Robinson and Bolhuis, 2004; Papanikou *et al.*, 2007). For further transportation, outside of the cell, or even into host cells, Gram-negative bacteria established dedicated secretion systems. Those can be classified into multiple systems from type I to type IX secretion system (Beeckman and Vanrompay, 2010; Green and Mecsas, 2016; Kooger *et al.*, 2018). Type I-VI have a β-barrel channel in the outer membrane in common, but otherwise are quite diverse (Green and Mecsas, 2016). The type I, III, IV, VI, IX system from one channel spanning the inner and outer membrane. On the other hand, the type II, V, VII, VIII secretion systems rely on the sec or tat pathway to export the cargo into the periplasm and only engage in export from there (Overview **Figure 1**)(Chagnot *et al.*, 2013).

The type I section system (T1SS) closely resembles the family of ATP-binding cassette (ABC) transporters, which are as the name states, ATP dependent and mostly associated with export of small molecules like antibiotics and toxins (Symmons *et al.*, 2009). Several different kind of type I systems can be found per cell used for different substrates (Delepelaire, 2004).

The Type II secretion system (T2SS) transports folded proteins from the bacterial periplasm outside the cell. Prior to export the substrate needs to be delivered into the periplasm by the Sec or Tat pathway followed by export from the periplasm to the environment (Green and Mecsas, 2016). Type II secretions

are not very specific, where some have only one or multiple substrates. Some of the secreted proteins are virulence associated (Korotkov *et al.*, 2012).

Type III secretion system (T3SS) has two applications (**Figure 1,** T3aSS T3bSS). One is the injectisome where it translocates effector proteins through a needle directly from the bacterial cytosol into the eukaryotic host cell. The other is in bacterial flagella where it exports flagella subunits, which allows for bacterial locomotion. At the core, both the flagellum and injectisome T3SS are used to transport proteins across the inner and out membranes(Deng *et al.*, 2017; Milne-Davies *et al.*, 2020). Since it is our major research interest it will be covered in more depth in a separate section.

The type IV secretion system (T4SS) has evolved from an early DNA secretion system to a system with various substrates. Single proteins, protein-protein and DNA-protein complexes have been reported to be translocated (Cascales and Christie, 2003). Similar to the T3SS, substrates are transported over both membranes and into other bacteria or eukaryotic cells (Green and Mecsas, 2016).

Type V secretion (T5SS) is dependent on protein delivery into the periplasm by the Sec pathway. In the next step, the proteins create their own outer membrane pore by incorporation of a β-barrel domain into the outer membrane (Pohlner *et al.*, 1987; Leyton *et al.*, 2012). Most of the type V secreted protein are virulence-associated and are toxins or binding proteins. Some well-known examples are the *Yersinia enterocolitica* adhesion protein YadA or the *S. flexneri* IcsA (Roggenkamp *et al.*, 2003; Brotcke Zumsteg *et al.*, 2014).

The type VI secretion system (T6SS) differs more from the other systems. Since this system resembles a molecular spear gun that shoots a phage tail-like structure and effector proteins into other bacterial or eukaryotic cells. The type VI is a more physical penetration system rather than one translocation (Pukatzki *et al.*, 2007; Russell *et al.*, 2014). It is well conserved and widely spread among Gram-negative bacteria (Russell *et al.*, 2011).

The type VII secretion system (T7SS) is only found in Gram-positive bacteria and was originally identified *Mycobacterium tuberculosis* (Stanley *et al.*, 2003). It is used in certain species to overcome a heavily lipidated layer of the cell envelope called the mycomembrane (Freudl, 2013). Multiple different systems can be found within one bacterium and their substrate are evolved in key roles during infection of the host cells (Bitter *et al.*, 2009; Houben *et al.*, 2012; Tinaztepe *et al.*, 2016; Damen *et al.*, 2020).

The name type VIII secretion system (T8SS) was assigned to the extracellular nucleation-precipitation pathway (ENP)(Kostakioti *et al.*, 2005; Desvaux *et al.*, 2009). It is associated with curli fibers assembly in bacterial biofilms (Bhoite *et al.*, 2019).

The Type IX secretion system (T9SS) is also known as the Por (porphyrin accumulation on the cell surface) secretion system. It is essential for pathogenicity in superphylum of Fibrobacteres–Chlorobi–Bacteroidetes and the β-barrel has with 36 polypeptide transmembrane domains. With this unusually high amount, it forms a 50 nm wide ring-shaped structures which is the largest β-barrel found so far (Gorasia *et al.*, 2016; Lasica *et al.*, 2017; Schiffrin *et al.*, 2017; Lauber *et al.*, 2018).

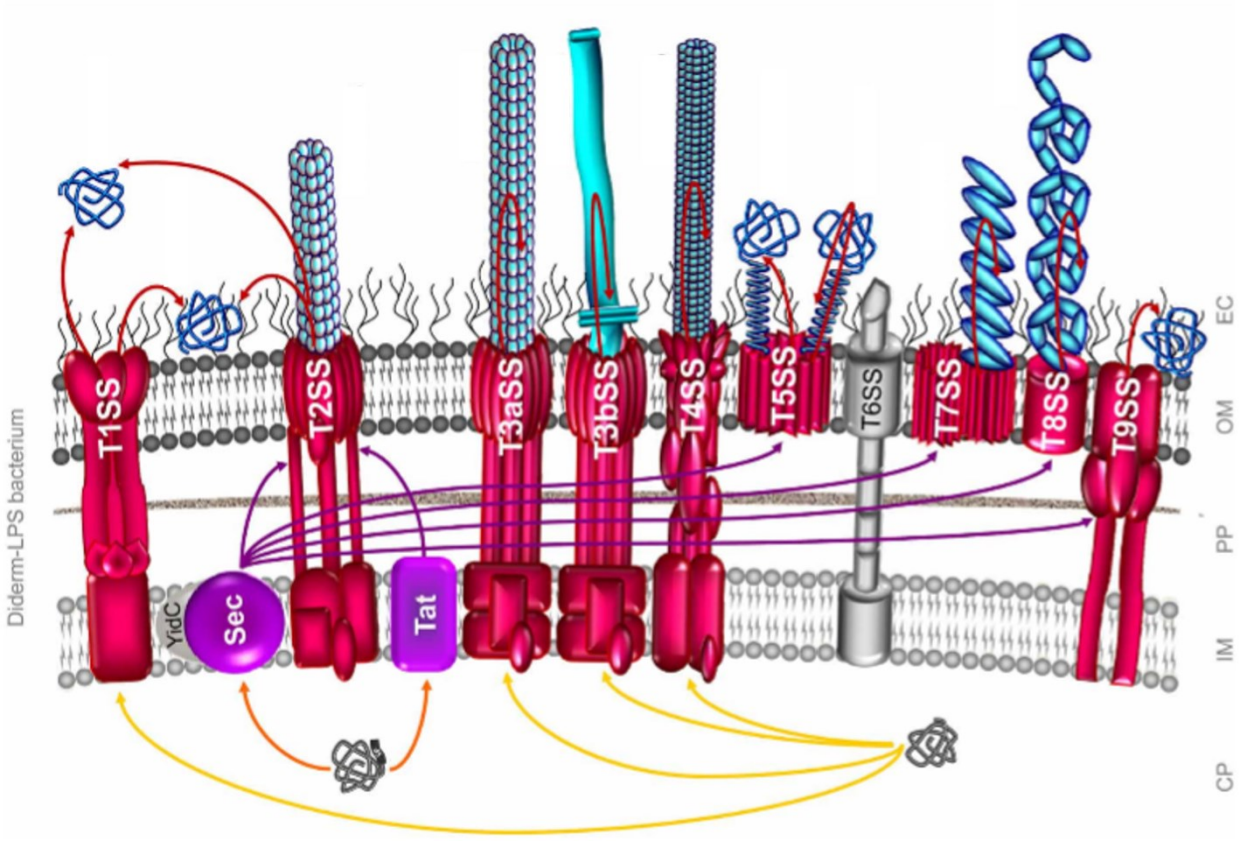

Figure 1 Different bacterial secretion systems.
Schematics of T1SS to T9SS located in the bacterial envelope in magenta and gray (T6SS). Proteins are recruited in the cytoplasm (CP) and guided to the secretion system via a signal peptide (SP). Type V,VII,VIII secretion systems span only the other membrane (OM) while others (T1,2,3a/b, 4,6,9SS) cross the inner (IM) and the OM as well as the peptidoglycan layer (PP) to secret proteins into the extracellular milieu (EC) or even into host cells (not displayed). The Sec and Tat system are displayed in violet and located in the inner membrane. Yellow arrows show the route of proteins without a clear N-terminal SP. Orange arrows display protein recruitment to the Sec or Tat system. Violet arrows indicate the route of proteins after export via Sec or Tat. Figure edited from (Chagnot et al., 2013)

1.2 The type III secretion system injectisome

Symbiont and pathogenic bacteria have developed multiple ways to interact with and survive in the host. Animal pathogens have to avoid or withstand the host's immune system, pass through living cells, or colonize the host. One way to facilitate this is by using the injectisome, a molecular nano-machine with a type III secretion system (T3SS) at its core (**Figure 2**). It is conserved in many pathogenic bacteria including *Salmonella*, *Shigella*, pathogenic *Escherichia coli* and *Yersinia* spp. and is used to deliver molecular toxins – so-called effector proteins – directly into the eukaryotic host cells. Due to years of research in different organisms, several nomenclatures exist. The common "Sct" nomenclature (Hueck, 1998; Diepold *et al.*, 2014) is used in this work for the injectisome components; when specifically referring to components of a particular species, the species initials are used as a prefix, e.g. *Ye*SctD for *Y. enterocolitica* SctD.

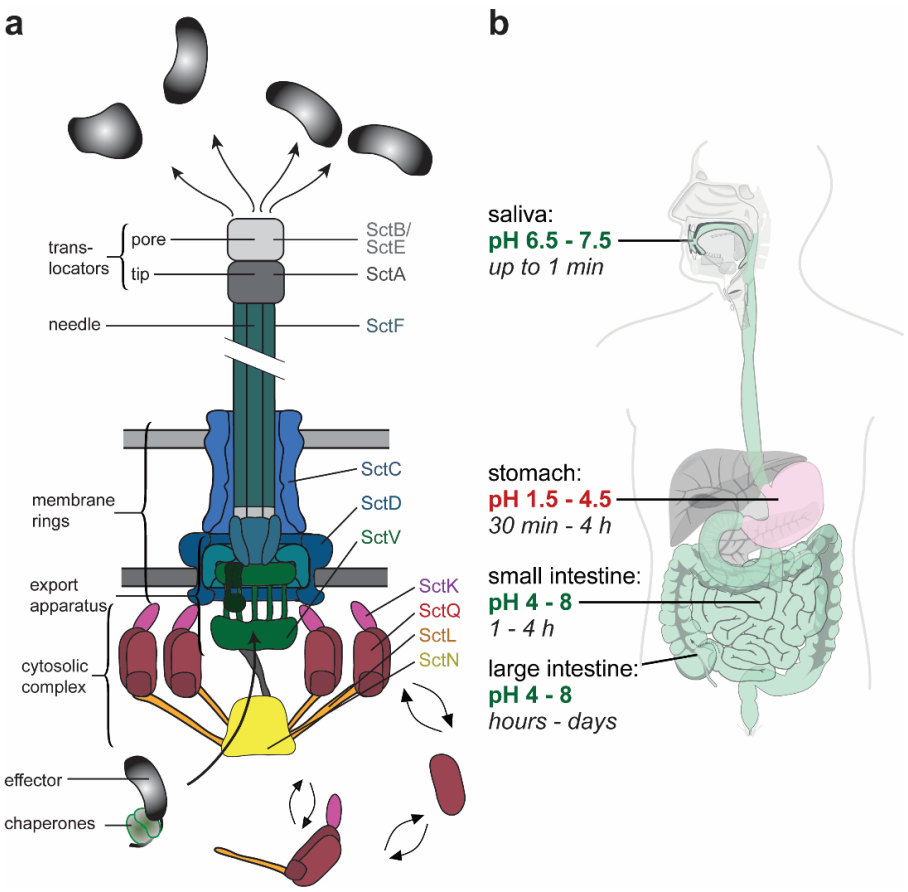

Figure 2 The injectisome and *Y. enterocolitcas* infections path and bacteria used in this study.
(a) Shematic repesentation of the injectisome with T3SS at its core. Adapted from Diepold and Wagner, 2014. Descritopns of the the main substructions can be found on the left side**.** On the right are the single components labeled that have been studied during my PhD. The double arrows indicate the exchange of cytosolic proteins between an injectisome bound and unbound state. **(b)** Schematic of the gastrointestinal system with typical retention times and pH range indicated. (Evans *et al.*, 1988; McClements and Li, 2010). Digestive tract image based on the public domain template https://commons.wikimedia.org/wiki/File:Digestive_system_diagram_de.svg.

The injectisome is closely related to the most abundant bacterial locomotion device, the flagellum. Both use a T3SS to export proteins out of the cell. While in case of the flagellum flagellin subunits are being exported, which assemble into a filament outside of the cell, needle subunits and effectors are exported in case of the injectisome (Diepold and Armitage, 2015; Deng *et al.*, 2017). Both systems use ion gradients to fuel the export of substrates (Paul *et al.*, 2008; Lee *et al.*, 2014), the flagellum rotates to propel the bacterium through the environment (Wadhams and Armitage, 2004; Sourjik and Wingreen, 2012), the injectisome needle is stable and optimized for translocation into eukaryotic host cells (Ibuki *et al.*, 2011; Abrusci *et al.*, 2012). This is done by creating a pore in the host cell membrane and thereby establishing a direct cytoplasmic connection between host and bacterium. While the structural components of the injectisome are highly conserved, the effectors differ among the different bacterial species (Büttner, 2012; Abby *et al.*, 2012). Generally, their function relates to the different lifestyles of the bacterial species and is mostly, but not always, connected to the pathogenicity. Effector functions range from modulating the cytoskeleton, invading and escaping cells, escaping endosomes, to inducing host cell death and coordinating symbiosis (Hueck, 1998; Coburn *et al.*, 2007b; Coburn *et al.*, 2007a; Miki *et al.*, 2010; Büttner, 2012; Rajashekar *et al.*, 2014; de Jong and Alto, 2018; de Souza Santos and Orth, 2019; Silva *et al.*, 2020a). In *Y. enterocolitica* the injectisome and its effectors are used to defend the bacteria against the primary immune host defense, inhibit inflammatory responses, and inducing apoptosis of immune cells in the lymphatic tissue (Navarro *et al.*, 2005; Letzelter *et al.*, 2006; Galán, 2009; Pha, 2016).

The overall structure of the injectisome can be divided into different sections (**Figure 2a**). A needle 61 ± 31 nm (mean) (Berger *et al.*, 2021) long and 20 Å wide ($SctF_{\sim 140}$)(small numbers indicate stoichiometry) with a pentameric needle tip ($SctA_5$)(Mueller *et al.*, 2005) which assembles outside of the cell (Broz *et al.*, 2007). It is anchored by two multimeric membrane rings that span the inner ($SctD_{24}$ and $SctJ_{24}$)(Yip *et al.*, 2005; Schraidt *et al.*, 2010) and outer membranes ($SctC_{15}$) (Schraidt and Marlovits, 2011). Located within the inner membrane ring, the export apparatus ($SctR_5S_4TUV_9$)(Abrusci *et al.*, 2014; Zilkenat *et al.*, 2016; Kuhlen *et al.*, 2018) can be found, which is in turn connected to the inner rod ($SctI_6$)(Zilkenat *et al.*, 2016; Dietsche *et al.*, 2016) of the needle. Together, the membrane rings form the basal body that encloses the export apparatus of the injectisome. At its cytosolic interface, the cytosolic components ($SctK_6$, $SctQ_{24}$/$SctQ_{c48}$, $SctL_{12}$, SctO and $SctN_6$)(Minamino and Macnab, 2000; Pozidis *et al.*, 2003; Akeda and Galán, 2005; Müller *et al.*, 2006; Bzymek *et al.*, 2012; McDowell *et al.*, 2016; Zhang *et al.*, 2017; Diepold *et al.*, 2017) are connected to cytosolic part of the inner membrane ring (SctD)(Hu *et al.*, 2017). The cytosolic components form a cage-like structure including an ATPase (SctN) and are essential for effector secretion. Due to their properties, assigned function and homology to the flagellum, they are also termed soluble components,

C-ring components (SctQ), or sorting platform (Lara-Tejero *et al.*, 2011; Diepold *et al.*, 2015; Diepold *et al.*, 2017).

1.2.1 Injectisome structure, stability and dynamics

1.2.1.1 The needle and basal body

The injectisome is a highly conserved molecular nano-machine (Abby *et al.*, 2012; Deng *et al.*, 2017). Despite its general conservation, several differences have been observed between species. A similar phenomenon was documented already for the flagellum (reviewed in more detail here: (Chaban *et al.*, 2015; Beeby *et al.*, 2020)). The overall structural differences seem to be minimal despite the different tailored applications. Berger *et al.*, 2021 (**Figure 3**) elucidated and compared the differences between the *Y. enterocolitica* injectisome and other species by Cryo-ET. Several things stood out here. Between different species, the diameters and electron densities of the basal body differ (**Figure 3b**). This is most apparent for SctD, which is barely visible in the inner membrane in *Y. enterocolitica* while it is strongly present in *Salmonella enterica* (**Figure 3b**). In addition, the cytosolic components display different geometries and electron densities between species as well (**Figure 3b**). Most stunning is that while SctQ forms clear separated pods in *S. enterica* and *S. flexneri*, *Ye*SctQ displays more of a patchy ring structure. While those are clear species specific adaptations, and may indicate the presence of more proteins or protein copies in the *Y. enterocolitica* system (Berger *et al.*, 2021), the biological and functional implications can only be deciphered in future experiments and with higher structural resolution. Based on the different shapes and electron densities of parts of the injectisome, the study elucidates once more the differences within the structural parts of the injectisome between species.

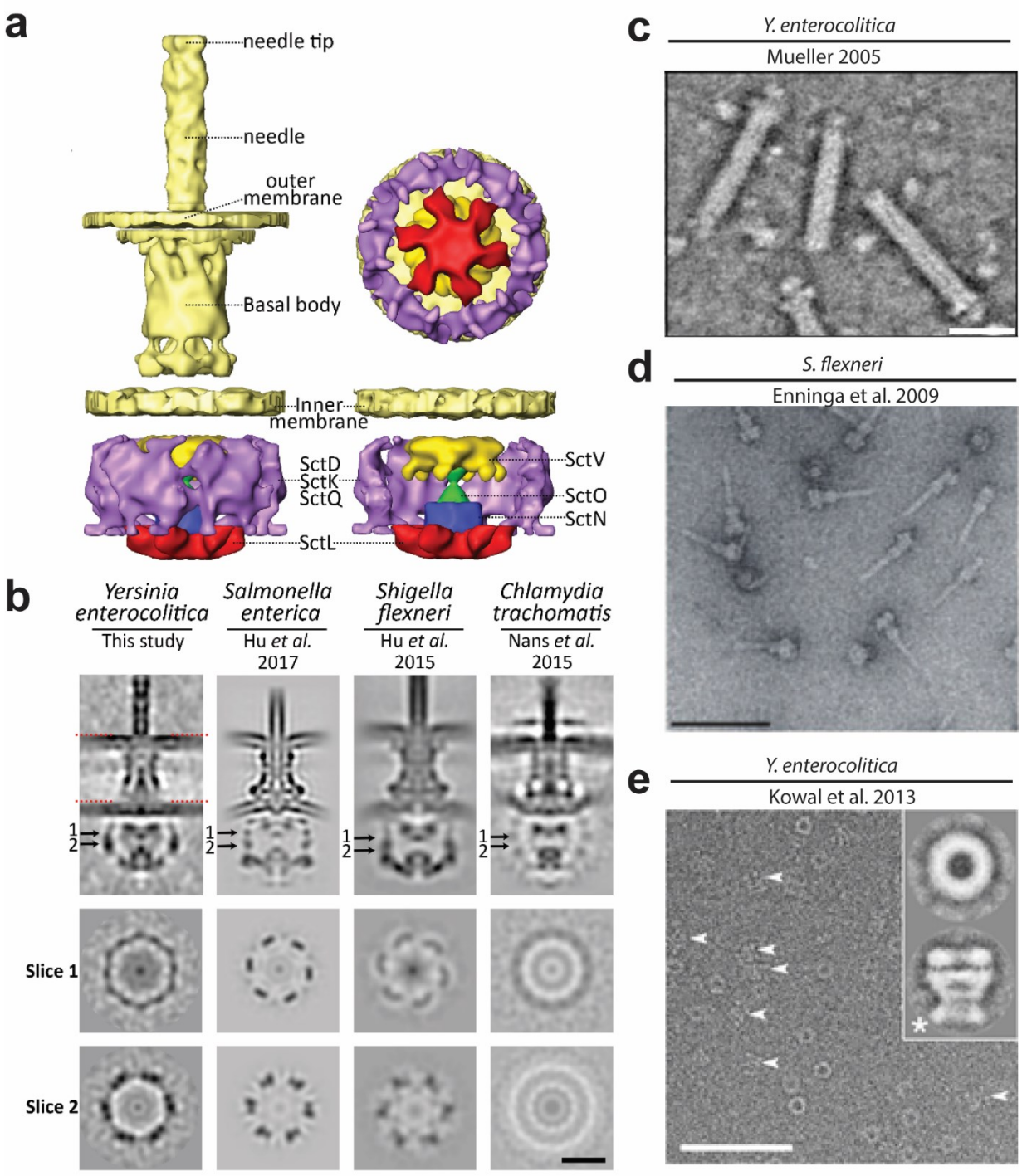

Figure 3 CryoET of the injectisome.
(a) Isosurface rendering model of the injectisome and cytosolic components with different angles. Left: whole injectisome, right top: bottom view, right left: parts of the SctQ-SctK-SctD complex removed. **(b)** Subtomogram average structures of the injectisome in different angles and species. Origin of data indicated above the figures. Scale bar: 20 nm. Arrows 1 and 2 indicate the position of the slices displayed in the bottom part of the figure. Figure part adapted from (Berger *et al.*, 2021). **(c)** Scanning transmission electron microscope (STEM) images of purified and negatively stained needles from the *Y. enterocolitica.* Scale bar, 20 nm (Mueller *et al.*, 2005). **(d)** Purified basal bodies with needles still attached and visualized with imaged by low-dose electron microscopy Scale bar: 120 nm. (Enninga and Rosenshine, 2009). (**e**) Purified SctC visualized by Cryo-EM. The inset displays top and side view Scale bars, 0.1 mm. Insets, 290 Å wide.

The injectisome needle is built up out of ~140 copies of the ~8.9 kDa protein, SctF, in a helical structure (Broz *et al.*, 2007) (**Figure 2a Figure 3**). Despite their large electron density of the needle (**Figure 3a**) and its ability to push up the host membrane (Nauth *et al.*, 2018; Berger *et al.*, 2021), needles can be sheared and purified with the needle tip still attached (**Figure 3c**) (Mueller *et al.*, 2005). Studies in *Y. enterocolitica, S. flexneri* and *S. enterica* indicated that the needle is involved in regulatory mechanisms like Ca^{2+} sensing (Blocker *et al.*, 2008), secretion activation (Kenjale *et al.*, 2005; Davis and Mecsas, 2007) and substrate regulation, respectively (Guo *et al.*, 2019).

The basal body of the injectisome includes three proteins, SctC, D and J, (Burkinshaw and Strynadka, 2014). It spans the outer and inner membrane and displays high electron density (**Figure 2a, Figure 3abe)**(Berger *et al.*, 2021). It is the core structure of the injectisome, which anchors the needle as well as the export apparatus and functions as a docking platform for the cytosolic components. It is a prime target for CyroEM (Hu *et al.*, 2015; Hu *et al.*, 2017; Berger *et al.*, 2021) and has been purified in one piece (**Figure 3d**) (Hodgkinson *et al.*, 2009). The secretin, SctC, assembles a large membrane pore out of 15 copies of the protein (Schraidt and Marlovits, 2011). Homologs can be found in other systems, like the T2SS and the type IV pili system (Silva *et al.*, 2020). It could be isolated in its oligomeric form and the structure has been solved in crystals and with Cyro-ET (**Figure 3e**) (Spreter *et al.*, 2009; Kowal *et al.*, 2013a; Bergeron *et al.*, 2013; Worrall *et al.*, 2016; Hu *et al.*, 2018). The C-terminus of the protein faces towards the needle and is located outside of the outer membrane, while the N-terminus faces in the direction of the cytosol. SctC can be separated into three globular domains. In the inner part of the ring, SctC forms a periplasmic gate, which opens up to incorporate the needle once exported (Worrall *et al.*, 2016). Interaction with the pilotin, SctG, takes place at the C-terminal S domain of the secretin (Worrall *et al.*, 2016)(**Figure 4a**). The interaction between the inner membrane ring protein SctD takes place at the N-terminus of SctC (Schraidt *et al.*, 2010). To overcome the mismatch of protein numbers in the basal body, (outer membrane ring, SctC, 15-mer, inner membrane ring, SctD/J, 24-mer) 5 monomers of SctC connect with eight monomers of SctD/J (Miletic *et al.*, 2020b).

SctD is ~45 kDa protein and forms the outer part of the inner membrane ring. It assembles into a 24-mer structure. The C-terminus of the protein is orientated in the direction of SctC while the N-terminus of the protein is located in the cytoplasm (Schraidt *et al.*, 2010; Miletic *et al.*, 2020b). Monomers of SctD most probably interact with SctC and SctJ (Bergeron *et al.*, 2015). A lysine at amino acid position 367 as well as the last C-terminal amino acids are key for assembly and interaction of SctD with SctC (Schraidt *et al.*, 2010). The SctD protein can be separated into 4 domains. Domain 1 is located in the periplasm and

connected by one transmembrane domain to the domains 2-4 (**Figure 4b**). Those form a 250 Å wide ring in the periplasm (Schraidt *et al.*, 2010). A modular architecture can be found in domains 2-4, which is mimicked in the other ring-forming proteins SctJ and SctC (Spreter *et al.*, 2009; Bergeron *et al.*, 2013). Domain 1 forms a cytoplasmic ring (Schraidt *et al.*, 2010). It contains a eukaryotic like Forkhead-associated-like (FHA-like) domain. While the typical phospho-threonine-binding sites formed by antiparallel β-sheets, is present, it seems to have no phosphorylation activity (Bergeron *et al.*, 2013; Almawi *et al.*, 2017). Further, periplasmic domain 1 is flexible and has been shown to change its conformation to interact with the cytosolic component protein SctK. While in absence of SctK it froms a homogenous ring, in its presences six patches are visible. It seems to be clear that those facilitate the change of symmetry from the 24-mer ring to the six pod structure found in the cytosol (Hu *et al.*, 2017). In *P. aeruginosa*, the structure of SctK has be solved recently for the first time. This allowed the identification of an electrostatic interphase critical for the SctK-SctD interaction and mutagenesis of key residues abolished the interaction of the two protein domains in bacterial two hybrid assays (Muthuramalingam *et al.*, 2020).

SctJ is the second part of the inner membrane ring (**Figure 2a**). It is a ~27 kDa protein and forms a 180Å wide ring made out of 24 copies of the protein. It is positioned in the inner membrane via an N-terminal Sec pathway signal. The protein can be separated into two globular domains, a transmembrane domain and a tail both located at the C-terminus (**Figure 4b**)(Schraidt *et al.*, 2010). In the assembled state, the N-terminus is located in the periplasm while the C-terminus phases upwards (Yip *et al.*, 2005; Schraidt *et al.*, 2010). It connects to SctD and links it with other proteins of the basal body (Bergeron *et al.*, 2015). The combination of the periplasmic membrane ring of SctD and SctJ appears to be the most stable part of the injectisome (Schraidt and Marlovits, 2011).

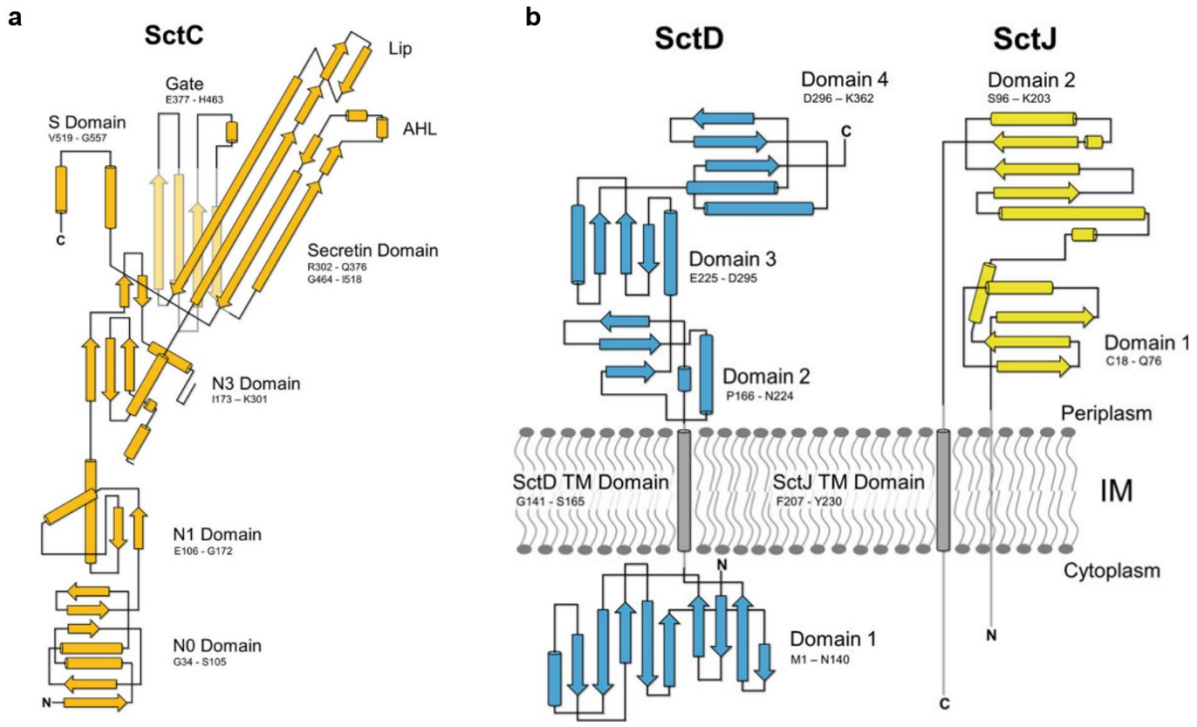

Figure 4 Topology of the basal body components.
Ribbon representations displaing the different domains and features of the points indicated by name on the top. **(a)** SctC (yellow, dark), **(b)** SctD (blue) and SctJ (yellow, light). In gray indicated is the inner membrane (IM) and the transmembrane domains (TM) of the respective proteins. (Miletic *et al.*, 2020b)

1.2.1.2 The cytosolic components

The cytosolic components, SctK, Q, L, N, and O, are located at the interface of the inner membrane (**Figure 2a, Figure 3a**). They interact with the basal body via SctD. SctK, Q, L and N are required for the successful assembly of the cytosolic complex, as well as for the secretion of effector proteins. In the absence of any of those components, the respective others only show a diffuse localization throughout the cytosol (Diepold *et al.*, 2010; Diepold *et al.*, 2017). *In vitro* experiments showed a linear interaction chain between SctK, Q, L and N (Jackson and Plano, 2000; Jouihri *et al.*, 2003; Spaeth *et al.*, 2009). Based on fluorescence labeling, the stoichiometries of the cytosolic components underneath the basal body have been calculated. SctK is assumed to be present in six copies, SctQ has 24 copies similar to the membrane ring SctD, $SctQ_c$ has most likely 48 copies. For SctL the estimated copy number is 12, while SctN oligomerizes in probably six copies (maybe 12) (Pozidis *et al.*, 2003; Akeda and Galán, 2005; Müller *et al.*, 2006; Zhang *et al.*, 2017; Diepold *et al.*, 2017). SctO could not be observed in these studies due to its low copy number. It is assumed to be present in one or two copies. In contrast to the basal body or the needle, the cytosolic

components are not a stable complex. It could be shown that SctQ exchanges with a cytosolic population with a half-time of around two minutes (**Figure 2a, Figure 6**) (Diepold *et al.*, 2015).

SctK is the only cytosolic protein that has no clear homolog in the flagellum system and is the least studied. It is the smallest of the essential cytosolic proteins and with six copies has the lowest abundance in the complex. At the basal body, it is located closest to the inner membrane ring and is potentially an adaptor between the membrane ring and the cytosolic components (**Figure 2a**) (Hu *et al.*, 2017). In *P. aeruginosa* the structure of SctK was solved recently by crystallization. This allowed the identification and of central amino acids responsible for the SctD-SctK interaction (Muthuramalingam *et al.*, 2020).

SctQ is the major pod or C-ring protein (**Figure 2a**). An additional internal translation site within the protein has been found. Thus the protein exists in two versions within the cell, either as full-length protein (SctQ) or as a shorter protein consisting only of the C-terminal part termed $SctQ_c$, both of which are essential for secretion (Yu *et al.*, 2011; Bzymek *et al.*, 2012). Three additional transcription products have been identified lately in *S. flexneri*, but their precise function and importance still needs to be clarified (Kadari *et al.*, 2019). While SctQ is homologous to the flagellar protein FliM, $SctQ_c$ resembles FliN (Yu *et al.*, 2011; Bzymek *et al.*, 2012). In the flagellum, the C-ring structure formed by FliM and FliN rotates; in contrast, the six pod structure of the injectisome is thought to be stationary. While *S. enterica* and *S. flexneri* display the six pods clearly, new data from *Y. enterocolitica* indicates that the pods include additional densities, again hinting more into the direction of a ring (Berger *et al.*, 2021). In *Chlamydia trachomatis* and *S. enteric*, SctQ has been show to interact with export cargo, especially with the chaperones which lead to the proposal of the sorting platform model (Spaeth *et al.*, 2009; Lara-Tejero *et al.*, 2011).

SctL has been named the spokes protein and is present as a hexamer of dimers underneath the basal body. It connects the SctQ pods with the hexameric ATPase SctN (**Figure 2a**). In a comparative CryoEM study, it has been shown that SctL, with its orientation and shape, is probably majorly responsible for overall geometry of the assembled cytosolic complex at the basal body (**Figure 2, Figure 3**) (Berger *et al.*, 2021). Besides these structural aspects, SctL has been shown to have a negative regulatory effect on the activity of the ATPase SctN in *Y. enterocolitica* and *S. flexneri* (Blaylock *et al.*, 2006; Case and Dickenson, 2018). In the flagellum, the SctN homologue FliH binds to flagella subunits export chaperones and has be hypothesized to serve as a dynamic substrate carrier (Bai *et al.*, 2014).

SctN itself is a hexameric ATPase located at the most distal side of the injectisome and is related to an F- and V-type ATPases (Ibuki *et al.*, 2011; Majewski *et al.*, 2019). It is held into position by a cage like structure underneath the injectisome basal body (**Figure 2, Figure 3**). SctN interacts with SctL and SctO and in its absence the interactions of cytosolic components in co-immunoprecipitation assays is strongly reduced. This suggests that SctN is needed to stablize the complexes of cytosolic components within the cell (Diepold *et al.*, 2017). SctN is thought to detach chaperones from its substrate and unfold effector proteins prior to export (Akeda and Galán, 2005). In the flagellum, SctN is thought to be the substrate loader that promotes the initial entry into the export apparatus (Bai *et al.*, 2014). SctO is the ATPase stalk or "ATPase lever arm" (Jensen *et al.*, 2020), and forms a ~140 Å sized structure made up of coiled-coils. CryoEM studies in *E.coli* revealed that it is positioned at a ~70˚ angle between SctN and SctV and was proposed to have a rotary catalytic function (Majewski *et al.*, 2019). Similar ATPase subunits have been found in F1-ATPase γ-subunit and the V1-ATPase D subunit (Braig *et al.*, 2000; Arai *et al.*, 2013; Notti and Stebbins, 2016). SctO links the export gate SctV, with the ATPase SctN **(Figure 2a**). SctV has been shown to bind to export cargo (Xing *et al.*, 2018) and has an open and close state (Terahara *et al.*, 2018; Inoue *et al.*, 2019). A recent study suggested that the ATPase catalyzes twisting of SctO. This in turn releases chaperone-cargo complexes from SctV and might also create a path into the export gate (Jensen *et al.*, 2020). Since this process might be aiding the export and not be essential for it, and might have species specific properties, it would fit with other findings which could show that SctN is not absolutely essential for the export of effector proteins but that the PMF if the driving force of export (Minamino and Namba, 2008; Paul *et al.*, 2008; Erhardt *et al.*, 2014).

Lara-Tejero *et al.*, 2011 showed that in blue native PAGE gels, translocators run in the same molecular weight as SctQ, presumably in a complex with SctK and SctL. Later SctN was included into the complex with the proposed role of the acceptor of injectisome substrate (Lara-Tejero, 2020). In the blue native gels, effectors and chaperones were only detected in low abundance together with the translocator proteins (Lara-Tejero *et al.*, 2011). Effectors only appeared in higher numbers within that complex once the translocators were deleted. Overall, Chaperones were detected more strongly than effector proteins. Based on that data, the authors proposed that this complex functions as a sorting platform involved in ordering and preparing the substrate in the cytosol for export (Lara-Tejero *et al.*, 2011). While the interpretation of the data has slightly changed over the years, this remains as of today the only publication actually coming close to the molecular mechanism of the hierarchical effector export (Deng *et al.*, 2017; Milne-Davies *et al.*, 2020; Lara-Tejero, 2020).

1.2.2 Assembly of the injectisome

As mentioned already, the injectisome is a conserved structure in different bacterial species. While the systems are homolog in structure, different cues are used to the start assembly like changes in pH, or oxygen tension (Chakravortty *et al.*, 2005; Marteyn *et al.*, 2010; Yu *et al.*, 2010; Büttner, 2012; Puhar and Sansonetti, 2014). In *Y. enterocolitica*, the temperature upshift from <30 to 37°C allows expression of the transcription factor VirF and triggers the assembly process (Cornelis *et al.*, 1989; De Nisco *et al.*, 2018). Assembly starts with the formation of the export apparatus in the inner membrane as well as secretin assembly (SctC) in the other membrane (Diepold *et al.*, 2010; Wagner *et al.*, 2010a; Diepold *et al.*, 2011; Diepold *et al.*, 2014; Diepold, 2020), both are translocated there by the sec system (Rapoza and Webster, 1993). While the inner membrane rings (SctJ and SctD) are stable in some organisms (Kimbrough and Miller, 2002; Schraidt and Marlovits, 2011), this is not the case in *Y. enterocolitica.* Here the secretin (SctC) needs to build up in the outer membrane first, aided by its pilotin (SctG) (Burghout *et al.*, 2004; Diepold *et al.*, 2010). This process may be needed to ensure proper peptidoglycan penetration, since the injectisome of *Y. enterocolitica* in contrast due others does not come with a dedicated enzyme to fulfill this task (Koraimann, 2003; Masi and Wandersman, 2010). After the SctC ring formation in the outer membrane, the inner membrane rings (SctD, SctJ), can enclose around the export apparatus and connect with the secretin, which completes the assembly of the basal body (Diepold *et al.*, 2010). The difference in stability of the membrane rings in different species led to the proposal of an outside-in and an inside-out model (Diepold *et al.*, 2010; Wagner *et al.*, 2010a; Diepold *et al.*, 2014). In the next step, the cytosolic components (SctKQLN) dock onto the inner membrane ring (SctD). While the SctD ring can form without SctJ, SctJ is needed for the docking of the cytosolic components (Diepold *et al.*, 2010). Now, the subunits of the inner rod and afterward the needle are exported. To coordinate needle length, pore formation, and subsequent effector translocation, the injectisome relies on several substrate switches.

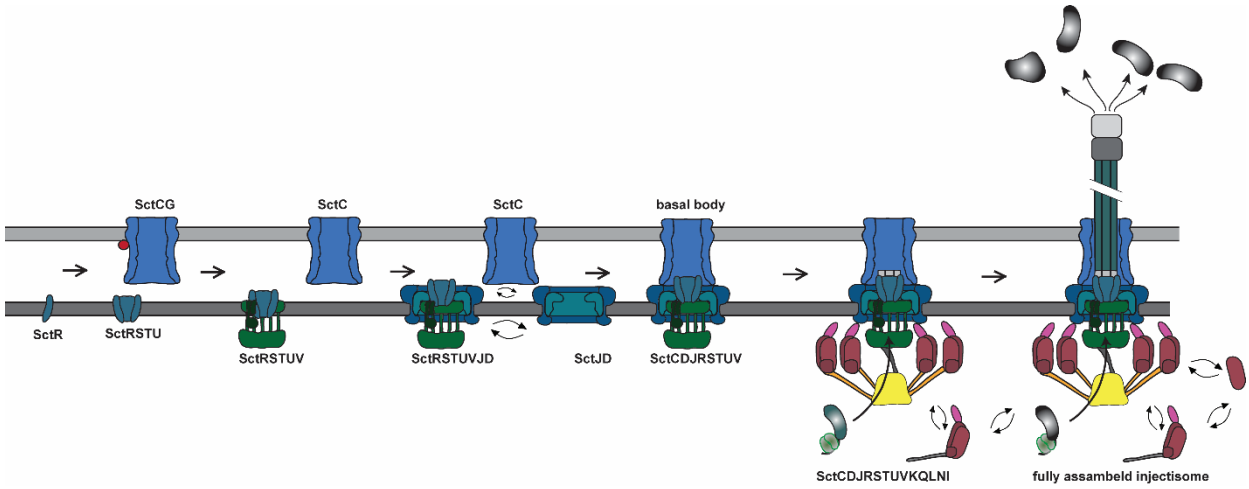

Figure 5 Schematic assembly of injectisome.
Names of proteins present in each step are indicated in the figure. Assembly steps are separated by arrows. Double arrow indicates instable assembly steps, or once present in other species then *Y. enterocolitica*. Gray lines represent the bacterial inner (dark) and outer (light) membrane. Assembly can start independently both in the inner and other membrane with the secretin (SctC) or the export apparatus (SctRSTUV). Once the Secretin is positioned and assembled with help of its pilotin (SctG), the inner membrane rings (SctDJ) form around the export apparatus and connect to the secretin. In a next step the cytosolic components (SctKQLN) dock onto the inner membrane ring. Next the Inner rod (SctI) and needle subunits (SctF) are exported. Only once the injectisome is built up completely, the needle tip (SctA) and the translocon subunits (SctEB) and effector secretion starts. A dapted from Diepold, 2020.

The first class of proteins exported, after assembly of the basal body are the inner rod and needle subunits (SctI and SctF, respectively). Once the needle reaches its defined length, measured by a molecular ruler SctP, a substrate switch occurs by interaction of SctP and SctU (Journet *et al.*, 2003; Wagner *et al.*, 2010). Now the hydrophilic translocator, SctA, is exported and assembles at the top of the needle in a pentameric needle tip (Mueller *et al.*, 2005). Once host cell contract is sensed by the needle tip (Veenendaal *et al.*, 2007; Roehrich *et al.*, 2013; Armentrout and Rietsch, 2016) or secreting conditions are applied by the media (Ca^{2+} chelation)(Fowler and Brubaker, 1994), the late substrate (translocators and virulence effectors) is exported. For that, Effector-chaperone complexes are recruited to the injectisome (Parsot *et al.*, 2003; Lara-Tejero *et al.*, 2011), held in an unfolded state by their cogent chaperones (Stebbins and Galán, 2001) and channeled into the export apparatus (Radics *et al.*, 2014; Miletic *et al.*, 2020a; Lyons *et al.*, 2021). The change from non-secreting conditions (high [Ca^{2+}]) to secreting conditions (low [Ca^{2+}]) leads also to an upregulation of the *yop* genes (Cornelis *et al.*, 1987; Pettersson *et al.*, 1996; Stainier *et al.*, 1997). This is caused by the export of the negative regulators YscM1 and YscM2 (Cornelis *et al.*, 1987; Rimpilainen *et al.*, 1992; Stainier *et al.*, 1997). A higher copy number of the pYV virulence plasmid (Wang *et al.*, 2016) under secreting conditions additionally causes a two fold upregulation of the structural components which assemble into new injectisomes in already existing clusters (Kudryashev *et al.*, 2015). Export of the hydrophilic translocon (SctE/B) results in the formation of a membrane pore which allows the passage of

the effector protein into the host (Schlumberger *et al.*, 2005; Enninga *et al.*, 2005; Mills *et al.*, 2008; Nauth *et al.*, 2018).

1.2.3 The dynamic of the cytosolic components

As mentioned above, the cytosolic components are not stationary bound to the injectisome basal body, but actually exchange between an injectisome bound and unbound state (**Figure 6**, **Figure 7a**) (Diepold *et al.*, 2015). The majority of the proteins are not associated within injectisome bound pods (*Ye*SctQ~86%, *Ye*SctL~56% (Rocha *et al.*, 2018)).

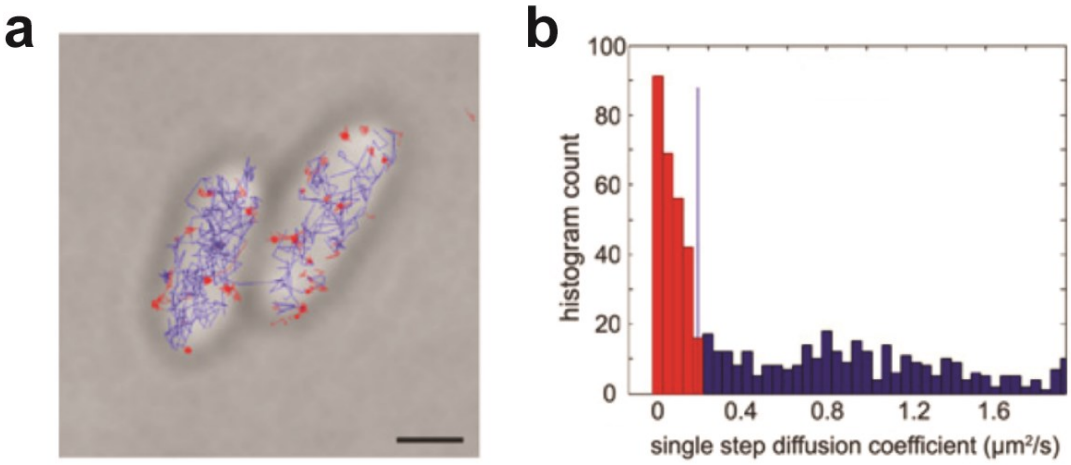

Figure 6 SctQ is present in two populations in the cytosol of SctQ.
(a) Distribution of PAmCh-SctQ within the cytosol of *Y. enterocolitica* measured by sptPALM**.** Stationary fraction displayed in red, mobile one in blue. Scale bar 1µm. (**b**) Quantification of single-particle tracking photoactivated localization Microscopy (sptPALM) measurements in Single step diffusion coefficients for PAmCh-SctQ in µm²/s. (Diepold *et al.*, 2015).

Through fluorescence recovery after photobleaching (FRAP) experiments, half-life recoveries for SctQ could be determined. Under non-secreting conditions (half-life recovery: 134.3 ± 16.1 seconds) the recovery was found to be slower than under secreting conditions (half-life recovery: 68.2 ± 7.9 seconds) (**Figure 7a**). For the other cytosolic components FRAP data is still missing, but the assumption is that they exchange together with SctQ (Wagner *et al.*, 2018; Milne-Davies *et al.*, 2020). Additional FRAP experiments with a nonfunctional ATPase mutant *Ye*SctN$_{K175E}$ showed only fast recovery (**Figure 7b**). Based on these observations, it was suggested that that the cytosolic complex underneath the injectisome is stabilized by the interaction with effector proteins and the ATP-bound ATPase (Diepold *et al.*, 2015). While there are no recovery data, it could be shown, that all cytosolic components exist in both an injectisome bound and cytosolic state (Johnson and Blocker, 2008; Diepold *et al.*, 2017; Rocha *et al.*, 2018; Bernal *et al.*, 2019). Also, all cytosolic components react to the state the injectisome is in (secreting/non-secreting) and is faster the diffusion in the cytosol under secreting conditions (**Figure 7c**). This effect is detectable

even in absence of the inner membrane ring, SctD, indicating that this change is independent of any sensing from the basal body or needle (Diepold *et al.*, 2017). A gradual change from 5 mM Ca^{2+} (non-secreting condition) to 5 mM EGTA (secreting conditions) tracked by FCS in combination with a secretion assay in *Y. enterocolitica* further revealed that the diffusion speed of SctQ and SctL correlates with the secretion output (**Figure 7b**) (Diepold *et al.*, 2017). Fluorescence (cross-) correlation spectroscopy (FCS) measurements and 3D single-particle tracking photoactivated localization microscopy (sptPALM) were further able to show that the cytosolic components do not diffuse alone in the cytosol, but form complexes with different diffusion behavior. The deletion of different cytosolic components overall increased diffusion speed of the tracked protein, which indicates abolished interactions (**Figure 7e)** (Diepold *et al.*, 2017; Rocha *et al.*, 2018). $SctQ_c$ is essential for the formation of these complex states. In the cytoplasm, three different populations of SctQ could be identified. They have been suggested to represent monomeric SctQ, oligomeric SctQ with $SctQ_c$ and correlation of diffusion speed indicates the third one could be SctQ and SctL diffuse in a complex. The potential existence of bigger complexes remained speculative at this point (Rocha *et al.*, 2018).

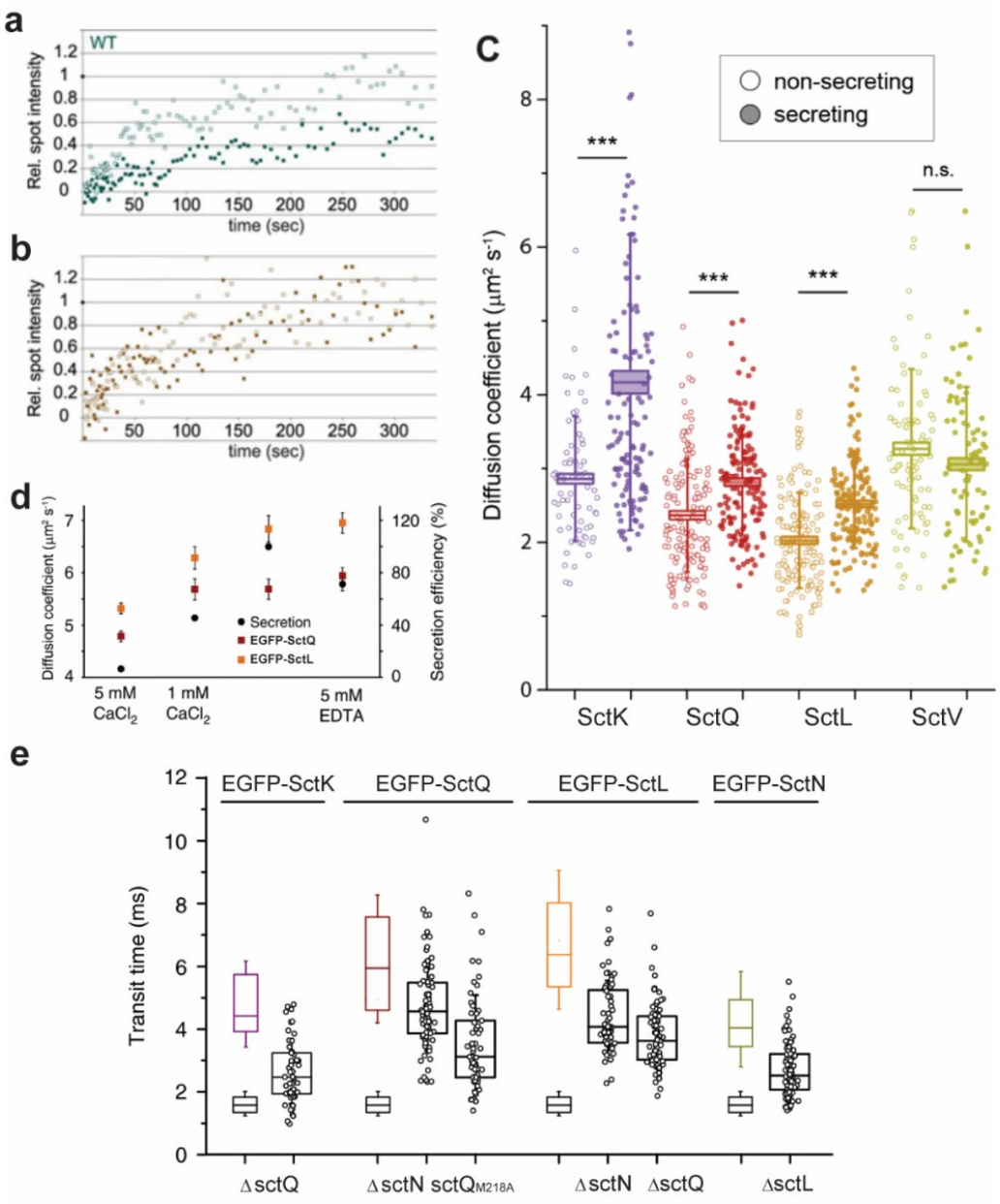

Figure 7 Dynamics of the cytosolic components.
Fluorescence recovery of (**a**) EFGP-SctQ, tracked over time in wild type (WT) background. (**b**) EFGP-SctQ, tracked over time in $SctN_{K175E}$ background. Circles represent intensity at the indicated time. In both (a),(b), measurements were taken under secreting (open) and non-secreting conditions (filled)(Diepold *et al.*, 2015). (**c**) FCS measurements of indicated cytosolic components (SctK,Q,L,N) under non-secreting (open) and secreting conditons (filled) ***P<0.001 (Diepold *et al.*, 2017) (**d**) FCS Diffusion in $\mu m^2/s^{-1}$ of EGFP-SctQ (Red) and EGFP-SctL (Orange) correlated with the amount of secreted effectors (black) in the transition from non-secreting (high Ca^{2+}) conditions to secreting condtions (low Ca^{2+}) (Diepold *et al.*, 2017). (**e**) Measured FCS transit time in (ms) of cytosolic components labeled with EGFP of the indicated cytosolic components at the top (SctL,Q,L,N) mesured in different mutations backgrounds and displayed as black boxplots with dots. Indicated at the bottom of the graph the mutation backgrounds (ΔSctQ, ΔSctN, $SctQ_{M218A}$ (internal translation site mutant), ΔSctN, ΔSctQ, ΔSctL). Colored boxplots on top represent WT measurements of the respective protein. Black small boxplots left denote EGFP diffusion for comparison. (Diepold *et al.*, 2015; Diepold *et al.*, 2017).

A study with native mass spectrometry (MS) in *Salmonella* Typhimurium investigated the different multimeric states in the cytosol (Bernal et al., 2019). The authors identified several sub-complexes including $SctQ_c$. The protein was mostly present in homodimers, but also homotetramers have been detected (Figure 8a) (Bernal et al., 2019). Bigger oligomeric complexes of StSctQ were identified ((SctQ(2$SctQ_c$), 2(SctQ(2$SctQ_c$)), as well as combinations of other cytosolic components (Figure 8a). It could be confirmed that SctL is mostly present as a dimer or built into a bigger complex size mainly 2(SctQ-(2$SctQ_c$)-2SctL) when diffusing in the cytosol. The biggest complexes found included four different proteins. The most abundant ones were: SctQ(2$SctQ_c$)-2SctL-SctN and 2(SctQ(2$SctQ_c$))-2SctL-SctN (Figure 8a). Interestingly, SctN was only found in complexes together with SctL (Bernal et al., 2019). This in turn fits the observation from a previous study where the deletion of *Y. enterocolitica*

SctN resulted in a drastic decrease of interactions in Co-immunoprecipitation assays (Diepold et al., 2017). Bead model reconstruction from the small-angle X-ray scattering done on the identified four protein complexes further suggested that those assume an L shape, which could be modeled and placed with a good agreement as one of six pods into the Cryo-ET structures from into the assembled *S*. Typhimurium (Figure 8b).

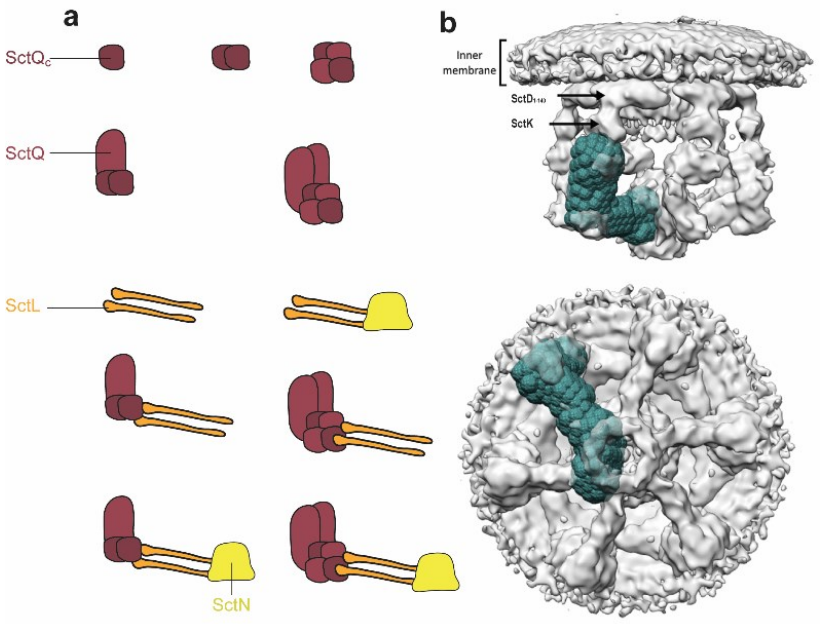

Figure 8 Representation of injectisome complexes found in the bacterial cytosol.
(**a**) Schematics of complexes found in higher abundance in the cytosol of *S.* Typhimurium: first row $SctQ_c$ homodimer, heterodimer and heterodimeric states; Second row: SctQ($SctQ_c$2) and 2(StSctQ($StSctQ_{c2}$)); third row: 2SctL and 2SctL-SctN; Fourth row: SctQ($StSctQ_{c2}$)-2SctL and 2SctQ($StSctQ_c$2))-2SctL; Fifth row: *SctQ(*$SctQ_{c2}$*)-2SctL-SctN and 2(SctQ(*$SctQ_{c2}$*))-2SctL-SctN* (**b**) Mode of Superpositioned L-shape based on SAXS bead model into already published CyroCT structure of *S.* Typhimurium. (Bernal *et al.*, 2019)

1.1 Model organisms

1.1.1 *Yersinia* spp. and *Yersinia enterocolitica*

The genus *Yersinia* was first established by van Loghem in 1944 named and in honor of A.J. Yersin. Yersin, who studied the bacteria in 1884 in Lausanne, Marburg and Paris, isolated, described and identified *Yersinia pestis* as the cause of the black death, formerly known as the *plague bacillus*, in 1894. Due to controversies about the discovery, the name *Y. pestis* only entered the *Approved List of Bacterial Names* in 1980 (Bibel and Chen, 1976; Hawgood, 2008). While *Yersinia* spp. is mostly associated with the past and the plague (Pastur. and 1894, n.d.; Mouton, 1975; Brossollet and Mollaret, 1994; Perry and Fetherston, 1997), outbreaks of all three species are reported on a regular and global basis (Nuorti *et al.*, 2004; Leslie *et al.*, 2011; Espenhain *et al.*, 2019).

Generally, *Yersinia* spp. are Gram-negative, rod-shaped gamma-proteobacteria (Bottone and Mollaret, 1977). Besides *Y. pestis*, the genus *Yersinia* holds 17 additional species. The two others known to cause diseases in mammals are *Y. pseudotuberculosis* and *Y. enterocolitica* and they are closely related (Koornhof *et al.*, 1999; Smego *et al.*, 1999). All of them cycle between the lymphoid tissue of mammalian hosts and the environment. *Y. pestis* is usually transmitted via a flea bite, whereas *Y. pseudotuberculosis* and *Y. enterocolitica* require the oral-fecal route for transmission. While the three different *Yersinia* species vary in their animal host, all can cause, to varying degrees, local and systemic diseases (Bottone and Mollaret, 1977; Straley *et al.*, 1993).

For this study, *Y. enterocolitica* has been used as the primary model organism. Infection with *Y. enterocolitica* occurs after consumption of contaminated food (Black *et al.*, 1978) or water (Keet, 1974), and undercooked pork was identified as the major source of transmission (Bottone, 1997; Fredriksson-Ahomaa *et al.*, 2006). *Y. enterocolitica* infection usually results in self-limiting gastro-enteric infections with associated symptoms like enteritis, ileitis and diarrhea. Inflammation of the lymphatic system is possible as well. In severe cases, a fatal systemic infection is possible (Cover and Aber, 1989; Koornhof *et al.*, 1999). If needed, a *Y. enterocolitica* infection is treatable with β-lactam or cephalosporin antibiotics (Gayraud *et al.*, 1993). Environmentally, *Y. enterocolitica* is widespread and can be found in different hosts like wild or in domesticated mammals or birds. At an environmental temperature of 4-28°C, growth of *Y. enterocolitica* has been shown and cells are flagellated and mobile (Bottone and Mollaret, 1977; Stenhouse and Milner, 1982).

After uptake in the human body, the shift to 37°C results in the loss of flagella and induction of virulence gene expression. Loss of the flagellum is attributed to the inhibition of flagellin transcription, which is regulated by the fliA-dependent σ^F promotors (Rohde *et al.*, 1994; Kapatral and Minnich, 1995). Despite the different pathogenicity, all pathogenic strains contain the pYV (plasmid of *Yersinia* virulence) plasmid in addition to its genome. The pYV is 70- to 75-kb and encodes the virulence-associated type III secretion system, also called injectisome and its cognitive effectors proteins and chaperones a arsenic resistance, the adhesion YadA and the partitioning system SpyAB (*Pathogenicity Islands and Other Mobile Virulence Elements*, 1999). Without the pYV, *Yersinia* is avirulent (Portnoy *et al.*, 1984; Bolin *et al.*, 1985; Straley *et al.*, 1993; Rohde *et al.*, 1999). Upon temperature shift from environmental temperature (below 30°C) to host temperature (37°C), a stem-loop structure in front of the master regulator VirF melts, allowing the effective translation of the injectisome genes (Hoe and Goguen, 1993; Rohde *et al.*, 1999). At 37°C and during active secretion, *Y. enterocolitica* shows an reduced growth rate, which can be quickly restored to normal after the stop of secretion (Carter *et al.*, 1980; Milne-Davies *et al.*, 2019). While this was contributed until lately to the metabolic burden of the injectisome and effectors, new results actually show that *Y. enterocolitica* adenylate energy charge is not affected (Milne-Davies *et al.*, 2019).

After uptake into the human body, *Y. enterocolitica* travels to the small intestine (**Figure 2b**) where they enter the Peyer's patches via M cells (Sabina *et al.*, 2011; Heroven and Dersch, 2014; Shoaib *et al.*, 2019). For initial attachment to the host cell and for successful infection, *Y. enterocolitica* relies on several adhesins. The most prominent on is the *Yersinia* adhesin A (YadA) (Meuskens *et al.*, 2019). Its length is tightly linked to the injectisome length and it interacts with collagen and fibronectin (Mota *et al.*, 2005; Mühlenkamp *et al.*, 2015). Once in contact with host cells, the injectisome is not very specific in its choice of host cell target and effector secretion has been shown with immune cells, epithelial cells and even red blood cells (Clerc *et al.*, 1986; Håkansson *et al.*, 1996; Armentrout and Rietsch, 2016; Nauth *et al.*, 2018; Bohn *et al.*, 2019). To reach the Peyer's patches, *Y. enterocolitica* travels the human body and gastrointestinal tract which can take between minutes to hours. During this time, the bacteria are exposed to a variety of low external pH (pH of 1.5 – 4.5) (**Figure 2b**) (Evans et al., 1988; McClements and Li, 2010). To cope with the acid stress, *Y. enterocolitica* developed a set of tools. While several decarboxylase or antiporter-dependent acid resistance systems, like glutamate-, arginine-, or lysine-dependent ones have been described in *E.coli, Y. enterocolitica* seems to rely mostly on an aspartate-dependent pathway (Foster, 2004; Hu *et al.*, 2010). Even more important for *Y. enterocolitica* is the urease enzyme, which has been shown to be vital for host colonization. It is constantly active and catalyzes the reaction from urease to ammonium thereby neutralizing proteins. The enzyme can make up 5-10% of the total proteome and

the OmpR response regulator of the EnvZ/OmpR system can further increase the levels of urease in response to low environmental pH, to increase the acid tolerance (Stingl and De Reuse, 2005; Hu *et al.*, 2009; Chen *et al.*, 2016). After passage through the gut and into the Peyer's patches, the injectisome and its effectors are key to inhibit cytoskeleton dynamics and fend of macrophages and neutrophils (Grosdent *et al.*, 2002).

1.1.2 *Pseudomonas aeruginosa*

Pseudomonas aeruginosa is a rod-shaped, opportunistic, Gram-negative, Gamma-protobacterium. It is an opportunistic human pathogen and is commonly found in the environment (Engel and Balachandran, 2009). For infection, it relies on a compromised epithelial barrier, as a result it is often associated with ventilator-associated pneumonia, post-operative infections or burn victims. Treatment is difficult since *P. aeruginosa* harbors resistance to many antibiotics and even with proper antibiotic treatment there is a mortality rate of up to 40% in immunocompromised or hospitalized patients. Thus, *P. aeruginosa* is listed number two on the World Health Organization (WHO) priority list (Hauser *et al.*, 2002; Lambert, 2002; Engel and Balachandran, 2009; Tacconelli and Magrini, 2017). During long-term cystic fibrosis infection, the bacteria can stay in the host for decades (Boucher, 2004). In contrast to *Y. enterocolitica, P. aeruginosa* harbors not only an injectisome (type III), but a wide range of secretion systems and pathogenicity factors. Type I, II, III, V and three type VI (Hemolysin-coregulated protein secretion island H-I, H-II, H-III) secretion systems have been found (Ma *et al.*, 2003; Lau *et al.*, 2005; Filloux *et al.*, 2008; Chatterjee *et al.*, 2020; Chen *et al.*, 2020). The injectisome is mostly used during early infection associated with fighting of macrophages and epithelial damage. Four effectors have been identified and *in vitro* effector secretion peaks after 2-3 hours after the induction of secretion (Engel and Balachandran, 2009; Lampaki et al., 2020). From the evolutionary perspective, the injectisome of *Y. enterocolitica* and *P.* aeruginosa are closely related. Injectisomes in general, can be divided into seven evolutionary groups, independently from the species in with they are found (Abby *et al.*, 2012), both the injectisome of *Y. enterocolitica* and *P. aeruginosa* belong to the Ysc-family of injectisomes (Lombardi *et al.*, 2019). Mutations in the injectisome of *P.* aeruginosa are commonly found in cystic fibrosis patients isolates (Jain *et al.*, 2008). This is probably to evade the immune system. Never the less, injectisome has been widely recognized as a potential target for novel therapeutics for *P. aeruginosa* (Engel, 2003; Lombardi *et al.*, 2019).

1.1.3 *Shigella flexneri*

Shigella flexneri is a rod-shaped, Gram-negative Gamma-protobacterium and can be divided in 13 serotypes (Jennison and Verma, 2004). Infections predominantly occur in the global south and in children under the age of five (Kotloff et al., 1999; Jennison and Verma, 2004). Bacterial transmission is mostly via the fecal-oral route and due to a lack of clean drinking water and proper sanitation. Treatment with antibiotics is possible, nevertheless especially against more widely used antibiotics, resistances are developing (Ashkenazi et al., 2003). *S. flexneri* is highly infectious and only ~100 cells are needed to cause diseases in adults (Formal, 1989). This is attributed to a very efficient survival during the gastro-internal passage by upregulation of acid resistance genes which allows *S. flexneri* to withstand exposure to a pH as low as 2.5 for up to two hours (Small et al., 1994). In the colon, they invade the mucosa and replicate within and between the junctions of the epithelial cells. The destruction of the epithelial layer is in the end what causes clinical symptoms like fever and watery to bloody diarrhea (Philpott et al., 2000; Jennison and Verma, 2004). Like both *Y. enterocolitica* and *P. aeruginosa*, *S. flexneri* uses injectisome. The *S. flexneri* injectisome is evolutionarily only distantly related to the one found in *Y. enterocolitica* and *P. aeruginosa* (Abby *et al.*, 2012). It is encoded on a virulence plasmid and *S. flexneri* utilizes its effector proteins to enter epithelial and M cells, as well as downregulate the immune response of the host (Perdomo et al., 1994; McCormick et al., 1998; Sakaguchi et al., 2002; Zurawski et al., 2009). Similar to *Y. enterocolitica*, *S. flexneri* is a widely used model organism for research on the injectisome with a strong emphasis on the structural aspects of the system (Martinez-Argudo and Blocker, 2010; Marteyn et al., 2012; Hu et al., 2015; Burgess et al., 2020).

2 Scope of the study

During my PhD, in the research group of Andreas Diepold at the Max Planck Institute for Terrestrial in Marburg, I wanted to investigate the function and regulation of the bacterial injectisome.

The injectisome is a complex nano-machine conserved in many pathogenic bacteria including *Yersinia, Salmonella,* and *Shigella* and is used to deliver molecular toxins – so-called effector proteins - into eukaryotic host cells. In *Y. enterocolitica* the effectors are used to defend the bacteria against the primary immune host defense in the lymphatic tissues. I wanted to investigate which events lead to the secretion of effectors and how the injectisome is regulated on the molecular level. For this, my main interest was on the cytosolic injectisome components, four proteins located at the interface of the basal body with the inner membrane (**Figure 2**). These proteins are the ATPase SctN, the spoke protein SctL, the C-ring protein SctQ, and an adapter protein, SctK. Recent research from our lab showed that these proteins shuttle between the injectisome-bound state and the cytosol, where they also interact with each other. Importantly, this behavior differs between secreting and non-secreting conditions and there is evidence that those components may be influenced by the environmental surroundings of the bacterium as well. While the dynamics have been well described in the past, any functional link between the effector secretion and the dynamics was still missing.

To shed light on the events at the cytosolic interface and to link the dynamics with the function of the system, I followed two major approaches. In the first approach, I characterized the effect of different environmental pH levels on the dynamics of the cytosolic components and the injectisome in general. By using flow cell-based TIRF microscopy, single particle tracking photoactivated localization microscopy (sptPALM) and functional assays, I characterized the impact that changes in environmental pH has on the injectisome and investigated the mechanism behind it. Our data shows that low outside pH results in loss of effector secretion and dissociation of the cytosolic components from the basal body - the first time that a study could link the dynamics of the cytosolic components with a direct functional output.

While this approach focused more on the regulatory aspects of the injectisome, the second one centered around the mechanisms of secretion. The cytosolic injectisome components interact with effector proteins in an ordered manner; however, how and when this interaction with the effectors proteins takes place and what the role of the dynamics in the cytosol are remained unclear in the past. To investigate this, we combined a mass spectrometry (MS)-based co-immunoprecipitation assay with (sptPALM) and functional assays. By comparison of the dynamics of the wild-type strain carrying the full set of effectors

with an effector-less strain, we investigated the impact of effector binding to the cytosolic injectisome components.

3 Results: Part I

3.1 Dynamic relocalization of the cytosolic type III secretion system components prevents premature protein secretion at low external pH

The findings presented in this study have been peer reviewed and accepted for publication on 12.02.21 at Nature Comminutions. doi: 10.1038/s41467-021-21863-4. A previous open access version is accessible at BioRxiv, doi: https://doi.org/10.1101/869214.

3.1.1 Authors and contributions

Stephan Wimmi, Alexander Balinovic, Hannah Jeckel, Lisa Selinger, Dimitrios Lampak, Emma Eisemann, Ina Meuskens, Dirk Linke, Knut Drescher, Ulrike Endesfelder & Andreas Diepold.

S.W. performed the majority of the experiments and data analysis and participated in study design and writing the manuscript. A.B. performed and analyzed the sptPALM experiment with support from S.W. H.J. provided coding for the automated spot detection. L.S., D.Lampaki and E.E. assisted in experiments and strain generation. I.M. performed the YadA binding experiments and participated in proofreading the manuscript. D.Linke, K.D. and U.E. provided supervision and participated in discussions and proofreading. A.D. conceived and designed the study, performed experiments and data analysis and wrote the manuscript. In case figures contain data or are mostly designed by co-authors, this will be noted in the figure legend.

3.1.2 Background

Y. enterocolitica is an extracellular gastrointestinal pathogen that employs its injectisome to downregulate immune responses and prevent inflammation after the penetration of the intestinal epithelium. For initial attachment to the epithelium, the bacteria employ a number of adhesins (Pepe *et al.*, 1995; Mikula *et al.*, 2013)., The two major adhesion factors at the early stage of infection are the autotransporters invasin (inv), which is already expressed at ambient temperatures (Pepe and Miller, 1993; Uliczka *et al.*, 2011) and *Yersinia* adhesin A (YadA) (Leo *et al.*, 2015); *inv yadA* double mutants are completely avirulent (Pepe *et al.*, 1995; Han and Miller, 1997). YadA is a key factor for establishing an infection (Meuskens *et al.*, 2019), which interacts with a variety of extracellular matrix molecules, including collagen and fibronectin (Mühlenkamp *et al.*, 2015). YadA length is tightly linked to the length of the injection needle of the T3SS, and establishes close contact to the host cells enabling injection (Mota *et al.*, 2005). *Y. enterocolitica* is

usually taken up with contaminated food or water. The shift from environmental to host temperature (37°C) induces expression and assembly of the injectisomes as well as YadA (Tertti *et al.*, 1992; Cornelis, 2006). The bacteria then have to pass the acidic environment of the stomach. During that time, the injectisome can already be present and ready for secretion of translocators (which form a pore in the host membrane and its connection to the needle, (**Figure 2**) and effectors. Since the injectisome readily translocates cargo into any host cell type it adheres to, including immune cells, epithelial cells and even red blood cells (Clerc *et al.*, 1986; Håkansson *et al.*, 1996; Armentrout and Rietsch, 2016; Nauth *et al.*, 2018; Bohn *et al.*, 2019), a distinct mechanism is needed to prevent premature activation of the injectisome during the passage of low pH parts of the gastrointestinal system, such as the stomach (external pH of 1.5 – 4.5 (Evans *et al.*, 1988; McClements and Li, 2010), (**Figure 2b**)), which would result in a loss of valuable resources, or even elicit immune responses.

3.1.3 Results

3.1.3.1 Resistance of *Y. enterocolitica* and its injectisome needles to low external pH

To investigate to which degree *Y. enterocolitica* can withstand a drop in external pH, *Y. enterocolitica* cultures in exponential growth phase were exposed to different pH for 30 minutes at 37°C. A subsequent dilution series on neutral pH agar showed high survival down to pH 4 (**Figure 9a**). Similarly, while the optical density of bacterial cultures slightly decreased over 90 min at pH 4 at 37°C, growth recovered at a reduced rate upon restoration of neutral pH (**Figure 9b**). Together, these results show that *Y. enterocolitica* tolerates temporary incubation down to pH 3, with limited fitness decrease at pH 4 and above. *Y. enterocolitica* adheres to host cells, other bacteria and abiotic surfaces by adhesins, most importantly the trimeric adhesin YadA and invasin (Leo *et al.*, 2015; Mühlenkamp *et al.*, 2015; Keller *et al.*, 2015). We thus tested whether low pH prevents the binding of YadA to collagen and more generally, of *Y. enterocolitica* cells to surfaces. Binding could be established at low pH in both cases, albeit at a significantly reduced level (**Figure 9cde,**). These results suggest that to avoid protein translocation into non-host cells, secretion itself might be prevented at low pH.

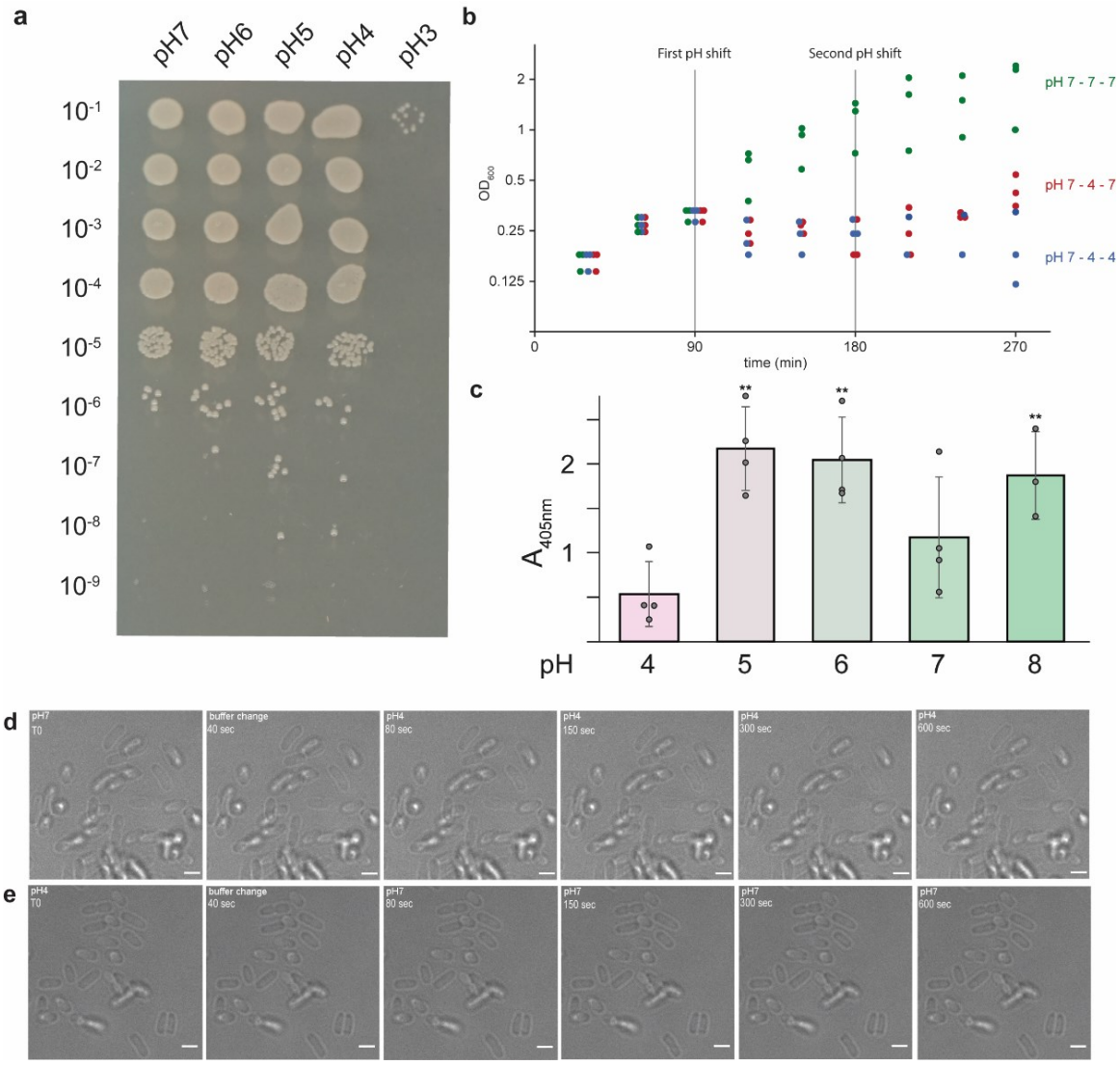

Figure 9 The *Y. enterocolitica* pH tolerance and its function low pH.
(a) Dilution drop test of *Y. enterocolitica* cultures incubated at the indicated pH at 37°C for 30 minutes. **(b)** Growth curve assay: *Y. enterocolitica* were inoculated to an OD_{600} of 0.12 from a stationary overnight culture. They were grown at pH 7 (28°C) for 90 min (0-90 min), collected by centrifugation and then resuspended in fresh medium (37°C) at pH 7 (green data points) or pH 4 (red and blue data points). Cultures were incubated for another 90 min (90-180 min), again collected by centrifugation, resuspended in fresh medium (37°C) at pH 7 (green and red data points) or pH 4 (blue data points), and incubated for further 90 min (180-270 min). OD_{600} values were recorded every 30 min. The results of three independent experiments are displayed. Experiments have been performed by Andreas Diepold and Stephan Wimmi. (**c**)Binding of the *Y. enterocolitica* adhesion YadA to collagen at the indicated pH values. Absorption at 405 nm resulting from Ni^{2+}-HRP binding to YadA-His_6 incubated with plate-absorbed calf collagen type I. n = 4 biological replicates (n = 3 for pH 8) with 3-8 technical replicates each, error bars denote standard deviation. **, statistically significant difference compared to pH 4, 0.001>p>0.0001 in a homoscedastic two-tailed t-test; all other pairwise comparisons do not differ in a statistically significant way (p>0.05). Experiments and analysis of panel c were done by Ina Meuskens. **(d)** Example micrographs from Time-lapse phase contrast video of *Y. enterocolitica* attached to a glass cover slip in a flow cell at pH 7. The buffer was exchanged from pH 7 to pH 4 buffered media during the experiment and cells were tracked for 600 seconds/10 minutes with a picture taken every 10 seconds. **(e)** Example micrographs from Time-lapse phase contrast video, *Y. enterocolitica* was attached to a glass cover slip in a flow cell at pH 4. During the experiment the buffer was changed from pH 4 to pH 7 and cells were tracked again for 10 minutes with a picture taken every 10 seconds. Scale bars, 2 µm, n = 3.

To test under which conditions *Y. enterocolitica* secretes injectisome substrates, we performed an *in vitro* secretion assay where *Y. enterocolitica* cells primed for secretion were subjected to secreting media in the range from pH 8 to pH 4. Indeed, we observed that secretion did not occur at low pH in both strains we commonly use in the lab, IML421asd (ΔHOPEMTasd) (does not harbor any virulence effectors) similar than in the wild type (WT) strain (strain with a full set of effector proteins) (**Figure 10ab**). This lack of secretion is not due to lower protein synthesis at pH 4 (**Figure 10c**), suggesting a specific mechanism to suppress secretion at low external pH.

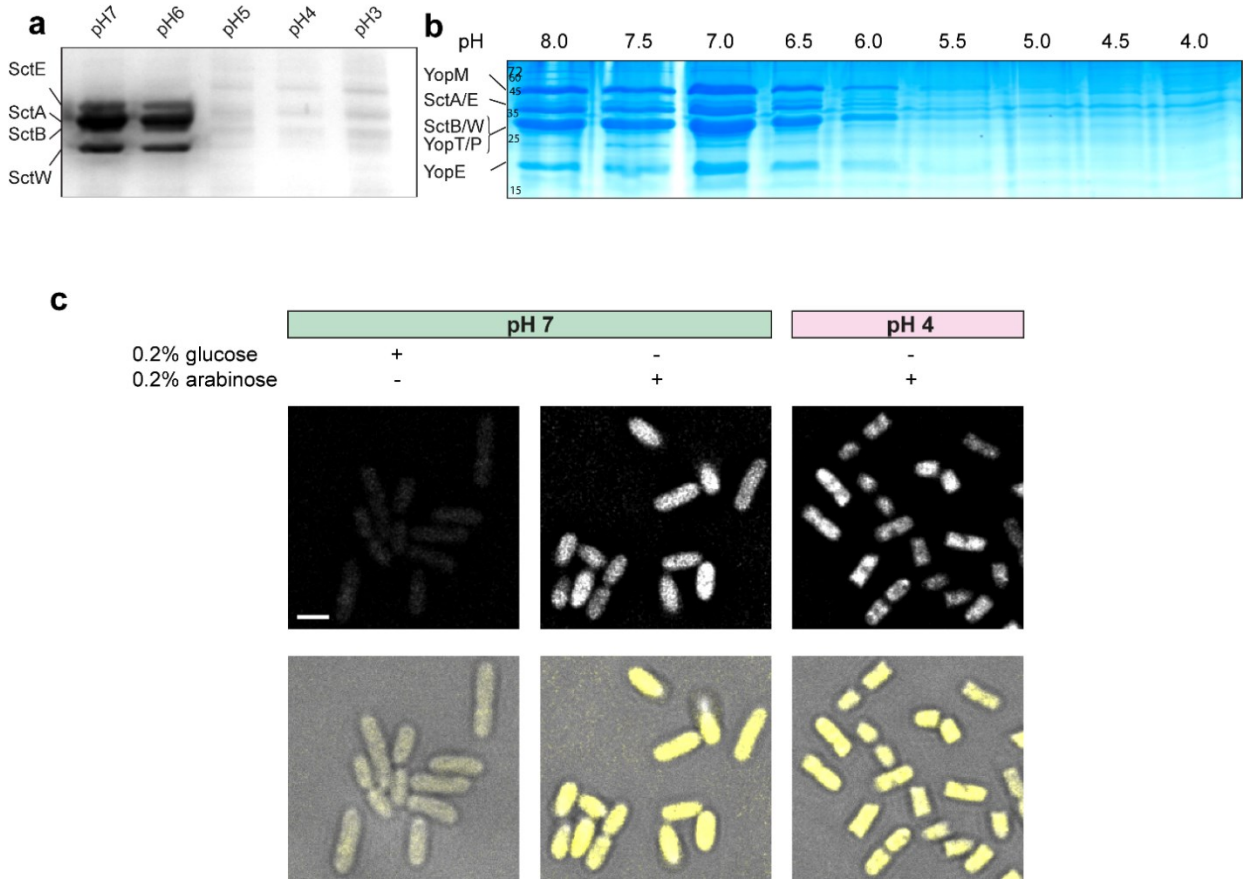

Figure 10 At low pH effector secretion is inhibited but protein biosynthesis still possible.
(a) *In vitro* secretion assay showing the export of native injectisome substrates (indicated on the left side) in strain with without effectors at the indicated external pH values. Black and white scan of a Coomassie-stained SDS-PAGE gel; **(b)** *In vitro* secretion assay showing the export of native injectisome substrates (indicated on the left side) in an effector strain containing all native virulence effectors at the indicated external pH values. Coomassie-stained SDS-PAGE gel; supernatant of $3*10^8$ bacteria per lane. n>5 independent experiments. **(b)** Effector-less *Y. enterocolitica* were grown at neutral pH and then subjected to different pH as indicated. EGFP expression was induced from a pBAD plasmid at the same time, and fluorescence was determined after 180 min. Top, fluorescence image in GFP channel, bottom, overlay of phase contrast (grey) and fluorescence (yellow). Scale bar, 2 µm, n = 3.

But how does *Y. enterocolitica* prevent secretion at low pH? To determine if the absence of secretion is due to a complete disassembly of injectisomes at that pH, we visualized the needles at different pH values and over time by labeling an introduced cysteine residue with a maleimide-linked dye (Milne-Davies *et al.*, 2019). The needles were stable at pH 4 over continued time periods (up to 120 minutes) (**Figure 11**, **Supplemental Figure 1**).

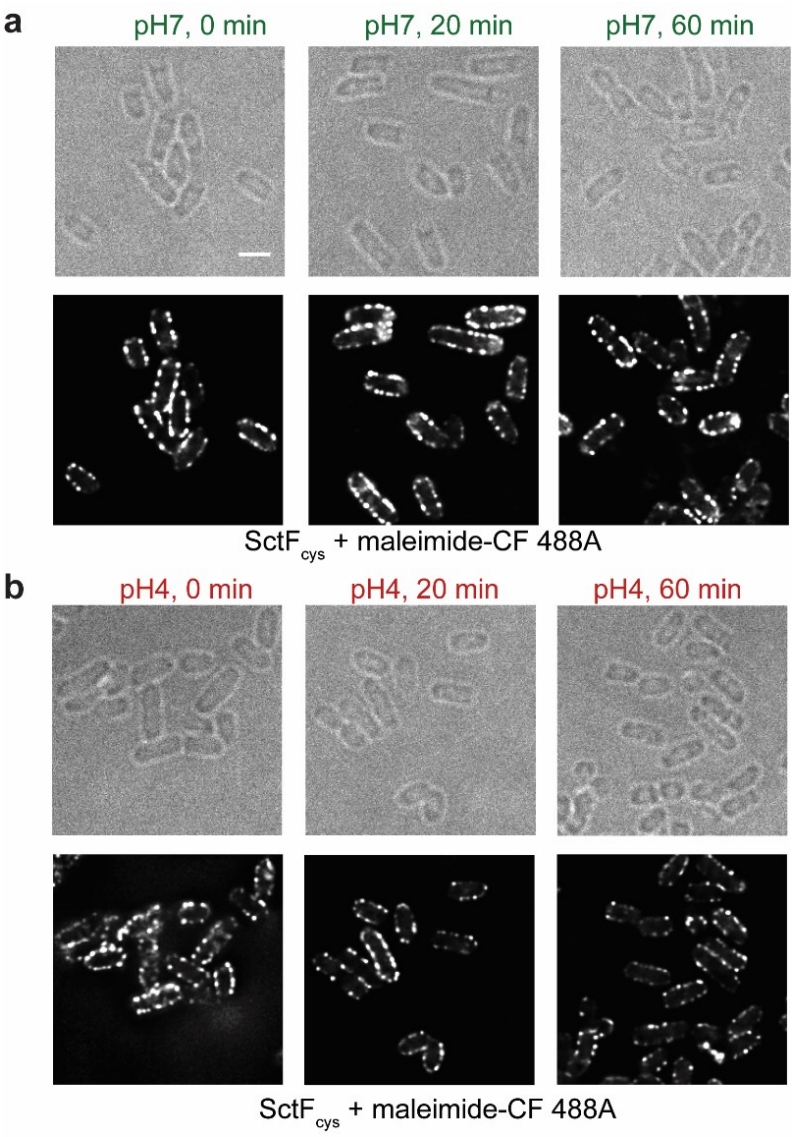

Figure 11 Staining of injectisome needles at the different indicated external pH values.
Fluorescent micrographs of live *Y. enterocolitica* cells over time. Indicated on top is the duration of **(a)** pH 7/**(b)** pH4 treatment. A strain expressing the mutated needle subunit SctF$_{S5C}$ was covalently labeled with maleimide-CF 488A. Experiments was performed at least 3 times with comparable results. Scale bar, 2 µm. Supplemental Figure 1 shows exposure to the indicated pH up to 120 min.

Taken together, *Y. enterocolitica* as well as its injectisome needles can withstand low external pH conditions, but still translocators and effectors are not secreted.

3.1.3.2 Association of the dynamic cytosolic injectisome components to the injectisome is temporarily suppressed at low external pH

We have recently found that the cytosolic injectisome components (SctK/Q/L/N) form a dynamic network, where protein exchange is connected to the function of the injectisome (Figure 2a) (Diepold et al., 2015; Diepold et al., 2017). Hence, we wondered whether these dynamic components could be involved in the inhibition of secretion at low pH. To investigate this question, we performed flow-cell-based total internal reflection fluorescence (TIRF) microscopy with functional N-terminal fluorescent protein fusions of the cytosolic components, expressed at native levels: EGFP-SctK, EGFP-SctQ, EGFP-SctL and EGFP-SctN (**Figure 2a**) (Diepold et al., 2010; Diepold et al., 2017). At neutral or near-neutral pH, the cytosolic components localized in foci at the bacterial membrane, which represent their injectisome-bound state (Diepold et al., 2010). However, at an external pH of 4, all cytosolic components lost this punctuate localization, and the proteins relocated to the cytosol (**Figure 12abc**).

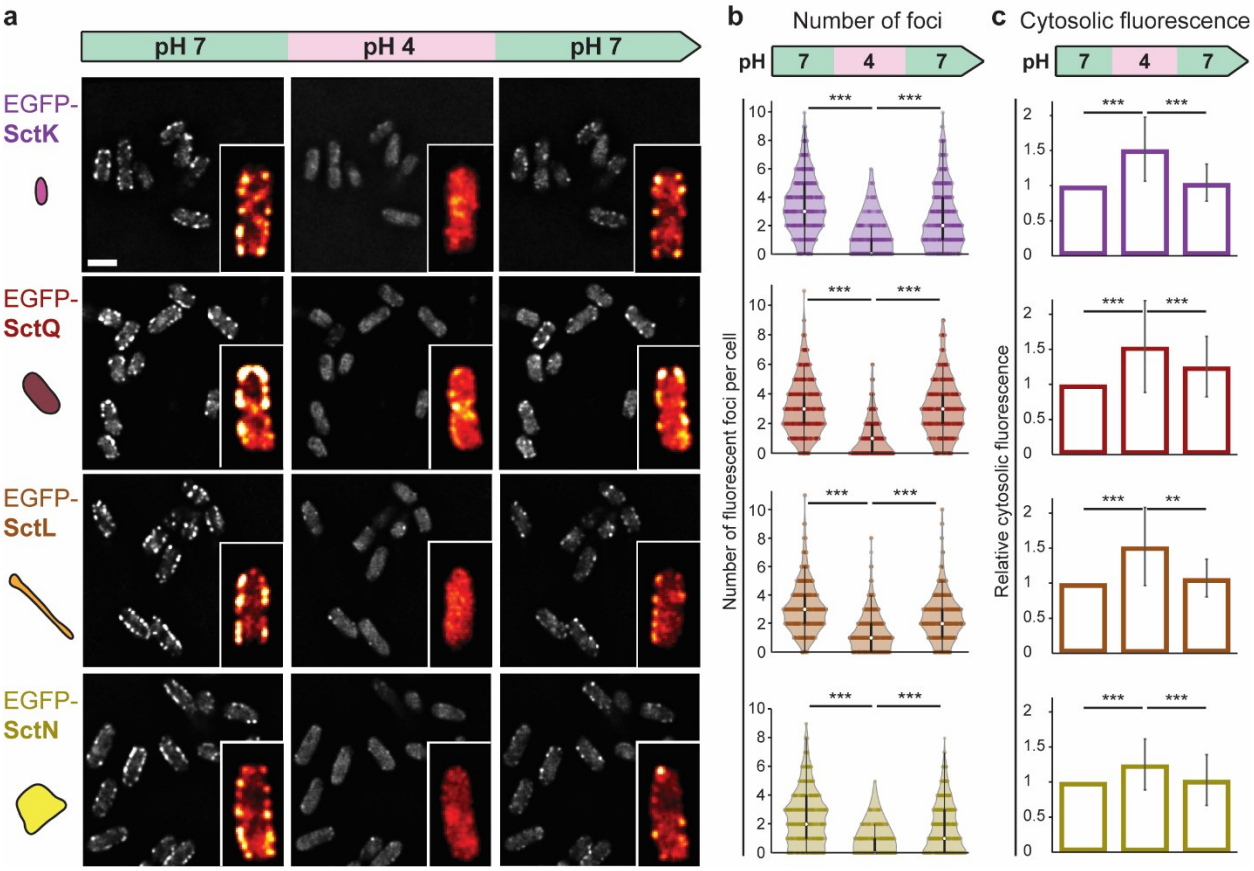

Figure 12 The cytosolic injectisome components temporarily dissociate from the injectisome at low external pH.
(a) Fluorescent micrographs of the indicated proteins in live *Y. enterocolitica*, consecutively subjected to different external pH in a flow cell. Images were taken under secreting conditions, 10 minutes after bacteria were subjected to the indicated pH. Insets, enlarged single bacteria, visualized with the ImageJ red-hot color scale. **(b)** Quantification of foci per bacterium for the strains and conditions shown in panel **(a)**. n = 453, 792, 466, 554 foci (from top to bottom) from three independent experiments. White circle denotes median, black bar denotes first and third quartile, black line denotes the lower/upper adjacent value. **(c)** Quantification of mean cytosolic fluorescence for the strains and conditions shown in panel **(a)**. n = 75 cells from 3 independent experiments per strain. Bars denote mean values. For **(a)** and **(c)**, error bars denote standard deviation; **/***, p<0.01/0.001 in homoscedastic two-tailed t-tests ((B): p~2*10-114/2*10-57, 4*10-102/1*10-51, 5*10-79/1*10-69, 8*10-89/2*10-51; **(c)**: p~8*10-18/7*10-13, 5*10-11/2*10-3, 2*10-13/3*10-9, 6*10-8/4*10-4 for differences between pH for first/second pH 7 incubation, respectively, from top to bottom). Experiments a for were performed >5, times respectively, with comparable results. Scale bars, 2 µm.

The relocation remained stable over time at low external pH (**Supplemental Figure 2**). Strikingly however, this phenomenon was reversible: Upon exposure to neutral external pH, the foci recovered within a few minutes (**Figure 12abc**). This effect was observed both under secreting and non-secreting conditions (**Figure 13a**), and was independent of the fluorophore or visualization tag that was used (**Figure 13b**). Notably, while the fluorescence of genetically encoded fluorophores such as EGFP is pH-dependent (Patterson *et al.*, 1997; Doherty *et al.*, 2010), the observed effect is not caused by the reduction of overall fluorescence in the cytosol (**Figure 13c**,**Figure 13cd**).

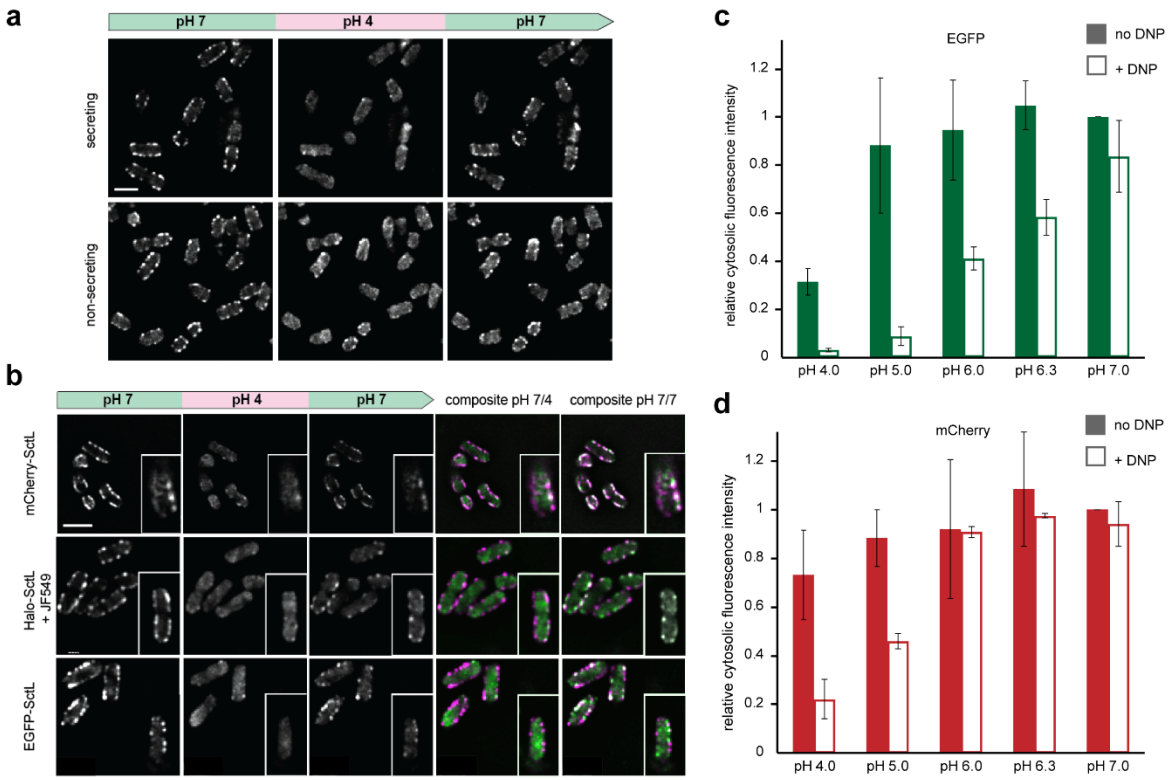

Figure 13 Dissociation of the cytosolic components at low external pH can be observed irrespective of the used visualization tag, and in both secreting and non-secreting conditions.
(a) Fluorescence micrographs of *Y. enterocolitica* EGFP-SctQ, incubated at the indicated external pH values under secreting conditions (top), or non-secreting conditions (bottom) over time. **(b)** Fluorescence micrographs of *Y. enterocolitica* expressing indicated labeled versions of SctL (replacing the WT gene by allelic exchange) at the indicated external pH values under secreting. Intensity of cytosolic fluorescence levels of EGFP and mCherry at different external pH. The cellular fluorescence levels of cytosolic EGFP **(c)** and mCherry **(d)** were determined at the indicated external pH, in absence (filled bars) and presence (empty bars, dotes represent single data points) of the ionophore 2,4-dinitrophenol (DNP, 2 mM), which adjusts the cytosolic pH to the external pH. Fluorescence per bacterium was determined by dividing the measured fluorescence above background by the number of bacteria per field of view, and normalized by the respective value at pH 7 in the absence of DNP. Error bars display the standard deviation of 3 independent experiments (2 independent experiments for mCherry + DNP). Bars denote mean values, single data points indicated by small circles. For each experiment, two fields of view were analyzed.

Dissociation and re-association of the cytosolic injectisome components in response to the external pH was reversible for several cycles (**Supplemental Figure 3**), and dissociation kinetics were similar under non-secreting and secreting conditions (presence of 5 mM $CaCl_2$ and EGTA, respectively) (**Supplemental Figure 4**). To quantify the kinetics of association and dissociation of SctQ, we monitored EGFP-SctQ foci in a microscopy flow cell after a pH change from 7 to 4 and *vice versa*. Foci gradually disappeared within two minutes under secreting conditions (**Figure 14**). Upon restoration of neutral external pH, this phenotype was reversed and foci were restored within a similar time range (**Figure 14**).

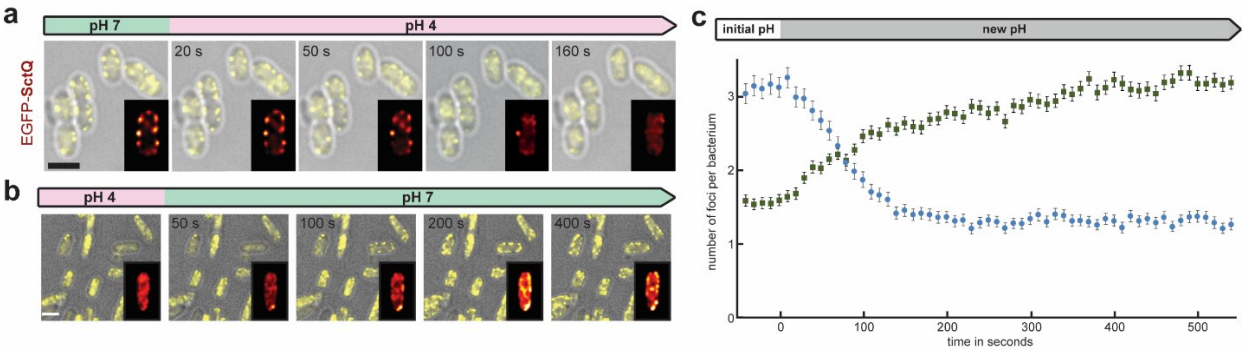

Figure 14 Re-association kinetics of EGFP-SctQ upon restoration of neutral external pH and quantification of disassociation and re-association kinetics.
(a) Kinetics of EGFP-SctQ dissociation after pH shift from 7 to 4. Overlay of phase contrast (grey) and fluorescence images (yellow); insets, enlarged single bacterium, visualized with the ImageJ red-hot color scale. **(b)** Kinetics of EGFP-SctQ re-association after pH shift from 4 to 7. Overlay of phase contrast (grey) and fluorescence images (yellow); insets, enlarged single bacteria, visualized with the ImageJ red-hot color scale. n = 3. Scale bar, 2 µm **(c)** The number of fluorescent EGFP-SctQ foci detected by BiofilmQ (see Material and Methods for details) was determined every 10 s in a flow cell upon changing the external pH at t=0, a) from 7 to 4 (blue circles; n = 337-349 detected). Raw data **Supplemental Figure 5**. Experiments were performed >5 times, with comparable results. Scale bars, 2 µm.

To test whether the recovery of foci was due to the synthesis of new proteins or if the previously bound proteins rebind to the injectisomes, we covalently labeled the pool of Halo-tagged SctL with the Janelia Fluor JF 646 Halo ligand dye (Grimm *et al.*, 2017) prior to the incubation at pH 4 to ensure that only the protein pool present at the time of labeling was fluorescent. Similar to the previous experiments, we observed a reversible loss of fluorescent foci at the membrane and an increase in cytosolic signal at pH 4 and rebinding of the fluorescent proteins upon changing pH to 7 (**Figure 15a**). The cytosolic components colocalize with the needle at the initial pH 7 (shown here SctL, others were also tested- data not shown) (**Figure 15bcd**) and an overlay of the micrographs at pH 7 before and after the incubation at pH 4 indicated that most foci reform at the same position as they previously appeared (**Figure 15, Figure 13ab**).

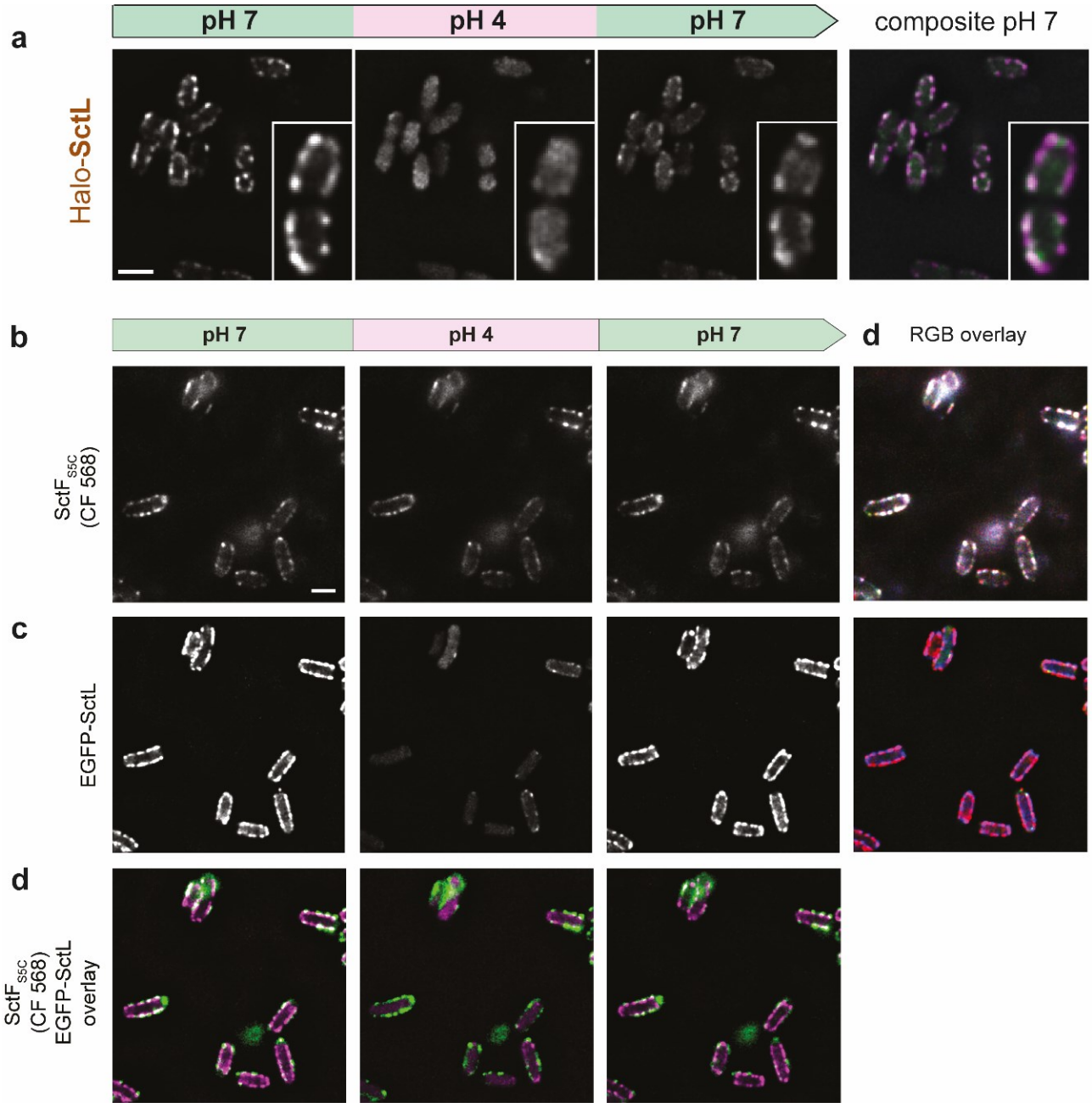

Figure 15 Localization of cytosolic subunit SctL labeled with JF dye and SctL in colocalization with the injectisome needle before, during and after incubation at pH 4.

(a) Fluorescence micrographs of Halo-SctL, labeled with JF 646 prior to the first image, during consecutive incubation at different external pH as before in **Figure 12**. Right, overlay of fluorescence distribution at pH prior to and after pH 4 incubation (red and green, respectively). Experiments 3 times, respectively, with comparable results. Scale bars, 2 µm. Fluorescence micrographs of *Y. enterocolitica* expressing **(b)** SctF$_{S5C}$ (from plasmid) and **(c)** EGFP-SctL (replacing the WT gene by allelic exchange). Micrographs were subsequently taken at the indicated external pH values under secreting conditions. SctF$_{S5C}$ was labeled with maleimide-CF 568 and visualized in the red channel. Bottom row, composite image of SctF$_{S5C}$ and mCherry-SctL (green and magenta, respectively). **(d)** composite images; red channel: pH 7 (first image on the left); green: pH 4 (second image on the left); blue: pH 7 (third image on the left) *n* = 3. Scale bars, 2 µm.

Taken together, our data indicate that the cytosolic components reversibly dissociate from the injectisome at low external pH. Upon exposure to neutral pH, proteins from the same pool rebind at the cytosolic interface of the injectisome, forming the potential basis for a regulatory mechanism for the prevention of secretion at low pH.

3.1.3.3 Molecular mechanism of extracellular pH sensing

What is the molecular basis for the dissociation of the cytosolic injectisome components at low external pH? To find out whether the pH is sensed intracellularly, we first tested the impact of the changed external pH on the cytosolic pH, using a ratiometric pHluorin GFP variant (pHluorin$_{M153R}$ (Miesenböck *et al.*, 1998; Morimoto *et al.*, 2011)) as a pH sensor. Upon changing the external pH from 7 to 4, the cytosolic pH dropped to a mildly acidic value (pH 6.3-6.4). This cytosolic pH was retained for at least 30 minutes at external pH 4, but quickly recovered upon re-establishment of neutral external pH (**Figure 16**).

To test if this mild drop in cytosolic pH directly causes the dissociation of the cytosolic complex, we treated bacteria with the proton ionophore 2,4-dinitrophenol, which attunes the cytosolic pH to the external pH (Hong *et al.*, 1979; Dechant *et al.*, 2010; Petrovska *et al.*, 2014) (**Supplemental Figure 6**), and visualized the localization of EGFP-SctQ at different pH values. EGFP-SctQ remained localized in foci representing assembled cytosolic complexes at pH 6.3 and 6.0 (**Figure 16b**), indicating that the observed disassembly of the cytosolic complex is not caused by the mild acidification of the cytosol.

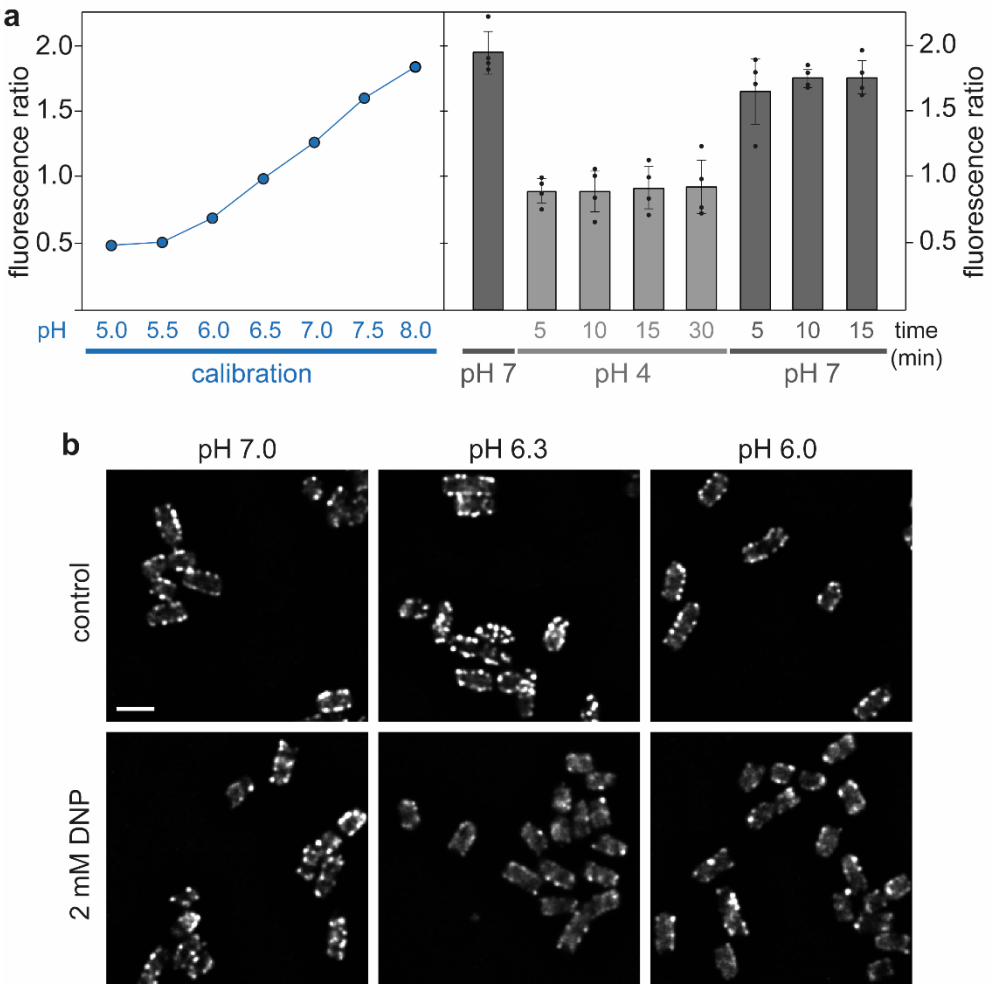

Figure 16 Low external pH leads to a small drop in cytosolic pH, which does not induce the dissociation of cytosolic injectisome components.
(**a**) Left, calibration of (Ex_{390nm}/Ex_{475nm}) fluorescence ratio of purified $pHluorin_{M153R}$ for the indicated pH values. Technical triplicate, error bars too small to display. Right, determination of cytosolic pH upon changing the external pH from 7 (first column) to 4 (columns 2-5) and back (columns 6-8). Fluorescence ratio (Ex_{390nm}/Ex_{475nm}) of bacteria expressing cytosolic $pHluorin_{M153R}$. n = 4, error bars denote standard deviation. (**b**) Fluorescence distribution of EGFP-SctQ in live *Y. enterocolitica* at indicated external pH in absence (top) or presence (bottom) of the ionophore 2,4-dinitrophenol (DNP). The experiment was performed 3 times with comparable results. At pH 4.0, no foci are present. Scale bar, 2 µm.

Based on above results, we searched for a periplasmic pH sensor. To this aim, we tested the effect of overexpression of the four candidate proteins that have periplasmic domains and influence the localization of the cytoplasmic components – SctC, SctD, SctJ and SctV (**Figure 2a**). We reasoned that if pH-induced partial dissociation of one of these components induces the dissociation of the cytosolic complex, overexpression of this component would shift the equilibrium towards the associated form of the protein itself and, in consequence, decrease dissociation of the cytosolic components at low pH. At pH 7 an induction of SctD with 0.001% L-arabinose, resulted in protein levels slightly below WT level, very low effector secretion and the appearance of first EGFP-SctQ foci already (**Figure 17abc**). At a surrounding pH of 4, 0.03% L-arabinose induction, and protein levels above WT level resulted in the appearance of

some EGFP-SctQ foci. Induction of SctD with 0.08% L-arabinose or higher and protein levels higher than WT, were even able to nearly restore a significant number of foci and the pattern of EGFP-SctQ observed at pH 7 (**Figure 17abc**). So indeed, overexpression of SctD strongly reduced the dissociation of the cytosolic component EGFP-SctQ at low external pH in an induction-dependent manner – while at wild-type SctD levels the number of EGFP-SctQ foci was strongly reduced at pH 4, bacteria with increased levels of SctD retained a higher number of EGFP-SctQ foci at pH 4.

Hereby the SctD level itself within the cell seemed to be the decisive factor which holds EGFP-SctQ in place. *In* trans complementation by *Pa*SctD showed a similar trend, although a higher amount of *Pa*SctD was needed to complement both effector secretion as well as foci appearance of EGFP-SctQ when expressed in *Y. enterocolitica* (**Figure 17def**, **Figure 18a**). In contrast, overexpression of SctC, SctJ or SctV, which did not influence effector secretion (**Figure 18d**), also did not interfere with pH-induced dissociation of the cytosolic components (**Figure 17ab**, **Figure 18bc**). Taken together, these results strongly support a central role for SctD in the reaction to low external pH.

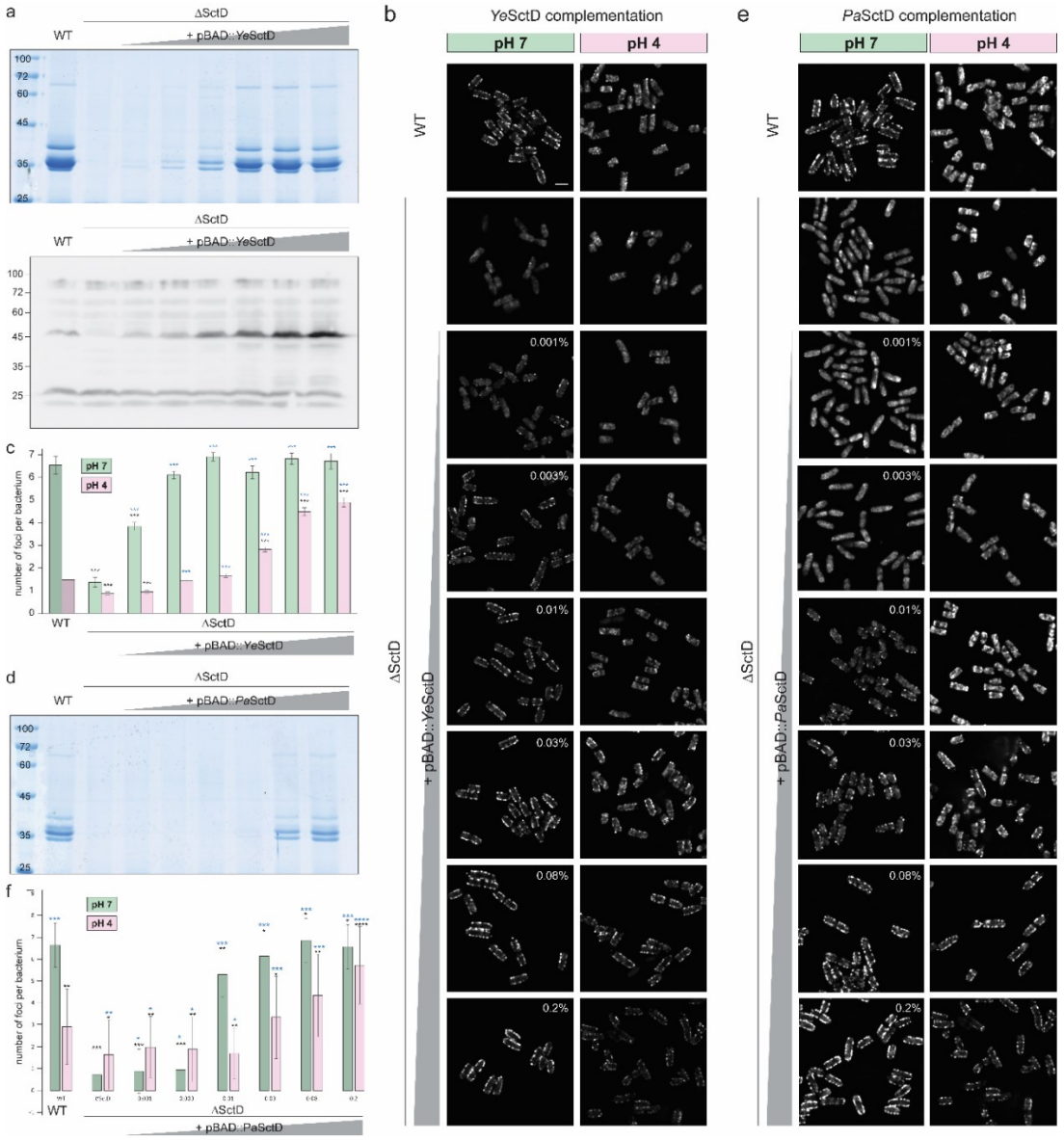

Figure 17 Influence of expression level of SctD on secretion and localization of the cytosolic components
(a) In vitro secretion assay (top) and immunoblot of total cellular protein anti-SctD (bottom) in EGFP-SctQ ΔSctD, complemented in trans by increasing induction levels of *Y. enterocolitica* SctD (from pBAD::YeSctD, ramp indicates increasing L-arabinose concentrations as shown in **(b)**). Left side, molecular weight marker (kDa); expected molecular weight of YeSctD, 46.9 kDa. **(b)** Localization of EGFP-SctQ in *Y. enterocolitica* EGFP-SctQ ΔSctD strains complemented in trans by YeSctD. Percentages indicate L-arabinose concentration. Wild-type (WT) EGFP-SctQ shown as control at top. Scale bar, 2 µm. **(c)** Quantification of EGFP-SctQ foci per bacterium for the strains and conditions shown in **(a)** and **(b)**. n = 34/148, 63/251, 111/193, 153/108, 106/355, 53/361, 80/133, 49/101 bacteria (pH 7/pH 4 from top to bottom) from at three fields of view (four fields of view for 0.001% and 0.2% induction at pH 7, as well as 0.2% induction at pH 4) in a representative experiment. Bars denote mean values, error bars denote standard deviation; blue ***, p<0.001 against WT; black ***, p<0.001 against ΔSctD in a homoscedastic two-tailed t-test, other comparisons not statistically significantly different (see Source data file for individual p values). **(d)** In vitro effector secretion assay in EGFP-SctQ ΔSctD, complemented in trans by increasing induction levels of P. aeruginosa SctD (from pBAD::PaSctD, ramp indicates increasing L-arabinose concentrations as shown in (e)). **(e)** Localization of EGFP-SctQ in *Y. enterocolitica* EGFP-SctQ ΔSctD strains complemented in trans by PaSctD. Percentages indicate L-arabinose concentration. Wild-type EGFP-SctQ shown as control at top. n = 2 independent experiments comparing all strains (n>10 independent experiments for individual strains in different combinations). Scale bar, 2 µm. **(f)** Quantification of EGFP-SctQ foci per bacterium for the strains and conditions shown in (b). The WT and ΔSctD deletions are in line one and two for comparison. Others display the indicated, rising, L-arabinose concentrations for induction of pBad::PaSctD. n>30 bacteria from at least three fields of view in a representative experiment. Error bars display standard deviation, black for pH7: ***, p<0.001; ** p=>0.01; *p>=0.1 against WT; blue ***, p<0.001 against ΔSctD. pH4: ****, p<0.0001; *** p=>0.001; **p>=0.1; *p=>0.1 against WT; blue ***, p<0.001 against ΔSctD.

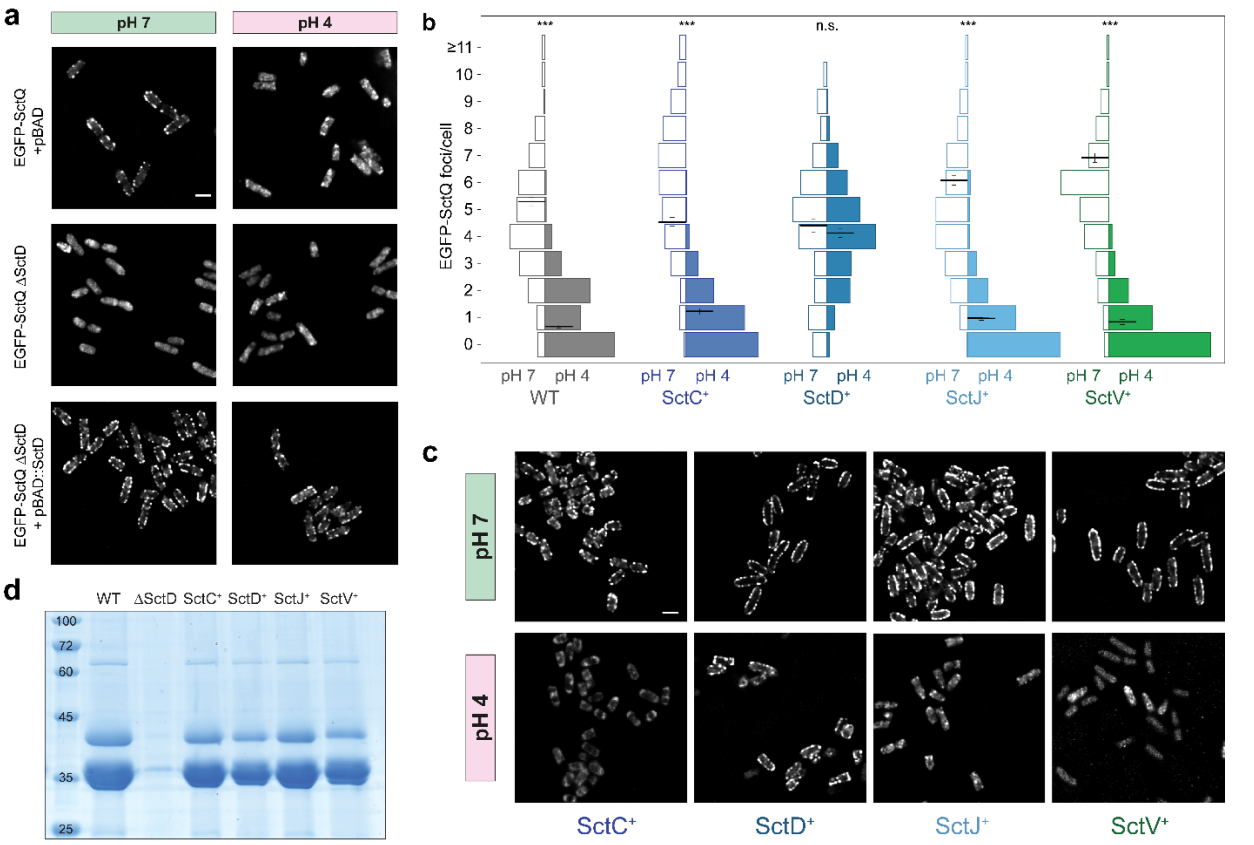

Figure 18 Overexpression of SctD, but not of SctC, SctJ or SctV suppresses the dissociation of the cytosolic components at low external pH.
(a) Cellular localization of EGFP-SctQ in live *Y. enterocolitica* at the indicated external pH. Top, wild-type; center, ΔSctD; bottom, additionally overexpressing SctD from plasmid. n = 3 independent experiments. **(b)** Quantification of EGFP-SctQ foci per bacterium in wild-type EGFP-SctQ strain and strains overexpressing the indicated proteins (induced by 0.2% L-arabinose), at external pH 7 (left, open) and pH 4 (right, filled). Black lines and error bars indicate mean number of foci and standard error of the mean. The number of foci at pH 7 and pH 4 does not differ significantly in strains overexpressing SctD (n.s., p=0.32 in a homoscedastic two-tailed t-test), but in all other strains (***, p~2*10-126, 3*10-43, 2*10-112, 3*10-106, 3*10-40 for WT and overexpression of SctC, SctJ and SctV, respectively). Bars display fraction of cells; n = 199/310, 203/149, 115/137, 205/279, 178/184 cells per strain and condition from 9/7, 8/10, 8/10, 9/9 8/9 fields of view (pH 7/pH 4 from left to right) from 3 independent experiments). **(c)** Cellular localization of EGFP-SctQ in the strains analyzed in (b), Scale bars, 2 µm. **(d)** *In vitro* secretion assay with overexpression of membrane components analyzed in (b) All tested strains show normal secretion. Secretion assay in wild-type EGFP-SctQ strains and strains overexpressing the indicated proteins (induced by 0.2% L-arabinose), as shown in abc. ΔSctD strain shown as a control. n = 3.

SctD is a bitopic inner membrane protein connecting the outer membrane (OM) ring to the cytosolic components (**Figure 2a**) (Ross and Plano, 2011; Hu *et al.*, 2017), that is an obvious candidate to act as a sensor for the external pH. Earlier studies showed that lack of SctD, or its inability to bind to SctC, leads to a similar cytosolic location of SctK/L/N/Q as observed at an external pH of 4 (**Figure 12a**) (Diepold *et al.*, 2010; Diepold *et al.*, 2017), and that the cytosolic domains of SctD connect to SctK via specific interactions (with four SctD binding to one SctK in *Salmonella* SPI-1) (Hu *et al.*, 2017; Tachiyama *et al.*, 2019; Muthuramalingam *et al.*, 2020). This suggests that structural rearrangements of SctD could lead to the dissociation of SctK and, subsequently, all other cytosolic components.

To investigate this hypothesis, we tested the behavior of SctD at low external pH by analyzing the localization of SctD. An EGFP-SctD fusion is stable and shows a slightly reduced effector secretion ((Diepold *et al.*, 2015), **Figure 19ab**).

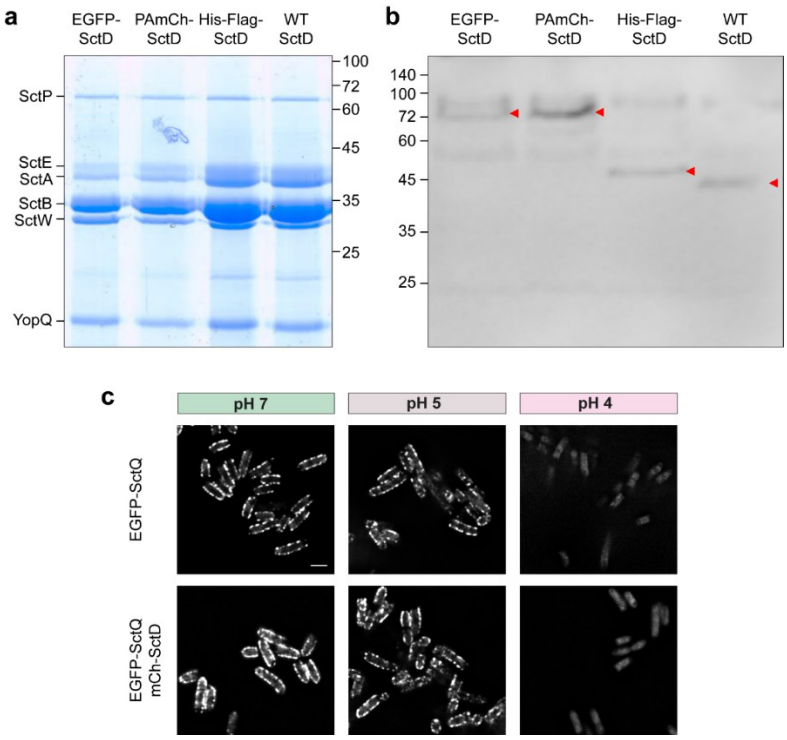

Figure 19 Functionality and stability of labeled SctD.
(**A**) *In vitro* secretion assay showing the export of native injectisome substrates (indicated on left side) in the indicated strains. Supernatant of $3*10^8$ bacteria per lane; left side, assignment of exported proteins. (**B**) Western blot using anti-SctD antibodies for total cellular protein of 2×10^8 bacteria per lane (strains as in (A)). Indicated proteins (expected molecular weight in kDa from left to right: 75.1, 74.9, 49.4, 46.7) indicated by red triangles. Left side, molecular weight in kDa. (**C**) Fluorescence micrographs of EGFP-SctQ in a strain otherwise wild-type (top) and in a strain also expressing mCherry-SctD (bottom) at the indicated external pH values. n = 3. Scale bar, 2 µm.

At pH 4, EGFP-SctD foci in the membrane became less clearly defined than at pH 7, with a concomitant increase in fluorescence throughout the membrane (**Figure 20a**). In contrast to the cytosolic components however, the SctD foci did not completely disappear, suggesting a reduced affinity at low external pH. Importantly, like the cytosolic components, SctD recovered its localization in foci at neutral external pH within minutes (**Figure 20a**). To study this unique phenotype in more detail, we performed single-molecule tracking of PAmCherry-SctD proteins in photoactivated localization microscopy (PALM). These experiments revealed that at an external pH of 7, more than 90% of the SctD molecules in the inner membrane were static (medium jump distance (mjd) of 0-60 nm, corresponding to the measurement uncertainty (Fukuoka *et al.*, 2007; Wieser and Schütz, 2008)); by contrast, at an external pH of 4, more than 40% of the SctD molecules became mobile within the membrane (**Figure 20b, Supplemental Figure**

7), indicating a dissociation from the core injectisome structure at low external pH. In line with these findings, the large injectisome export apparatus component SctV-EGFP retained its localization within foci at pH 4; however, these foci (likely representing the SctV nonamers) became mobile within the membrane (**Figure 20c**, **Supplemental Figure 8**). The same behavior has been detected for SctV-EGFP in the absence of SctD (Diepold *et al.*, 2011), supporting the notion that at an external pH of 4, SctV is released from the SctD structure. To test whether the N-terminal fluorophore tag influences the stability of the nner membrane ring, we localized EGFP-SctQ, which depends on the presence of the inner membrane ring for its localization (Diepold *et al.*, 2010), at different external pH. The fusion of mCherry to SctD did not influence the formation of EGFP-SctQ foci in any tested condition (**Figure 19c**), suggesting a labeling-independent effect of external pH on SctD assembly.

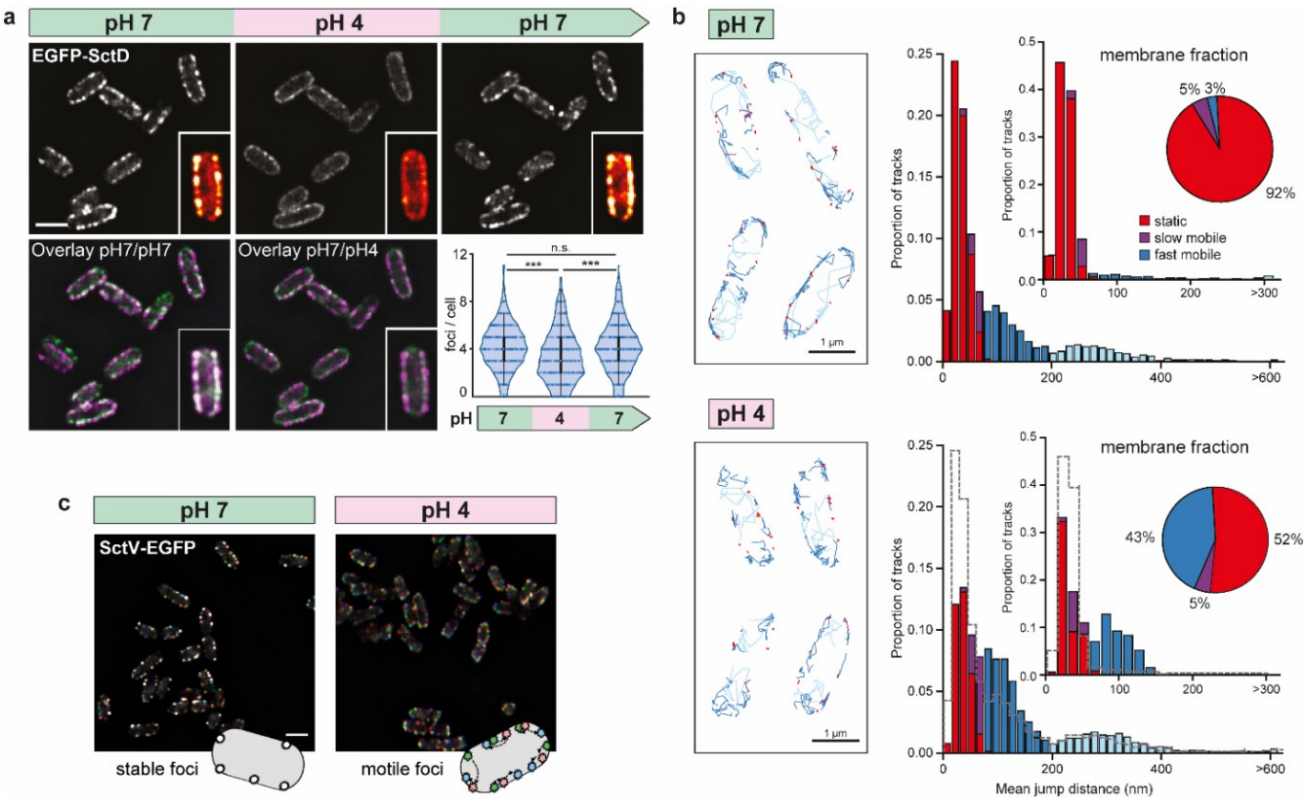

Figure 20 The bitopic inner membrane protein SctD reacts to low external pH

(a) Fluorescent micrographs of EGFP-SctD in live *Y. enterocolitica*, consecutively subjected to different external pH in a flow cell. Images were taken under secreting conditions, 10 minutes after bacteria were subjected to the indicated pH. Insets, enlarged single bacteria, visualized with the ImageJ red-hot color scale. Bottom, overlays of fluorescence at pH 7 before pH change (magenta) and pH 7 after pH change or pH 4 (green). Bottom right, quantification of foci per bacterium. n = 468 cells from three independent biological replicates. White circle denotes median, black bar denotes first and third quartile, black line denotes the lower/upper adjacent value. ***, p<0.001 in homoscedastic two-tailed t-tests; n.s., difference not statistically significant (p~2*10-11, 2*10-8, 0.42 for pH7/4, pH 4/7 and pH 7/7, respectively). **(b)** PAmCherry-SctD dynamics in living *Y. enterocolitica* example cells (left) and histograms (right) of the mean jump distances (MJD) of PAmCherry-SctD trajectories weighted by the number of jump distances used for calculating each MJD. Only trajectories with more than 6 one-frame jumps are shown and included into the analysis. Upper panel was measured at pH 7, lower panel at pH 4. Trajectories are assigned into two diffusive states: static (red) and mobile (violet and blue fractions) based on the experimental localization precision. Mobile trajectories are sorted into three MJD categories: lower than 60 nm (violet), lower than 195 nm (dark blue) and higher than 195 nm (light blue). Counts were normalized to the total number of trajectories. At pH 7 we acquired 29,859 trajectories (60% static, 2% mobile <60 nm MJD, 25% mobile from 60-195 nm MJD, 13% mobile >195 nm MJD; 19,473 membrane-bound trajectories). At pH 4 we acquired 33,036 trajectories (34% static, 4% mobile <60 nm MJD, 44% mobile from 60-195 nm MJD, 18% mobile >195 nm MJD; 21,600 membrane-bound trajectories). The bin size of 15 nm was calculated using the Freedman-Diaconis rule. Inset histograms and pie plot display statistics of only membrane-bound trajectories. The number of trajectories of membrane-bound static PAmCherry-SctD molecules decreases in pH 4 (92% to 52%), while the number of diffusing PAmCherry-SctD with MJDs <195 nm (dark blue bars) increases (3% to 43%). The fast fractions of PAmCherry-SctD molecules of MJDs >195 nm (light blue), only visible for the whole cell analysis, remain constant. Grey dashed lines in the pH 4 panels represent the outlines of the pH 7 analysis. Experiment performed by Alexander Balinovic and Stephan Wimmi. Figure design Alexander Balinovic **(c)** Spatial stability of SctV-EGFP foci over time at the indicated external pH. Three images of the same focal plane were taken at 10 s intervals. Green/blue/red channel correspond to t = 0/10/20 s. See Suppl. Fig. 17 for single time points and larger fields of view. The experiment was performed three times with similar results. Scale bars, 2 µm.

3.1.3.4 Physiological advantage of temporary suppression of type III secretion at low pH

We reasoned that bacteria could benefit from the dissociation of the cytosolic injectisome components at low external pH to suppress secretion in the low pH parts of the gastrointestinal system, including the stomach, where pH values of 4 and below prevail, and where injectisome activation might lead to energy depletion or even elicit immune reactions. If this would be the case, bacteria with a similar infection route, but not bacteria that do not pass the gastrointestinal tract during normal infection, and therefore are not under evolutionary pressure to suppress injectisome activity at low pH, would be expected to display the same pH dependence for the localization of cytosolic injectisome components. We therefore tested the localization of cytosolic components at low external pH in *S. flexneri* and *P. aeruginosa*. *S. flexneri* is a gastrointestinal pathogen that uses an evolutionarily distant injectisome, but like *Y. enterocolitica*, needs to pass the stomach to invade the colonic and rectal epithelium. In contrast, the injectisome of *Y. enterocolitica* and *P. aeruginosa* are closely related (Abby *et al.*, 2012), but the infection strategies of the two species differ. *P. aeruginosa* is not a gastrointestinal pathogen and mainly enters the host body through wounds. *S. flexneri* GFP-*Sf*SctN (Burgess *et al.*, 2020) formed fewer and less distinct foci than *Y. enterocolitica* EGFP-*Ye*SctQ and *P. aeruginosa* EGFP-*Pa*SctQ (**Error! Reference source not found.**), p ossibly due to the lower stoichiometry of SctN compared to SctQ. Most importantly, in agreement with the hypothesis that the dissociation of cytosolic components at low external pH is a conserved adaptation to the passage of low pH parts of the gastrointestinal system during a normal infection, the fraction of *S. flexneri* GFP-*Sf*SctN with foci significantly decreased at pH 4, whereas *P. aeruginosa* EGFP-*Pa*SctQ cells showed a small, non-significant decrease (**Figure 21ab**).

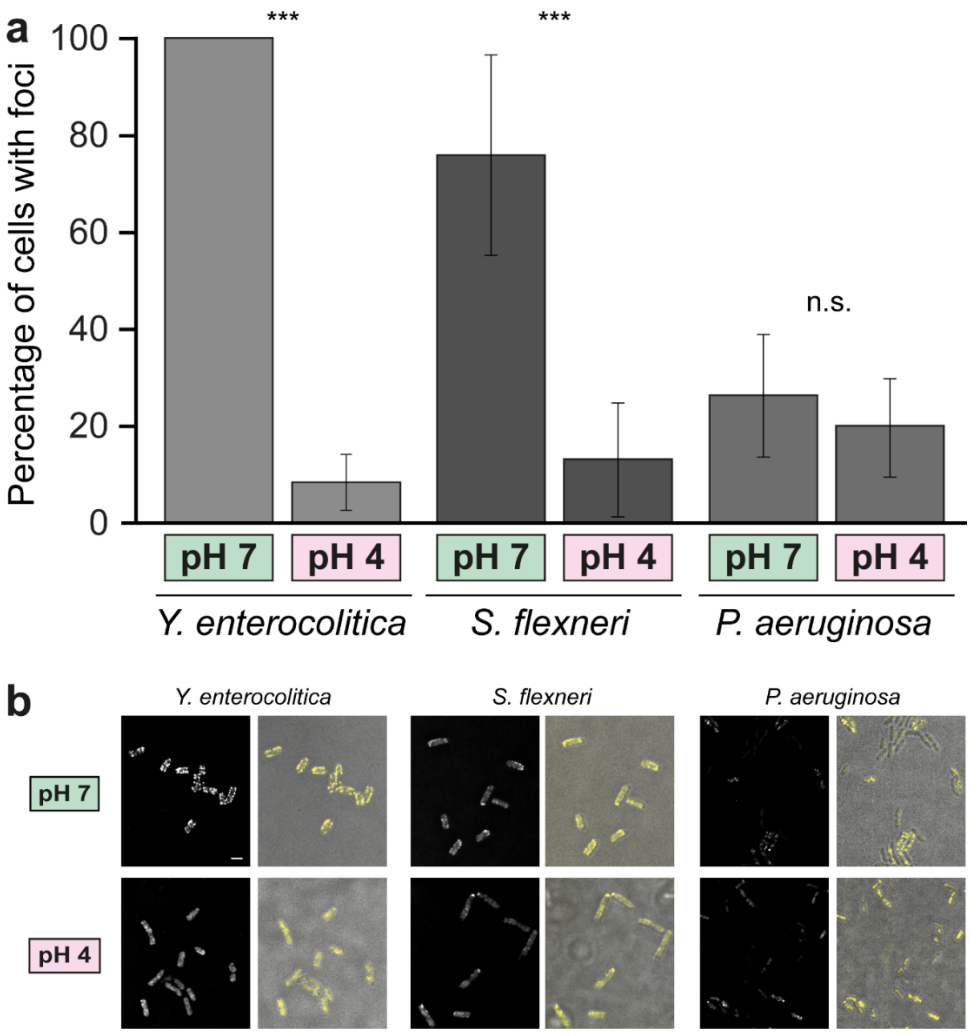

Figure 21 The effect of external pH on the assembly of cytosolic injectisome components is species-specific
(a) Percentage of bacteria with fluorescent foci at the indicated external pH for *Y. enterocolitica* EGFP-*Ye*SctQ, *S. flexneri* GFP-SfSctN, and *P. aeruginosa* EGFP-PaSctQ, respectively. n = 1134/1270, 530/691, 1078/926 bacteria from 20, 22, 25 fields of view (pH 7/pH 4 from left to right) from 3 independent experiments per condition. Bars denote mean values, error bars denote standard deviation between fields of view. n.s., difference not statistically significant; ***, p<0.001 in a two-tailed homoscedastic t-test (p~2*10-44, 6*10-16, 0.053, respectively) **(b)** Representative micrographs of *Y. enterocolitica* EGFP-SctQ, *S. flexneri* GFP-SctN, and *P. aeruginosa EGFP-SctQ* at the indicated external pH values. Right side, overlays of phase contrast (grey) and fluorescence (yellow). Brightness of the *S. flexneri* images was increased two-fold to account for the lower stoichiometry of SctN in comparison to SctQ. n = 3. Scale bar, 2 µm.

To determine a potential molecular mechanism for this effect, we looked for amino acids in the periplasmic portions of the injectisome that can be protonated at pH 4, but not at pH 7 (Asp, Glu, His) in *Y. enterocolitica* and *S. flexneri*, but not in *P. aeruginosa*. As no such amino acids could be identified (**Supplemental table 1**), we focused on protonatable amino acids that differ between *Y. enterocolitica* and *P. aeruginosa* (**Supplemental Figure 9**). Single amino acid substitutions, as well as the combination of all four substitutions still led to dissociation of the cytosolic component SctQ, as well as a loss of secretion at pH 4 (**Supplemental Figure 10**). Notably, a *Y. enterocolitica* ΔSctD strain could be

complemented for secretion by *in trans* expression of *Pa*SctD, which showed the same expression level-dependent suppression of the dissociation of the cytosolic components at low external pH as *Ye*SctD (**Figure 17d-f**). Taken together, these results and the clear effect of SctD overexpression (**Figure 18**) suggest that the effect of the pH is conveyed by gradual rearrangement of intermolecular interactions rather than by discrete salt bridges.

In the more pH-neutral intestine, *Y. enterocolitica* need to pass the M cells across the intestinal epithelium. Afterwards, the injectisome must be ready to manipulate immune cells. To test whether the reversible dissociation of the cytosolic injectisome components supports a fast activation of the injectisome once back at neutral pH, we monitored protein secretion over time after a temporary drop of external pH to 4. We found that secretion was suppressed at low pH, but restarted 20-40 minutes after reaching neutral pH (**Figure 22a**). Notably, this recovery is much faster than the onset of effector secretion after *de novo* assembly of the injectisome by a temperature change to 37°C (**Figure 22a**), supporting the notion that bacteria benefit from the temporary dissociation of the cytosolic subunits at low pH in two ways: This mechanism suppresses protein secretion at low external pH, while ensuring a timely reactivation upon reaching a pH-neutral environment (**Figure 22b**).

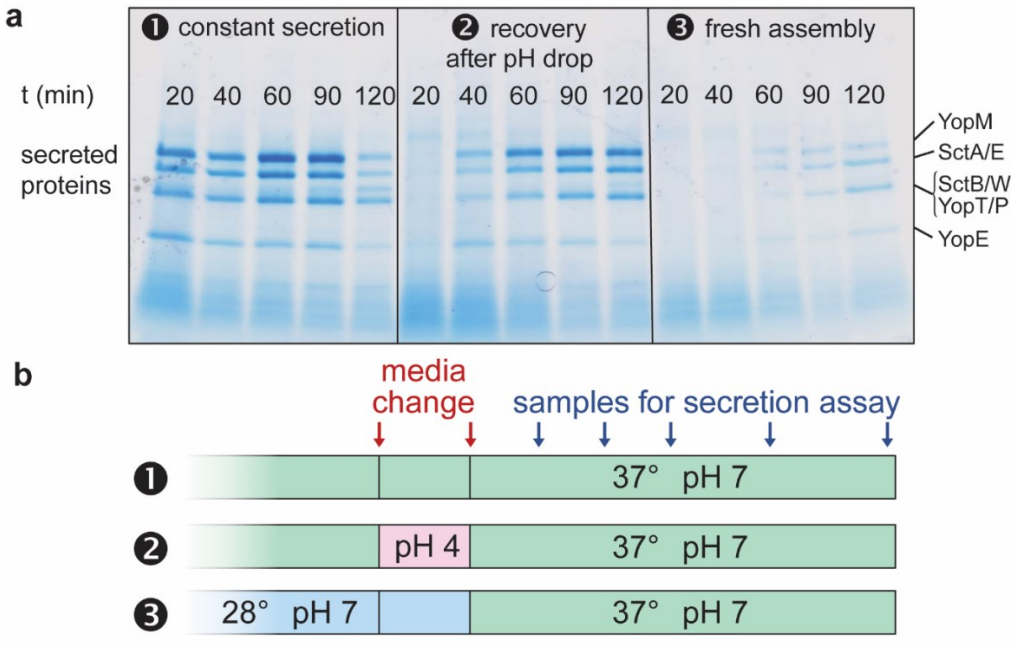

Figure 22 Temporary suppression of Injectisome activity at low external pH enables a fast re-activation of secretion
(a) *In vitro* secretion assay showing the proteins exported by the injectisome in an *Y. enterocolitica* effector strain at the given time points after the second media change, (1) under constantly secretion-inducing conditions, (2) after a temporary change of the external pH to 4, (3) after incubation at 28°C, where expression of injectisome components and effectors is downregulated and no injectisomes are assembled. Right side, exported effectors, based on (Iriarte and Cornelis, 1998; Diepold *et al.*, 2012). n = 3. **(b)** Schematic explaining the experiment described above.

3.1.3.5 Summary and Model

In this study, we identified a novel pH sensing mechanism that prevents the activity of the injectisome at low external pH conditions and allows a fast resumption of effector secretion once the pH is neutral again. Upon entry into the host organisms assembly of the injectisome starts and off target translocation is already possible (**Figure 11**, **Figure 23**) (Clerc *et al.*, 1986; Håkansson *et al.*, 1996; Armentrout and Rietsch, 2016; Nauth *et al.*, 2018; Bohn *et al.*, 2019). In low pH arrays the bitopic transmembrane protein SctD at least partially disassociates (**Figure 20**) which leads a to exclusively cytosolic localization of the cytosolic components (**Figure 13**, **Figure 15**, **Figure 23**). Thereby effector secretion is prevented (**Figure 9**, **Figure 22**), even in case of contacted of the needle contact to a host cell membrane. Once the pH is neutral again all injectisome components reassemble in their original location and effector secretion can be resumed (**Figure 22**, **Figure 23**).

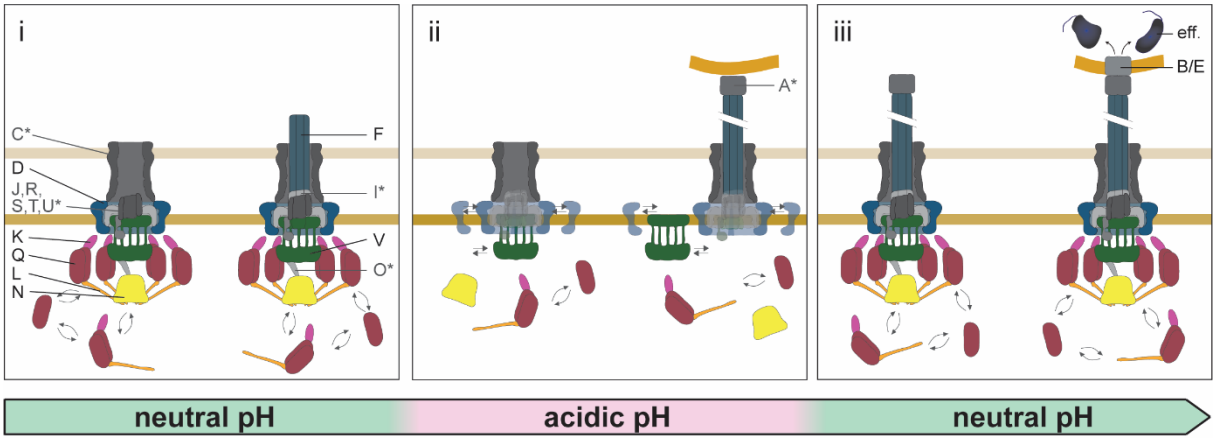

Figure 23 Model of the pH-dependent suppression of injectisome activity.
From left to right: (i) Assembly of the injectisome upon entry into host organisms; cytosolic components bound and exchanging with cytosolic pool. (ii) Prevention of effector translocation upon host cell attachment in low pH environment, because cytosolic components are exclusively cytosolic. (iii) Re-association of cytosolic components to the injectisome and effector translocation upon host cell contact in neutral body parts. Letters represent protein identifiers (common Sct nomenclature); eff., effectors. Proteins whose localization was not specifically tested are indicated by asterisks and grey shading. Straight double arrows indicate diffusion in membrane; curved double arrows indicate exchange of cytosolic subunits or subcomplexes between the cytosolic and the injectisome-bound state.

3.1.4 Additional results

3.1.4.1 *In trans* expression of *P. aeruginosa* needle subunits cannot compliment a *Y. enterocolitica* needle deletion

In the process of identifying the pH sensor, we screened multiple possible candidates within the injectisome. First, we turned to the needle (SctF). The needle is located outside of the cell (**Figure 2a**), exposed directly to all environmental changes and has been associated with other sensing and regulatory process like sensing calcium levels or host cell contract (Torruellas *et al.*, 2005; Deane *et al.*, 2006; Shaulov *et al.*, 2017). Since we observed a reduced sensitivity of *P*aSctQ towards low pH (**Figure 21**), we wondered if replacing the needle may transfer that phenotype. To investigate this hypothesis, we expressed a WT *Pa*SctF and a stainable cysteine mutant *Pa*SctF$_{N6C}$ in trans from a pBAD plasmid. In contrast to SctD (**Figure 17**), neither of these constructs complemented the deletion of *Ye*SctF.

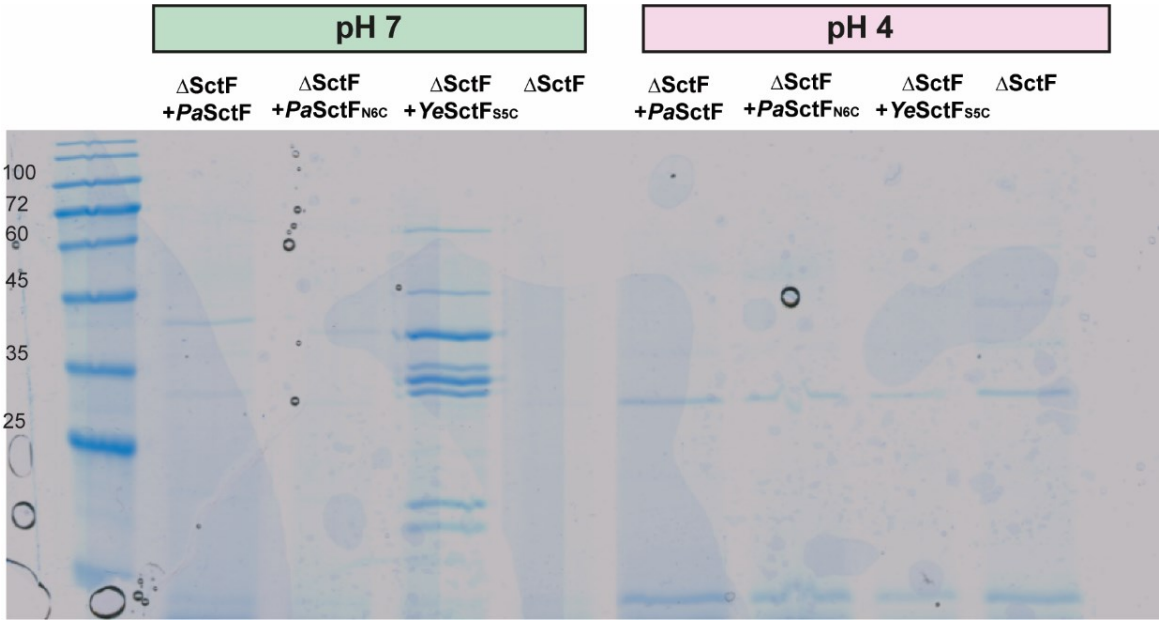

Figure 24 *In vitro* secretion assay with in trans complementation of the needle subunit, SctF.
Shown here is the export of native injectisome substrates of ΔSctF strains, complimented with the indicated SctF version (*Pa*SctF, *Pa*SctF$_{N6C}$,*Ye*SctF$_{S5C}$, the mutations *Pa*SctF$_{N6C}$,*Ye*SctF$_{S5C}$ were introduced into the needle genes, to allow staining with maleimide dye) exposed to different external pHs of 7 (left) or 4 (right). Samples are bacterial supernatant of 3x10^8 bacteria analyzed on a SDS-PAGE gel. Molecular weights in kDa of the protein standards lines are indicated on the left. n = 3 independent experiments.

3.1.4.2 Deferred complementation of *Y. enterocolitica* basal body deletions is possible but does not mimic the pH phenotype

Since we could show (**Figure 22**) that effector secretion starts after the pH 4 treatment within 20-40 minutes, which is faster than new assembly of the injectisome, we hypothesized that this delay in secretion may be the time that it takes to synthesize and incorporate new proteins into the already existing machinery. Therefore we complimented deletions of the needle (SctF), the secretin (SctC), the outer part of the inner membrane ring (SctD), the inner part of the inner membrane ring (SctJ), and the major export apparatus protein (SctV) (**Figure 2**) from a pBAD plasmid 2 hours after the temperature shift and tracked the time that it takes to start secretion (**Figure 25**). While SctF, SctC, SctD and SctJ complemented faster than new assembly (60-90 minutes) (**Figure 22**), it took nearly as long to complement the deletion of SctV. The temporal resolution of these experiments is very low and does not account for transcription, translation, and folding time, however, none of them matched the pattern that we observed after the pH treatment.

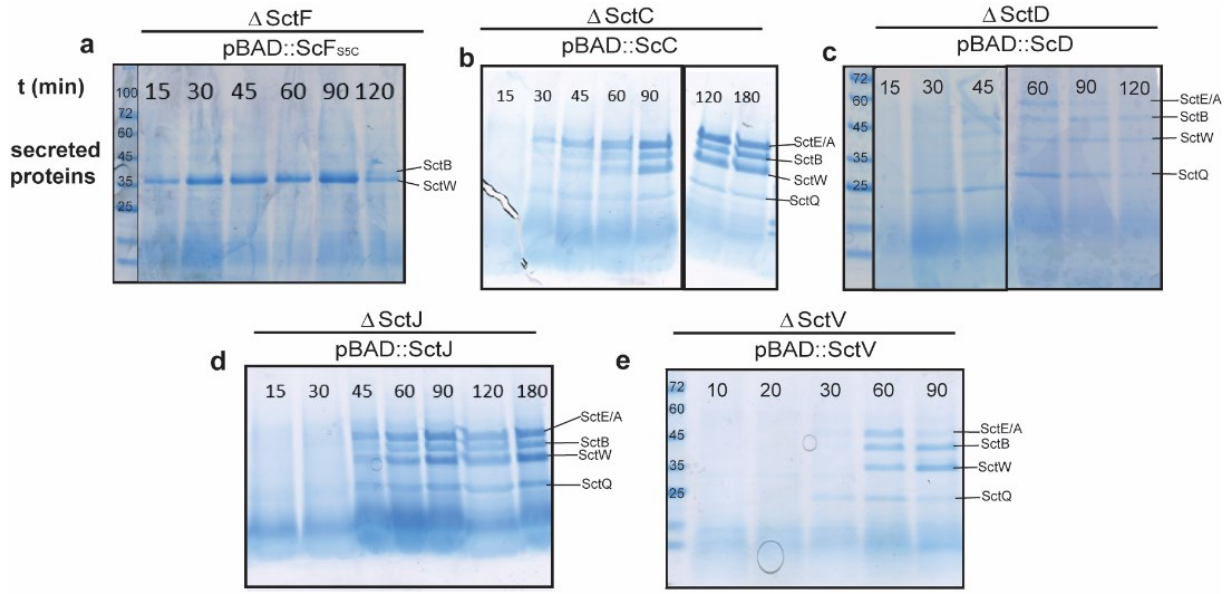

Figure 25 Influence of deferred complementation on effector secretion.
Complementation of chromosomal deletions of **(a)** SctF, **(b)** SctC, **(c)** SctD, **(d)** SctJ, **(e)** SctV. Complementation was done by *in trans* expression of respective proteins (**(a)** pBAD::SctFs5c, **(b)** pBAD::SctC, **(c)** pBAD::SctD, **(d)** pBAD::SctJ, **(e)** pBAD::SctV). Protein expression was induced 2h after temperature upshift to 37°C with 0.2% L-arabinose. Numbers on top indicate time intervals in which samples were taken in minutes. Indicated on the left, were applicable, molecular weight standard, on the right name of the effectors, based on (Iriarte and Cornelis, 1998; Diepold et al., 2012) Samples per lain normalized to in supernatant of $3*10^8$ bacteria. Molecular weights in kDa of the protein standards lines are indicated where applicable. n = 1.

3.1.4.3 Intracellular protein levels of SctD determine foci stability of EGFP-SctQ in *Y. enterocolitica*

Since this was the case, we focused on the expression levels of *Ye*SctD. As shown earlier (Figure 17), both *Ye*SctD and *Pa*SctD complement the deletion of SctD, in the case of *Pa*SctD complementation was only possible with higher induction levels. To evaluate the effect of *Ye*SctD further, we compared the complementation of secretion and localization of different *Ye*SctD levels after 3 and 5 hours (**Figure 26**). After 3 h of induction, only higher amounts of L-arabinose correspond with high protein levels in the cells (**Figure 26b)**. Only these high amounts were sufficient to compliment the deletion of SctD and result in foci localization of EGFP-SctQ at the membrane at pH 4 (**Figure 26ad**). After 5h of induction, the low levels of L-arabinose do not correspond with low protein levels in the cell anymore and all induction levels show similar effects on secretion and localization of EGFP-YscQ as the higher induction levels used before (**Figure 26**). This shows, that the overall protein level within the cells determines if EGFP-SctQ foci are stable at pH4. The needed protein level can be either reached by high induction or by a longer expression time of SctD from plasmid.

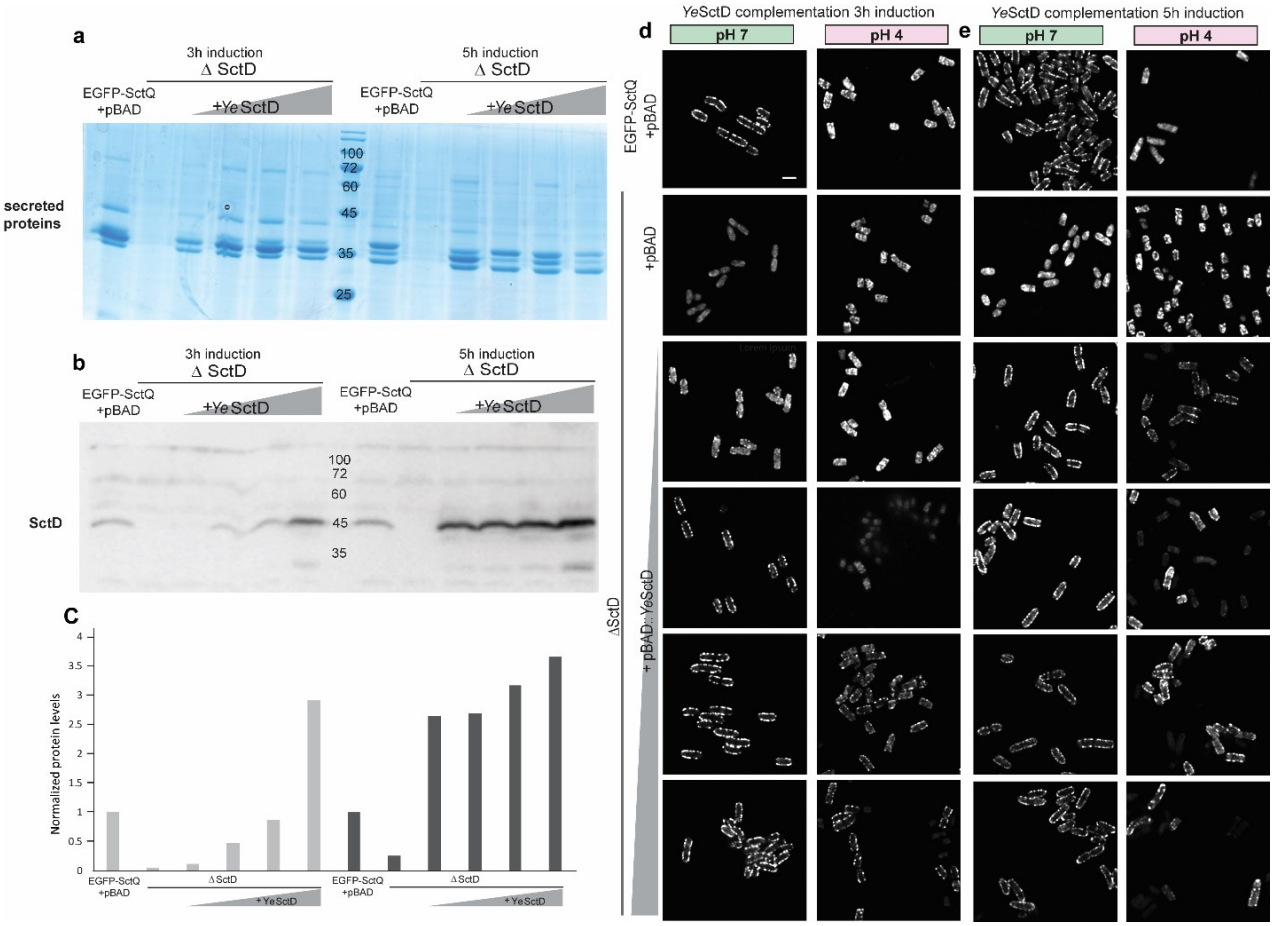

Figure 26 Influence of expression level of SctD on secretion and localization of the cytosolic components over time.
(a) *In vitro* secretion assay with EGFP-SctQ ΔSctD completed in trans with pBAD::SctD. Loaded was supernatant from supernatant of 3x10^8 bacteria. **(b)** Immunoblot of total cellular protein anti-SctD. EGFP-SctQ ΔSctD, complemented by increasing induction levels of *Y. enterocolitica* SctD (from pBAD::YeSctD, ramp indicates increasing L-arabinose concentrations: 0.01%, 0.03% 0.08% 0.2%). Molecular weight standard in kDa located in the middle of the Gel. Expected molecular weight of SctD, 46.9 kDa. **(c)** Quantification of western blot bands in **(b)** corresponding to the band of SctD running at the respective size. Band intensity was measured with ImageJ-Fiji and normalized against WT EGFP-SctQ levels. **(d)** Localization of EGFP-SctQ in *Y. enterocolitica* EGFP-SctQ ΔSctD strains complemented with different increased expression levels of SctD. All panels include a control WT EGFP-SctQ + pBAD and ΔSctD + pBad. The panel shows the respective result after three hours, the right one after 5 hours. This figure shows results from one representative experiment while similar result have been observed in different combinations and 2 replications (n = 2). Scale bar, 2 µm.

3.1.4.4 Fixation of *Y. enterocolitica* inner membrane ring with the crosslinker BS3

After we identified SctD as the most likely candidate for the pH sensor (**3.1.3.3**), we hypothesized that we should be able to prevent disassociation of SctD if we stabilize the SctD ring at pH 4. We tried to crosslink the inner membrane ring with the crosslinker bis(sulfosuccinimidyl)suberate (BS3). BS3 is a membrane impermeable crosslinker that might allow to fix the proteins at the outside of the cell while leaving the inner cell interacted. Since no literature values for crosslinking in *Y. enterocolitica* were available, we screened for the right fixation conditions. A low concentration (<10 mM) of BS3 had no visible effects after

15 and 30 minutes on EGFP-SctD foci. They also did not result in an increased crosslinking of cells in strains lacking the major adhesin, YadA (non- aggregation mutant) (**Figure 27a**). To test fixation of the SctD transmembrane ring, a strain expressing EGFP-SctD was crosslinked with 10 mM and 50 mM BS3 for 30 minutes and afterwards exposed to pH4 and pH7 buffered media (**Figure 27b**). While 10 mM BS3 resulted in partially stable clusters of EGFP-SctD, no difference could be observed in the cluster pattern of cells treated with 50 mM BS3 compared to pH 7. This indicates that under these conditions the transmembrane rings are completely crosslinked. To investigate which effect the fixation had on the cytosolic components, 50 mM of BS3 was used to fix a strain expressing EGFP-YscQ and exposed to pH7 and pH4. Both conditions resulted in abnormal foci pattern of EFGP-SctQ. The amount of overall foci was reduced, they varied a lot in size and were not confined to a next to equal distribution around the membrane (**Figure 27c**). To test if this was a side effect of the cross linker, we turned to a purely cytosolic version of EGFP-YscQ and cytosolic GFP (expressed from a pBAD plasmid). In both, the addition of BS3 resulted in fluorescence spots along the membrane, indicating that the chosen concentration of BS3 is responsible for the abnormal pattern observed before. Based on these results, the attempts to fix SctD with BS3 were not continued.

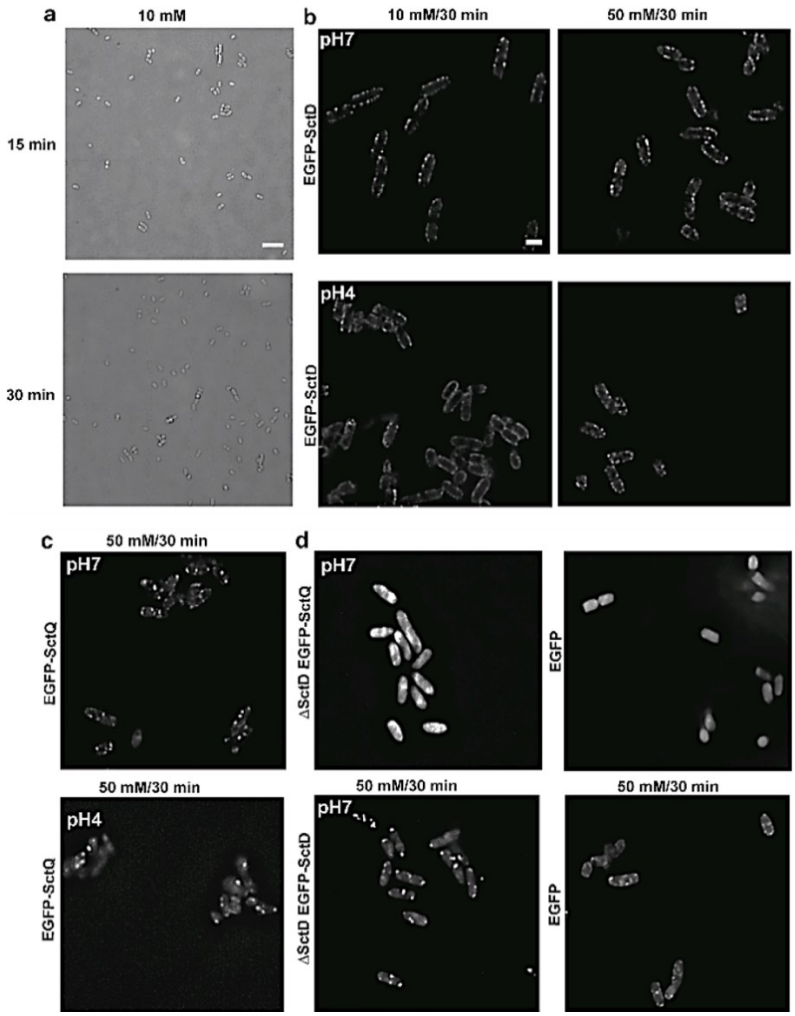

Figure 27 Effects of the crosslinker BS3 in different concentrations.
(a) *Y. enterocolitica* ΔYadA cells treated for 15 or 30 minutes with 10 mM BS3, scale bare 5 µm. **(b)** Localization of EGFP-SctD at pH 7 and pH 4 in cells treated with 10 or 50 mM BS3 for 30 minutes. Scale bar 2 µm **(c)** Localization of EGFP-SctQ at pH 7 and pH 4 treated with 50 mM BS3. **(d)** EGFP-SctQ ΔSctD strain and EGFP expressed from the pBAD plasmid induced with 0.2% L-arabinose, treated with 50 mM BS3. Representative results from >3 independent experiments with different combinations of strain used but the same trend.

3.1.4.5 CCCP treatment results in a stop of secretion and purely cytosolic localization of EGFP-SctQ

Next, we wanted to test if the complete uncoupling of the membrane potential by CCCP (Carbonylcyanid-m-chlorphenylhydrazon) has a similar effect to low external pH on the injectisome. Previously it has been shown that uncoupling of the PMF by CCCP results in an inhibition of effector export in *Y. enterocolitica*, as well as for subunit export of the flagella (Wilharm *et al.*, 2004; Paul *et al.*, 2008; Wilharm and Heider, 2014).

Since the *Y. enterocolitica* experiments have been conducted with another strain (*Y. enterocolitica* WA-314 (Wilharm et al., 2004)), we first evaluated the effect of CCCP on our model organism (**Figure 28a**).

While 15 µM of CCCP resulted in a slight decrease in effector secretion, 40 µM were sufficient to abolish secretion completely. Next, we tested to effect of CCCP on the subcellular localization of the cytosolic components. In the low ranges no effects were visible. At 40 µM CCCP the foci along the membrane were completely gone and the cells displayed only cytosolic fluorescence, similar to the phenotype of low external pH. With higher concentrations of CCCP, cells started to show two to three large foci per cell with a tendency to be polar (**Figure 28b**). Since the abolishment of secretion resulted in purely cytosolic localization of EGPF-SctQ which mirrored the observed phenotype of the pH treatment (**Figure 13**), we tested if this also holds true for the recovery of secretion (**Figure 28c)**. Strikingly, secretion recovered in less than 15 minutes after β-mercaptoethanol treatment, which reverses the effects of CCCP, (**ii**) and showed more similarities to the WT control secretion (**Figure 28c)** (**i**) than to the pH treated strain (**iii**). This indicated that the phenotype observed by exposing *Y. enterocolitica* to CCCP, is based on a different mechanism compared to the phenotype observed by pH exposure (**Figure 13**, **Figure 28**).

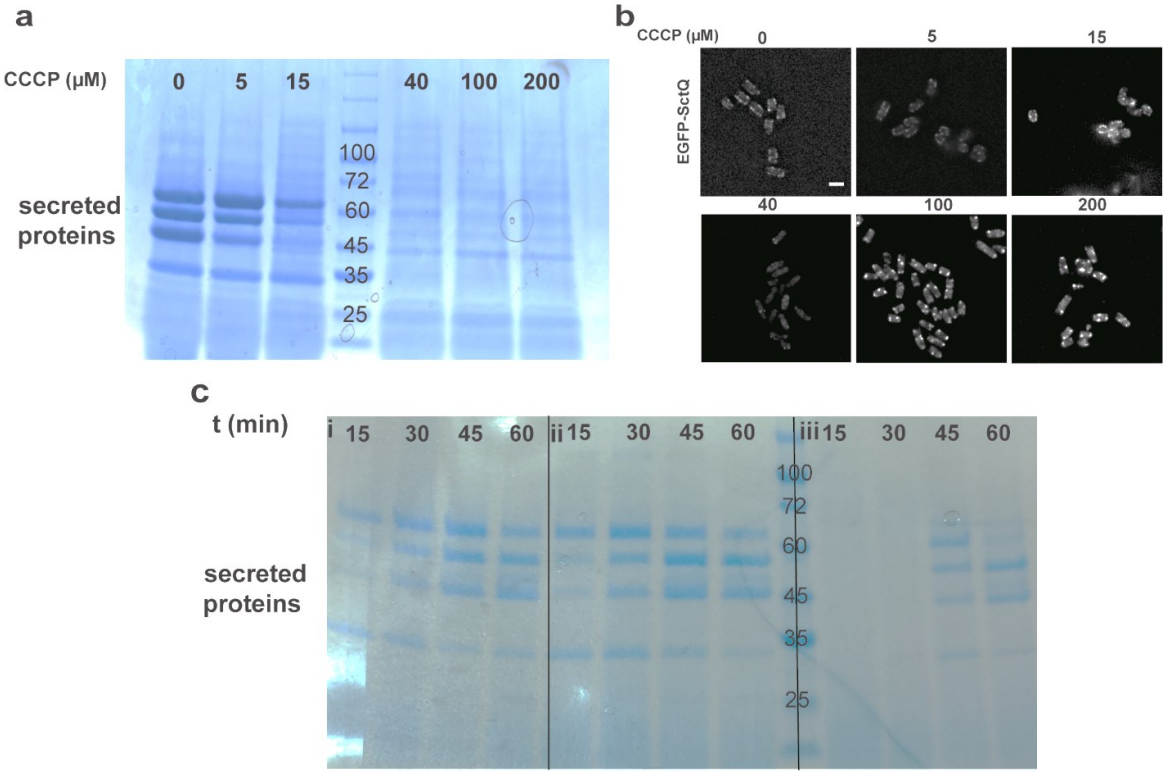

Figure 28 Effect of CCCP on secretion and localization of cytosolic components.
(a)(c) Secretion assay with WT effector strain, normalized to $3x10^8$ bacteria per lane. **(a)** Indicated on the top of the gel are different concentrations of CCCP ranging from 0 µM to 200 µM (n = 1). **(b)** Micrographs of *Y. enterocolitica* expressing EGFP-SctQ from its native locus. Numbers on top indicate different concentrations of CCCP from 0 µM to 200 µM. **(c) i:** WT secretion assay as control, **ii:** secretion assay with bacteria treated first with CCCP for 10 minutes and then, at time point 0 exposed to β-mercaptoethanol. **iii** late temperature shift, were bacteria have only been shifted to 37°C to start assembly of the injectisome at time point 0. Numbers on top indicate minutes past since time point 0. Molecular weight standard with indicated protein sizes in kDa can be found in the middle of the gel or towards the right respectively.

The overall performed experiments showed that total proteins levels in the cell are more important than inductions of expression in long term experiments and that a physiological saturation is reached after 5h of expression. Additionally, our results show that new expression and incorporation of proteins have different secretion recoveries than the pH effect (**Figure 22**, **Figure 25**). This brings an additional piece of evidence that the secretion recovery after pH treatment, (**Figure 22**) is more due to redistributions of proteins rather than new production.

3.1.5 Dynamic exchange of protein subunits within the basal body

"Life is change" (Tusk *et al.*, 2018), but for some life includes a bit more change than for others. The stator components of the flagellum exchange (Block and Berg, 1984) and DNA polymerase complexes are in a state of constant turnover (Aberg and Duderstadt, 2016). The cytosolic components at the basal body of the injectisome have been shown to be mobile and exchange with a rate about two minutes, the injectisome basal body do not (Diepold *et al.*, 2015; Diepold *et al.*, 2017). Its two membrane rings, the needle, and the inner membrane gate are presumed to be stable. They are stable enough to be visible in subtomograph averages in great detail (Kudryashev *et al.*, 2013; Butan *et al.*, 2019), they co-purify as a complex (Enninga and Rosenshine, 2009; Kowal *et al.*, 2013a; Kudryashev *et al.*, 2013; Muthuramalingam *et al.*, 2020). Nevertheless, our data clearly shows that the inner membrane ring SctD reversibly disassociates from its position around the needle and export apparatus into the membrane at low pH (**Figure 20**). This raises the question, if there is maybe exchange of basal body subunits at neutral pH as well. To investigate this, we established a "fluorescence intensity dilution exchange assay". In this approach, we used a strain with a chromosomally encoded EGFP-SctD and a pBAD plasmid with an L-arabinose inducible SctD version. First, we assembled the injectisomes through the temperature upshift from 28°C to 37°C for two hours. At this point, the injectisomes are completely assembled and effector secretion has started (Diepold *et al.*, 2010). One of the used cultures contained glucose to inhibit expression of SctD from the start. After two hours of assembly at 37°C, the expression of unlabeled SctD was induced by addition of 0.2% L-arabinose in the second culture. In this setup, visualization took place after 1 hour of expression with 0.2% L-arabinose. The glucose culture was used as a control, here the WT protein levels in the cell and subcellular localizations, in this case 24mers of SctD located at the injectisome with a little membrane background was visible **(Figure 29a**). For the "fluorescence intensity dilution exchange assay", two scenarios are possible now: either there is no exchange and the localization of the protein of interest looks like the control; or like in case of SctD, the original membrane signal located in precise foci fluorescence is diluted. Which would result in a distribution of the fluorescence, in this case

of SctD in the inner membrane. This could be seen in our experiments (**Figure 29b).** To observe protein expression, we monitored SctD and EGFP-SctD expression over time via western plot (**Figure 29cd).** While the levels of EGFP-SctD stay constant over time, the levels of unlabeled SctD are nearly twice as high as WT level after only 10 minutes of expression (**Figure 29cd)**.

With the fluorescence intensity dilution exchange assay we provide a novel way to look at protein dynamics and exchange. The application of this approach show for the first time convincing evidence for the inner membrane ring SctD to have subunit exchanging dynamics as well.

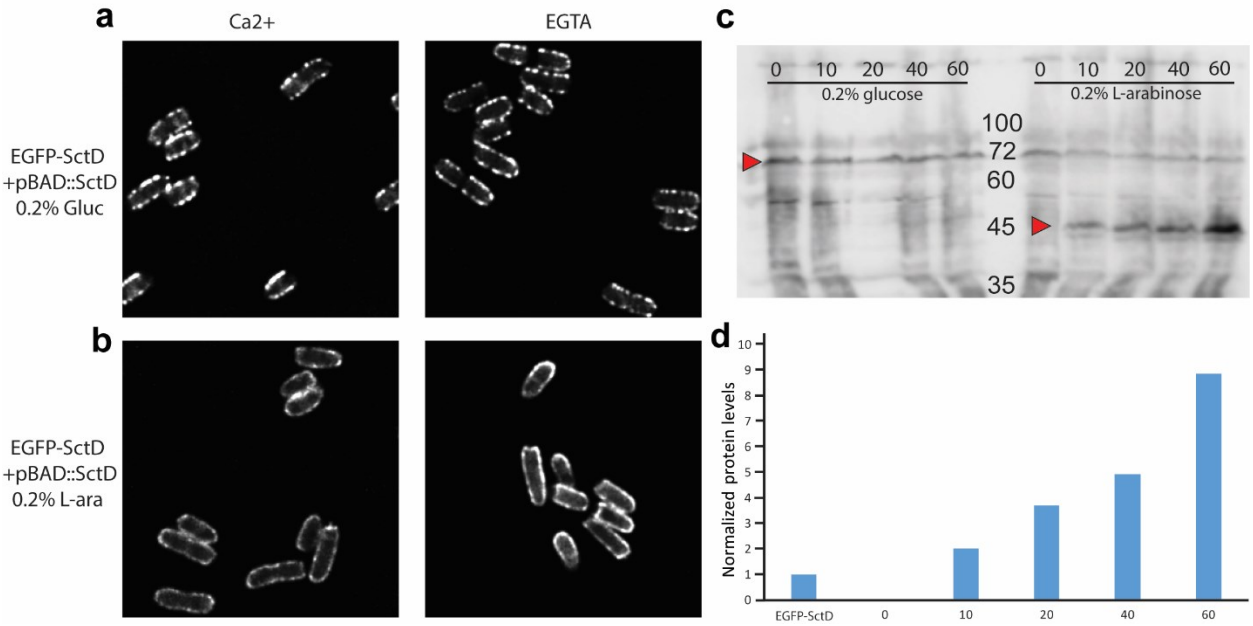

Figure 29 Fluorescence intensity dilution exchange assay one the inner membrane ring SctD.
(a) Micrographs of *Y. enterocolitica* harboring a pBAD::SctD plasmid and a EGFP-SctD version on the chromosome. Expression is inhibited with 0.2% glucose. **(b)** Same strain as in (a), this time expression of the SctD is initiated by addition of 0.2% L-arabinose. Micrographs were acquired 1 h after expression was imitated. Experiment has been performed in two independent replications (n = 2). **(c)** immunoblot of total cell protein with anti-SctD antibody, numbers on top indicate time point at which the sample were taken in minutes. Molecular weight marker (kDa) in the middle for protein size comparison. The expected molecular weight of SctD is 46.9 kDa while the expected molecular weight of EGFP-SctD is 76.8 kDa. The ***** indicate respective protein sizes. **(d)** Quantification of SctD expressed from the pBAD plasmid shown on the right side of the immunoblot in (c). Measurements normalized against the WT levels (EGFP-SctD). Shown here are results of one representative experiment. Different experiments with expression of pBAD::YscD have been performed with a similar trend visible, overall n = 2.

4 Discussion I

4.1 Discussion - Dynamic relocalization of the cytosolic type III secretion system components prevents premature protein secretion at low external pH

On their way through the gastrointestinal system, bacteria encounter a multitude of different pH environments. Importantly, the highly acidic stomach acts as natural barrier for food-borne infections. Gastrointestinal pathogens express factors that facilitate survival in these conditions, such as urease, of which high amounts are exported in *Y. enterocolitica* (Young *et al.*, 1996; Stingl and De Reuse, 2005; Hu *et al.*, 2009; Heroven and Dersch, 2014; Chen *et al.*, 2016). It was not known, however, if and how the activity of the injectisome, an essential virulence factor for many gastrointestinal pathogens, is regulated under these conditions. Although the injectisome target cells are downstream of the stomach for most gastrointestinal pathogens, cells in the low pH parts of the gastrointestinal system can be accessible and bacteria can attach to host cells at low pH (**Figure 9ce**). Our data support the notion that bacteria prevent premature injection into host cells at this stage by directly using the external pH as a cue for the temporary suppression of the injectisome. While parts of the injectisome, including the needle, remain stable, the cytosolic components dissociate in an acidic environment (pH 4 and below). This effect persists at low external pH; however, once the bacteria encounter neutral external pH, both adherence via the adhesin YadA to collagen is significantly increased (**Figure 9c**), and the binding of the cytosolic components is restored (**Figure 12**). Bacteria conceivably benefit from this mechanism, which prevents premature effector translocation into any eukaryotic cells in contact in the acidic regions of the gastrointestinal tract, an event that would be energetically expensive and might elicit immune responses. Once the pH-neutral intestine is reached, secretion is restarted within 20-40 minutes, which is significantly faster than *de novo* synthesis of injectisomes at this time (**Figure 22**). This is in line with earlier observations where assembly of injectisomes by fluorescence microscopy and the resulting secretion was only observed about 60 minutes after induction of injectisome assembly by temperature shift to 37°C (Diepold *et al.*, 2010).

We found that similarly to *E. coli* (Slonczewski *et al.*, 1981; Krulwich *et al.*, 2011), *Y. enterocolitica* can partially compensate for acidic external environment, and that at an external pH of 4.0, the cytosolic pH remained at 6.3-6.4 (**Figure 16**). When we used a proton ionophore to create this cytosolic pH at a similar external pH, the cytosolic injectisome components remained bound to the injectisome (**Figure 16**), suggesting that the external pH is not sensed in the bacterial cytosol. A central open question is how

exactly the pH change is sensed in the extracytosolic space. We found that overexpression of SctD, which shifts the equilibrium towards association to the injectisome, strongly represses the pH-dependent dissociation of the cytosolic components (**Figure 17**, **Figure 18**). This is not the case for any of the other tested proteins with extracytosolic domains, SctC, SctJ or SctV, pointing out SctD as the prime candidate for conveying the effect of low external pH. The bitopic inner membrane component SctD could react to a drop in external pH with its periplasmic domain and then transmit this signal to the cytosol. Indeed, our data show that the localization of SctD within the membrane clearly differs between external pH of 7 and 4 (**Figure 20**). Interestingly, SctD is one of the least conserved genes in the injectisome, especially in comparison to its direct structural neighbors, the highly conserved SctC secretin ring in the OM, as well as SctJ and the export apparatus proteins in the inner membrane (Diepold *et al.*, 2014). While this low sequence similarity impedes a multi-sequence alignment to identify conserved differences between the Injectisome of gastrointestinal and non-gastrointestinal pathogens (**Supplemental table 1**), except for the closely related *Y. enterocolitica* and *P. aeruginosa* (**Supplemental Figure 9**), it supports the notion that SctD is involved in species-specific adaptation of the injectisome, such as pH sensing. This hypothesis is further substantiated by the finding that in *P. aeruginosa*, which does not pass the gastrointestinal system during a normal infection, the effect of low pH is significantly restricted, with the majority of EGFP-SctQ foci remaining present at low external pH (**Figure 21**). Mutation of candidate amino acids in *Ye*SctD or even complementation of *Y. enterocolitica* ΔSctD with *Pa*SctD did not phenocopy the lack of pH sensitivity, suggesting that a broader reversible conformational change at low pH is responsible for the observed effect. It is currently unclear at which interface(s) this effect takes place; however, the lack of phenotype of overexpression of the other injectisome components with periplasmic domains (SctC, SctJ and SctV) makes the interface between neighboring SctD molecules the prime candidate for a pH-dependent temporary dissociation.

Both possible types of pH sensing, direct structural change and rearrangement of intermolecular interactions, are used by biological systems: The *E. coli* membrane-integrated transcriptional regulator CadC senses acidic pH through direct protonation of a charged surface patch in its C-terminal periplasmic domain, and transduces the signal to the cytosol by its N-terminal cytosolic domain (Haneburger *et al.*, 2011). Similarly, the *P. syringae* injectisome effector AvrPto transitions from a largely unfolded state in the mildly acidic bacterial cytosol to a well-defined fold in the neutral host cytosol (Dawson *et al.*, 2009). Perhaps most strikingly, the highly ordered multimeric structures of bacteriophages undergo large-scale structural changes at low pH, that are reversible (Helenius *et al.*, 1980; Mauracher *et al.*, 1991; Taylor *et al.*, 2002). Our data show a reversible partial delocalization of SctD at low external pH (**Figure 20**). The

presence of SctD is required for binding of any cytosolic injectisome component (Diepold *et al.*, 2010; Diepold *et al.*, 2017), most likely through a direct contact of four SctD to one SctK at the cytosolic interface of the inner membrane (Hu *et al.*, 2017), indicating that this partial displacement of SctD (**Figure 20**) is causal for the dissociation of the cytosolic injectisome components.

The dissociation and re-association kinetics of the cytosolic components of the injectisome revealed binding/unbinding half-times of about one to two minutes under secreting conditions (**Figure 13d**, **Figure 14**, **Supplemental Figure 4**). These values are strikingly similar to the exchange rate of SctQ at the injectisome (Diepold *et al.*, 2015), suggesting that at low external pH, primarily the re-association of the cytosolic components is prevented. Notably, recovery of fluorescent foci at pH 7 appears to be faster and more pronounced for the proteins close to SctD (SctK and SctQ) compared to the more distant components (SctL and especially SctN) (**Figure 12**); however, both visual and automated spot detection are influenced by the stoichiometry of the respective components, which makes comparisons across different parts of the injectisome difficult.

The mobile fraction of SctD at low external pH diffuses with a coefficient of 0.006-0.048 µm²/s, which is similar to other freely diffusing membrane proteins, including the unbound flagella stator GFP-MotB (Leake *et al.*, 2006; Lenn *et al.*, 2008; Kumar *et al.*, 2010; Mika *et al.*, 2014). This finding is compatible with passive diffusion of SctD in the inner membrane under these conditions, which allows a rebinding within few seconds.

SctD is a core component of the injectisome basal body that is reliably copurified in purified needle complexes (Kimbrough and Miller, 2000; Spreter *et al.*, 2009) and has an early role in injectisome assembly (Diepold *et al.*, 2014). While the dissociation of such a central protein upon external cues might be counterintuitive, dynamic exchange of structural components of large protein complexes and molecular machines has been shown in other cases, in particular for the flagellum (reviewed by (Tusk *et al.*, 2018)) and the DNA replisome (Mueller *et al.*, 2019), showing that structural and functional roles in a complex and protein exchange are not mutually exclusive.

While the effect of low external pH on the injectisome can be clearly observed in our experiments, it is difficult to estimate its role during infection. Activation of the injectisome by host cell contact can differ from activation by low calcium levels (Kusmierek *et al.*, 2019) and the exposure of *Y. enterocolitica* to different pH, as well as the extent of possible host cell contact in the low pH parts of the gastrointestinal system (Koziolek *et al.*, 2015) are unclear. In particular, it remains to be determined whether invasin,

whose regular downregulation at 37°C is prevented at acidic pH (Pepe *et al.*, 1994) contributes to host cell binding under these conditions. Nevertheless, the described adaptation of injectisome function at low pH may explain the so-far enigmatic benefit of the dynamic exchange of the cytosolic parts of the injectisome during its function. Notably, the observed dissociation of the cytosolic proteins in response to low external pH may not reveal the complete mechanism for suppression of injectisome activity at this pH. The observation that the dissociation of the cytosolic components occurs at a slightly lower pH (between 4 and 5) than the loss of effector secretion (which occurs between pH 5 and 6), and that the re-initiation of secretion occurs later than the initial recovery of foci indicates that other factors might participate in this phenotype. While we were up to this point, not able to take those two different observations apart, it remains imaginably that a first mechanism within the export apparatus spots effector recreation and only after the pH drops even further the inner membrane ring and the cytosolic components disassociate. If that is the case, it would imply even more that effector secretion needs to be prevented at low pH since two regulatory mechanisms are in place to ensure that. The slightly delayed activation of secretion after restoration of neutral pH could also be explained by the time required for re-associating SctV to the machinery (the cytosolic components can already bind to the membrane rings in the absence of SctV (Diepold *et al.*, 2010). *Y. enterocolitica* may in fact benefit from this lag, as it delays the antiphagocytic effects of the injectisome effectors, which otherwise may hamper the passage of *Y. enterocolitica* through the M cells that is required to access the lymphoid follicles of the Peyer's patches (Cornelis, 2002). As it is currently unclear to which extent *Y. enterocolitica* and other gastrointestinal pathogens directly contact cells in the low pH parts of the gastrointestinal system, including the stomach, this may be equally or even more beneficial for the bacteria than the direct suppression of secretion at low external pH. Our finding that overexpression of SctD strongly reduces dissociation of the cytosolic injectisome components at low pH, while retaining the secretion ability of *Y. enterocolitica* might be exploited in future infection experiments to investigate this question.

Like the *Y. enterocolitica* injectisome, the intracellular *S. enterica S*PI-2 injectisome is strongly influenced by the external pH; however, the mechanism described for *S*PI-2 differs from the one described in this study. Injectisome assembly and secretion of the translocon components in *S*PI-2 are activated by the low pH of the surrounding vacuole (around pH 5.0) (Rappl *et al.*, 2003; Yu *et al.*, 2010). After this step, neutral pH, most likely indicative of a successfully established connection to the neutral host cytosol, leads to the disassembly of a gatekeeper complex, which in turn licenses the translocation of effectors (Yu *et al.*, 2010). Strikingly, a single amino acid exchange in the export apparatus protein $SctV_{V632d}$, governs this pH-dependent effect (Yu *et al.*, 2018). Both the sensory and the functional connection between the pH and

injectisome activity differ between *Salmonella S*PI-2 and *Y. enterocolitica*, which highlights the high degree of functional adaptability of the injectisome.

In this study, we found that dynamic exchange of cytosolic components of the injectisome enables to suppress the activation of the injectisome at low external pH in *Y. enterocolitica*. Strikingly, this effect was also observed in *S. flexneri*, indicating a conservation in gastrointestinal pathogens, but not in *P. aeruginosa*, which does not pass low pH regions during normal infections. Our data highlight that not only the effector repertoire, but also dynamics and function of injectisome are adapted to the specific environment of the respective bacteria. This newly described pathway is a striking showcase for the variety and sophistication of mechanisms that allow bacteria to use different aspects of injectisome assembly and function, including protein dynamics, to tailor the activity of this essential virulence mechanism to their specific needs during infection.

4.2 Acknowledgments for this work

We thank Nicholas Dickenson (Utah State University, Logan, USA) for the kind sharing of *S. flexneri* GFP-Spa47, Sophie Bleves (Aix-Marseille University, FR) for the *Pseudomonas aeruginosa* PAO1 strain, Marc Erhardt (Humboldt University Berlin, Germany), Tohru Minamino (Osaka University, Japan), and Gero Miesenböck (University of Oxford, UK) for the pHluorin$_{M153R}$ DNA, Luke Lavis (Janelia Research Campus, USA) for the kind donation of Janelia Fluor dyes, and Malte Buchholz (University of Marburg, Germany) for helpful discussions about gastrointestinal infection pathways. We are also grateful to Carlos Helbig and Bartosz Turkowyd (Max Planck Institute Marburg, Germany and Carnegie Mellon University, USA) for analysis scripts.

4.3 Discussion - Additional results from 3.1.4

In chapter 3.1, we described the molecular effects of low pH on the injectisome. During the process we unraveled the molecular mechanism of pH sensing within the cells of *Y. enterocolitica*. To investigate if the needle protein SctF has a role in pH sensing, we attempted a heterologous complementation of the needle with *Pa*SctF. SctF is located outside the cell and therefore exposed directly to the environmental conditions surrounding the cell. It senses the calcium levels and host cell contact, which triggers the substrate switch during the infection in the human body (Torruellas *et al.*, 2005; Deane *et al.*, 2006; Shaulov *et al.*, 2017). Most interestingly, in the *S. enterica* SPI-2 system, the needle and the translocon are actually involved in conveying the neutral pH signal of the phagosome membrane to the export apparatus (Yu *et al.*, 2010). Since *P. aeruginosa* show less sensitivity towards low pH (**Figure 21**), *Pa*SctF was a prime candidate for investigating the pH sensor. Although some components of the injectisome can be heterologously cross-complemented (e.g SctD **Figure 17**), others are no (ExsB this study**,** Pcr3 (YscX) and Pcr4 (YscY) (Gurung *et al.*, 2018)). Our results suggest that in case of SctF the latter applies (**Figure 24**). Although we could not test expression of *Pa*SctF from the pBAD promotor, the pBAD system is robust and has been widely used for successful protein expression (including needle subunits) in this study and others in the past (**Figure 11**)(Milne-Davies *et al.*, 2019; Lindner *et al.*, 2020). To actually check the expression a (mass spectrometry) MS analysis of total cell samples would be needed.

We could not establish complementation by late expression of injectisome components from plasmid 2 hours after exposure to 37°C and start of assembly of the injectisome that mimicked the phenotype of low pH treatment (**Figure 25**). Noteworthy at this point is that while all experiments do not mimic the pH treatment, the number of replications of most of the experiments is quite low and to draw valid conclusions, the experiments would need to be performed in parallel and in multiple replications. Nevertheless, our data provides additional evidence that new protein biosynthesis and fresh assembly is not responsible for the fast injectisome reassembly and restauration of the secretion after pH 4 treatment (**Figure 22**). Instead, our experiments underline that already existing proteins facilitate the reassociation of the cytosolic components to the basal body and subsequently the restart of secretion. This also indicates that the delay we observed in secretion restart is more likely due to the reincorporation of proteins rather than to new biosynthesis of proteins (**Figure 22, Figure 25)**. Our experiments may additionally challenge the existing models for exclusive unidirectional linear injectisome assembly (Diepold *et al.*, 2010; Wagner *et al.*, 2010a). The export and assembly of the needle subunits is fast and swift after the start of expression, which is not surprising (**Figure 25a**). In this scenario, the basal body is

preassembled already and the needle subunits can be exported as quickly as they are synthesized resulting in secretion within under 15 minutes (**Figure 5**, **Figure 25a**) (Diepold *et al.*, 2014). For SctC this is different, it is needed in its assembled from to stabilize the inner membrane rings which lead to the proposal of the outside in model (**Figure 5**). In a linear assembly, were we have upregulation of genes followed step by step incorporation of different proteins into the machinery, it takes 60-120 minutes until establishing full effector secretion (**Figure 22**). The Assembly of the whole basal body takes ~60 minutes, since only then the cytosolic fluorescence of EGFP-SctQ is visible in precise membrane spots (Diepold *et al.*, 2010). Since we see fast secretion of effectors (30-45 minutes) (**Figure 25b**), this suggests a preassembly of other injectisome components like the export apparatus or possibly also the presents of SctD and SctJ in the inner membrane in an unassembled state. Once the secretin ring is established the already present and preassembled parts only have to connect to new assembling SctC. This would support the theory that the assembly in different species does not differ between inside out and outside in model but that it can starts independently at different points, suggested by Diepold (2019). It is also possible that the bottle neck in the assembly line is not the positioning and assembly of subunits into a machine, but rather the time it takes to produce the proteins involved. Since biosynthesis can be reduced in our experiments to SctC, the time it takes to start secretion is reduced. Both of these mentioned scenarios would explain the delayed secretion restart in the case of late SctD complementation, as well as late SctC expression (**Figure 25bc)**.

For SctJ and SctV, inner components of the basal body (**Figure 2**), incorporation in the injectisome and restart of secretion after complementation takes more time (**Figure 25**). In case of SctJ complementation, secretion restart is slightly faster than in case of SctD complementation, but slower than for SctV complementation. Since SctJ and SctV are components located within the SctD ring this is not surprising. This overall restart of secretion is still faster than fresh assembly. This may indicate that it is possible, although time-consuming, for SctJ to assemble inside the already existing membrane ring of SctD. Further this may imply that the membrane rings are more dynamic then originally presumed and in line with our hypothesis that the membrane ring is able to open up (**4, Figure 19**) (Schraidt and Marlovits, 2011). After the expression of SctV, it takes ~45 minutes to restart effector secretion (**Figure 25**). With that it is around 5-25 minutes slower than the pH treatment, but also 15-75 minutes fast then new assembly (**Figure 22**) (Diepold *et al.*, 2010). Earlier we speculated that the time it takes to restart secretion, is mainly caused by the time it takes to incorporate the different injectisome components back in their original positions. Since SctV is not essential for the assembly of the rest of the injectisome and all the other critical components should be present at the point of SctV expression already, it is reasonable to assume that the time it takes to start secretion, is the time needed for the incorporation of SctV in an already existing injectisome rather

than “waiting” for a new injectisome to be assemble for the incorporation of SctV (Diepold *et al.*, 2010). For this to be possible, again there needs to be a shortcut in the assembly pathway of the injectisome, contradicting the assumption of a strictly ordered step by step assembly. While exactly mirroring the pH treatment secretion pattern, our data suggest in conclusion that we not only observe protein relocation and distribution within the cell during and after the pH treatment (**3.1**), but also that there might be a bypass within the known mechanism of injectisome assembly. This may be facilitated by more subunit exchange then originally assumed in the basal body (Enninga and Rosenshine, 2009; Diepold *et al.*, 2010; Wagner *et al.*, 2010a).

Although our attempts to crosslink extracytosolic proteins with the membrane impermeable cross-linker (BS3) were not successful, our results indicate that the concentration should be between 10 mM and 50 mM with an incubation time of 30 minutes (**Figure 27***).* A concentration of 50 µM has been successfully used previously with purified proteins and in association with bacteriophages (Al-Eryani *et al.*, 2016; Ghuman *et al.*, 2018). In *Agrobacterium tumefaciens*, higher concentrations up to 10 mM were successful (Pan *et al.*, 1993). Otherwise applications of BS3 were focused on eukaryotic studies according to studies cited on the manufacturing homepage. This difference may also explain why problems with membrane permeability have been encountered (**Figure 27**). The overall idea of stabilizing the SctD ring nevertheless remains promising. As discussed earlier, the addition of more SctD protein pushes the equilibrium in the membrane towards the oligomer ring state (**4**) creating an artificial stabilization of the SctD ring. That stability could result in stable foci of EGFP-SctQ at pH4 as well. In the future, it would be interesting to test other cross-linker or introduce specific cysteine bounds, which could be cross-linked on the outside by oxidative treatment (Lippa and Goulian, 2012).

Similar to DNP, CCCP is an ionophore that uncouples the protein motive force across the membrane. Concentration of 10 µM in *Y. enterocolitica* WA-314 up to 100 µM in other bacteria have been used to neutralize the PMF at the membrane and the optimum concentration varied between species and the used growth medium (Ghoul *et al.*, 1989; Wilharm *et al.*, 2004). While our CCCP experiment lacks proper number of replications the phonotype is striking (**Figure 28**). At a concentration of 40 µM, the same concentration used for *E. coli* K12 previously as uncouppeler of PMF (Yerushalmi *et al.*, 1995), the localization of the cytosolic components matches the phenotype of *Y. enterocolitica* exposed to low pH (purely cytosolic localization of EGFP-SctQ, **Figure 12**). On top of that the presence of 40 µM CCCP also inhibited secretion, which has been already documented (Wilharm et al., 2004). After recovery from low pH, it takes 20-40 minutes, to recover the effector secretion (**3.1, Figure 22**), whereas after CCCP

treatment secretion restarts almost immediately after the reversal with β-mercaptoethanol (**Figure 28**). While the CCCP results are being preliminary, the secretion after CCCP exposure starts under 15 minutes. The secretion after pH exposure stars only after 20-40 minutes, this points in the direction of a different mechanism behind those two phenotypes. Interestingly, this mechanism would involve the cytosolic components as regulatory network as well but at the same time may not undergo major, time-consuming, restructuration of the membrane components in the sensing process (**Figure 20**). It could be possible that complete collapse of the PMF is sensed by the cytosolic components, or that the PMF is partly needed for their proper assembly at the basal body and once it is restored the assemble back again immediately. Further experiments are needed to investigate both the nature of this phenotype as well its molecular function.

In summary, we learned that the *Pa*SctF needle does not complement the deletion of *Ye*SctF. None of the complementation of the basal body mimic the phenotype of the pH exposure, they allowed new insights into the assembly process and while the BS3 crosslinking was not as sensitive as we hope for, the fixation of the inner membrane ring SctD remains a promising approach to investigate the dynamics in the injectisome.

Some of these results are striking and it is interesting to speculate with and about but most of them are not well worked out at this point. Further investigation would be needed to validate and investigate those hints.

4.4 Discussion - Dynamic exchange of protein subunits within the basal body

Protein dynamics, movement and changing interactions are an essential part of microbial life. This not only applies to bacterial secretion (Diepold *et al.*, 2015; Diepold *et al.*, 2017; Milne-Davies *et al.*, 2020), but also chemotaxis, cell cycle organization and even DNA replication and segregation (Treuner-Lange and Søgaard-Andersen, 2014; Tusk *et al.*, 2018). To investigate protein dynamics within the cell, a set of different tools and techniques have been established. FRAP (fluorescence recovery after photobleaching), FRET (Förster resonance energy transfer), sptPALM and FCS (fluorescence correlation spectroscopy) are the most commonly used ones and while all have their individual strengths, they all require specialized equipment and expertise in the process to apply those meaningfully. With the "fluorescence intensity dilution exchange assay" we provide a fast and easy tool to investigate global protein dynamics. A first test run enabled us already to show convincingly that the inner membrane ring SctD exchanges subunits in the already assembled injectisome (**Figure 29**). At the same time those early experiments already point out a drawback of this new method. The limiting factor in this assay is protein biosynthesis and protein folding of the respective protein of interest and the used fluorophores rather than the dynamics itself. If for example sfGFP already takes on average 13.6 minutes to mature (Pédelacq *et al.*, 2006; Lambert, 2019), the temporal resolution is always bound to that time and only afterwards the protein exchange can be observed. At this point we can also not exclude, that there is an incorporation bias towards the unlabeled version of SctD expressed from the plasmid. Nevertheless, it is a powerful tool and it will be interesting to see how fare we can reduce the temporal resolution with more experiments. The initial data are very promising since we see at least a significant expression of SctD already after 10 minutes (**Figure 29cd**) which translates into a dilution of EGFP-SctD foci. In addition, FRAP can be used to validate our results with an already established method. The incorporation of more proteins of the basal body, SctC, SctV, as well as the cytosolic components will allow us to benchmark the assay further for a broader application outside of membrane proteins. On top the implantation of a dual color approach, EGFP-tagged protein expressed from the chromosome and a red fluorescent protein, mCh or mScarlet-i-C1 expressed for the pBAD plasmid will enable us to visualize both the native and the addition levels of proteins within the cell. It will also prevent an incorporation bias towards the untagged protein. While we have established and proven the principle of this new technique to look at proteins dynamics and turnovers, further validation and application is still needed in the future.

While it has recently become obvious that more and more formally stable multi-protein complexes actually exchange subunits while performing their task in the cells, this is quite novel for the injectisome

(Enninga and Rosenshine, 2009; Tusk *et al.*, 2018). Here it has been established that the components in the cytosol are mobile (Diepold *et al.*, 2015; Diepold *et al.*, 2017; Rocha *et al.*, 2018), but the paradigm based on the fact, that SctD assembles intrinsically in a 24-mer ring around SctJ (purified SctJ even forms rings on its own), the many interactions between SctD, SctJ and SctC and the fact that they together purify as the basal body was that especially the inner membrane rings are highly stable, if not the most stable part of the system at all (Yip *et al.*, 2005; Enninga and Rosenshine, 2009; Schraidt *et al.*, 2010; Schraidt and Marlovits, 2011; Kowal *et al.*, 2013b; Kudryashev *et al.*, 2013; Bergeron *et al.*, 2015; Diepold *et al.*, 2015; Butan *et al.*, 2019; Miletic *et al.*, 2020b; Muthuramalingam *et al.*, 2020). With the first set of experiments we presented in this study, our view of the inner membrane ring SctD changes now (**Figure *29***). While we see clear indications for protein exchange it is noteworthy is that with the expression of proteins from the pBAD plasmid and continuous induction, the cell encounters an 8.9 fold upregulation of the native protein levels. Although our experiments indicate protein exchange, to be more quantitative, more elaborate experiments are needed to ensure that the amount of access protein is not changing the turnover rate of the ring complex. In the future it will be interesting to determine as well if SctC shows protein turnover. Here FRAP experiments suggest otherwise but since they were only conducted in a temporal magnitude of 10 minutes (Diepold *et al.*, 2015), the low temporal resolution of our approach could actually be an advantage here. The same applies to SctV (Diepold *et al.*, 2015), which is held in position by the inner membrane rings SctD, SctJ (Diepold *et al.*, 2011). Further, will be especially of interest to investigate if the dynamics of SctD include SctJ or if the inner part of the inner membrane ring and export apparatus remain stable while the outer ring proteins are exchanging. Maybe our approach even has the potential to answer why in the injectisome two concentric membrane rings are needed in the first place while the flagellum only has one (FliF (Thomas *et al.*, 2001; Diepold and Armitage, 2015)). The dynamics of SctD could also link and/or explain the bypass of the linear assembly order described in **4.3**. The most intriguing speculation of all, that need to be investigated is that the dynamics of the cytosolic components, which have been described in great detail and for which a mechanistically explanation is still missing, could be linked to, or even caused by, a slower turnover rate of their binding site in the inner membrane, SctD. If the dynamics of SctD are influenced by the state the injectisome is in, secreting or non-secreting conditions, similar to the cytosolic components this would be a first indication in that direction (Diepold *et al.*, 2015; Hu, et al., 2017; Diepold *et al.*, 2017). At this point we were able to show already that there is protein turnover in the inner membrane ring SctD while this is intriguing, more experiments are needed to elaborate the details of the dynamic and their biological function.

5 Results: Part II

5.1 Binding of effector proteins to the cytosolic injectisome components and their role in secretion in *Y. enterocolitica*

At this point this study is a manuscript in preparation, while it is not finished yet goal is to publish it within the postdoc wrap up phase following my PhD.

5.1.1 Authors and contributions

Stephan Wimmi, Alexander Balinovic, Carlos Helbig, Moritz Stahl, Jörg Kahnt, Timo Glatter Ulrike Endesfelder & Andreas Diepold

S.W. performed sample preparation, data analysis and participated in study design and wrote the manuscript. A.B. performed and analyzed the sptPALM experiment with support from S.W.. M.S. and C.H. assisted in sample preparation for the sptPALM measurements. J.K and T.G. performed MS analysis. U.E. provided data analysis, supervision, study design and participated in discussions. A.D. conceived and designed the study and analyzed data.

5.1.2 Background

In contrast to the basal body of the injectisome, the cytosolic components are mobile in the cytosol and exchange between an injectisome-bound and unbound state (**Figure 2**). While the transition of effector proteins through the needle and the events at the export gate have been recently elucidated by CryoET/EM (Radics *et al.*, 2014; Hüsing *et al.*, 2020; Miletic *et al.*, 2020a; Lyons *et al.*, 2021) less is known about the events happening in the cytosol. Despite multiple attempts to answer how the path of substrates from the bacterial lumen to the injectisome looks like, it is still unclear today. At the moment, the most-cited evidence for the interplay between effectors, chaperones and the cytosolic components is Lara-Tejero *et al.*, 2011. Here the localization of export cargo (Translocators, Chaperones, Effectors) and the sorting platform protein (SctQ) could be shown in the same molecular weight complex in blue native gels (Lara-Tejero *et al.*, 2011). The experiments are well thought of, in a fest step mostly translocators are detected. If they are deleted, mimicking export, chaperones and effectors or detected more abundantly (Lara-Tejero *et al.*, 2011). Since the export substrate localizes quite broadly on those gels, to draw solid conclusions remains challenging. Direct binding of SctQ to the effector chaperones could be shown in Chlamydia as well (Spaeth *et al.*, 2009) and a deletion of any of the cytosolic components results in a

secretion deficit strain (Diepold *et al.*, 2017). In conclusion, SctQ seem to have a key for the function of the system. Further, it has been also observed that the dynamics of the cytosolic components differ between the different states that the machinery is in (secretion and non-secretion conditions) (Diepold *et al.*, 2017). However, the actual biological function and purpose of the dynamics are not yet clear. A popular theory is that the cytosolic compounds, mainly SctQ, shuttle or assist in the shuttling of effector proteins from the bacterial lumen to the injectisome or at least increases the local concentration of export substrate at the injectisome (Diepold *et al.*, 2015; Soto *et al.*, 2017; Diepold *et al.*, 2017; Rocha *et al.*, 2018; Wagner *et al.*, 2018; Lara-Tejero, 2020).

5.1.3 Aim of the study

We wanted to investigate the role of the cytosolic components and clarify the precise task of SctQ in the processes that lead to effector export by screening for new interactions of SctQ in the cytosol. In addition, we speculated that if the cytosolic components are involved in the shuttling process of effectors, it would be within reason to assume that their diffusion behavior changes by binding or interacting with an increasing amount of secretion substrate cargo. To test this hypotheses, we compared the dynamics of SctQ in strains carrying different loads of secretion substrates. To this aim, we performed sptPALM measurements on SctQ in a strain lacking the main virulence effectors YopH, O, P, E, M, T (effector-less strain), and a WT strain (effector-less strain) carrying the full set of effector proteins under non-secreting conditions (low expression of effectors) and secretion conditions (high expression of effectors). At this point, our data indicates that the presence of additional substrate cargo slows done the diffusion speed of SctQ within the cytosol. Furthermore, our measurements indicate that the composition of the subcomplexes formed by SctQ and the other cytosolic components changes between secreting and non-secreting conditions.

5.1.4 Results

5.1.4.1 Identifying novel interactors of the cytosolic components

Due to its proposed role in the sorting platform, SctQ would a prime candidate to check for direct interactions with export cargo. Therefore, we performed a co-immunoprecipitation experiment with PAmCh-SctQ as bait protein to screen for this interaction (**Supplemental table 2**). While the efficiency of the IP was low, the known interactors (SctL, SctQ and SctN) and the closely associated SctV could be pulled in a higher concentration than the background (**Supplemental table 2**). While some effector chaperones (SycD and SycH) and translocators (YopB/D) and regulatory effectors (SctW and YopQ) could be pulled

down, their concentration is not significantly above the background levels. So this approach does not seem to be every promising and we need to find another way to address this.

Since the CoIP results did not unequivocally uncover any novel interaction partners, we concluded that the interaction to the cytosolic sorting complex, as well as it interactions to its cargo, may be too transient to be co-purified with the injectisome components. Thus, we decided to change our approach and use single-particle tracking photoactivated localization microscopy (sptPALM) to investigate the impact of the effector proteins on the cytosolic sorting platform component SctQ. This method allows to investigate the localization and diffusion behavior of proteins within living cells. Therefore, sample fixation, cell lysis and purification are not needed, although it allows *in situ* understanding at the same time. As a result, we established a collaboration with to lab of Dr. Ulrike Endesfelder.

5.1.4.2 Difference in cargo levels between different strains used in this study

To interpret our results, it was important to quantify the changes in cargo levels (translocators, effectors and chaperones (Spaeth *et al.*, 2009; Lara-Tejero *et al.*, 2011) between the different strains and conditions. To this aim and estimate the relative abundance of cargo per SctQ based on spectral counts from total cell proteomics measurements. We chose three different strains and conditions which we expected to have different levels of cargo: the effector-less strain, non-secreting; the strain with effectors, non-secreting (low expression of effectors); strain with effectors, secreting conditions (high expression of effectors). **Figure 30** shows the normalized amount of cargo per SctQ detected per strain (raw counts in **Supplemental table 3**). As expected, the effector-less strain showed a low ratio of cargo per SctQ in spectral counts. In contrast, there was 1.89 times more cargo in a low expression of effectors strain with effector strain, non-secreting compared to effector-less strain. In the strain with high expression of effectors (secreting conditions), we detected 7.88 times more cargo per SctQ.

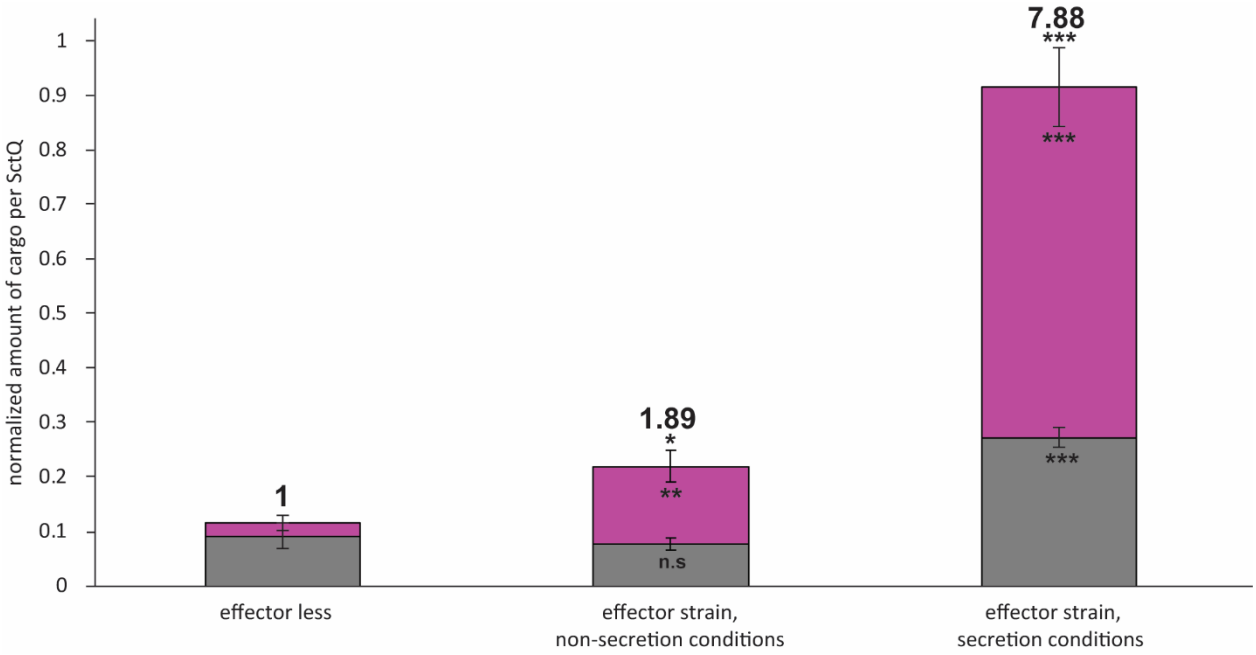

Figure 30 Amount of cargo per SctQ based on mass spectrometry spectral counts and normalized on effector strain secretion conditions.
Total amount of effector cargo per indicated strain and condition per SctQ present in that strain and condition. Displayed in gray are the translocators and regulators (SctB (YopD), YopQ, SctE (YopB), YopP, YopR) while virulence effector proteins are displayed in magenta (YopH, YopO, YopP, YopE, YopM, YopT). The experiment has been performed in three independent replicates within one day (n = 3) and the arrow bars denote the standard deviation. *, p<0.05, **, p<0.006, ***, p>0.003; against the effector-less strain values. Asterisk underneath the error bar indicate P values for the respective fraction (translocators/ effectors). Asterisk on top indicate P values of the total cargo. Number on top of the graphs indicate ratios against the effector-less strain under non-secretion conditions. MS samples processed by Jörg Kahnt.

5.1.4.3 Establishing a working protocol for sptPALM for *Y. enterocolitica*

In a first step, the optimal experimental conditions for sptPALM with *Y. enterocolitica* needed to be established. Since the reduction of auto-fluorescence and background are key for this method, samples are usually rigorously washed and grown in minimal medium or pre-bleaching. The tradeoff one has to consider in sptPALM experiments is background that increases the number of false tracks, against the physiological state of the cell and comparability with the usually used full media conditions (**9.2.1** BHI).

In our case, the protocol included media changes after expression and assembly of the injectisome from BHI to minimal microscopy media, 30 minutes prior microscopy. Additionally, the samples needed to be washed three times in twice the volume with EZ Rich Defined Medium - (Teknova) (EZRD). EZRD-medium is a widely used non-fluorescent microscopy medium. Since growth and injectisome activation were reduced when *Y. enterocolitica* was grown in EZRD-medium it was necessary to stay as close as possible to the standardized conditions, the exposure to EZRD-medium should be limited. So in our protocol, a pre-

incubation step in BHI was included, to ensure effective secretion and avoid cell lysis. After the washing steps, cells were resuspended in EZRD-medium and finally spotted on an EZRD-medium agarose pad. For transport and visualization under the sptPALM microscope, agarose pads were sealed with gene frames to prevent any leakage or drying out of the sample. The PALM images were taken with an exposure time of 15 ms, 20000 frames and with laser intensities of 561 nm- 800W/cm^2 together with an activation plus every 10 frames at 405 nm- 1W/cm^2. To analyze the data, a threshold of 3000 counts was set for localization. Only tracks longer than six steps were accepted. To further reduce unspecific background, we only accepted tracks that started with a UV-pulse or up to two frames after it.

The protocol gave robust results for sptPALM in both effector-less strain and the effector strain (**Figure *31*ab**)**.** By using the "swift" software package, provided by the Endesfelder Lab, we were able to visualize and quantify the acquired trajectories. Tracking of localizations and calculation of the medium jump distance (MJD) showed a slow diffusing injectisome-bound population of PAmCH-SctQ at the membrane (peak **I,** maximum at 42 nm) and a fast diffusing population of PAmCh-SctQ in the cell lumen (peak **II-V,** maxima at 177, 267, 317, 377 nm) (**Figure 31ab)**. The injectisome bound fraction displayed mean jump distances around under 60 nm (peak **I**)(which is assumed to be the resolution limit reachable for sptPALM (Wieser and Schütz, 2008)) while the cytosolic fraction was most prominent in an MJD fraction from 100-700nm (**Figure 31ac**). As control for our localizations, we tracked PamCH-SctQ in an ΔSctD strain (**Figure 31de**). This resulted in the strong reduction of that stationary peak (peak **I,** maximum at 42 nm) and purely cytosolic population of PAmCh-SctQ (peak **II,** maximum at 272 nm). Since the binding site at the injectisome basal body for the cytosolic components is missing now, this was expected (Diepold *et al.*, 2010; Diepold *et al.*, 2017). To further ensure that no membrane bound artefacts were included in our analysis, we focused on the cytosolic fraction of the trajectories and excluded membrane foci from here on (**Figure 31f**). Overall, our initial data shows that our approach works and can be applied now for broader sptPALM measurements in *Y. enterocolitica*.

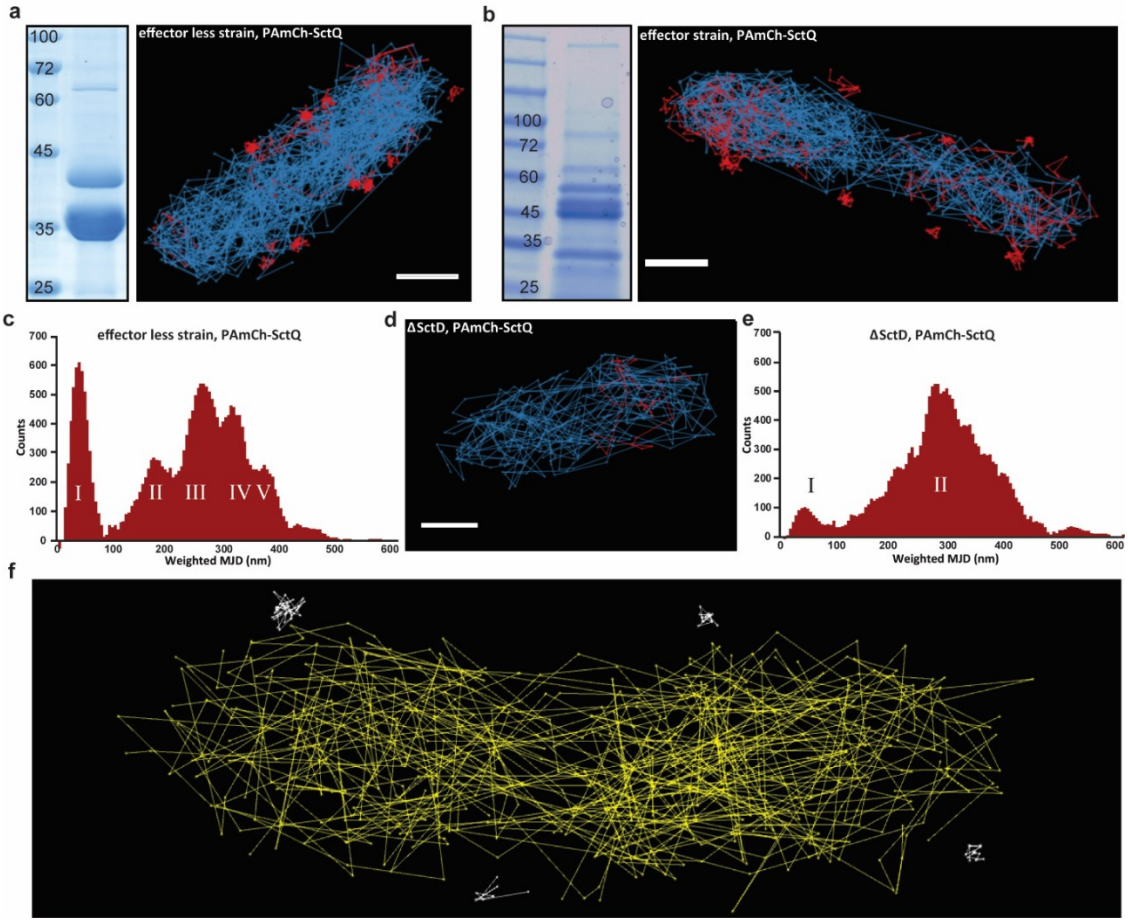

Figure 31 Establishing sptPALM in *Y. enterocolitica* effector-less and effector strain.
(a) Left: *In vitro* secretion assay with an effector-less strain. Right: PAmCherry-SctQ dynamics in an example *Y. enterocolitica* effector-less cell. **(b)** Left in secretion assay with the effector strain harboring a full set of effector proteins. Right: Dynamics of PAmCherry-SctQ in an example living *Y. enterocolitica* effector harboring cell. (ab) red trajectories: slow fraction in <180 nm median jump distance (MJD), fast fraction in blue >180 nm MJD. Scale bar 500nm mean jump distances MJD. **(c)** Histogram of the mean jump distances MJD PAmCH-SctQ an effector-less strain background with membrane bound and cytosolic fraction. **(d)** Example *Y. enterocolitica* cell with a SctD deletion resulting in a purely cytosolic fraction of PAmCH-SctQ. **(e)** Quantification in MJD of the strain background displayed in (d). (**f**) *Y. enterocolitica* cell with cytosolic trajectories marked for analysis in yellow and membrane fraction excluded white. Measurements performed in collaboration with Alexander Balinovic.

5.1.4.4 Impact of injectisome secretion and non-secretion conditions on diffusion in the cytosol

Since non-secreting and secreting conditions are quite different in cell physiology (Milne-Davies *et al.*, 2019) and secreting conditions result in an upregulation of injectisome components (2.45x in Kudryashev *et al.*, 2015) as well as effector proteins (**Figure 30**), we tested if this has any impact of the diffusion of PAmCh in the cytosol in an effector strain background (

Figure 32). Due to the fact, that both the mobility distribution curve and the mean MJD of PamCH-SctQ in the effector strain, non-secretion conditions and secretion conditions are similar (non-secretion conditions: median347.7 nm; secretion: 360.7 nm) and the two different conditions have nearly no effect

on the peak distribution of the histogram, we concluded that the different states have no influence on global protein diffusion within *Y. enterocolitica*.

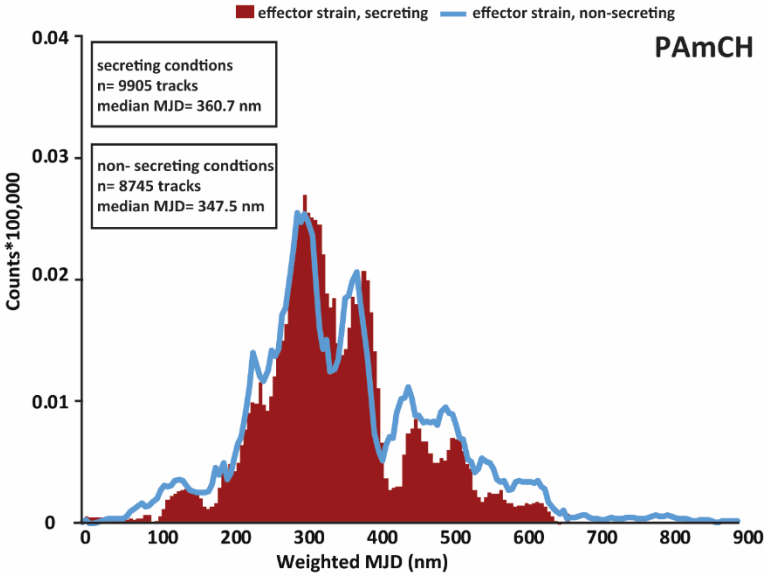

Figure 32 Different conditions of the injectisome have no major impact on diffusion.
Histogram displaying weighted MJD's based on sptPALM measurements under secreting and non-secreting conditions. Red: Effector strain expression PAmCh from a pBAD plasmid under secreting conditions. blue: Same strain under non-secretion conditions. In both cases the expression from the pBAD plasmid was induced with 0.05% L-arabinose. Y-axis Counts*100,000. In boxes number of counts analyzed and median MJD Secreting conditions 1 dataset (n = 1), non-secreting condition 2. Measurements performed in collaboration with Alexander Balinovic.

Next, we established baseline measurements by tracking how PAmCh-SctQ diffuses in a pYV$^-$ strain, which lacks the virulence plasmid and consequently all other injectisome genes. The fluorophore displayed uniform diffusion throughout the cytosol (**Figure 33ab**) with a small peak at 100 nm (**I**), a global maximum in the middle of the graph (peak **II** at 372.5 nm) and a shoulder at 482.5 nm (**III**) (**Figure 33ab**). As a reference point, we measured PAmCh alone in a pYV$^-$ background, which exhibited closely to gaussian distribution with a central peak at 397.5 nm (**II**) and shoulder at 507 nm (**III**). In comparison, the tracking of PAmCh-SctQ and PAmCh (26.8 kDa) alone did not display major differences, which is also reflected by the median MDJs. However, the maximum peak (**II**) from the PAmCh-SctQ (61.2 kDa) strain, is shifted to the left and is thereby slower when compared to PAmCh diffusion. So as a result, the diffusion speed of PAmCh slows down in pYV$^-$ bacteria when it is expressed as a fusion protein together with SctQ (PAmCh-SctQ). This was not only expected to happen but also nicely elucidates that addition of a molecular mass to our fluorophore, here the 34.4 kDa of the SctQ protein, results in a reduction of diffusion within the cytosol.

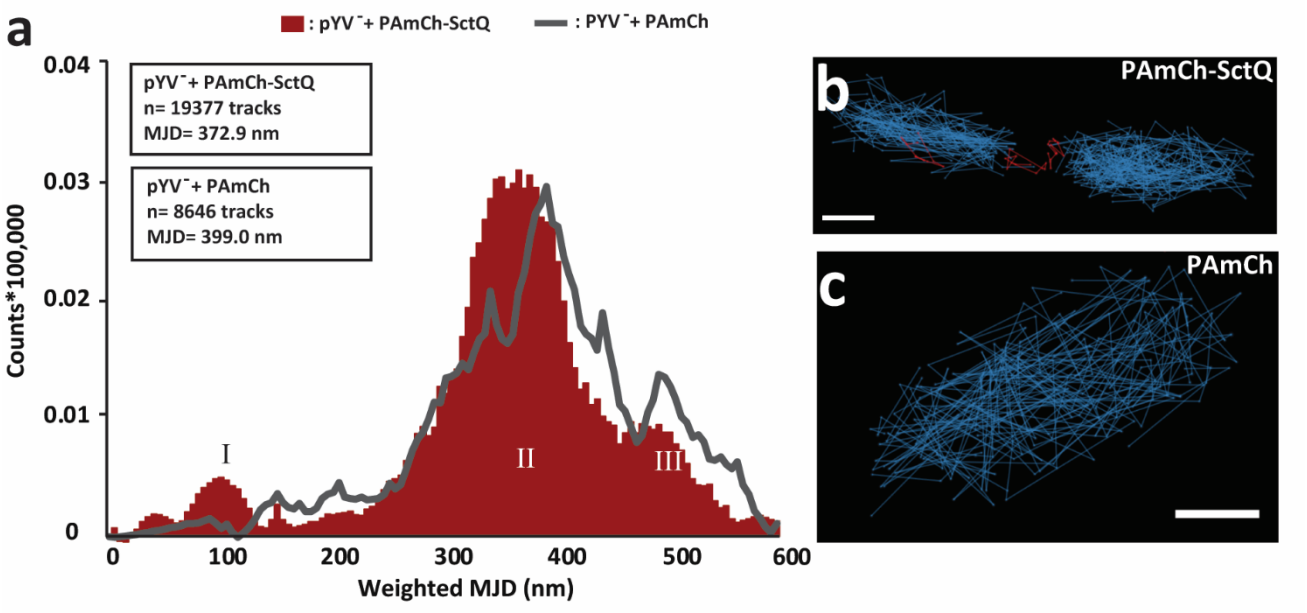

Figure 33 PAmCh-SctQ diffuses slower than PAmCh in a pYV⁻ background.
(a) Histogram MJD of PAmCh-SctQ (red) and PAmCh (gray line), both proteins are expressed in trans from a pBAD plasmid induced with 0.05% L-arabinose. Counts*100,000. Trajectories are weighted by the number of jump distances used for calculating each MJD PAmCherry/PAmCherry-SctQ (n = 1 dataset). Roman numbers (I-III) for peak identification. Boxes on the left side legend with number of tracks analyzed for the respective histograms and median MJD. On the right side dynamics in an example *Y. enterocolitica* cell with **(b)** PAmCh-SctQ and (**c**) PAmCh, slow fraction in red <180 nm MJD, fast fraction in blue >180 nm MJD. Scalebar 500 nm. Measurements performed in collaboration with Alexander Balinovic.

5.1.4.5 Impact of the presence of cargo on SctQ

But what happens when the full system is present and how does the presence of additional interactors (cytosolic components) and cargo (virulence effectors) influence the behavior of SctQ in the cytosol? To answer that question, we measured strains and conditions in which different amounts of export cargo are present in the cell (**5.1.4.2**). The measurements of PAmCh-SctQ in the effector-less strain resulted in a slower diffusion than the strains measured before (**Figure 34a**). The histogram displayed a central peak around 272.5 nm (**II**), a left shoulder with a maximum at 192 nm (**I**), three times smaller than the main peak and a right shoulder at 372 nm (**III**). The central peak of the population is shifted to the left compared to pYV⁻ PAmCh and pYV⁻ PAmCh-SctQ (**Figure 34a, gray and blue line**), which is also reflected in the median MJDs that are 78/113 nm lower than for PamCh alone (**Figure 34a**), corresponding to slower diffusion. Considering the amount of cargo in the cell at this point is still every low (**Figure 30**), the shifts are most likely due to the presence of the other cytosolic components SctK, L, N in the cell. This would be in line with previous results of the cytosolic components, suggesting the presence of subcomplexes within the cytosol(Diepold *et al.*, 2017; Rocha *et al.*, 2018; Bernal *et al.*, 2019).

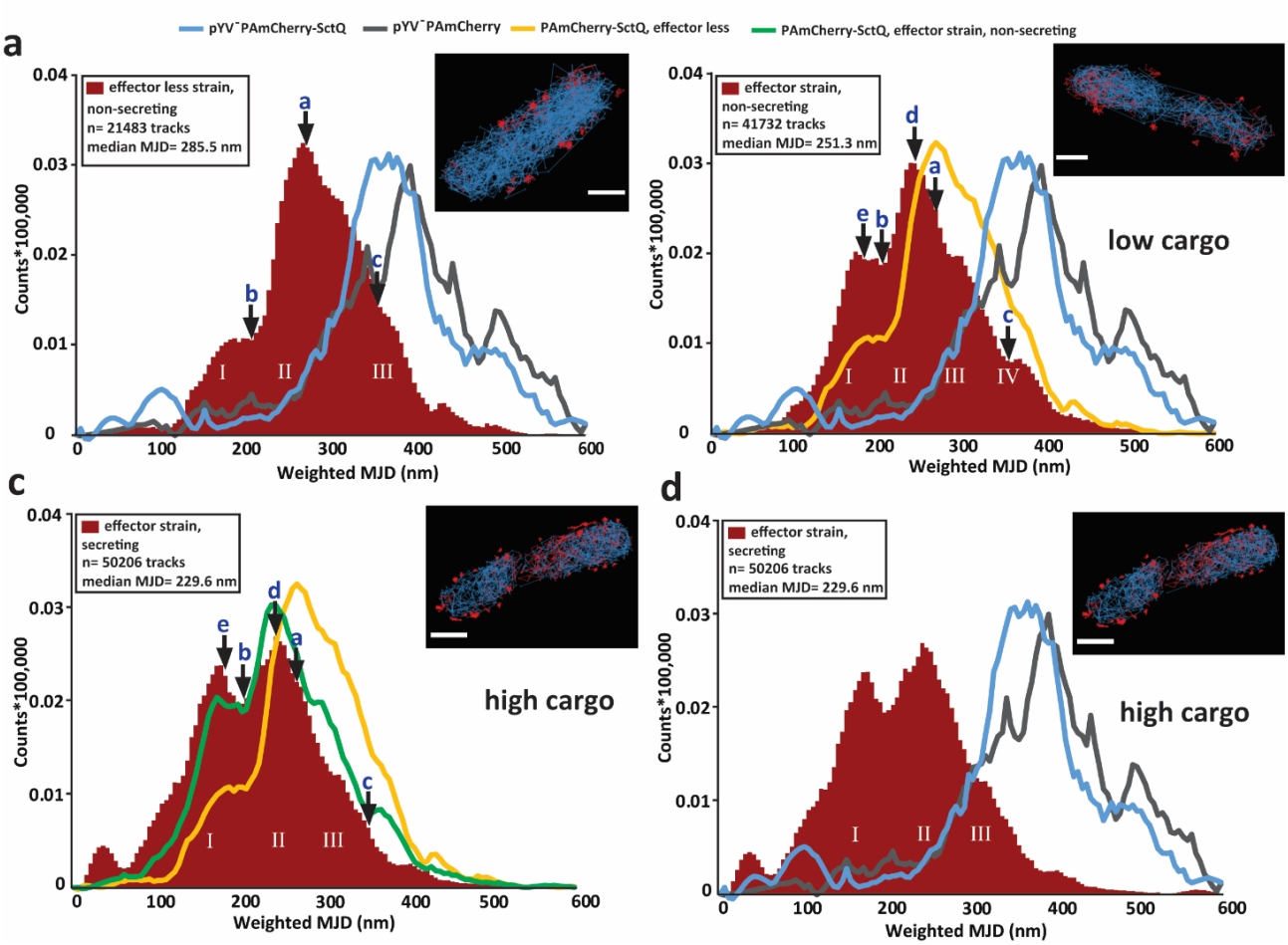

Figure 34 Impact of different amounts of cargo on diffusion behavior of PAmCh-SctQ.
(a) Red: Histogram of the mean jump distances (MJD) of PAmCherry-SctQ in effector-less, strain background (n = 3 datasets), **(b)** in effector strain, non-secreting conditions background (n = 5 datasets). **(c)/(d)** in effector strain, secreting background and (n = 3 datasets). Right number of analyzed tracks and median MJD. Roman numbers (I-IV) for peak identification. Right: Example PAmCherry-SctQ trajectories from the respective strain, slow fraction in red <180 nm MJD, fast fraction in blue >180 nm MJD. Scale bar 500 nm. **grey line**: pYV⁻ PAmCh expressed from pBAD plasmid and induced with 0.05% L-arabinose. **blue line**: pYV⁻ PAmCh-SctQ expressed from pBAD plasmid and induced with 0.05% L-arabinose, **yellow line**: PAmCherry-SctQ in effector-less background and non-secreting conditions. **green line:** PAmCherry-SctQ in effector strain, non-secreting background and non-secreting conditions. **a**: Theoretical diffusion speed of full single pod. **b**: Theoretical diffusion speed in MJD of a fully sorting platform with all six pod structure. **c**: Theoretical diffusion speed of SctQ oligomers. **d**: MJD of fully assembled sorting platform, including the molecular weight of 24 effector proteins. **e**: Theoretical diffusion speed of single pod including the molecular weight of four effector proteins (**Figure 35**). Measurements performed in collaboration with Alexander Balinovic.

In order to correlate measured MJD with the presence of potential subcomplexes of the cytosolic components, we calculated the theoretical JD (in nm) of different possible subcomplexes (**Supplemental table 5**). For this we assumed that the proteins diffuse by Brownian motion (unknown viscosity, crowding, confinement or charge effects). The results for the pod came with 346.19 nm close to the highest peak we measured (**II**) (272.5 nm) (**Figure 34a**)(theoretical JD PAmCh: 1372.98 nm, SctQ oligomer: 791.51 nm, fully assembled sorting platform: 145.15 nm). Since this peak does not correspond to PAmCh-SctQ alone, which we measured (**Figure 34a**) and the most prominently identified assembled subunit within the

cytosol was the assembled single pod complex **(a)** (Bernal *et al.*, 2019) (**Figure 35, Figure 34a**) we calculate the theoretical JDs for the other complexes based on their molecular weight in kDa and the assumption that the single pod corresponds to the 272.5 nm peak (**II**) (**Figure 35,Supplemental table 4**). A complete sorting platform ring (**Figure 35b**), would have a JD of 195 nm (**Figure 34a**,) and the smallest stable SctQ oligomer complex would have a MJD of 350 (**Figure 35c**, **Figure 34a**). Thus would indicate that the larger left shoulder fraction (**I**) (**Figure 34a**) is actually a fully assembled sorting platform (**Figure 35b**), while the small right shoulder (**II**) corresponds to the SctQ oligomer (**Figure 35c**). This assignment strikingly fits to our measured data. To check if we see an assembly of SctQ in foci in the cytosol, we performed TIRF microscopy. The used microscope here has a less sensitive photon detector and a lower temporal resolution than the sptPALM setup, which allows us to see complex oligomers up to the hexameric SctK, but no monomers. Indeed we were able to observe foci clusters and quantify the appearance and disappearance of EGFP-SctQ in the cytosol (**Supplemental Figure 11**). Thereby again indicating the presence of bigger subcomplexes of SctQ within the cytosol.

Schematic	Stoichiometry	Molecular weight in kDa	calculated diffusion speed in JD
a 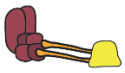	1x SctK, 4x (SctQ + 2 $SctQ_C$), 2x SctL, 1x SctN	451.48	270
b 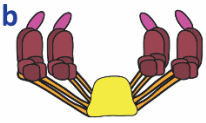	6x (1x SctK, 4x (SctQ + 2x$SctQ_C$), 2x SctL, 1x SctN	2708.88	195
c 	1x (SctQ + 2x$SctQ_C$)	82.22	350
d 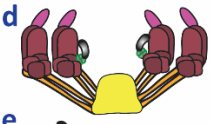	6x (1x SctK, 4x (SctQ + 2x$SctQ_C$), 2x SctL, 1x SctN, 24 effector proteins	4682.16	173
e 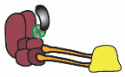	1x SctK, 4x (SctQ + 2x$SctQ_C$), 2x SctL, 1x SctN, 4 effector proteins	780.36	240
f 	1x (SctQ + 2x$SctQ_C$), 1 effector protein	164.71	312

Figure 35 Identification of diffusion patterns.
(a)-(f): Schematics of different assumed states in which the cytosolic components can be in, displayed together with together with their, arrow names in the figures **(a-f)**, as well as stoichiometry of the complex, Molecular weight in kDa and the calculated diffusion speed in jump distance (JD). Calculations of diffusion speed in MJD done by Ulrike Endesfelder and Alexander Balinovic.

In a next step, we visualized PAmCh-SctQ in the effector strain, non-secreting conditions. This resulted again in the MJD distribution shifting to the left (average MJD 251 nm). The center peak (**II**) shifted slightly from 270 nm (yellow line) to 242 nm MDJ (**Figure 34bd**). This shift brings the peak (**II**) away from the

calculated MJD of a single pod state (**Figure 35a**) and closer to the calculated MJD of a single pod including four effector proteins (240.7 nm) (**Figure 35e**). Further, the presence of effector proteins within the cell caused an upshift of the left shoulder (**I**) to nearly twice the detected counts and a right shift from 192 nm (peak) to now 177 nm (**Figure 34b**) Thereby the peak (**I**) comes closer to the estimated diffusion speed of a fully assembled sorting platform with 24 effector proteins bound (**Figure 35d, Figure 34b**). At the same time the small right shoulder (**III**) associated with the SctQ oligomer (**Figure 35c**) decreased in abundance (**Figure 34b**). These results now show that for the first time the presence of effector protein cargo has an influence on the diffusion behavior of SctQ and the cytosolic components. Since the overall diffusion speed of PAmCh-SctQ slowed done with more cargo/effectors, this ultimately needs to be attributed to some kind of cargo interaction of the cytosolic sorting platform components. That the same time, the shifts in the population might be an indication for a switches from empty subunit diffusion to loaded once (**Figure 34ab, Figure 35**).

Now we were curious if a more drastic increase in cargo/effectors also would have a proportional effect on the diffusion of SctQ (**Figure 30**). To test this, we measured the diffusion of PAmCh-SctQ in a effector strain background under secretion conditions (**Figure 34cd**). While the overall changes were not as drastic as before (median MJD change from 251 nm to 229 nm, difference to PAmCh-SctQ now 143 nm (**Figure *34***) the left shoulder peak (**I**) (maximum at 177 nm) slightly increased in abundance and now was close to the detected counts of the center peak at 251 nm, thus creating a local maximum at the calculated MJD of the single pod with effectors **(Figure 34,e**) and local small minimum at the calculated MJD of the single pod without effectors **(Figure 35e, Figure 34 arrow 2**). To get a better idea of how this left shoulder (**I**) changes with the conditions and strain, we the calculated the ratios between the different detected counts. In effector strain, non-secreting conditions the left shoulder is elevated 3.4 times in respect to the left shoulder (**I**) in the effector-less strain. Under secreting conditions, the shoulder (**I**) is even 4.9 times higher than in the effector-less strain. While this does not reflect the total changes of cargo in the cells quantified by MS (1/1.89/7.88) (**Figure 30**) it states a big chance by the addition of effector proteins rather than their levels.

Our results indicate that by increase in the amount of effectors cargo, the overall diffusion speed of SctQ slows down and possibly pushes the distribution of assembled subunits in the cytosol away from a SctQ oligomers (**Figure 35c**) and single pods (**Figure 35a**) to fully assembled six pod structures (**Figure 35b, Figure 34ab**). Further the data suggests a shift from empty pods (**Figure 35a**) to cargo loaded pods (**Figure**

***35*e**) and even cargo loaded fully assembled sorting platforms with effector proteins (**Figure 35d**), which still diffuse around the cytosol (**Figure 34bc**).

5.1.4.6 SctD does not strongly impact the diffusion of cytosolic SctQ and its effector binding

Since the presence of effectors reduces the diffusion speed of SctQ, we wondered which injectisome components are needed for this phenotype. First, we tested if cargo export and binding to the basal body was actually essential for the reduction of diffusion speed of SctQ and for the formation of the differently diffusion fractions we observed (**Figure 34**). We tracked PAmCh-SctQ in a strain where the inner membrane ring SctD, the binding site of the cytosolic components with the basal body, was deleted (**Figure 36**). In a effector-less strain, the deletion of SctD increased the median MJD from 285 nm to 301 nm (**Figure 36a**). The center peak (**III**) moved to the left from 270 nm to 307 nm, however a shoulder at 270 nm remains visible (**II**), although less prominent. At the same time, the left shoulder (**I**) decreased in abundance by approximately a factor of 2 (**Figure 36a**). This would indicate that while SctD is not needed to establish the described subpopulations as shown in **5.1.4.5 (Figure 35abc**), it may be needed to stabilize both the fully assembled sorting platform complex **(Figure 35b**), as well as the single pod **(Figure 35a**).

In the effector, non-secreting ΔSctD strain, with the addition of more cargo compared to the effector-less strain, the center peak (**II**) showed nearly no difference to the WT (**Figure 36b**). The left shoulder (**I**) increased slightly in abundance and the transition between the two fractions (**I->II**) is not as sharp anymore as in the WT (**yellow line Figure 36b**). The change from the effector-less strain to the effector strain, non-secreting, resulted in the micrographs in a visible increase in the red (slow) trajectories with no distinct subcellular localization. Interestingly, the presence or absence of virulence effectors has a bigger influence on the overall cytosolic mobility of SctQ than in the WT (median MJD: ΔSctD= 59.8 nm difference, WT= 34.2 nm) (**Figure 36ab**). While the connection to the basal body does not seem to be needed to establish the different populations of SctQ (**Figure 35**), SctD may be needed to stabilize those in the effector strain (**Figure 36a**). This does not seem to be the case in presence of the effectors under, non-secreting conditions (**I+II**) (**Figure 36b**). Although, it is tempting to speculate that since the slope between the center peak (**II**) and shoulder (**I**) is not as high anymore, SctD may be needed in this case for proper transition between those two states (**Figure 36b**).

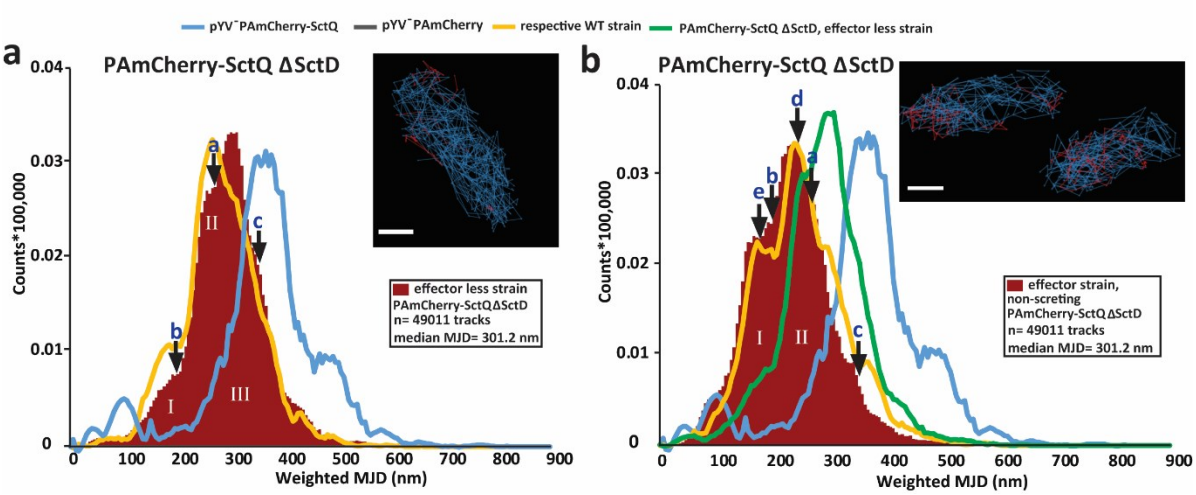

Figure 36 Impact of the inner membrane ring, SctD, on the cytosolic diffusion of SctQ.
Histogram of mean jump distances (MJD) in ΔSctD Strain. Red: MJD of PAmCh-SctQ in **(a)** effector-less strain (n = 5) **(b)** effector strain, non-secreting background strain (n = 3). Left: number of analyzed tracks and median MJD. Right: example PAmCherry-SctQ ΔSctD trajectories, slow fraction in red <180 nm MJD, fast fraction in blue >180 nm MJD. Scale bar 500 nm. The **blue line** displays MJD of pYV⁻ PAmCh-SctQ expressed from pBAD plasmid and induced with 0.05% L-arabinose. The **yellow line** displays the respective WT measurements from **Figure 34** while the **green line** represents the measurements from figure a. **a-e**: Theoretical diffusion speeds of different assumed cytosolic states (**Figure 35**). Measurements performed in collaboration with Alexander Balinovic.

5.1.4.7 SctK does not strongly impact the diffusion of cytosolic SctQ and its effector binding

After investigating the role of the basal body, we focused on the role of cytosolic components themselves in SctQ diffusion and interaction with cargo, starting with SctK. SctK is a 23.95 kDa protein with no clear homologue in the flagellum and connects the rest of the cytosolic sorting platform with the membrane ring SctD. To check if SctK is needed for the formation of the described sub-population in the PAmch-SctQ diffusion (**Figure 35**) and if the presence of SctK is required for a reduction in overall MJD by the addition of cargo, we tracked PAmCh-SctQ in a ΔSctK mutant effector-less and an effector strain, non-secreting conditions (**Figure 37**). The deletion of SctK did not have a big influence on the behavior of SctQ in the effector-less strain. The center peak stayed in the same position as the WT (**Figure 37a yellow line**) and the left shoulder (**I**) decreased a bit in abundance of detected counts compared to the WT. The addition of cargo into the cytosol by the effector strain, non-secreting, resulted in an overall reduction of median MJD by 57.3 nm in the ΔSctK mutant. This is also reflected in the micrographs. Here the increase of red (slow) tracks in the cytosol in the effector strain (**Figure 37b**). Further in the effector strain, non-secreting, the central peak (**III**) was reduced about a third, while the left shoulder (**II**) increased to nearly the same abundance as in the WT (**Figure 37b**). In addition to that a new local maximum appeared at 122 nm (**I**). Overall, these results show that SctK has no influence on the reduction of MJD. This indicates that SctK is not directly involved the cargo/effector recruitment. Since the transition between the left shoulder (**I**)

and central peak (**II**) is less clear in the effector-less strain (**Figure 37a**), this suggests that the interaction with the basal body may be needed to stabilize and facilitate the assembly of fully assembled sorting platforms from single pods. The appearance of new local maximum (**I**) could suggest that basal body connection is also needed for proper disassembly (**Figure 37b**).

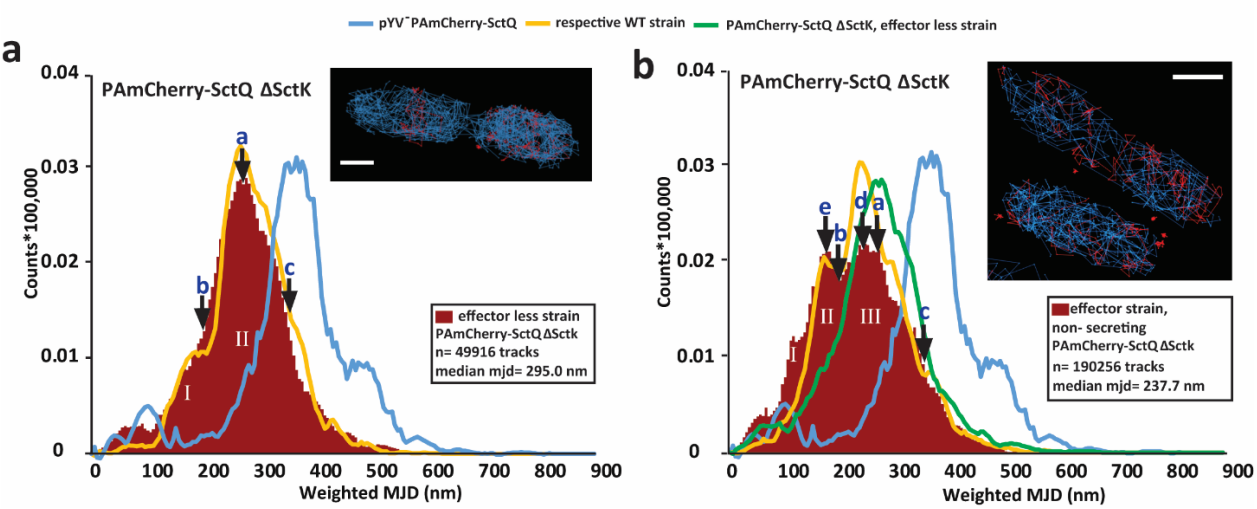

Figure 37 Impact of adaptor protein deletion SctK on the cytosolic diffusion of SctQ.
Histograms of PAmCh-SctQ in ΔSctK strains, **(a)** without virulence effector in effector-less background, (n = 4). **(b)** With virulence effectors (n = 2). Left: number of tracks analyzed for the respective blot and median MJD. Right: example of PAmCherry-SctQ ΔSctK trajectories, slow fraction in red <180 nm MJD, fast fraction in blue >180 nm MJD. Scale bar denotes 500 nm. **Yellow line** displays WT measurements in the respective background, **blue line** shows the MJD of pYV⁻ PAmCh-SctQ expressed from pBAD plasmid, induced with 0.05% L-arabinose and the **green line** represents the measurements from figure a. a-e: Theoretical diffusion speeds of different assumed cytosolic states as displayed in **Figure 35**. Measurements performed in collaboration with Alexander Balinovic.

5.1.4.8 SctL does not strongly impact the diffusion of cytosolic SctQ and its effector binding

Next, we decided to investigate SctL. SctL forms dimers (Bernal *et al.*, 2019), has a molecular weight of 24.93 kDa and connects the SctQ oligomers to the SctN hexamers underneath the injectisome (**Figure 2**). The deletion of SctL in an effector-less strain resulted in a reduction of abundance at the central peak (**II**), as well as the left shoulder (**I**). One part of the right shoulder increased substantially (**III**) to nearly the same size then the central peak (**II**) while a small maximum appeared even more right (**IV**). Based on the calculated MJD and the assumption that the central peak corresponds to one single pod (**Figure 35**), this would suggest that we shift the populations from a single pod (**Figure 35a**), which can now not assemble anymore, to mostly SctQ oligomers (**Figure 35c, Figure 38a)** and probably even smaller states (**IV**). SctQ still appears to interact with something (**I+II**), but the fractions are not as defined as previously seen in the left shoulder.

The addition of effector cargo to the system results in the overall reduction of median MJD by 60.1 nm, which reflected the increase of red trajectories throughout the cytosol displayed in the example cells (**Figure 38b**). The left shoulder (**I**) increases in comparison to **Figure 38a,** but did not reach WT levels (**yellow line Figure 38b**). The right shoulder (**III**) is still more dominant than in the previous measurements but has now one maximum (**Figure 38b**) again instead of two (**III**+**IV**) (**Figure 38a**). While the overall cargo loading still seems to work, this suggest that in the absence of SctL the signal or trigger for assembly of the single pods and fully formed sorting platforms results in misassembled and non-assembled of the sorting platforms.

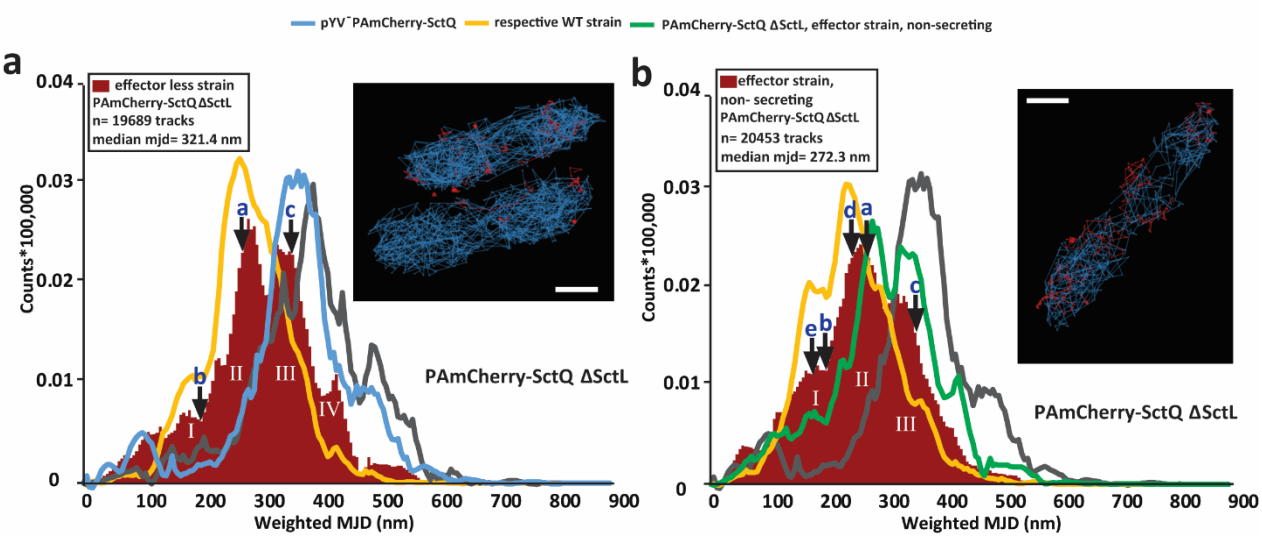

Figure 38 Impact of deletion of the negative regulator protein SctL on the cytosolic diffusion of SctQ.
Histograms displaying the MJD of PAmCh-SctQ in a ΔSctL strain, **(a)** measurements in the effector-less background and **(b)** in the effector background, non-secreting. Both: (n = 3) Left: number of tracks analyzed to generate this graph and median MJD in nm. Right: example of PAmCherry-SctQ ΔSctL trajectories, slow fraction in red <180 nm MJD, fast fraction in blue >180 nm MJD. **Yellow line** displays WT measurements in the respective background from **Figure 34**, **blue line** shows the MJD of pYV⁻ PAmCh-SctQ expressed from pBAD plasmid and induced with 0.05% L-arabinose and the **green line** represents the measurements from figure a, ΔSctL without effector proteins. **a-e**: Theoretical diffusion speeds of different assumed cytosolic states as displayed in **Figure 35**.. Measurements performed in collaboration with Alexander Balinovic.

5.1.4.9 SctL without SctQ is not able to form distinct subpopulations

To further investigate the role of SctL within the sorting platform, we directly tracked PAmCh-SctL in a ΔSctQ strain with effector proteins (effector strain, non-secreting). Here the median is at 270.3 nm and similar to the SctQ trajectories under effector, secretion conditions with some red tracks visible in the example cells, but no obvious patterns are observed. The center peak of the histogram is divided (**II**+**III**) into a bigger fraction with a maximum at 257 nm (**II**)and another that is a bit smaller with a maximum at 279 nm (**III**) (**Figure 39**). Overall the populations of effector strain, non-secreting, PAmCh-SctL ΔSctQ and effector strain, non-secreting PAmCh-SctQ ΔSctL are in the same area and the bigger maximum (**II**) of

PAmCh-SctL ΔSctQ at 257 nm correlates well with the calculated diffusion speed of a single pod, which is not present in this strain. Similar to a ΔSctQ strain, it would be possible that misinteraction occurs once the right partner is not present.

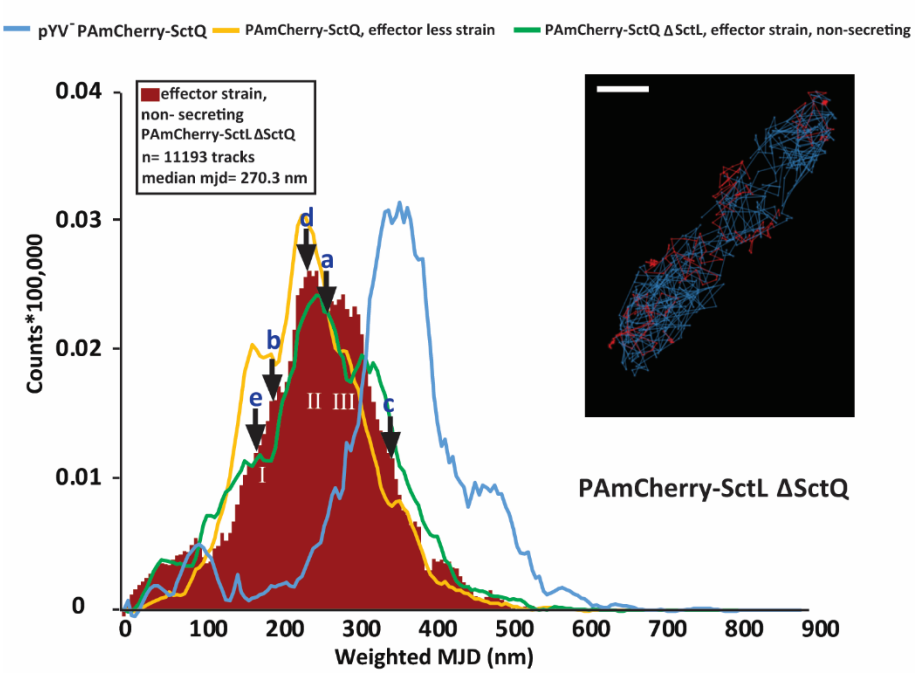

Figure 39 Diffusion behavior of PAmCh-SctL in ΔSctQ effector strain, non-secreting.
The red region displays is the histogram of PamCh-SctL (n = 2). Left: total number of tracks analyzed for this histogram and median MJD. Right: example of *Y. enterocolitica* PAmCh-SctL ΔSctQ cell with trajectories blotted, slow fraction in red <180 nm MJD, fast fraction in blue >180 nm MJD. **Yellow line** in the histogram displays WT measurements effector strain, non-secreting from **Figure 34**, **blue line** shows the MJD of pYV⁻ PAmCh-SctQ expressed from pBAD plasmid and induced with 0.05 % L-arabinose. The **green line** represents the measurements PAmCh-SctQ ΔSctL. a-e: Theoretical diffusion speeds of different assumed cytosolic states as displayed in **Figure 35**. Measurements performed in collaboration with Alexander Balinovic.

5.1.4.10 SctN is needed to form stable and distinct subpopulations

To complete our analysis of the cytosolic components, we tracked PAmCh-SctQ in a ΔSctN strains in both effector-less and effector, strain background under non-secreting conditions. SctN is a hexameric ATPase and is localized at cytosolic interface of the injectisome bound sorting platform and has a molecular weight of 47.71 kDa per monomer. Notably, SctN is besides SctQ the other protein of the cytosolic components for which an interaction with effectors and chaperones has been shown already (Akeda and Galán, 2005; Spaeth *et al.*, 2009; Lara-Tejero *et al.*, 2011). Deletion of SctN results in a distribution similar to a Gaussian distribution of PAmCh-SctQ around 300 nm MJD (**I**) in the effector-less background (**Figure 40a**). The left shoulder is not really visible anymore and the right shoulder shifted up to around 390 nm and is more prominent (**II**). Additionally, a second right shoulder appeared (**I**). While the overlap between the effector-less strain and ΔSctN background is still relatively large, the center of peak (**I**) is less sharp than

before (**Figure 40a**). Distribution and position may suggest a constant binding and unbinding of subunits and effectors, which do not stay in transient interactions or a complete collapse of the cytosolic interactions. Distinct changes can be observed with the addition of effector proteins, non-secreting conditions (**Figure 40b**), where the overall MJD is at 307.3 nm and the majority of the trajectories are under 200 nm MJD (**I**) (**Figure 40b**). The histogram displays multiple wholes and the correlation with previous states is not visible anymore (**Figure 40b**). Further cells start to display larger accumulations of tracks at the poles on top of the population within the cytosol. This may suggest that without effectors the interactions in the cytosol are very transient and may fall apart quickly which resulting in the Gaussian-like distribution (**Figure 40a**). The introduction of effector proteins may result in protein misfolding and aggregation of a majority of SctQ and in a magnitude that this are exclusions to the poles(**Figure 40b**).

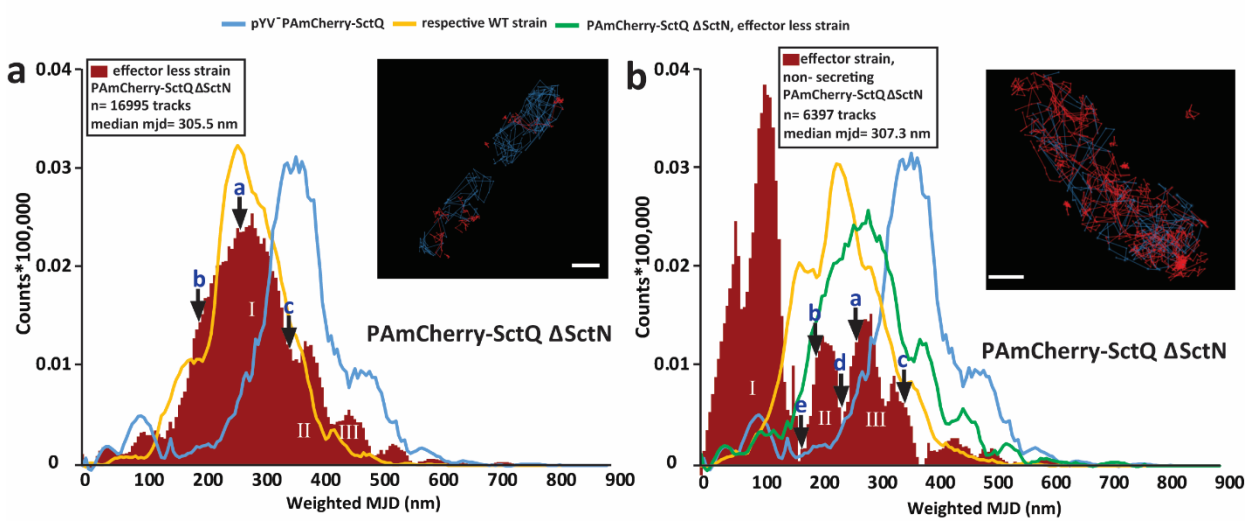

Figure 40 Impact of ATPase deletion SctN on the cytosolic diffusion of SctQ.
Histogram of PAmCh-SctQ MJD's in ΔSctN strain measured without and with effector proteins in the cell. **(a)** Measurements in an effector-less strain background. **(b)** Measurements in a effector strain, non-secreting. Left Box: number of foci analyzed for this histogram and median MJD, right: example cell with trajectories botted. Slow fraction in red <180 nm MJD, fast fraction in blue >180 nm MJD (n = 3). **Yellow line** displays effector-less/effector strain measurements from **Figure 34**, the **blue line** shows the MJD of pYV⁻ PAmCh-SctQ expressed from pBAD plasmid and induced with 0.05% L-arabinose and the **green line** represents the measurements PAmCh-SctQ ΔSctL. **a-e**: Theoretical diffusion speeds of different assumed cytosolic states as displayed in **Figure 35**. Measurements performed in collaboration with Alexander Balinovic.

5.1.4.11 Impact of effector cargo on SctQ alone

In an attempt to narrow down the effect the addition of cargo, in form of effectors, has on the diffusion of SctQ, we built up a minimal system. To this aim, we expressed PAmCh-SctQ from a constitutive promotor (pACYC184) in pYV⁻ strain and added, from the inducible *pBAD* promotor on a separate plasmid, increasing amounts of the effector YopO and its cognate chaperone SycO (*pBAD::sycO-yopO*. SycO) (**Figure 41**). Tracking of PAmCh-SctQ alone, in a strain where SycO and YopO expression was inhibited by addition

of 0.2% glucose, resulted in a histogram with several local maxima ((**I**) 192 nm, (**II**) 267 nm, (**III**) 307 nm, (**IV**) 372 nm, (**V**) 432 nm, (**VI**) 472 nm, (**VII**) 532 nm) where the cells display homogenous trajectories. The (**II**) 267 nm and (**IV**) 372 nm peaks are close to the peaks observed for PAmch-SctQ effector-less strain, as well as for the calculated MJD for the fully assembled pod (**Figure 35a**) and for a SctQ oligomer (**Figure 35c**).

Interestingly the expression of SycO and YopO by induction of with 0.05% L-arabinose results in an increase of median MJD from 327.2 nm (0.2% glucose) to 336.5 nm (**Figure 40ab**). Additionally, a drastic change in distribution could be observed which is now only present in one central peak (**I**)(337 nm). The trajectories within the cells seem to increase compared to the previous conditions but stay homogenous (**Figure 40b**). The main peak (**I**) in the histogram does not correlate with any of the peaks observed prior but, strikingly were previously a local minimum was located (between (**III**) and (**IV**)332 nm (**Figure 40a**) the new global maximum is located now (**I**) (**Figure 40b**). It may be possible that the introduction of effector proteins pushes all SctQ molecules from an equilibrium state of different oligomers into a single oligomeric cargo bound state.

Further increase in effector cargo (0.2% L-arabinose), splits the single peak (**I**) (**Figure 40b**) again into a left maximum (**I**) at 172 nm and a (**II**) right maximum around 477 nm with a strong shoulder (**III**) (**Figure 40c**). Overall those measurements look more similar to the non-included measurements (**Figure 40a**) then to the low induced once (**Figure 40b**). The trajectories show an increase in slow red tracks corresponding to peak (**I**), while the blue tracks seem be less dense. The median MJD is reduced to 306.9 nm (0.05% L-arabinose: 336.5 nm). The central peak overlaps mostly with the peak measured with 0.05% L-arabinose (**Figure 40b**). The left peak overlaps to a certain degree with the histogram measured for PAmCh-SctQ in a effector strain background, as well as the calculated MJD, for fully assembled sorting platform. Although the addition of effector and chaperone proteins has a clear influence on the MJD and shape of the histogram, it remains hard to pinpoint their exact nature.

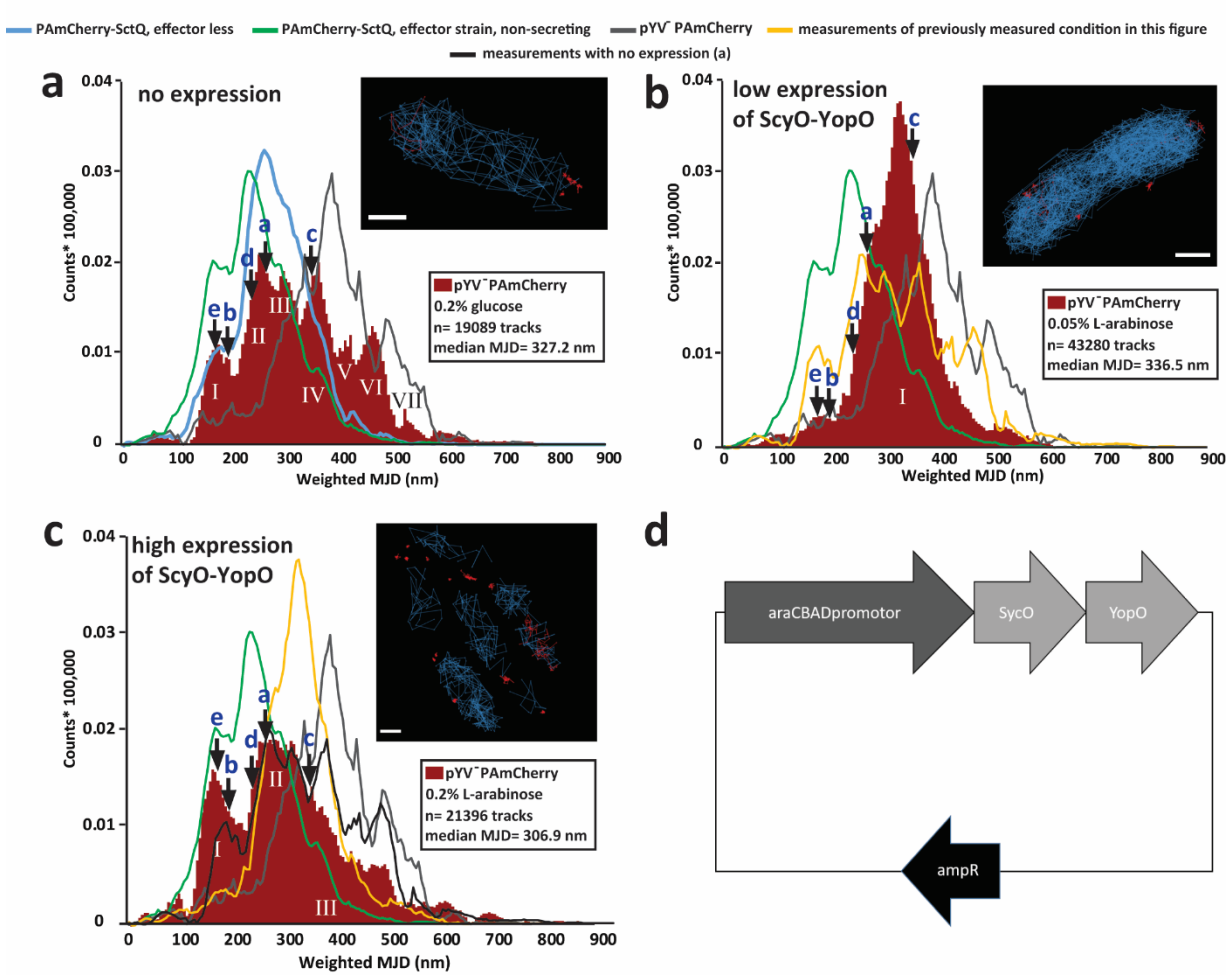

Figure 41 Impact of SycO and YopO on the diffusion of SctQ in a pYV⁻ strain.
Histogram of PAmCh-SctQ constitutively expressed from the pACYC184 plasmid in a pYV⁻ strain together with: **(a)** SycO and YopO on the pBAD plasmid, expression inhibited by addition of 0.2% glucose; **(b)** Expression induced with 0.05% L-arabinose; and **(c)** Expression induced with 0.2% L-arabinose. Upper right: example cells of *Y. enterocolitica* pYV⁻ in respective condition with trajectories of PAmCh-SctQ blotted. Slow fraction in red <180 nm MJD, fast fraction in blue >180 nm MJD.s Lower right: number of tracks analyzed for the blot and median MJD. **Grey line:** pYV⁻ PAmCh expressed from pBAD plasmid and induced with 0.05% L-arabinose. **Blue line:** PAmCh-SctQ in the effector-less background. **Green line:** PAmCh-SctQ in effector strain, non-secreting background. **Yellow line:** Previous condition measured in this figure (n = 4). a-e: Theoretical diffusion speeds of different assumed cytosolic states as displayed in **Figure 35**. Measurements performed in collaboration with Alexander Balinovic.

At this point our collective results indicate that the addition of effector cargo to the cytosol of *Y. enterocolitica* has a clear effect on the diffusion of SctQ and slows down the MJD by at least 34 nm. Since the deletions of SctD, SctK and SctL show no major effects on the interaction of effector proteins with SctQ (**Figure 36**, **Figure 37**, **Figure 38**) they do not seem to be involved in this phenotype, although SctL may be needed to prevent misassembly under secretion conditions. The deletion of SctN on the other hand seems to abolish formations of precise sub-complexes under non-secreting conditions (**Figure 40**). Addition of more effector proteins leads to multiple maxima and a near stationary population within the cytosol (**Figure 40**). This could point out a central role of SctN for preassembly of complexes and effector

recruitment. Our attempts to build up a system with only SctQ resulted at least in one concentration in the formation of one homogeneous peak, which could correspond to the SctQ effector loaded state (**Figure 41**). This could suggest that while binding of effectors to SctQ seems does not require SctN (**Figure 41**), it may has a role in stabilizing the sorting platform interactions as well as removing loaded effectors from SctQ. The slowing down effect by addition of the effector proteins is clearly documented with these experiments. The change in SctQ diffusion as well as the results of the deletion strain, strongly indicates an interaction between SctQ and the effector proteins. Further our data indicates, that the addition of effector proteins into the system, triggers a rearrangement of the interactions within the cytosol. Where this effect originates precisely from and if this is due to the direct or interaction of SctQ and the effector in the cytosol, still needs to be found out. Despite our best efforts, the identification of the members and stoichiometries of the observed transient complexes remains speculative at this point.

6 Discussion II

6.1 Discussion - Binding of effector proteins to the cytosolic injectisome components and their role in secretion in *Y. enterocolitica*

In our study, we investigated the impact of effector proteins on the molecular dynamics of the *Y. enterocolitica* injectisome cytosolic components, also termed the sorting platform. This was done to with the ultimate goal to clarify the effector - sorting platform interactions. Previous work showed that the cytosolic components form large diffusing complexes in the cytosol, even in the absence of the membrane ring SctD (Diepold *et al.*, 2017; Rocha *et al.*, 2018). While the complexes are influenced by the status of the system (secreting/non-secreting), the exact composition is still debated (Lara-Tejero *et al.*, 2011; Diepold *et al.*, 2017; Rocha *et al.*, 2018; Bernal *et al.*, 2019; Lara-Tejero, 2020). Further, the impact of the effector proteins on these complexes has not been investigating *in vivo* (Lara-Tejero *et al.*, 2011; Diepold *et al.*, 2017). Here we present the first evidence that the effector proteins bind to the major pod protein, SctQ, thereby slowing down its overall diffusion speed in the cytosol (**Figure 34**). Deletions of the inner membrane anchor protein SctD, or the other cytosolic components SctK, SctL do not appear to impact the binding, indicating that the interaction with SctQ is directly involved in the process, while SctN seems to be needed for proper subunit assembly.

6.2 Identification of novel binding partners via CoIP and quantification of Cargo in different strain backgrounds

In an initial attempt to investigate the interactions of the cytosolic components, we performed a CoIP assay with PAmCh-SctQ in the effector-less strain background (**Supplemental table 2**). Our results confirmed the previous findings that the cytosolic components, SctK, SctQ, SctL and SctN interact with each other (Diepold *et al.*, 2017; Bernal *et al.*, 2019). In terms of subunit composition in the cytosol, this attempt did yield any information exciding the already published once. Here the Halo-SctQ/Halo-SctL gentle and specific co-immunoprecipitation method revealed that all four cytosolic components can form stable interactions, where SctN seems to be the stabilization and anchor point of those interactions since they are not detectable anymore upon SctN deletion (Diepold *et al.*, 2017; Bernal *et al.*, 2019). At this point we were able to confirm those interactions. Further, we were unable to gather more substantial evidence for interactions of chaperones, effectors or other regulatory proteins with SctQ by this CoIP

(**Supplemental table 2**). Previous more gentle methods like Yeast two-hybrid assays (Spaeth *et al.*, 2009) and blue native pages (Lara-Tejero *et al.*, 2011) that do not rely on copurification, were able to see interactions of SctQ and chaperones in the past (Spaeth *et al.*, 2009; Lara-Tejero *et al.*, 2011), while other CoIP approaches failed as well (Diepold *et al.*, 2017). Overall the biggest bottleneck in the current CoIP protocol is sufficient cell lysis. Although we were able to open up some cells, a substantial amount of sample remained in the pellet. Different sonication methods, as well as spheroplastation, did not improve cell lysis. Before continuing with further experiments, this needs to be addressed. Using a French press to open up the cells, stop supplementing DAP to maybe weaken the cell wall, or a more aggressive pre-digestion with lysozyme could be options. A transition from the effector-less strain to the effector background may allow easier cell disruption as well since these bacteria are not grown with the addition of DAP in the media and therefore may have a weaker cell wall. The incorporation of secreting conditions into the experiment would additionally allow us to screen more efficiently for interactions between effectors, chaperones, and the cytosolic components since under secreting conditions the virulence effectors are substantially upregulated (**Figure 30**) (Büttner, 2012; Deng *et al.*, 2017; Milne-Davies *et al.*, 2019). At this point and to the best of our knowledge, it is the first time that anyone has compared the amounts of export substrate present within the *Y. enterocolitica* cells under the different conditions on a protein level (**Figure 30**). The quantification of effectors and chaperones in two of the tested conditions (effector strain) under secreting and non-secreting conditions indicated that a small pool of effector proteins are pre-synthesized before export. Although the data also shows a small number of false positives in our measurements (**Figure 30**) (the effector-less strain, has no virulence effectors, a small amount of them is detected), this is in order with experiments previously performed in our lab (unpublished work PhD thesis Milne-Davis 2021). Overall, since the interactions of the cytosolic components with the secretion cargo appeared to be too transient to be detected with the CoIP method, we turned to another approach.

6.3 Secreting and non-secretion conditions do not influence the diffusion of cytosolic PAmCh

To investigate the impact of effector proteins on the cytosolic components we established a protocol for sptPALM in *Y. enterocolitica* (**Figure 31**). First, we analyzed the diffusion of PAmCh under secreting and non-secreting conditions. The resulting histograms indicated that global cytosolic diffusion is not affected by the activation of the injectisome (

Figure 32). Given that a number of essential cell maintenance processes rely on diffusion (Min system, Par system, chemotaxis (Treuner-Lange and Søgaard-Andersen, 2014; Surovtsev and Jacobs-wagner, 2018), it is not too surprising that a process that is evolutionary optimized to ensure cell survival does not interfere with one of the essential processes within the cell.

6.4 Interactions with effectors and injectisome components soll down the diffusion of PAmCh-SctQ

Next, we investigated the diffusion speed of PAmCh and PAmCh-SctQ in a pYV^- strain (**Figure 33**). The addition of the 34.35 kD protein SctQ, to the 26.8 kDa PAmCh slowed down the diffusion (ΔMJD of 26.1 nm) (**Figure 34**). Since protein diffusion does not linearly correlate with the molecular weight of the proteins (Kumar *et al.*, 2010; Parry *et al.*, 2014) this was not surprising. The measurements in a pYV^- strain, that has now other injectisome components, together with *in trans* expression of SctQ and the effector YopO as well as its cognate chaperone SycO showed a direct effect on the diffusion of PAmCh-SctQ (**Figure 41ab**). A high expression of SycO and YopO mimicked more the diffusion of non-induced experiment (**Figure 41ac**), than the low induced version and came with an addition of stationary PAmCh-SctQ in clusters visible in the micrographs (**Figure 41b**). This could suggest two things: At high expression, the used native operon structure (SycO-YopO) could reach its limits which leads to mostly expression of SycO alone, instead of expression of both proteins. The elevated SycO levels could in turn result in an aggregation of PAmCh-SctQ explaining the clusters. The other possibility would be that the high expression of SycO and YopO themselves, lead to aggregations and due to that SycO, YopO are not available anymore to interact with PAmCh-SctQ. Those bigger aggregation bodies could be what we see as clusters, while the rest of the PAmCh-SctQ population is diffusing freely in the cytosol. This would explain the similarity to the non-induced measurements. Never the less, together with already published data our results indicate again that we have a binding of effectors proteins to SctQ (**Figure 41**) (Spaeth *et*

al., 2009; Lara-Tejero *et al.*, 2011). After establishing this baseline, we transitioned to measurements in the complete system. The first measurements already indicated by a change in MJD and orientation of the of SctQ population that PAmCh-YscQ is not diffusing alone in the effector-less strain background peak (**I**) (**Figure 34a**). This is in agreement with previous work, which suggested that a formation of a SctL-SctQ as complex, together with different other states of the sorting platform components in the cytosol (**Figure 34**, **Figure 35**, **Figure 39**, **Figure 42**)(Diepold *et al.*, 2017; Rocha *et al.*, 2018; Bernal *et al.*, 2019).

6.5 Identification of subcomplexes based on theoretical MJDs

The assumption that one fully assembled pod of the sorting platform complex might be the highest abundant peak in our diffusion measurements is based on three aspects. (i) The fact that Bernal *et at*. 2018 identified amongst others, pre-assembled pods as most abundant form in a population of different bigger and smaller complexes in cytosolic components in *S. enterica* with native MS. (ii) While Brownian diffusion using Einstein-Stokes can just be an estimate for the diffusion of the pod in the cell (unknown viscosity, crowding, confinement or charge effects), it yields an theoretical expectation value of 346.19 nm as JD for the pod **(a)** which is close to the diffusion of the most abounded peak in our measurements (**II**). (iii) Since we measured the diffusion of PAmCh-SctQ alone and it displayed a faster diffusion behavior (**Figure 33**), this can be excluded. Noteworthy at this point is also that the measurements of PAmCh and PAmCh-SctQ are more affected by the confinement of the cell and are probably representing an underestimation of their speed which becomes visible by looking at their theoretical JDs (PAmCh: 1372.99 nm, SctQ oligomer: 791.51 nm). Based on this argumentation, we tentatively assigned molecular weights and assembly states to the peaks detected in the sptPALM measurements (**Figure 35**). These values are theoretical and the assignment of the reference point, the fully assembled pod, lacks direct experimental evidence at the moment. Nevertheless, this allows us in the PAmCh-SctQ measurements in effector-less strain to identify the left shoulder (**I**) as potential fully assembled sorting platform (**b**) and the smaller right shoulder (**II**) as SctQ oligomer (**c**) (**Figure 34**, **Figure 35**). That this point it needs to be noted, that while those values are based on theoretical assumptions, they fit strikingly the maximum of our measured data (**I**)-(**III**) (**a**-**c**) (**Figure 34**, **Figure 35**). In favor of this assignment is that the identified SctQ oligomer (**c**) (**III**) diffuses with 350 nm MJD, close to the median MJD of PAmCh-SctQ in the pYV$^-$ (**II**) (median MJD 372 nm, left part of the peak 357 nm) (**Figure 33**). While an SctQ oligomer diffusion state has also been identified already (Rocha *et al.*, 2018; Bernal *et al.*, 2019), the fully assembled sorting platform remained speculative in the past.

6.6 Effector proteins bind to SctQ and alter the interactions of all cytosolic components

Changing from the effector-less strain under non-secreting conditions to the effector strain, non-secreting conditions, slows down the overall diffusion speed of SctQ (**Figure 34b**). The presence of effector proteins (non-secreting) in this still moderate concentration (**Figure 30**), influences the median diffusion speed of the cytosolic components already. This finding itself is novel and has to our knowledge not been shown before (**Figure 34ab**).

The effect on the diffusion of SctQ is drastic and suggests major changes in the interaction dynamics or diffusion behavior of SctQ (**Figure 34**). The calculated diffusion speeds of SctQ further indicate that this is caused by more than the sole addition effector proteins to the subunit in the cytosol (**f**) (**Figure 35**). This indicates that with the addition of the effector proteins, a rearrangement of the cytosolic interactions of the sorting platform components takes place. In the full systems, the left local maximum (**I**) (**Figure 34ab**) (peak 177 nm MJD) is more pronounced in the presence of effectors. Since we see differences of abundance on the peaks (**I-III**), it is tempting to speculate that this contributed to changes in cytosolic interaction with the introduction of effector proteins (**Figure 34**). Based on calculated diffusion the two major peaks, the later local (**I**) (177 nm) and global maximum (**II**) (242 nm) would fit strikingly to the theoretical MJDs of a single pod (**e**) and the fully assembled sorting platform (**d**) in an effector loaded state (**Supplemental table 5**, **Figure 34**, **Figure 42**).

The addition of more effector proteins by induction of secretion did not result in drastic changes (**Figure 34c**). Noteworthy, the center peak (**II**) was reduced, while the left peak (**I**) was slightly increased. This suggests again that the observed change in diffusion can be attributed to the presence of effector proteins that trigger changes in interactions of the sorting platform rather than to only effectors being loaded according to their abundance within the cell (**Figure 30**). Since the changes in median MJD (**Figure 34**) do not correlate directly with the changes in cargo (**Figure 30**), this could be attributed to an early saturation of binding sites of the sorting platform. If that's the case the dynamics underneath the injectisome (Diepold *et al.*, 2017) might be needed to ensure a constant supply of effector proteins to the system.

It was shown earlier (Diepold *et al.*, 2017 in the effector-less strain that interactions of the cytosolic components get more transient under secreting conditions. Since we do not see a decrease in the left shoulder (**I**) (**Figure 34**), this state (**b**/**d**) must either have a high turnover rate or must be stabilized by the presence of the effectors. Increasing the amount of effector loaded sorting platforms within the cytosol

under non-secreting conditions, could be one way to ensure already that the injectisome is constantly able to export cargo once activated and to reach the high export rate of thousand effectors per minute described in the literature (Schlumberger *et al.*, 2005).

Less likely but it cannot be fully excluded at this point is also, that the effectors do not directly bind to SctQ, but to SctN and we only see the downstream effect of interaction. This would also mean that the introduction of effectors under non-secreting conditions in the effector strain results in stronger interactions between the cytosolic sorting platform components (**Figure 30**, **Figure 34**). Since it has been shown on the other hand that interactions between cytosolic components get more transient under secreting conditions (Diepold *et al.*, 2017), the test deletion (ΔSctD,K,L) do not influence the effector binding and we see a response in the MJD of SctQ alone after induction of effector proteins (**Figure 41**), this is less likely. Tracking of SctN with sptPALM in the future would allow us to investigate this and the overall role of SctN further.

6.7 SctD, SctK and SctL are not evoled in effector binding

To determine the role of the inner membrane ring component SctD and its cytosolic interactor SctK as well as the connection of the cytosolic components to the basal body we introduced PAmCh-SctQ into different deletion backgrounds (ΔSctK **Figure 36,** ΔSctD **Figure 37**). The overall diffusion speed of PAmCh-SctQ was not affected in both strains. This indicates that the dynamic interactions resulting in the reduced diffusion speed of PAmCh-SctQ in the presence of effectors, work independently of connection to and the presence of the basal body, which is in line with previous results (Diepold *et al.*, 2017). The decrease of the slopes (left shoulder (**I**), (**I**)→(**II**) (**Figure 36**) and (**I**)→(**II**) (**Figure 37**) and reduction in abundance between different attributed states (**a-f**) (**Figure 36**, **Figure 37**), could additionally hint that while the connection is not needed to establish the different diffusion states, it aids in the correct assembly and or transition between them (single pod (**a/e**) and the full sorting platform (**b/d**) (**Figure 35**, **Figure 42**). If that is true, the presence of the additional local maximum at 117 nm MJD, close to being stationary, could be interpreted as the first indication of misinteraction in the dynamic process (**Figure 37b**).

Similar to the deletion of SctK, the deletion of SctL does not show an effect on the general reduction in SctQs MJD by the addition of effector proteins (**Figure 38**). SctL is one of the direct interaction partners of SctQ and establishes the interaction of SctQ to SctN at the injectisome (**Figure 42**). This argues again that a direct interaction of effectors and SctQ is needed to slow down the diffusion of SctQ and trigger the

change in cytosolic interactions. It could also suggest that interaction change within the cytosolic sorting platform components and that in the absence of the right interactors another is bound. Since direct interactions between SctQ and SctN could not be identified via native mass spectrometry (Bernal *et al.*, 2019), but have been shown in CoIPs, although probably of an indirect nature (Diepold *et al.*, 2017), it is difficult to pinpoint what happens here exactly. While it is tempting to speculate that the left peak (**I**) in this strain (172 nm) corresponds not to the fully assembled sorting platform, but to a less stable or non-linear interaction between SctQ, SctN and SctK without SctL but solid evidence is lacking for this at the moment (**Figure 38**). If one assumes that these interactions without SctL can happen but are less stable than interactions of all four cytosolic components, the fact that this peak (**I**) (172 nm) is reduced in the ΔSctL strain by half in abundance compared to the WT would at least fit to the assumption of reduced stability.

6.8 SctN is needed to stabilize cytosolic complexes

In a SctN deletion background, all previously observed peaks for PAmCh-SctQ are shifted (**Figure 40a**). So the deletion of SctN seems to abolish most interactions of SctQ with other proteins. This would be in agreement with previous experiments indicating that SctN is required to stabilize the interactions of the cytosolic components (**Figure 40**) (Diepold *et al.*, 2017). Due to the fact that SctL and SctK are still present in the strain, they might interact very transiently with SctQ. If those interactions are not stabilized by SctN anymore, this could result in the near to Gaussian shape that we observe (**Figure 40a**). The introduction of effector proteins has a striking effect on the PAmCh-SctQ ΔSctN strain. Diffusion of SctQ slows down and the distribution of the MJD is not at all close to Gaussian distribution anymore (**I**)-(**III**) (**Figure 40b**). This suggests that the presence of effectors in the cell triggers an increased assembly of pods (**a**) and sorting platforms (**b**). Since SctN, which is required for proper assembly, is absent in this strain, these subassemblies mislocalize. Studies from Bernal and colleagues (2019) in *Salmonella* with native MS and Diepold and colleagues (2017) in *Y. enterocolitica* with CoIP, were able to identify cytosolic complexes (Sct,K,Q,L) in the absence of SctN. In the later, the occurrences of those were strongly reduced. While in *Y. enterocolitica* (Diepold *et al.*, 2017) and *S. flexneri* (Johnson and Blocker, 2008), SctN is essential for assembly of the cytosolic components, in *Salmonella* those complex can form in the absence of SctN (Lara-Tejero *et al.*, 2011; Zhang *et al.*, 2017). Overall the phenotype presented by the ΔSctN strain is very impressive, it is not in order with previous visualizations of EGFP-SctQ in ΔSctN which could show to be

just cytosolic future (Diepold et al., 2010; Diepold et al., 2017) and needs to be further evaluated in the future.

Taken together, our study has shown for the first time that the presence of effector proteins slows done the diffusion speed (MJD) of the cytosolic pod protein SctQ (**Figure 42**). While more experiments are needed, this suggests that SctQ is the direct target for the effector interaction of the sorting platform. Additionally, the association of local and global minima and maxima with theoretical MJDs, permits us to speculate about different assembly and interaction states of the cytosolic sorting platform. Here the higher ordered states seem to increase in abundance upon the introduction of effectors. Interestingly the increase of effectors within the cell does not correspond with the increase of those higher or slower diffusing states. Further research, especially the tracking of PAmCh-SctN in different background (effector-less strain/effector strain/pYV$^-$ and +/- effectors) will allow us to test the theories brought forth by our speculations and further clarify how the adaptive dynamic network governs protein export and order via the injectisome.

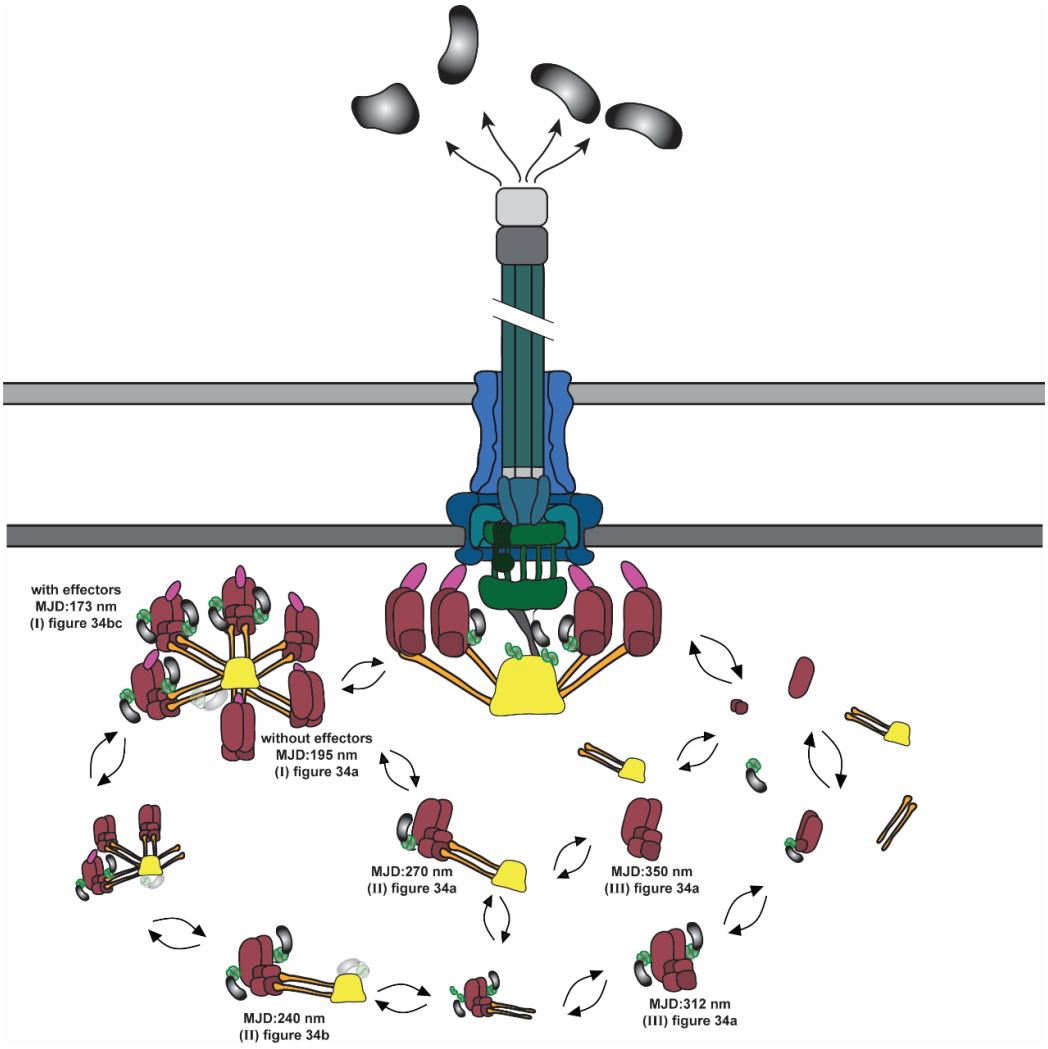

Figure 42 Schematic representation of interactions in the cytosol of *Y. enterocolitica*.
Model representing the possible interactions within the cytosol. Bigger and with theoretical MJD and figure and peak assignment are the states that we were able to present evidence for also listed in figure (**Figure 35**). Represented in smaller comics and without MJD assigned are states that we know exist from previous research (Diepold *et al.*, 2017; Rocha *et al.*, 2018; Bernal *et al.*, 2019), or transient states that may exist in the assembly of the bigger complexes. Black and green effectors are states of which experimental evidence exists, transparent ones have not been directly observed.

6.9 Acknowledgments for this work

We thank Bartosz Turkowyd (Max Planck Institute Marburg, Germany; currently Carnegie Mellon University, Pittsburgh, PA, USA) for his contribution in the first test runs of the experimental setup, as well as data analysis and continuous help with coding and scripts as well as input for data analysis and discussions.

7 Overall conclusions and outlook

During my PhD I set out to investigate the molecular function and regulation of the bacterial type three injectisome of *Y. enterocolitica*.

I investigated and described the effect caused by low environmental pH on the injectisome of *Y. enterocolitica*. Using a combination of flow-cell-based TIRF microscope, sptPALM, protein overexpression and functional assays, we found that in gastrointestinal pathogens the cytosolic injectisome components are temporarily released from injectisome at low external pH. This mechanism prevents effector secretion in acidic environments such as the stomach. Notably, this is the first time that the dynamics of the cytosolic components have been linked to a mechanical function and physiological benefit. We were further able to identify SctD as the protein that detects the low external pH in the periplasm. Its partial dissociation from the inner membrane ring causes in turn the dissociation of the cytosolic injectisome components from the injectisome. Upon restauration of neutral pH, this is reversed resulting in a fast recovery of effector secretion. Further, a dissociation of SctD can be prevented by *in trans* overexpression of the protein which leads to a stabilization of SctD clusters in the membrane. In conclusion, our findings indicate that the cytosolic components form an adaptive regulatory interface, which regulates injectisome activity in response to environmental conditions (such as the pH). During our research on that topic, we did several additional experiments that did not make it into the manuscript. Collectively, they suggest that the injectisome basal body is more dynamic than the field assumes right now. By defining and utilizing a “fluorescence intensity dilution exchange assay” we were further able to show that SctD subunits can be exchanged in an assembled injectisome. While in both those approaches more experiments are needed they have the potential to significantly change our view on the injectisome while extending our knowledge on the architecture of this molecular nano-machine. We will follow those promising directions during my postdoc wrap-up phase.

In the second project, I described the impact of effector proteins on the dynamics of the cytosolic components in an attempt to elucidate how the cytosolic components contribute to effector selection and export on a molecular level. We were able to show that the presence of effector proteins slows down the overall diffusion speed of the cytosolic component SctQ. At this point our data suggests a direct, transient interaction of the effector/chaperon proteins to the SctQ. SctK and SctL are not needed to establish those interactions and that effector binding to SctQ still occurs in those in export deficient strains lacking SctK or SctL. Our measurements and the correlations with the calculated MJDs based on the molecular weight of the proteins further suggest a shift in the arrangements of the sorting platform

components in the cytosol. This could be the transition from monomers to the assembly of single pods and/or from single pods to a completely assembled sorting platform. While we made significant progress on the impact of effector proteins on SctQ, SctL, and SctK and could show that the connection of the basal body (SctD) is of less importance, we still need to further investigate the diffusion behavior of SctN in more detail to clarify its role in the sorting platform. Similar to the initial results of the previous topic, the open questions will be followed up during my postdoc wrap-up phase.

8 Supplemental figures and tables

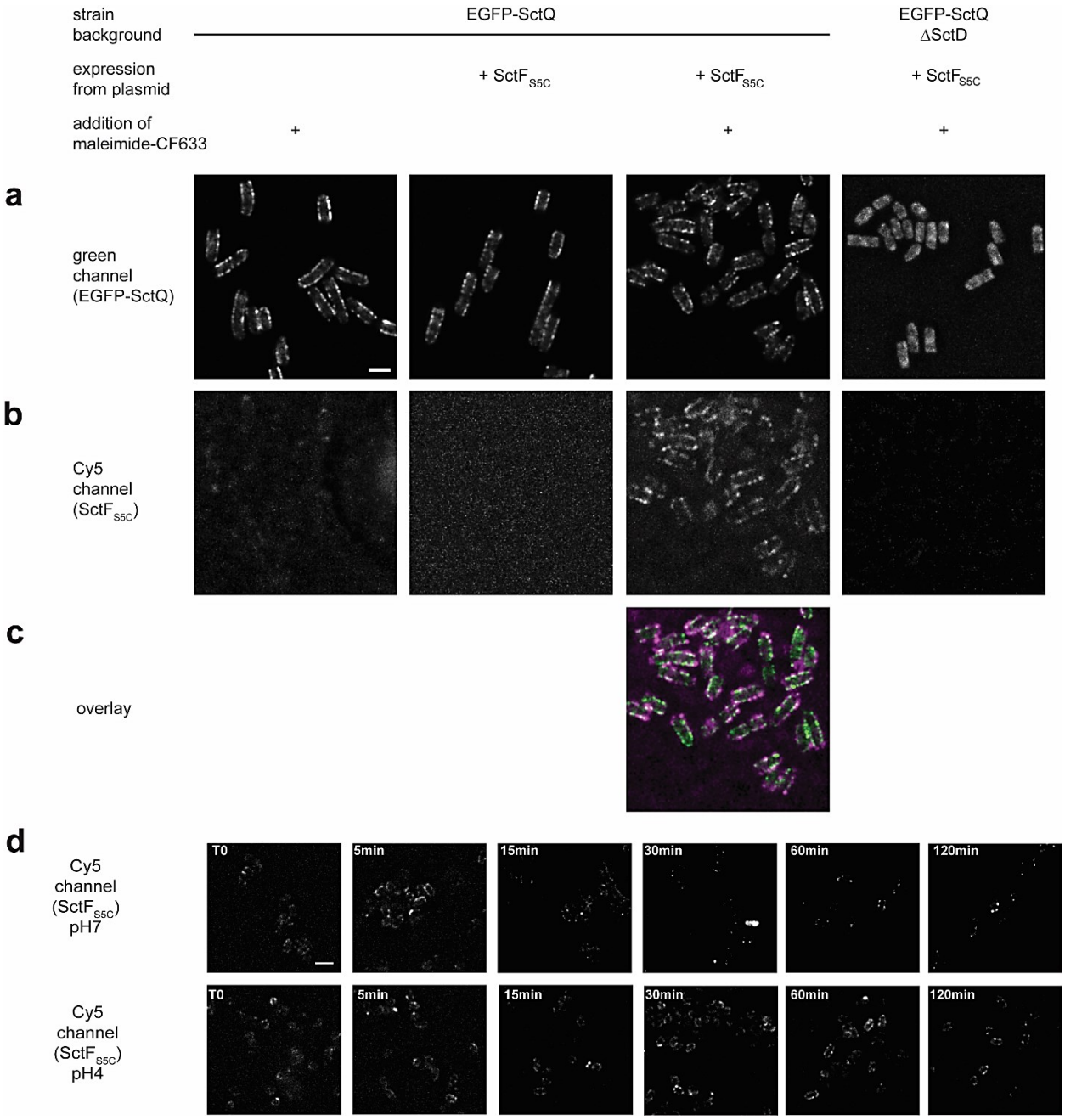

Supplemental Figure *1* Specificity of maleimide-based labeling of SctF$_{S5C}$
Fluorescence micrographs of *Y. enterocolitica* strains expressing **(a)** EGFP-SctQ from the native chromosomal locus and **(b)** SctF$_{C5S}$ from plasmid a pBAD plasmid. Where indicated, induced with 1.0% L-arabinose. Bacteria were stained using CF 633 maleimide dye, where indicated, and imaged in the green and Cy5 channel **(c)**shown in magenta in the overlay). Experiments were carried out in 3 independent repetitions (n = 3). **(b)** Time course microscopy expressing SctF$_{C5S}$ from its native locus on the chromosome. The bacteria were stained again with a CF 633 maleimide dye and incubated for the indicated time. The experiment was carried out in 2 independent. Scale bar, 2 µm.

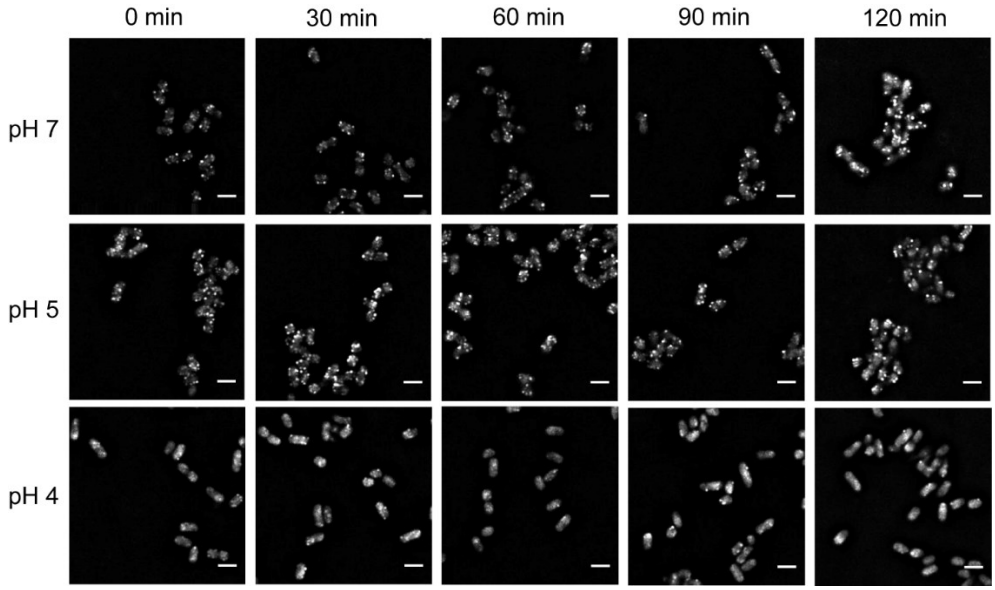

Supplemental Figure 2 The localization of the cytosolic components remains stable over time.
Fluorescence micrographs of *Y. enterocolitica* EGFP-SctQ, incubated at the indicated external pH values under secreting conditions over time. n = 2. Scale bars, 2 µm.

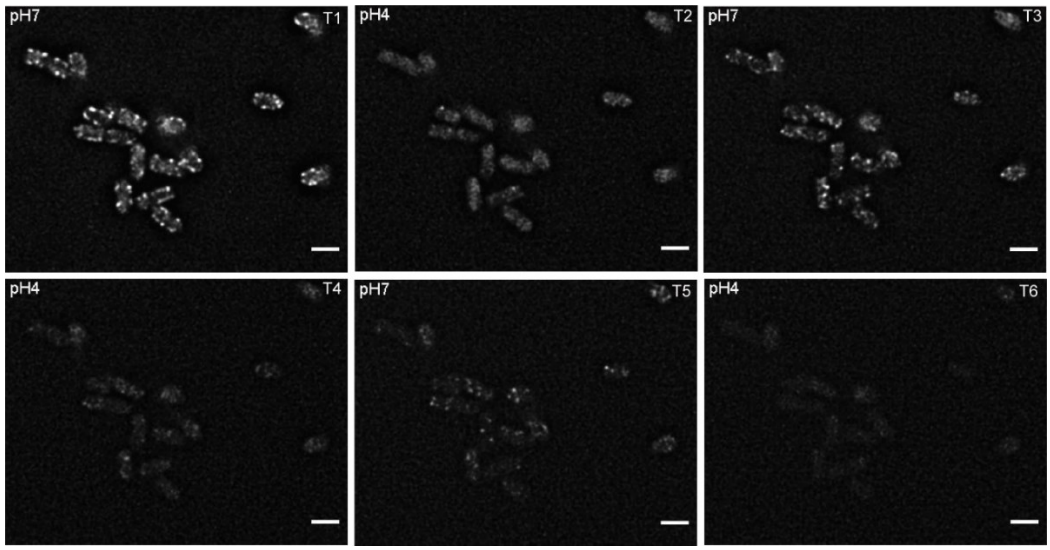

Supplemental Figure 3 The pH-induced dissociation and re-association of EGFP-SctK to the injectisome can be repeated for several cycles.
Excerpt from time-lapse video of *Y. enterocolitica* expressing EGFP-SctK attached to a glass cover slip in a flow cell. After flow was started the buffer was toggled every 5 minutes between pH 7 to pH 4, as indicated. For the video Micrographs were acquired every 10 seconds displyed here are the toggled intervals. Scale bar 2 µm, n = 2.

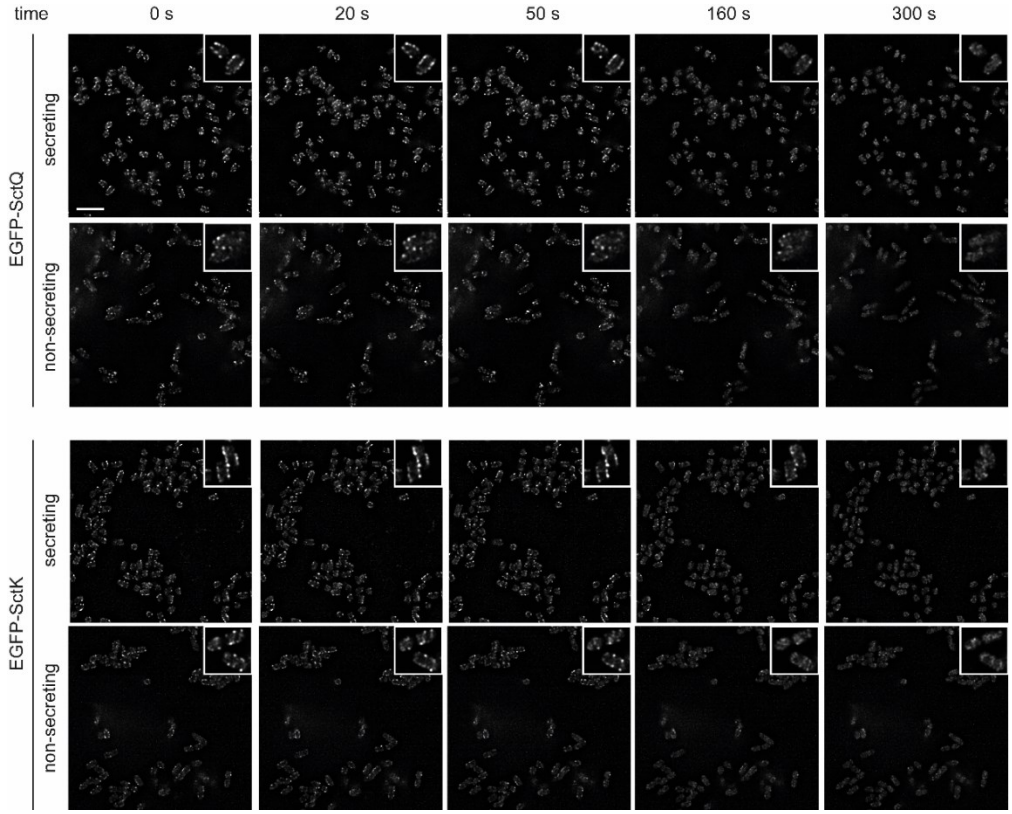

Supplemental Figure 4 Fluorescence micrographs of *Y. enterocolitica* EGFP-SctQ or EGFP-SctK subjected to pH 4.
EGFP-SctQ or EGFP-SctK at the given time periods after subjecting the bacteria to an external pH of 4 in a flow cell, under secreting conditions (rows 1 and 3), or non-secreting conditions (rows 2 and 4) Scale bar, 5 µm; insets show enlarged sections of the micrographs. n = 3 independent experiments for EGFP-SctQ; n = 2 independent experiment for EGFP-SctK.

A

t (s)	-40	-30	-20	-10	0	10	20	30	40	50	60	70	80	90	100	110	120	130	140	150	160	170	180	190	200	210	220	230	240	250	260	270	280	290	300	310	320	330	340	350	360	370	380	390	400	410	420	430	440	450	460	470	480	490	500	510	520	530	540
16	0	0	0	1	0	0	1	1	0	0	0	0	0	0	0	0	0	0	0	0	0	0	0	0	0	0	0	0	0	0	0	0	0	0	0	0	0	0	0	0	0	0	0	0	0	0	0	0	0	0	0	0	0	0	0	0	0	0	0
15	0	1	0	0	0	0	0	0	1	0	1	1	0	0	0	0	0	0	0	0	0	0	0	0	0	0	0	0	0	0	0	0	0	0	0	0	0	0	0	0	0	0	0	0	0	0	0	0	0	0	0	0	0	0	0	0	0	0	0
14	1	0	1	1	0	1	1	2	0	2	1	1	0	0	0	0	0	0	0	0	0	0	0	0	0	0	0	0	0	0	0	0	0	0	0	0	0	0	0	0	0	0	0	0	0	0	0	0	0	0	0	0	0	0	0	0	0	0	0
13	0	0	1	1	2	0	0	0	1	1	1	1	0	1	0	0	0	0	0	0	0	0	0	0	0	0	0	0	0	0	0	0	0	0	0	0	0	0	0	0	0	0	0	0	0	0	0	0	0	0	0	0	0	0	0	0	0	0	0
12	2	1	0	0	2	2	0	0	0	0	0	0	0	1	0	1	0	0	0	0	0	0	0	0	0	0	0	0	0	0	0	0	0	0	0	0	0	0	0	0	0	0	0	0	0	0	0	0	0	0	0	0	0	0	0	0	0	0	0
11	1	0	1	1	1	1	1	0	0	1	1	1	1	1	0	0	0	1	0	0	0	0	0	0	0	0	1	0	0	0	0	0	0	0	0	0	0	0	0	0	0	0	0	0	0	0	0	0	0	1	0	0	0	0	0	0	0	0	0
10	0	3	1	1	1	0	1	2	2	0	1	0	0	0	2	2	0	0	0	0	0	0	0	0	0	0	0	0	0	0	0	0	0	0	0	0	0	0	0	0	0	0	0	0	0	0	0	0	0	0	0	0	1	0	0	0	0	0	0
9	4	4	5	5	1	3	6	3	5	2	1	2	2	1	2	1	2	0	0	0	1	0	0	0	0	0	0	0	0	0	0	0	0	0	0	1	0	0	0	0	0	0	0	0	0	0	0	0	0	0	1	0	0	0	1	1	0	0	0
8	7	10	8	11	7	9	3	5	5	6	6	3	4	5	1	1	2	2	3	2	2	0	1	1	1	0	2	0	0	1	0	1	0	1	1	1	0	0	0	2	0	0	0	0	1	0	0	0	0	1	1	2	1	1	0	0	2	0	0	1
7	15	13	9	9	14	19	14	12	9	11	9	4	6	4	4	2	2	4	0	3	1	1	0	0	0	2	1	1	1	1	0	2	1	1	1	3	4	0	1	1	1	0	1	0	3	1	2	1	0	1	1	3	0	0	2	2	0	2	1	2
6	21	23	24	28	23	22	23	25	19	16	14	13	10	8	6	4	5	4	1	2	1	4	6	3	3	3	5	1	2	2	2	3	0	0	2	1	2	2	3	5	2	2	0	4	2	2	6	1	3	0	2	1	4	2	1	1	2	4	3
5	42	42	42	35	34	36	35	29	29	26	21	24	18	17	19	12	13	11	7	9	5	7	3	8	7	3	4	8	6	6	2	3	5	6	3	5	5	7	6	4	12	6	6	5	6	7	6	7	6	7	4	2	3	7	6	7	6	3	6
4	48	57	60	53	72	68	63	54	51	36	46	39	35	28	19	24	23	26	25	20	21	15	14	20	14	15	13	14	16	16	22	11	19	15	16	22	16	18	18	18	14	21	17	15	12	13	11	19	15	11	17	19	14	12	22	11	14	13	10
3	57	51	50	62	50	49	48	64	57	74	57	46	46	49	55	55	48	36	36	39	41	44	44	35	48	32	31	26	34	32	32	29	34	38	35	39	37	40	28	30	28	31	25	33	36	33	30	31	29	41	40	36	35	35	34	45	33	26	31
2	43	40	48	40	41	35	40	43	57	56	55	76	65	72	66	58	66	66	68	60	73	72	74	66	56	77	74	67	71	68	68	64	65	63	78	61	64	64	78	73	65	63	79	69	62	61	81	77	80	65	59	60	72	71	66	66	58	67	70
1	30	24	24	23	25	29	31	37	35	49	47	62	57	63	69	70	83	83	90	79	81	82	86	92	85	91	95	86	93	96	103	97	92	73	90	93	96	89	83	100	98	91	100	107	93	94	79	94	87	96	95	97	95	91	92	98	106	93
0	78	80	75	77	76	70	84	77	76	83	86	91	99	106	111	118	138	116	124	119	124	122	117	125	119	120	123	131	128	118	122	127	120	126	126	119	121	106	115	127	113	119	121	111	114	133	111	128	112	130	122	128	114	113	121	119	123	123	128

B

t (s)	-40	-30	-20	-10	0	10	20	30	40	50	60	70	80	90	100	110	120	130	140	150	160	170	180	190	200	210	220	230	240	250	260	270	280	290	300	310	320	330	340	350	360	370	380	390	400	410	420	430	440	450	460	470	480	490	500	510	520	530	540
12	0	0	0	0	0	0	0	0	0	0	0	0	0	0	0	0	0	0	0	0	0	0	0	0	0	0	0	0	0	0	0	0	0	0	0	0	0	0	0	0	0	0	0	0	1	0	0	0	0	1	0	0	0	0	0	0	0	0	0
11	0	0	0	0	0	0	0	0	0	0	0	0	0	0	0	0	0	0	0	0	0	0	0	0	0	0	0	0	0	0	0	0	0	0	0	0	0	0	0	0	0	0	0	0	0	0	0	0	0	0	1	0	0	0	0	0	0	0	0
10	0	0	0	0	0	0	0	0	0	0	0	0	0	0	0	0	0	1	0	0	0	0	0	0	0	0	0	0	0	0	0	0	1	0	0	0	0	0	0	1	0	0	0	0	0	0	0	0	0	0	1	0	0	0	0	0	0	0	0
9	0	0	0	0	0	0	0	0	0	1	0	0	0	0	2	1	0	0	0	1	0	1	0	0	0	0	1	2	3	1	0	0	0	0	1	0	1	2	0	1	1	1	0	0	1	0	0	1	1	1	0	1	1	2	0	0	1	0	1
8	0	1	1	0	2	0	0	0	0	1	0	0	1	3	1	2	0	0	3	2	4	1	4	1	3	3	2	3	2	1	2	2	4	3	3	6	2	6	0	2	5	5	5	0	5	3	3	2	2	4	3	5	1	1	4	3	1	1	
7	2	0	1	4	1	2	1	1	0	2	1	1	2	3	2	4	4	9	3	6	2	4	4	1	8	3	5	5	4	3	4	5	3	6	1	8	4	5	8	9	10	9	11	11	14	10	11	10	10	7	5	10	9	14	8	6	9	7	10
6	4	3	4	6	4	5	5	6	1	3	1	3	4	3	8	7	6	6	10	7	8	5	14	12	13	8	6	11	10	9	11	14	18	19	21	13	20	16	13	16	17	22	19	17	22	22	19	24	17	14	28	17	18	20	22	24	17	21	15
5	7	8	7	5	6	10	10	4	5	9	12	15	15	12	10	21	13	12	17	22	27	16	17	25	18	25	24	29	30	26	30	18	23	24	30	34	26	27	37	28	35	33	28	28	29	30	36	38	32	41	29	31	37	32	32	32	37	42	38
4	22	23	20	17	18	21	20	39	23	27	35	27	28	38	47	47	50	58	56	45	40	52	47	43	47	55	57	49	49	55	57	50	56	47	63	47	51	60	54	56	54	60	55	51	60	53	57	48	61	50	71	61	65	54	68	55	62	51	71
3	47	36	41	35	43	43	51	41	59	76	72	81	65	70	71	72	83	79	79	80	90	80	90	96	89	84	75	78	87	83	81	73	79	77	57	81	70	77	79	86	83	73	74	86	80	72	72	68	75	67	65	79	67	81	80	81	75	90	74
2	72	78	79	84	73	71	81	100	65	90	100	98	100	100	88	83	76	82	84	87	74	90	95	76	86	76	85	78	65	79	70	84	79	73	88	81	72	77	83	76	70	91	74	78	65	89	63	65	78	79	78	83	65	70	65	67	79	72	72
1	106	112	102	109	117	104	99	105	61	90	86	84	85	77	67	60	79	65	57	59	65	63	48	55	42	47	51	52	53	51	47	59	49	54	47	48	63	46	45	42	46	26	47	40	40	35	61	56	42	49	38	25	40	35	40	44	33	38	45
0	87	86	90	87	75	80	78	45	26	43	28	20	31	23	26	31	18	19	27	23	22	22	19	22	19	20	23	14	22	18	20	22	16	20	14	15	17	18	11	13	11	12	17	10	10	11	9	16	12	12	14	11	5	6	11	8	9	10	6

Supplemental Figure 5 Distribution of number of EGFP-SctQ fluorescent foci over time upon change of external pH.
Number of bacteria with n (blue font, left) detected spots over time (in seconds, top row); relates to Suppl. Fig. 9. **(a)** Dissociation of foci upon shift of external pH from 7 to 4. **(b)** Re-association of foci upon shift of external pH from 4 to 7. Spot numbers per bacterium were determined using the customized BiofilmQ software for 337-349 bacteria (top) / 328-347 bacteria (bottom, except for t=40 s, where n = 240 detected bacteria) from three independent experiments in each case. Darker colors identify combinations with a higher number of bacteria.

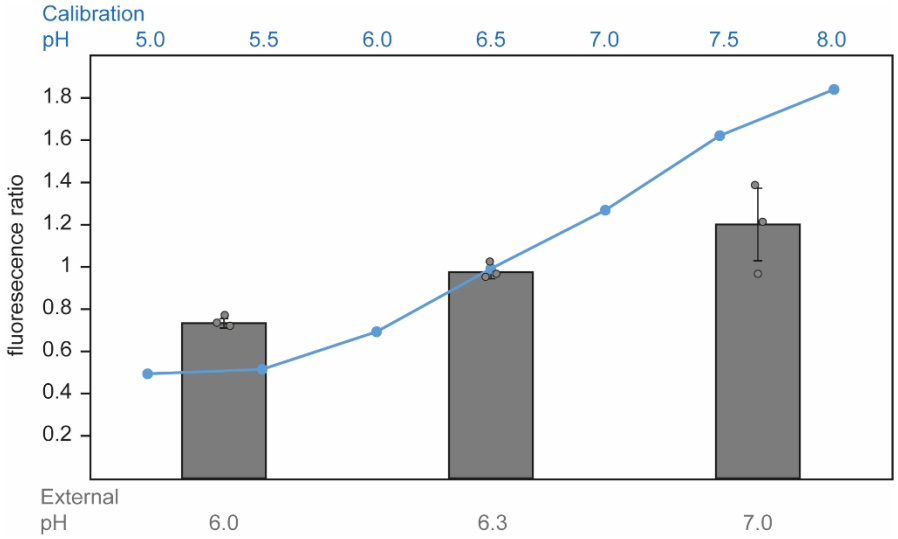

Supplemental Figure 6 Internal pH is equilibrated with external pH upon DNP treatment.
Blue curve, calibration of (Ex_{390nm} / Ex_{475nm}) fluorescence ratio of purified $pHluorin_{M153R}$ for the pH values indicated on the top (blue) (see Fig. 3A). Technical triplicate, error bars too small to display. Grey bars, determination of cytosolic pH upon incubating bacteria at the indicated external pH values (bottom) in presence of 2 mM DNP. Fluorescence ratio (Ex_{390nm} / Ex_{475nm}) of bacteria expressing cytosolic $pHluorin_{M153R}$. n = 3, error bars denote standard deviation

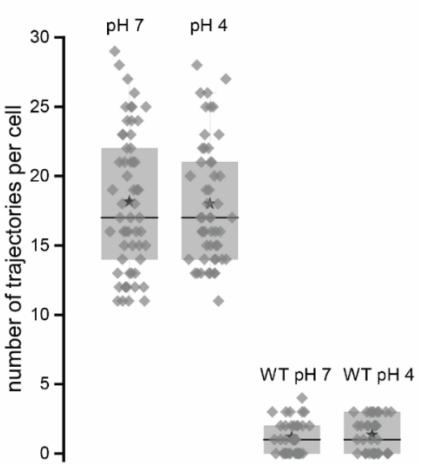

Supplemental Figure 7 Number of SctD trajectories in *Y. enterocolitica* cells at pH 7 and pH 4 compared to the number of false positives measured in WT cells.
Number of PAmCherry-SctD trajectories per single living *Y. enterocolitica* cells at pH 7 and at pH 4. Both exhibit a medium trajectory number of 17 trajectories per cell and a mean of 18.2 ± 5.1 s.d. (pH 7) and 18.0 ± 4.4 s.d. (pH 4). As a control, strains expressing PAmCherry-SctD were mixed with WT cells during the sample preparation. False positive trajectories from the background signal of single WT cells in the same movies yield a median of one false positive trajectory per cell for both conditions and a mean of 1.2 ± 1.1 s.d. (pH 7) and 1.3 ± 1.2 s.d. (pH 4). Symbols in the histogram are black star mean, black line median, whisker range 5-95% and box range 25-75%.
.

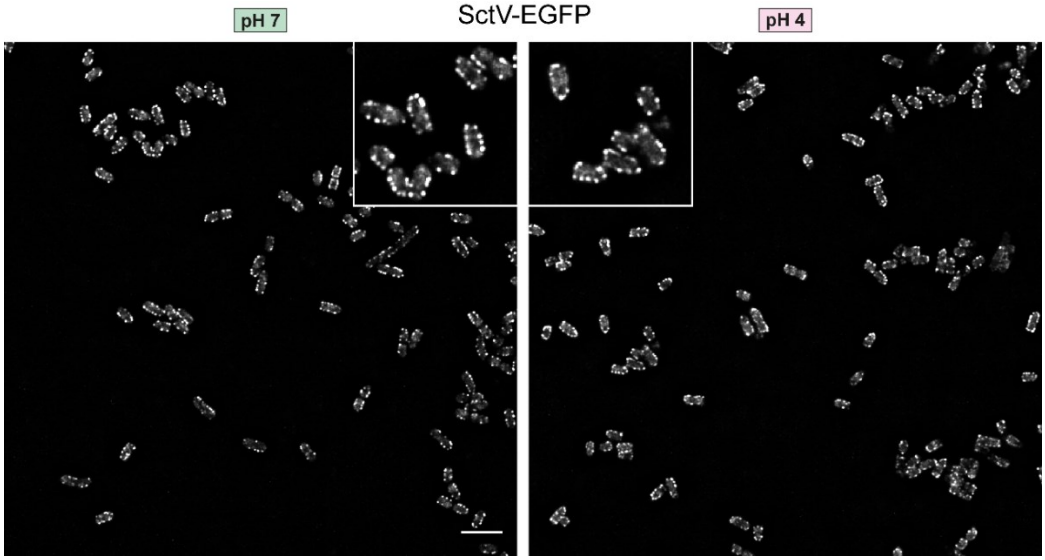

Supplemental Figure 8 SctV-EGFP forms fluorescent foci at external pH of 7 and 4.
Single micrographs of *Y. enterocolitica* SctV-EGFP at the indicated external pH. Scale bar, 5 µm. Insets 2x enlarged. n = 3. See Fig. 5C for RGB overlay of time course microscopy.

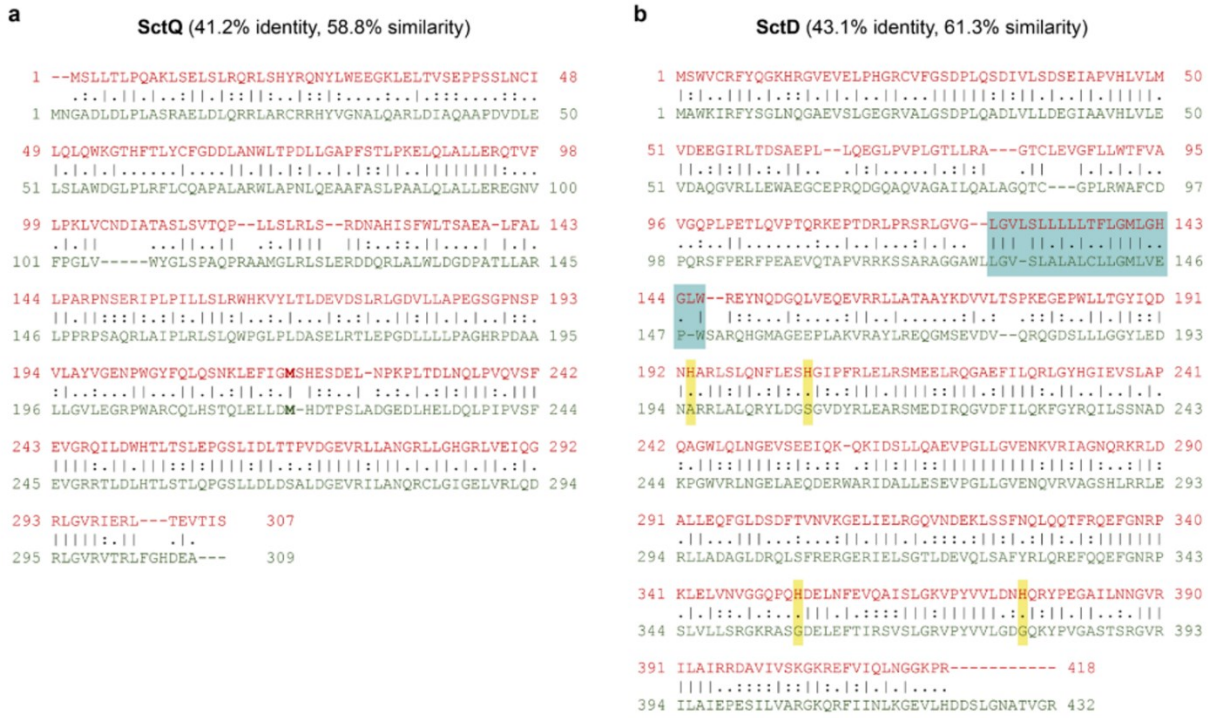

Supplemental Figure 9 Sequence conservation of injectisome components in *Y. enterocolitica* and *P. aeruginosa*.
Pairwise sequence alignment of SctQ (**A**) and SctD (**B**). Red, *Y. enterocolitica* sequences (NP_052404, NP_052414); green *P. aeruginosa* PAO1 sequences (NP_250385, NP_250408). Alignments created with EBI EMBOSS Needle (https://www.ebi.ac.uk/Tools/psa/emboss_needle/). Bold M indicates internal translation start site of $SctQ_C$ (amino acid 218 in *Y. enterocolitica*) (Yu *et al.*, 2011; Bzymek *et al.*, 2012). Turquoise background indicates region of trans-membrane helix (TMH) for *Y. enterocolitica* SctD, as predicted by Phobius (Käll *et al.*, 2007). The regions upstream and downstream of the TMH correspond to the cytosolic and periplasmic parts of the structure, respectively. Amino acids highlighted in yellow were identified as potentially important for pH sensing in SctD. See Suppl. Table 1 for multi-species alignment including additional proteins used in this study.

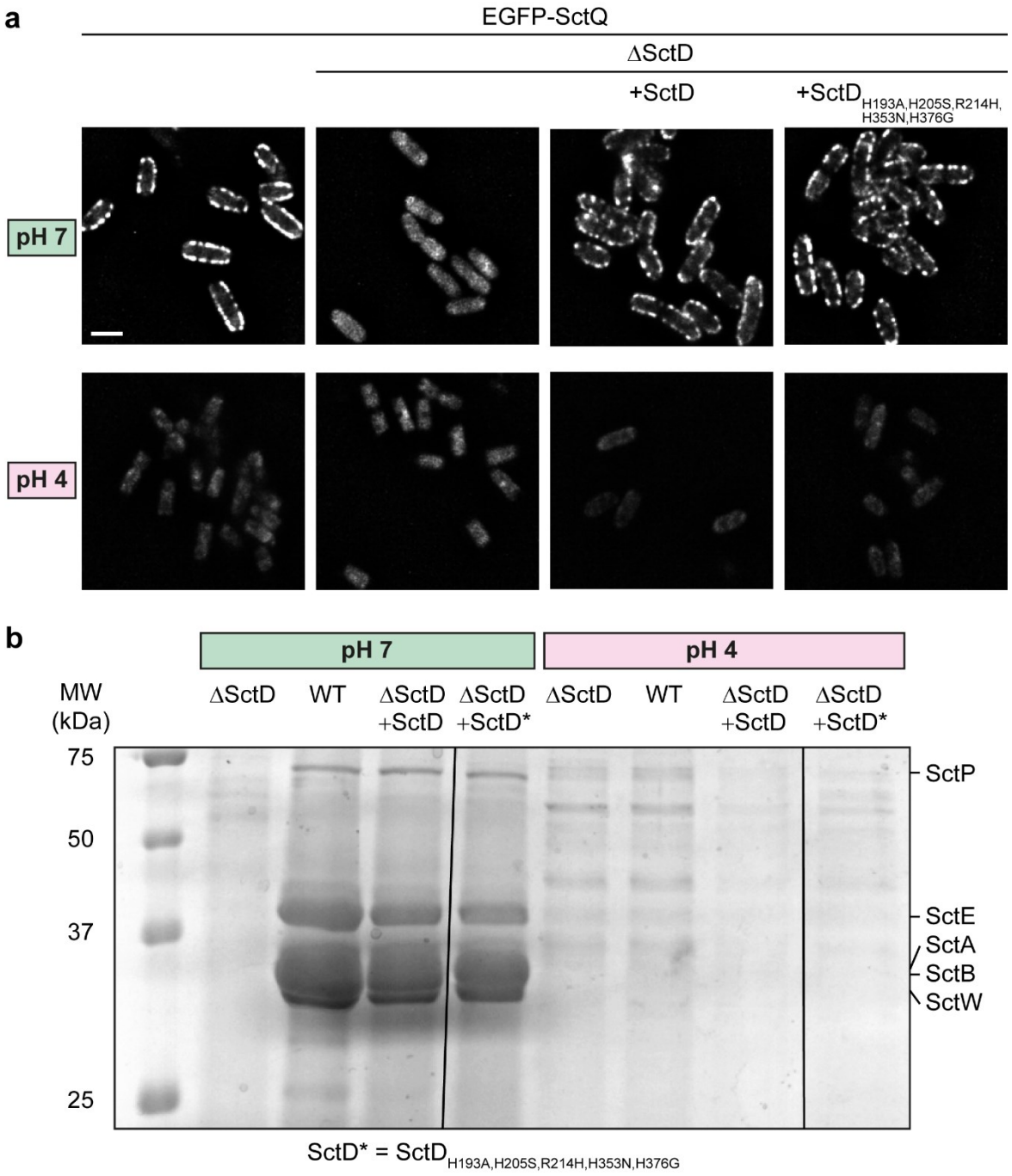

Supplemental Figure 10 Point mutations in SctD do no suppress the pH-dependent dissociation of cytosolic injectisome components and suppression of secretion at low external pH.

(a) Fluorescence micrographs of *Y. enterocolitica* EGFP-SctQ in strains lacking SctD (column 2-4) and complemented *in trans* with wild-type SctD (column 3) or an SctD multiple point mutant (see main text for details), at pH 7 (top) or pH 4 (bottom). The mutant SctD confers the same phenotype on SctQ localization as wild-type SctD under both conditions. Scale bar, 2 µm. **(b)** *In vitro* secretion assay showing the export of native injectisome substrates in the strains used in (A), at external pH of 7 (left) or 4 (right). All samples were analyzed on the same SDS-PAGE gel, vertical lines denote the omission of intermediate lanes. Molecular weight in kDa and exported proteins are indicated and the left and right side, respectively. Black and white scan of a Coomassie-stained SDS-PAGE gel; supernatant of $3*10^8$ bacteria per lane. n = 3. Experiment b performed by Emma Eisemann.

Supplemental table 1 Multiple sequence alignment of injectisome components

Multiple sequence alignments for transmembrane and cytosolic injectisome components analyzed in this study (SctC, D, J, V, K, Q, L, N) from different species (*Y. enterocolitica, Y. pestis, P. aeruginosa, S. flexneri* and *S. enterica* SPI-2). (a) Overview of protein similarity. Identical and similar amino acids were determined by a BlastP pairwise protein alignment (https://blast.ncbi.nlm.nih.gov) of the given proteins with the Y. enterocolitica W22703 pYVe227 homolog, using standard settings, only displaying best homology stretches with E values < 0.1. *: no clearly homologous protein known; n.d.: no homology stretch with E < 0.1 detected. (b) Multiple sequence alignment. Sequence alignment was performed using Clustal Omega 1.2.4 (https://www.ebi.ac.uk/Tools/msa/clustalo/) 4 using NCBI protein sequences for the strains listed in (A). Phylograms (Clustal Omega Guide Tree, standard settings, real branch length) are displayed below the individual alignments. For SctV, the result of a Phobius topology prediction (http://phobius.sbc.su.se/) 3 is displayed for Y. enterocolitica. For amino acids predicted to be located in the periplasm or extracellular space, His residues in Y. enterocolitica are marked in red. Neutral amino acids at the equivalent position in P. aeruginosa are marked in blue. For none of these amino acids, the aligned His residue was conserved for S. flexneri. Val-632 in SPI-2 SctV 5 is marked in green.

A

protein function	**Sct name**	*Yersinia pestis* EV NIIEG		*Pseudomonas aeruginosa* PAO-1		*Shigella flexneri* 2a str. 301		*Salmonella enterica subsp. enterica* serovar Typhimurium str. LT2; SPI-2			Protein length of *Y. entero-colitica* homolog
		Identity (*similarity*) to *Y. enterocolitica* homolog in amino acids									
secretin	**SctC**	594	*601*	370	*466*	158	*276*	155	*256*		607
outer MS ring protein	**SctD**	413	*418*	179	*261*	32	*60*	57	*100*		418
inner MS ring protein	**SctJ**	243	*243*	171	*204*	56	*98*	77	*129*		244
major export app. prot.	**SctV**	699	*702*	556	*630*	277	*441*	281	*435*		704
accessory cytos. prot.	**SctK**	206	*207*	84	*116*	9	*17*	*	*		209
C ring protein	**SctQ**	301	*305*	124	*178*	18	*31*	25	*36*		307
stator	**SctL**	208	*208*	115	*155*	n.d.	*n.d.*	35	*72*		223
ATPase	**SctN**	438	*439*	357	*385*	178	*256*	225	*275*		439

		Identity (*similarity*) to *Y. enterocolitica homolog in %*								**Average identity**	***Average similarity***
secretin	**SctC**	97.9%	*99.0%*	61.0%	*76.8%*	26.0%	*45.5%*	25.5%	*42.2%*	52.6%	*65.9%*
outer MS ring protein	**SctD**	98.8%	*100.0%*	42.8%	*62.4%*	7.7%	*14.4%*	13.6%	*23.9%*	40.7%	*50.2%*
inner MS ring protein	**SctJ**	99.6%	*99.6%*	70.1%	*83.6%*	23.0%	*40.2%*	31.6%	*52.9%*	56.0%	*69.1%*
major export app. prot.	**SctV**	99.3%	*99.7%*	79.0%	*89.5%*	39.3%	*62.6%*	39.9%	*61.8%*	64.4%	*78.4%*
accessory cytos. prot.	**SctK**	98.6%	*99.0%*	40.2%	*55.5%*	4.3%	*8.1%*	*	*	35.8%	*40.7%*
C ring protein	**SctQ**	98.0%	*99.3%*	40.4%	*58.0%*	5.9%	*10.1%*	8.1%	*11.7%*	38.1%	*44.8%*
stator	**SctL**	93.3%	*93.3%*	51.6%	*69.5%*	n.d.	*n.d.*	15.7%	*32.3%*	40.1%	*48.8%*
ATPase	**SctN**	99.8%	*100.0%*	81.3%	*87.7%*	40.5%	*58.3%*	51.3%	*62.6%*	68.2%	*77.2%*

SctC

```
CLUSTAL O(1.2.4) multiple sequence alignment

Sf_SctC   --------MKKFNIKSLTLLIVLLPLIVNANNIDSHLLEQNDIAKYVAQSDTVGSFFERF     52
S2_SctC   -----MVVNKRLI---LIL--LFILNTAKSDELS----WKGNDFTLYARQMPLAEVLHLL     46
Ye_SctC   MAFPLHSFFKRVLTGTLLL----LSSYSWAQELD----WLPIPYVYVAKGESLRDLLTDF     52
Yp_SctC   MAFPLHSFFKRVLTGTLLL----LSNYSWAQELD----WLPIPYVYVAKGESLRDLLIDF     52
Pa_SctC   --------MRRLLIGGLLA--LLPGAVLRAQPLD----WPSLPYDYVAQGESLRDVLANF     46
           ::.  *      :: :.       *:  : ..: :

Sf_SctC   SALLNYPIVVSKQAAKKRISGEFDLSNPEEMLEKLTLLVGLIWYKDGNALYIYDSGELIS     112
S2_SctC   SENYDTAITISPL-ITATFSGKIPPGPPVDILNNLAAQYDLLTWFDGSMLYVYPASLLKH     105
Ye_SctC   GANYDATVVVSDK-INDKVSGQFEHDNPQDFLQHIASLYNLVWYYDGNVLYIFKNSEVAS     111
Yp_SctC   SANYDATVVVSDK-INDKVSGQFEHDNPQDFLQHIASLYNLVWYYDGNVLYIFKNSEVAS     111
Pa_SctC   GANYDASVIVSDK-VNDQVSGRFDLESPQAFLQLMASLYNLGWYYDGTVLYVFKTTEMQS     105
       .  : : :*  . .**.:  * :*: ::  .* : **. **::  :

Sf_SctC   KVILLENISLNYLIQYLKDANLYD-HRYPIRGNISDKTFYISGPPALVELVANTATLLDK     171
S2_SctC   QVITFNILSTGRFIHYLRSQNILSSPGCEVKEITGTKAVEVSGVPSCLTRISQLASVLDN     165
Ye_SctC   RLIRLQESEAAELKQALQRSGIWE-PRFGWRPDASNRLVYVSGPPRYLELVEQTAAALEQ     170
Yp_SctC   RLIRLQESEAAELKLALQRSGIWE-PRFGWRPDASNRLVYVSGPPRYLELVEQTAAALEQ     170
Pa_SctC   RLVRLEQVGEAELKRALTAAGIWE-ARFGWRADPSGRLVHVSGPGRYLELVEQTAQVLEQ     164
       ::: ::   :  *  .: .   :  . : . :**  : : : * *::

Sf_SctC   QVS--SIGTDKVNFGVIKLKNTFVSDRTYNMRGEDIVIPGVATVVERLLNNGKALSNRQA     229
S2_SctC   AL--IKRKDSAVSVSIYTLKYATAMDTQYQYRDQSVVVPGVVSVLREMSKTS-VPTSS-T     221
Ye_SctC   QTQIRSEKTGALAIEIFPLKYASASDRTIHYRDDEVAAPGVATILQRVLSDATIQQVT-V     229
Yp_SctC   QTQIRSEKTGALAIEIFPLKYASASDRTIHYRDDEVAAPGVATILQRVLSDATIQQVT-V     229
Pa_SctC   QYTLRSEKTGDLSVEIFPLRYAVAEDRKIEYRDDEIEAPGIASILSRVLSDANVVAVG-D     223
         .  . : . : *: : . *  . *.:.: **:.::: .: . .

Sf_SctC   QNDPMPPFNITQKVSEDSNDFSFSSVTNSSILEDVSLIAYPETNSILVKGNDQQIQIIRD     289
S2_SctC   NNGS-----P-------------------ATQALPMFAADPRQNAVIVRDYAANMAGYRK     257
Ye_SctC   DNQRIPQAAT--------------------RASAQARVEADPSLNAIIVRDSPERMPMYQR     270
Yp_SctC   DNQRIPQAAT--------------------RASAQAKVEADPSLNAIIVRDSPERMPMYQR     270
Pa_SctC   EPGKLRP--G--------------------PQSSHAVVQAEPSLNAVVVRDHKDRLPMYRR     262
       :                  . * * *:::*:.  .:  :

Sf_SctC   IITQLDIAKRHIELSLWIIDIDKSELNNLGVNWQGTASFGDSFGASFNM-----------     338
S2_SctC   LITELDQRQQMIEISVKIIDVNAGDINQLGIDWGTAVSLGGKKIAFNTG----LNDG---     310
Ye_SctC   LIHALDKPSARIEVALSIVDINADQLTELGVDWRVGIRTGNNHQVVIKTTGDQSN---IA     327
Yp_SctC   LIHALDKPSARIEVALSIVDINADQLTELGVDWRVGIRTGNNHQVVIKTTGDQSN---IA     327
Pa_SctC   LIEALDRPSARIEVGLSIIDINAENLAQLGVDWSAGIRLGNNKSIQIRTTGQDSEEGGGA     322
       :* ** . **:.: *:*:: :: :**::*   *..

Sf_SctC   ---SSSASISTLDGNKFIASVMALNQKKKANVVSRPVILTQENIPAIFDNNRTFYVSLVG     395
S2_SctC   --GASGFSTVISDTSNFMVRLNALEKSSQAYVLSQPSVVTLNNIQAVLDKNITFYTKLQG     368
Ye_SctC   SNGALGSLVDARGLDYLLARVNLLENEGSAQVVSRPTLLTQENAQAVIDHSETYYVKVTG     387
Yp_SctC   SNGALGSLIDARGLDYLLARVNLLENEGSAQVVSRPTLLTQENAQAVIDHHETYYVKVTG     387
Pa_SctC   GNGAVGSLVDSRGLDFLLAKVTLLQSQGQAQIGSRPTLLTQENTQAVLDQSETYYVRVTG     382
        : .   . . ::. : *:.. .* : *:* ::* :* *::*: *:*. : *

Sf_SctC   ERNSSLEHVTYGTLINVIPRFSSRG---QIEMSLTIEDGTGNSQSNYNYNNENTSVLPEV     452
S2_SctC   EKVAKLESITTGSLLRVTPRLLNDNGTQKIMLNLNIQDGQQSD------TQSETDPLPEV     422
Ye_SctC   KEVAELKGITYGTMLRMTPRVLTQGDKSEISLNLHIEDGNQKP------NSSGIEGIPTI     441
Yp_SctC   KEVAELKGITYGTMLRMTPRVLTQGDKSEISLNLHIEDGNQKP------NSSGIDGIPTI     441
Pa_SctC   ERVAELKAITYGTMLKMTPRVVTLGDTPEISLSLHIEDGSQKP------NSAGLDKIPTI     436
       :. :.*: :* *:::.: **. . .  :* :.* *:** .    ..  . :* :

Sf_SctC   GRTKISTIARVPQGKSLLIGGYTHETNSNEIISIPFLSSIPVIGNVFKYKTSNISNIVRV     512
S2_SctC   QNSEIASQATLLAGQSLLLGGFKQGKQIHSQNKIPLLGDIPVVGHLFRNDTTQVHSVIRL     482
Ye_SctC   SRTVVDTVARVGHGQSLIIGGIYRDELSVALSKVPLLGDIPYIGALFRRKSELTRRTVRL     501
Yp_SctC   SRTVVDTVARVGHGQSLIIGGIYRDELSVALSKVPLLGDIPYLGALFRRKSELTRRTVRL     501
Pa_SctC   NRTVIDTIARVGHGQSLLIGGIYRDELSQSQRKVPWLGDIPYLGALFRTTADTVRRSVRL     496
       .: : : * : *:**::** :    .:* *..** :* :*: :   :*:
```

```
Sf_SctC   FLIQPREIKESSYYNTAEYKSLISEREIQKTT----QIIPSETT---L--------LEDE   557
S2_SctC   FLIKASVVNNGISHG-------------------------------------------   497
Ye_SctC   FIIEPRIIDEGIAHHLA----LGNGQDLRTGILTVDEISNQSTTLNKLLGGSQCQPLNKA   557
Yp_SctC   FIIEPRIIDEGIAHHLA----LGNGRDLRTGILAVDEISNQSTTLNKLLGGFQCQPLNKA   557
Pa_SctC   FLIEPRLIDDGVGHYLA----LNNRRDLRGGLLEIDELSNQSLSLRKLLGSARCQALAPA   552
       *:*:  :.:. :

Sf_SctC   KSL---------VSYLNY---------------------------------       566
S2_SctC   -----------------------------------------------------       497
Ye_SctC   QEVQKWLSQNNKSSYLTQCKMDKSLGWRVVEGACTPAQSWCVSAPKRGVL       607
Yp_SctC   QEVQKWLSQNNKSSYLTQCKMDKSLGWRVVEGACTPAESWCVSAPKRGVL       607
Pa_SctC   RAEQERLRQAGQGSFLTPCRMGAQEGWRVTDGACPKDGAWCVGAERGN--       600
```

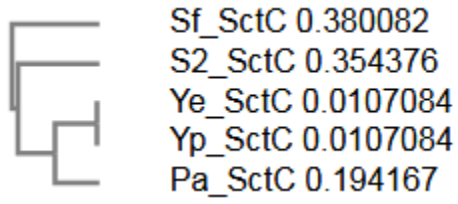

SctD

```
CLUSTAL O(1.2.4) multiple sequence alignment

Sf_SctD   ----MSEAKNSNLAPFRLLVKLTNGVGDEFPLYYGNNLIVLGRTIETLEFGNDNFPENII     56
S2_SctD   MAYLMVNPKSSWK--IRF----LGHVLQGREVWLNEG---------NLSLGEKGCDICIP     45
Pa_SctD   ---------MAWK--IRF----YSGLNQGAEVSLGEG---------RVALGSDPLQADLV     36
Ye_SctD   ---------MSWV--CRF----YQGKHRGVEVELPHG---------RCVFGSDPLQSDIV     36
Yp_SctD   ---------MSWV--CRF----YQGKHRGVEVELPHG---------RCVFGSDPLQSDIV     36
            :   *:       :  ..      :*..   :

Sf_SctD   PVTDSKSDGIIYLTISKDNICQFSDEKGEQIDIN--------------------------     90
S2_SctD   L-AINE---KIIL--REQADSLFVDAGKARVRVNGRRFNP---NKPLPSSGVLQVAGVAI     96
Pa_SctD   L-LDEG---IAA-----VHLVLEVDAQGVRLLEWAEGCEPRQDGQAQVAGAILQ-ALAGQ     86
Ye_SctD   L-SDSE---IAP-----VHLVLMVDEEGIRLTDSAEPL--LQEGLPVPLGTLLR-AGTCL     84
Yp_SctD   L-SDSE---IAP-----VHLVLMVDEEGIRLTDSAEPL--LQEGLPVPLGTLLR-AGSCL     84
          .          *  ::

Sf_SctD   ---SQFNSFEYDGISFH----------LKNMREDKSRGHILNGMYKNHSVFFFFAV--IV     135
S2_SctD   AFGKQD-------------------CELADYQIPVSRS----GYWWLAGVFLIFIGG-MG     132
Pa_SctD   TCGPLRWAFCDPQRSFPERFPEAEVQTAPVRRKSSARA----GGAWLLGVSLALALCLLG     142
Ye_SctD   EVGFLLWTFVAVGQPLPETLQVPTQRKEPTDRLPRSRL----GVG-LGVLSLLLLLTFLG     139
Yp_SctD   EVGFLLWTFVAVGQPLPETLQVPTQRKEPTDRLPRSRL----GIG-LGVLSLLLLLTFLG     139
                    :  :*   *   : : :  :

Sf_SctD   VLII-IFSLSLKKD-----EVKEIAEIIDDKRYGIVNTGQCNYILAETQNDAVWASVA--     187
S2_SctD   VLLS----ISGQPETVNDLPLRV-KFLLDK--------SNIHYVRAQWKEDGSLQLSGYC     179
Pa_SctD   MLVE-PWSARQ-HGMAGEEPLAKVRAYLRE--------QGMS-EVDVQRQGDSLLLGGYL     191
Ye_SctD   MLGHGLWREYNQDGQLVEQEVRRLLATAAY--------KDVV-LTSPK-EGEPWLLTGYI     189
Yp_SctD   LLGHGLWREYNQDGQLVEQEVRRLLATAAY--------KDVV-LTSPKKEGEPWLLTGYI     190
       :*         :              :.   .

Sf_SctD   ------------LNKTGFTKCRYILVSNKEINRIQQYINQRFPFINLYVLNLVSDKAELL     235
S2_SctD   SSSEQMQKVRATLESWG-VMYRDGVICDDLLVREVQDVLIKMGYPHAEVSSE---GPGS-     234
Pa_SctD   EDNARRLALQRYLDGSG-VDYRLEARSMEDIRQGVDFILQKFGYRQILSSNAD--KPGW-     247
Ye_SctD   QDNHARLSLQNFLESHG-IPFRLELRSMEELRQGAEFILQRLGYHGIEVSLAP--QAGW-     245
Yp_SctD   QDNHARLSLQNFLESHG-IPFRLELRSMEELRQGAEFILQRLGYHGIEVSLAP--QAGW-     246
             *: *  *  . . : : : : :: :

Sf_SctD   VFLSKERNSSKDTELDKLKNALIVEFPYIKNIKFNY--LSDHNARGDA----KGIFTKVN     289
S2_SctD   VLIHD-DIQ-MDQQWRKVQPLL-ADIPGLLHWQISHSHQSQGDDIISA-IIENGLVGLVN     290
Pa_SctD   VRLNG-ELAEQDERWARIDALLESEVPGLLGVENQVRVAGSHLRRLERLLADAGLDRQLS     306
Ye_SctD   LQLNG-EVSEEIQ-KQKIDSLLQAEVPGLLGVENKVRIAGNQRKRLDALLEQFGLDSDFT     303
Yp_SctD   LQLNG-EVSEEIQ-KQKIDSLLQAEVPGLLGVESKVRIAGNQRKRLDALLEQFGLDSDFT     304
       : :       ::. * :.* :  : .  ..   .   *:  ..

Sf_SctD   VQYKEICENNKVTYSVREELTDEKLELINRLISEHKNIYGDQYIEFSVLLID-----D--     342
S2_SctD   VTP------MRRSFVISGVLDESHQ---RILQETLAALKKKDPA-LSLIYQDIAPSHDES     340
Pa_SctD   FRE------RGERIELSGTLDEVQLSAFYRLQREFQQEFGNRPS-LVLLSRGKRASGDEL     359
Ye_SctD   VNV------KGELIELRGQVNDEKLSSFNQLQQTFRQEFGNRPK-LELVNVGGQPQHDEL     356
Yp_SctD   VNV------KGELIELRGQVNDEKLNSFNQLQQTFRQEFGNRPK-LELVNVGGQPQHDEL     357
       .       :  : : :   *     .  : :: .   *

Sf_SctD   DFKGKSY----LNSKDSYVMLNDKHWFFLDKNK---------------------------     371
S2_SctD   KYLPAPVAGFVQSRHGNYLLLTNKERLRVGALLPNGGEIVHLSADVVTIKHYDTLINYPL     400
Pa_SctD   EFTIRSV----SLGRVPYVVLGDGQKYPVGASTSRGVRILAIEPESILVARGKQR--FII     413
Ye_SctD   NFEVQAI----SLGKVPYVVLDNHQRYPEGAILNNGVRILAIRRDAVIVSKGKRE--FVI     410
Yp_SctD   NFEVQAI----SLGKVPYVVLDNHQRYPEGAILNNGVRILAIRRDAVIVSKGKRE--FVI     411
       .:      : *::* : .  .

Sf_SctD   ------------------- 371
S2_SctD   DFK---------------- 403
Pa_SctD   NLKGEVLHDDSLGNATVGR 432
Ye_SctD   QLNGGKPR----------- 418
Yp_SctD   QLNGGKPR----------- 419
```

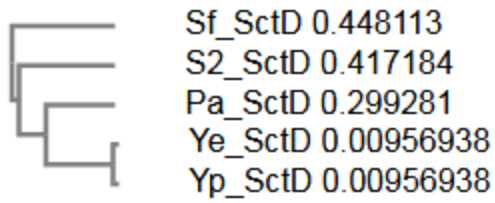

SctJ

```
CLUSTAL O(1.2.4) multiple sequence alignment

Sf_SctJ   -----MIRYKGFILFLLLMLIGCEQREELISNLSQRQANEIISVLERHNITARKVDGGKQ     55
S2_SctJ   ----MKVHRIVFLTVLTFFLTACD--VDLYRSLPEDEANQMLALLMQHHIDAEKKQEEDG     54
Pa_SctJ   MRRTVKGLSRMALLALVLALGGCK--VELYTGISQKEGNEMLALLRSEGVSADKQADKDG     58
Ye_SctJ   ----MKVKTSLSTLILILFLTGCK--VDLYTGISQKEGNEMLALLRQEGLSADKEPDKDG     54
Yp_SctJ   ----MKVKTSLSTLILILFLTGCK--VDLYTGISQKEGNEMLALLRQEGLSADKEPDKDG     54
              * : * .*.  :* .: : :.*:::::* . : * *  .

Sf_SctJ   GISVQVEKGTFASAVDLMRMYDLPNPERVDISQMFPTDSLVSSPRAEKARLYSAIEQRLE     115
S2_SctJ   -VTLRVEQSQFINAVELLRLNGYPHRQFTTADKMFPANQLVVSPQEEQQKINFLKEQRIE     113
Pa_SctJ   TVRLLVEESDIAEAVEVLKRKGYPRENFSTLKDVFPKDGLISSPIEERARLNYAKAQEIS     118
Ye_SctJ   KIKLLVEESDVAQAIDILKRKGYPHESFSTLQDVFPKDGLISSPIEELARLNYAKAQEIS     114
Yp_SctJ   KIKLLVEESDVAQAIDILKRKGYPHESFSTLQDVFPKDGLISSPIEELARLNYAKAQEIS     114
       : : **:. . .*:::::: . *. .  ..:** : *: ** * ::   *.:.

Sf_SctJ   QSLVSIGGVISAKIHVSYDLEEKNISS--KPMHISVIAIYDSPKESELLVSNIKRFLKNT     173
S2_SctJ   GMLSQMEGVINAKVTIALPTYDE--GSNASPSSVAVFIKYSPQVNMEAFRVKIKDLIEMS     171
Pa_SctJ   HTLSEIDGVLVARVHVVLPEERDGLGRKSSPASASVFIKHAADVQLDAYVPQIKQLVNNG     178
Ye_SctJ   RTLSEIDGVLVARVHVVLPEEQNNKGKKGVAASASVFIKHAADIQFDTYIPQIKQLVNNS     174
Yp_SctJ   RTLSEIDGVLVARVHVVLPEEQNNKGKKGVAASASVFIKHAADIQFDTYIPQIKQLVNNS     174
        * .: **: *:: :   . .    :*: :  : :  :** :::

Sf_SctJ   FSDVKYENISVILTPKEEYVYTNVQPVKEV----------KSEFLTNEVIYLFLGMAVLV     223
S2_SctJ   IPGLQYSKISILMQPA-EFRMVADVPARQTFWIMDVINANKGKVVKWLMKYPYPLMLSLT     230
Pa_SctJ   IEGLSYDRISVVLVPSAGVRQVPLAPRFESVFSIQVAEHSRGRLLGLF---------GLL     229
Ye_SctJ   IEGLAYDRISVILVPSVDVRQSSHLPRNTSILSIQVSEESKGRLIGLL---------SLL     225
Yp_SctJ   IEGLAYDRISVILVPSVDVRQSSHLPRNTSILSIQVSEESKGHLIGLL---------SLL     225
       : .: *..**::: *     *       :...:       *

Sf_SctJ   VILLVWAFKTG--WFKRNKI       241
S2_SctJ   GLLLGVGILIGYFCLRRRF-       249
Pa_SctJ   LALLLASNLAQFFWHRQRG-       248
Ye_SctJ   ILLLPVTNLAQYFWLQRKK-       244
Yp_SctJ   ILLLPVTNLAQYFWLQRKK-       244
        **       ::.
```

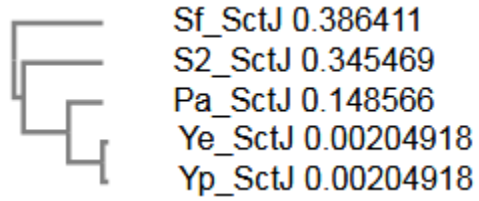

SctV

```
CLUSTAL O(1.2.4) multiple sequence alignment

Sf_SctV   ---------MIQSFLKQVSTKPELIILVLMVMIIAMLIIPLPTYLVDFLIGLNIVLAILV     51
S2_SctV   MRSWLGEGVRAQQWLSVCAGRQDMVLATVLLIAIVMMLLPLPTWMVDILITINLMFSVIL     60
Pa_SctV   -------MNDLSGLLGRVGERKDILLVVLLLAVVFMMVLPLPPLLLDILIAVNITISVVL     53
Ye_SctV   ------MNPHDLEWLNRIGERKDIMLAVLLLAVVFMMVLPLPPLVLDILIAVNMTISVVL     54
Yp_SctV   ------MNPHDLEWLNRIGERKDIMLAVLLLAVVFMMVLPLPPLVLDILIAVNMTISVVL     54
              *  . : :::: .::: : *:::*** ::*:** :*: :::::

Sf_SctV   FMGSFYIERILSFSTFPSVLLITTLFRLALSISTSRLILVDADAGKIITTFGQFVIGDSL     111
S2_SctV   LLIAIYLSDPLDLSVFPSLLLITTLYRLSLTISTSRLVLLQHNAGNIVDAFGKFVVGGNL     120
Pa_SctV   LMMSVYIGSPLQFSVFPAVLLITTLFRLALSVSTTRMILLQADAGQIVNTFGSFVVGGNL     113
Ye_SctV   LMIAIYINSPLQFSAFPAVLLVTTLFRLALSVSTTRMILLQADAGQIVYTFGNFVVGGNL     114
Yp_SctV   LMIAIYINSPLQFSAFPAVLLVTTLFRLALSVSTTRMILLQADAGQIVYTFGNFVVGGNL     114
       :: :.*:  *.:*.**::**:***:**:*::**:*::*:: :**:*: :**.**:*..*

Sf_SctV   AVGFVIFSIVTVVQFIVITKGSERVAEVAARFSLDGMPGKQMSIDADLKAGIIDAAGAKE     171
S2_SctV   TVGLVVFTIITIVQFIVITKGIERVAEVSARFSLDGMPGKQMSIDGDLRAGVIDADHART     180
Pa_SctV   VVGIIIFLIITIVQFLVITKGAERVAEVSARFSLDAMPGKQMSIDGDMRAGVIDVNEARA     173
Ye_SctV   IVGIVIFLIITIVQFLVITKGSERVAEVSARFSLDAMPGKQMSIDGDMRAGVIDVNEARE     174
Yp_SctV   IVGIVIFLIITIVQFLVITKGSERVAEVSARFSLDAMPGKQMSIDGDMRAGVIDVNEARE     174
       **:::* *:*:***:***** ******:******.*********.*::**:**. *:

Sf_SctV   RRSILERESQLYGSFDGAMKFIKGDAIAGIIIIFVNLIGGISVGMSQHGMSLSGALSTYT     231
S2_SctV   LRQHVQQESRFLGAMDGAMKFVKGDTIAGIIVVLVNIIGGIIIAIVQYDMSMSEAVHTYS     240
Pa_SctV   RRAVIEKESQMFGSMDGAMKFVKGDAIAGLIIIVVNILGGIAIGVTQKGLSTADALQLYA     233
Ye_SctV   RRATIEKESQMFGSMDGAMKFVKGDAIAGLIIIFVNILGGVTIGVTQKGLAAAEALQLYS     234
Yp_SctV   RRATIEKESQMFGSMDGAMKFVKGDAIAGLIIIFVNILGGVTIGVTQKGLAAAEALQLYS     234
       * :::**:: *::******:***:***:*::.**::**: :.: * .:: : *: *:

Sf_SctV   ILTIGDGLVSQIPALLISISAGFIVTRVNGD-SDNMGRNIMSQIFGNPFVLIVTSALALA     290
S2_SctV   VLSIGDGLCGQIPSLLISLSAGIIVTRVPGEKRQNLATELSSQIARQPQSLILTAVVLML     300
Pa_SctV   VLTVGDGMVSQVPALLIAITAGIIVTRVSSDESADLGSDIGEQVVAQPKALLIGGLLLVL     293
Ye_SctV   ILTVGDGMVSQVPALLIAITAGIIVTRVSSEDSSDLGSDIGKQVVAQPKAMLIGGVLLLL     294
Yp_SctV   ILTVGDGMVSQVPALLIAITAGIIVTRVSSEDSSDLGSDIGKQVVAQPKAMLIGGVLLLL     294
       :*::***: .*:*:***:::**:***** .:  ::. :: .*: :* ::: . : :

Sf_SctV   IGMLPGFPFFVFFLIAVTLTALFYYKKVVEKEKSL------SESDSSGYTGTFDI-----     339
S2_SctV   LALIPGFPFITLAFFSALLALPIILIRRK-KSVVS----------ANGVEAPEK--DSMV     347
Pa_SctV   FGLIPGFPTLTFLALALLVGGGGYFMLWRQRAQASAGSRDLPALLAQGAGAPSAKARGKA     353
Ye_SctV   FGLIPGFPTVTFLILALLVGCGGYMLSRKQ-SRNDEANQDLQSILTSGSGAPAARTKAKT     353
Yp_SctV   FGLIPGFPTVTFLILALLVGCGGYMLSRKQ-SRNDEANQDLQSILTSGSGAPAARTKAKT     353
       :.::**** ..: :: :             :.* .

Sf_SctV   --DNSHDSSLAMIENLDAISSETVPLILLFAE---NKINANDMEGLIERIRSQFFIDYGV     394
S2_SctV   PG--------------------ACPLILRLSP----TLHSADLIRDIDAMRWFLFEDTGV     383
Pa_SctV   GGGKPKAGRLAEQ----EEFALTVPLLIDVDASLQERLEAMSLNEELVRVRRALYLDFGV     409
Ye_SctV   SG--ANKGRLGEQ----EAFAMTVPLLIDVDSSQQEALEAIALNDELVRVRRALYLDLGV     407
Yp_SctV   SG--ANKGRLGEQ----EAFAMTVPLLIDVDSSQQEALEAIALNDELVRVRRALYLDLGV     407
                 : **:: .    :.: :  : :* :: * **

Sf_SctV   RLPTILYRTSNELKVDDIVLLINEVRADSFNIY--FDKVCITDENGDIDALGIPVVST--     450
S2_SctV   PLPEVNIEVLPEPTEKLTVLLYQE-PVFSLSIPAQADYLLIGADASVVG------DSQTL     436
Pa_SctV   PFPGIHLRFNEAMGDGEYLVQLQEVPVAR--GCLRPGWLLVRERAAQLELLAVPHEPAEL     467
Ye_SctV   PFPGIHLRFNEGMGEGEYLISLQEVPVAR--GELKAGYLLVRESVSQLELLGIPYEKGEH     465
Yp_SctV   PFPGIHLRFNEGMGEGEYIISLQEVPVAR--GELKAGYLLVRESVSQLELLGIPYEKGEH     465
       :* : .     :: :* .     . : :  . :

Sf_SctV   SYNERVISWVDVSYTENLTNIDAKIKSAQDEFYHQLSQALLNNINEIFGIQETKNMLDQF     510
S2_SctV   PNGMGQICWLTKDMAHKAQGFGLDVFAGSQRISALLKCVLLRHMGEFIGVQETRYLMNAM     496
Pa_SctV   QVPGEEASWVEQAHQDRLERSGCACLGLEQVLTWHLSHVLREYAEDFIGIQETRYLLEQM     527
Ye_SctV   LLPDQETFWVSVEYEERLEKSQLEFFSHSQVLTWHLSHVLREYAEDFIGIQETRYLLEQM     525
Yp_SctV   LLPDQEAFWVSVEYEERLEKSQLEFFSHSQVLTWHLSHVLREYAEDFIGIQETRYLLEQM     525
           *:   ..     . .: :  *. .* .  :::*:***: ::: :
```

```
Sf_SctV   ENRYPDLLKEVFRHVTIQRISEVLQRLLGENISVRNLKLIMESLALWAPREKDVITLVEH     570
S2_SctV   EKNYSELVKELQRQLPINKIAETLQRLVSERVSIRDLRLIFGTLIDWAPREKDVLMLTEY     556
Pa_SctV   EQGYGELVKEAQRIVPLQRMTEILQRLVGEDISIRNMRAILEAMVEWGQKEKDVVQLTEY     587
Ye_SctV   EGGYGELIKEVQRIVPLQRMTEILQRLVGEDISIRNMRSILEAMVEWGQKEKDVVQLTEY     585
Yp_SctV   EGGYGELIKEVQRIVPLQRMTEILQRLVGEDISIRNMRSILEAMVEWGQKEKDVVQLTEY     585
       * * :*:** * : :::::* ****:.* :*:*::: *: :: *. :****: *.*:

Sf_SctV   VRASLSRYICSKIAVSGEIKV-VMLSGYIEDAIRKGIRQTSGGSFLNMDIEVSDEVMETL     629
S2_SctV   VRIALRRHILRRLNPEGKPLPILRIGEGIENLVRESIRQTAMGTYTALSSRHKTQILQLI     616
Pa_SctV   IRSSLKRYICYKYSSGNNILPAYLLDQAVEEQIRGGIRQTSAGSYLALDPAITQAFLERV     647
Ye_SctV   IRSSLKRYICYKYANGNNILPAYLFDQEVEEKIRSRVRQTSAGSYLALDPAVTESLLEQV     645
Yp_SctV   IRSSLKRYICYKYANGNNILPAYLFDQEVEEKIRSGVRQTSAGSYLALEPAVTESLLEQV     645
       :* :* *:* :  .:   :. :*: :* :***: *:: :.  . .:: :

Sf_SctV   AHALRELRNAKKNFVLLVSVDIRRFVKRLIDNRFKSILVISYAEIDEAYTINVLKTI---     686
S2_SctV   EQAL----KQSAKLFIVTSVDTRRFLRKITEATLFDVPILSWQELGEESLIQVVESIDLS     672
Pa_SctV   RQTVGDLAQMQNRPVLIVSMDIRRYVRKLVESDYAGLPVLSYQELTQQINIQPLGRIVL-     706
Ye_SctV   RKTIGDLSQIQSKPVLIVSMDIRRYVRKLIESEYYGLPVLSYQELTQQINIQPLGRVCL-     704
Yp_SctV   RKTIGDLSQIQSKPVLIVSMDIRRYVRKLIESEYYGLPVLSYQELTQQINIQPLGRICL-     704
       :::  : . . .::.*:* **::::: :  .: ::*: *: :  *: : :

Sf_SctV   ---------    686
S2_SctV   EEELADNEE    681
Pa_SctV   ---------    706
Ye_SctV   ---------    704
Yp_SctV   ---------    704
```

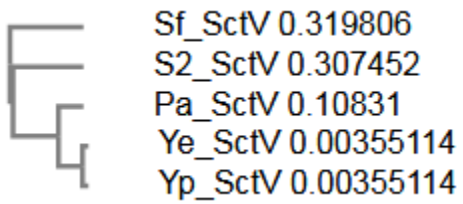

Phobius (http://phobius.sbc.su.se) topology prediction for Ye_SctV:

```
FT  TOPO_DOM   1   17    CYTOPLASMIC.
FT  TRANSMEM   18   36
FT  TOPO_DOM   37   41    NON CYTOPLASMIC.
FT  TRANSMEM   42   61
FT  TOPO_DOM   62   72    CYTOPLASMIC.
FT  TRANSMEM   73   93
FT  TOPO_DOM   94  104    NON CYTOPLASMIC.
FT  TRANSMEM  105  131
FT  TOPO_DOM  132  199    CYTOPLASMIC.
FT  TRANSMEM  200  220
FT  TOPO_DOM  221  231    NON CYTOPLASMIC.
FT  TRANSMEM  232  259
FT  TOPO_DOM  260  279    CYTOPLASMIC.
FT  TRANSMEM  280  298
FT  TOPO_DOM  299  303    NON CYTOPLASMIC.
FT  TRANSMEM  304  321
FT  TOPO_DOM  322  704    CYTOPLASMIC
```

SctK

```
CLUSTAL O(1.2.4) multiple sequence alignment

Sf_SctK   MIRMDGIYKKYLSIIFDPAFYINRNRLNLPSE----LLENGVIRSEINNLIINKYDLNCD     56
Ye_SctK   ---MMENYITSFQLRFCPAAYLHLEQLPSLWRSILPYLPQWRDSAHLNAALLDEFSLDTD     57
Yp_SctK   ----MENYITSFQLRFCPAAYLHLEQLPSLWRSILPYLPQWRDSAHLNAALLDEFSLDTD     56
Pa_SctK   ------MPLTAYQLRFCPARYIHESHLPAVLLRLLPALPDWRRQSVLNAWLLEQLELDCA     54
           . .: * ** *:: .:*     * :  : :* :::: .*:

Sf_SctK   IEPLSGVTAMFVANWNLLPAVAYFIGSQESRLINHSEMVISYYGG--------KISKQGE     108
Ye_SctK   YEEPHGLGALPLQPQSQLELLLCRLGL-----VLHGEAIRRCVLASPLQQLLTLVNQETL     112
Yp_SctK   YEEPHGLGALPLQPQSQLELLLCRLGL-----VLHGEAIRRCVLASPLQQLLTLVNQETL     111
Pa_SctK   FRMPAQLGGLALYPQAALERTLGWLGA-----LLHGQALRQVLDGARVRRIRAQIGEQGQ     109
       .  : .: :   *   :*   : *.: :   .     :.::

Sf_SctK   A------AIRSGFWHLIAWK----ENISVGIYERINLLFNPIALEGNYTPVERNLS-RL-     156
Ye_SctK   RQIIVQHELLIGPWP-TNWQRPLPTEIESRTMIQSGLAFWLAAMEPQPQAWCKRLSLRLP     171
Yp_SctK   RQIIVQHELLIGPWP-THWQRPLPTEIESRTMIQSGLAFWLAAMEPQPQAWCKRLSLRLP     170
Pa_SctK   RFCLEQLDLLIGRWP-PGWQRALPENPEEGYFRRCGLAFWLAACSDADCGFSRRLRLRLR     168
           : * *  *:   : .   : .* *  * .    :.* **

Sf_SctK   ------NEGMQYAKRHFTGIQTSCL---------------  175
Ye_SctK   LA--TPSEPWLVAESQRPLAQTLCHKLVKQVMPTCSHLFK  209
Yp_SctK   LA--TPSEPWLVAESQRPLAQTLCHKLVKQVTPTCSHLFK  208
Pa_SctK   LEAMPAPADWTFDEQRRSLARTLCLKVARQASDECFHLLN  208
             : :  :* *
```

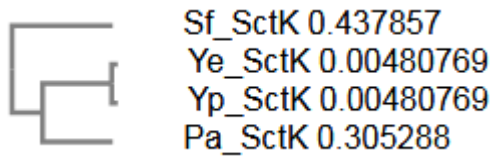

SctQ

```
CLUSTAL O(1.2.4) multiple sequence alignment

Sf_SctQ   ------------------------------------------------------------     0
S2_SctQ   ------------------MLRIANEERPWVEILPTQGATIGELTLSMQQYPVQQGTLFTI     42
Pa_SctQ   MNGADLDLPLASRAELDLQRRLARCRRHYVG-------NALQARLDIAQAAPDVDLELSL     53
Ye_SctQ   --MSLLTLPQAKLSELSLRQRLSHYRQNYLW-------EEGKLELTVSEPPSSLNCILQL     51
Yp_SctQ   --MSLLTLPQAKLSELSLRQRLSHYQQNYLW-------EEGKLELTVSEPPSSLNCILQL     51


Sf_SctQ   --------------MCGDWVIR-IDTLSFLKKKYEVFSGFSTQES--LLHL---SKCVFI     40
S2_SctQ   NYHNELGRVWIAEQCWQRWCEGLIGTANRSAIDPELLYGIAEWGLAPLLQASDATLCQNE     102
Pa_SctQ   AWDGLPLRFLCQAPALARWLAPNLQEAAFASLPAALQLALLEREGN----VFPGLVWYGL     109
Ye_SctQ   QWKGTHFTLYCFGDDLANWLTPDLLGAPFSTLPKELQLALLERQTV----FLPKLVCNDI     107
Yp_SctQ   QWKGTHFTLYCFGNDLANWLTADLLGAPFFTLPKELQLALLERQTV----FLPKLVCNDI     107
                *  :      : .:

Sf_SctQ   ESSSVFSIPELSDKITFRITNEIQYATTGSHLCCFSSSLGIIYFDKMPVLRNQVSLDSLH     100
S2_SctQ   PPTSC---SNLPHQLALHIKWTVEEHEFHSIIFTWPTGFLRNIVGELSAERQQIYPAPP-     158
Pa_SctQ   SPAQP---RA-A--MGLRL--SLERD--DQRLALWLDGDPATLLARLPPRPSAQRLAIP-     158
Ye_SctQ   ATASL---SVTQ--PLLSL--RLSRD--NAHISFWLTSAE-ALFALLPARPNSERIPLP-     156
Yp_SctQ   ATASL---SVTQ--PLLSL--RLSRD--NAHISFWLTSAE-ALFALLPARPNSERIPLP-     156
        :.      : :  :.    : : .   . :  .

Sf_SctQ   HLLEFCLGSSN--VRLATLKRIRTGDIIIVQKLYNLL--------------------LCN     138
S2_SctQ   VVVPVYSGWCQL--TLIELESIEIGMGVRIHCFGDIRLGFFAIQLPGGIYA---RVLLTE     213
Pa_SctQ   --LRLSLQWPGLPLDASELRTLEPGDLL--------------L-LPAGHRPDAALLGVLE     201
Ye_SctQ   --ILLSLRWHKVYLTLDEVDSLRLGDVL--------------L-APEGSGPNSPVLAYVG     199
Yp_SctQ   --ILISLRWHKVYLTLDEVDSLRLGDVL--------------L-APEGSGPNSPVLAYVG     199
        : .       : :. * :

Sf_SctQ   QVIIGDYIVNDNNEAKIN----LSESNGESEHTEVSLALFNYDDINVKVDFILLEKNMTI     194
S2_SctQ   DNTMKFDELVQDIETLLASGSPMSKSDGT--------SSVELEQIPQQVLFEVGRASLEI     265
Pa_SctQ   GRPWARCQLHSTQLELLDMHDTPSLADGE--------DLHELDQLPIPVSFEVGRRTLDL     253
Ye_SctQ   ENPWGYFQLQSNKLEFIGMSHESDELNPK--------PLTDLNQLPVQVSFEVGRQILDW     251
Yp_SctQ   ENPWGYFQLQSNKLEFIGMSHESDELNPE--------PLTDLNQLPVQVSFEVGRQILDW     251
           : .   :   . :       : :::  * * : . :

Sf_SctQ   NELKMYVENELFKFPDDIVKHVNIKVNGSLVGHGELVSIEDGYGIEISSWMVKE--- 248
S2_SctQ   GQLRQLKTGDVLPVGGCFAPEVTIRVNDRIIGQGELIACGNEFMVRITRWYLCKNTA 322
Pa_SctQ   HTLSTLQPGSLLDLDSALDGEVRILANQRCLGIGELVRLQDRLGVRVTRLFGHDEA- 309
Ye_SctQ   HTLTSLEPGSLIDLTTPVDGEVRLLANGRLLGHGRLVEIQGRLGVRIERLTEVTIS- 307
Yp_SctQ   HTLTSLEPGSLIDLTTPVDGEVRLLANGRLLGHGRLVEIQGRLGVRIERLTEVTIS- 307
        *   ..:: .  . .* : .*  :* *.*:  .  :.:
```

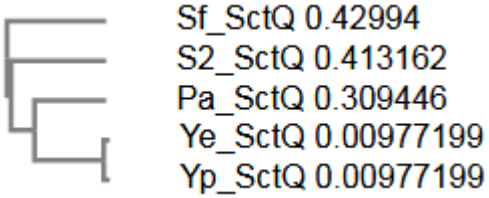

SctL

```
CLUSTAL O(1.2.4) multiple sequence alignment

Sf_SctL   MKVCNMQKGTLPVSRHHAYDGVVIKRIEKEL-----CKTIKDRDTESKKKAICVIKEATK     55
S2_SctL   -----MSFTSLPLTEIN-HKLPARNIIESQW-ITL-QLTLFAQEQQAKRVSHAIVSSAYR     52
Pa_SctL   -------------------MLPFVELDASRVRLAPGQALLRARDYQDYLSANRLVEAARE     41
Ye_SctL   -----MSQTC--QTGYA-YMQPFVQIIPSNLSLACGLRILRAEDYQSSLTTEELISAAKQ     52
Yp_SctL   -------------------MQPFVQIIPSNLSLACGLRILRAEDYQSSLTTEELISAAKQ     41
                     :  ..     : .: :  : ::. * .

Sf_SctL   KAESLRIDAV-------CDGYQIGIQTAF---EHIIDYICEWKLKQNENRRNIEDYITSL     105
S2_SctL   KAEKIIRDAYRYQREQKV-EQQQ--ELACLRKNTLEKMEVEWLEQHVKHLQDDENQFRSL     109
Pa_SctL   RAAEIEREAHEVYQEQKRLGWEAGLEEARLRQAGLIQETL---LRCNRYYRQVDRQLGEV     98
Ye_SctL   DAEKILADAQEVYEQQKQLGWQAGMDEARTLQATLIHETQ---LQCQQFYRHVEQQMSEV     109
Yp_SctL   DAEKILADAQEVYEQQKQLGWQAGMDEARTLQATLIHETQ---LQCQQFYRHVEQQMSEV     98
       * .: :*      :  : *   : .    : . :. : : .:

Sf_SctL   LSENLHD-ERIISTLLEQWLSSLRNTV-TELK-----------------VVLPKCNLALR     146
S2_SctL   VDHAAHHIKNSIEQVLLAWFDQQSVDSVMCHRLARQAT-AMAEEGALYLRIHPEKEALMR     168
Pa_SctL   VLQAVRKVLRH--------YDAVEL----TLAATREALALVSNQKQVILHVQPEQLAAVR     146
Ye_SctL   VLLAVRKILND--------YDQVDM----TLQVVREALALVSNQKQVVVRVNPDQAGTIR     157
Yp_SctL   VLLAVRKILND--------YDQVAM----TLQVVREALALVSNQKQVVVRVNPDQAGAIR     146
       :  :. .     .              : *.  :*

Sf_SctL   KKLELDLHKYRSDVKIILKYSE--------GNNYIFCSGNQVVEFSPQDVISGVKIELAE     198
S2_SctL   ETFGKRFTLI-----IEPGFSPDQAE---------LSSTRYAVEFSLSRHFNALLKWL--     212
Pa_SctL   EQVARVLKDF-----PEVGYLEVVGDARLDQGGCILETEIGIIDASLDSQLAALQAALTE     201
Ye_SctL   EQIAKVHKDF-----PEISYLEVTADARLDQGGCILETEVGIIDASIDGQIEALSRAIST     212
Yp_SctL   EQIAKVHKDF-----PEISYLEVTADARLDQGGCILETEVGIIDASIDGQIEALSRAIST     201
       : .        :        : :  :: * . : .:  :

Sf_SctL   KLTK--------NDKKYFKELAHKKLRQIAEDLLKENPVND  231
S2_SctL   -----RNGEDKRGSDEY------------------------  224
Pa_SctL   SVARSGEEEGDAG---------------------------  214
Ye_SctL   TLGQMKVTEEE-----------------------------  223
Yp_SctL   TLGQMKVTE--------------------------------  210
```

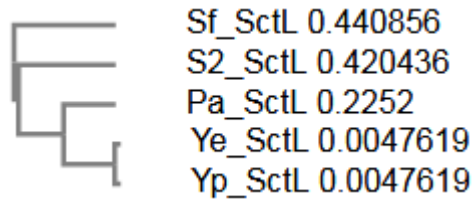

SctN

```
CLUSTAL O(1.2.4) multiple sequence alignment

Sf_SctN   ---------------MSYTKLLTQLSFPNRISGPILETSLSDVSIGEICNIQAGIESNEI     45
S2_SctN   ---MKNELMQRLRLKYPPPDGYCRWGRIQDVSATLLNAWLPGVFMGELCCIKPGEE----     53
Pa_SctN   MPAPLSPLIVRMRHAIEGCRPIQIRGRVTQVTGTLLKAVVPGVRIGELCQLRNPDQSL--     58
Ye_SctN   -MLSLDQIPHHIRHGIVGSRLIQIRGRVTQVTGTLLKAVVPGVRIGELCYLRNPDNSL--     57
Yp_SctN   -MLSLDQIPHHIRHGIVGSRLIQIRGRVTQVTGTLLKAVVPGVRIGELCYLRNPDNSL--     57
                    .  ::. :*:: : .* :**:* ::  :

Sf_SctN   VARAQVVGFHDEKTILSLIGNSRGLSRQTLIKPTAQFLHTQVGRGLLGAVVNPLGEVTDK     105
S2_SctN   --LAEVVGINGSKALLSPFTSTIGLHCGQQVMALRRRHQVPVGEALLGRVIDGFGRPLDG     111
Pa_SctN   ALLAEVIGFQQHQALLTPLGEMLGVSSNTEVSPTGGMHRVAVGEHLLGQVLDGLGRPFDG     118
Ye_SctN   SLQAEVIGFAQHQALLIPLGEMYGISSNTEVSPTGTMHQVGVGEHLLGQVLDGLGQPFDG     117
Yp_SctN   SLQAEVIGFAQHQALLIPLGEMYGISSNTEVSPTGTMHQVGVGEHLLGQVLDGLGQPFDG     117
        *:*:*:  :::* : . *:   :    :. **. *** *:: :*. *

Sf_SctN   FAVTDNSEILYRPVDNAPPLYSERAAIEKPFLTGIKVIDSLLTCGEGQRMGIFASAGCGK     165
S2_SctN   RELPD---VCWKDYDAMPPPAMVRQPITQPLMTGIRAIDSVATCGEGQRVGIFSAPGVGK     168
Pa_SctN   SPPAE--PAAWYPVYRDAPQPMSRRLIERPLSLGVRAIDGLLTCGEGQRMGIFAAAGGGK     176
Ye_SctN   GHLPE--PAAWYPVYQDAPAPMSRKLITTPLSLGIRVIDGLLTCGEGQRMGIFAAAGGGK     175
Yp_SctN   GHLPE--PAAWYPVYQDAPAPMSRKLITTPLSLGIRVIDGLLTCGEGQRMGIFAAAGGGK     175
        :   :    *  * * *: *::.**.: *******:***:: * **

Sf_SctN   TFLMNMLIEHSGADIYVIGLIGERGREVTETVDYLKNSEKKSRCVLVYATSDYSSVDRCN     225
S2_SctN   STLLAMLCNAPDADSNVLVLIGERGREVREFIDFTLSEETRKRCVIVVATSDRPALERVR     228
Pa_SctN   STLLASLVRNAEVDVTVLALVGERGREVREFIESDLGEQGLRRSVLVVATSDRPAMERAK     236
Ye_SctN   STLLASLIRSAEVDVTVLALIGERGREVREFIESDLGEEGLRKAVLVVATSDRPSMERAK     235
Yp_SctN   STLLASLIRSAEVDVTVLALIGERGREVREFIESDLGEEGLRKAVLVVATSDRPSMERAK     235
       : *: * .  .* *: *:******* * ::  ..:  :.*:* **** :::* .

Sf_SctN   AAYIATAIAEFFRTEGHKVALFIDSLTRYARALRDVALAAGESPARRGYPVSVFDSLPRL     285
S2_SctN   ALFVATTIAEFFRDNGKRVVLLADSLTRYARAAREIALAAGETAVSGEYPPGVFSALPRL     288
Pa_SctN   AGFVATSIAEYFRDQGRRVLLLMDSLTRFARAQREIGLAAGEPPTRRGYPPSVFAALPRL     296
Ye_SctN   AGFVATSIAEYFRDQGKRVLLLMDSVTRFARAQREIGLAAGEPPTRRGYPPSVFAALPRL     295
Yp_SctN   AGFVATSIAEYFRDQGKRVLLLMDSVTRFARAQREIGLAAGEPPTRRGYPPSVFAALPRL     295
       * ::**:***:** :*::* *: **:**:*** *::.***** .  ** .** :****

Sf_SctN   LERPGKLKAGGSITAFYTVLLEDDDFADPLAEEVRSILDGHIYLSRNLAQKGQFPAIDSL     345
S2_SctN   LERTGMG-EKGSITAFYTVLVEGDDMNEPLADEVRSLLDGHIVLSRRLAERGHYPAIDVL     347
Pa_SctN   MERAGQS-ERGSITALYTVLVEGDDMSEPVADETRSILDGHIVLSRKLAAANHYPAIDVL     355
Ye_SctN   MERAGQS-SKGSITALYTVLVEGDDMTEPVADETRSILDGHIILSRKLAAANHYPAIDVL     354
Yp_SctN   MERAGQS-SKGSITALYTVLVEGDDMTEPVADETRSILDGHIILSRKLAAANHYPAIDVL     354
       :** *   *****:****:*.**: :*:*:*.**:***** ***.** .::**** *

Sf_SctN   KSISRVFTQVVDEKHRIMAAAFRELLSEIEELRTIIDFGEYKPGENASQDKIYNKISVVE     405
S2_SctN   ATLSRVFPVVTSHEHRQLAAILRRCLALYQEVELLIRIGEYQRGVDTDTDKAIDTYPDIC     407
Pa_SctN   HSVSRVMNQIVDDDQRHAAGRLREWLAKYEEVELLLKIGEYQKGQDSEADRAIEKIGAIR     415
Ye_SctN   RSASRVMNQIVSKEHKTWAGDLRRLLAKYEEVELLLQIGEYQKGQDKEADQAIERIGAIR     414
Yp_SctN   RSASRVMNQIVSKEHKTWAGDLRRLLAKYEEVELLLQIGEYQKGQDKEADQAIERMGAIR     414
       : ***: :....:: *. :*. *: :*:. :: :***: * : . *: :  :

Sf_SctN   SFLKQDYRLGFTYEQTMELIGETIR-  430
S2_SctN   TFLRQSKDEVCGPELLIEKLHQILTE  433
Pa_SctN   QWLRQGTHETSDYAQACAQLRSLCA-  440
Ye_SctN   GWLCQGTHELSHFNETLNLLETLTQ-  439
Yp_SctN   GWLCQGTHELSHFNETLNLLETLTQ-  439
       :* *.       :
```

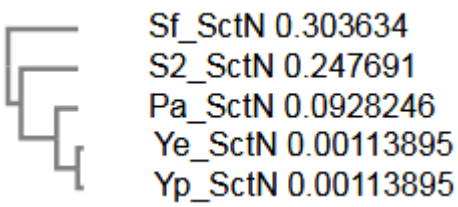

Supplemental table 2 Spectral counts from PAmCh-YscQ CoIP in effector-less background strain. Displayed here are the results of a CoIP with PamCh-YscQ as bait. Spectral counts hits are sorted by Injectisome components, Chaperones and Effectors/translocators. first Colum shows the results for PAmCh-SctQ expressed for am pBAD plasmid in a pYV$^-$ background strain (no injectisome components), second effector-less strain with a chromosomal encoded PAmCh-SctQ, third effector-less strain with PAmCh alone expressed from a pBAD plasmid and fourth shows a the spectral count results for an unlabeled effector-less strain. Colum five displays the PAmCh-SctQ effector-less strain results minus the pBad::PAmCh results, bold numbers indicate positive results. The last Colum displays the Ratio of detected protein per background substracted PamCh-SctQ detected with the chromosomal encoded fusion protein. n = 1. Sample handeling in the MS facaillity performed by Jörg Kahnt.

Detected spectral counts	**PAmCh-SctQ pYV-**	**PAmCh-SctQ WT**	**pBAD::PAmCh WT**	**neg. ctrl. dHOPEMTasd +pBad**
mCHERRY	439	147	365	32
YadA	0	47	69	57
Injectisome components				
YscC_possible_misannotation	0	2	2	0
YscW	0	7	3	0
YscJ	0	19	5	0
YscV	0	6	0	0
YscQ	453	71	6	17
YscL	0	9	2	0
YscN	0	21	1	0
Chaperones				
SycD	0	17	9	0
SycH	0	4	3	0
Effectors				
YscP	0	0	0	0
YscB	0	3	0	0
YopQ	0	9	1	0
YopD	0	6	7	0
YopB	0	4	7	0
YopN	0	2	5	0
YopD_partial	0	1	2	0

Supplemental table 3 spectral counts for detected Effectors in indicated strains

		MRS40 EGTA	MRS40 EG	MRS40 EG	8	MRS40 CA	MRS40 CA	dHOPEMT	4	dHOPEMT
	YopH	361	478	400	37	37	38	0	10	0
	YopD	211	230	223	32	41	36	45	50	52
	YopE	194	255	203	36	41	47	2	6	2
	YopO	83	116	98	21	20	23	7	13	8
	YopQ	35	43	43	5	10	8	12	19	12
	YopB	44	58	48	7	8	7	8	11	10
	YopP	9	9	8	6	6	6	4	7	6
	YopR	2	1	1	4	5	3	7	8	7
	YopM	19	19	22	5	8	8	0	1	0
	YopT	1	1	3	1	0	0	0	0	0
Sum all:		959	1210	1049	154	176	176	85	125	97
		MRS40 EGTA			MRS40 CA			dHOPEMTasd		
	Average Sum	1072.666667			168.6667			102.3333		
	Stdev Sum	103.827849			10.3709			16.75974		

Supplemental table 4 Molecular weight of cytosolic sub complexes.

Protein	YscK	PAmCh-YscQ	YscQc	YscL	YscN	effector	**MW complex**
MW monomer	23.95	62.51	9.99	24.93	47.71	82.22	
Complex							
complete sorting platform	6	24	48	12	6		**2708.88**
single pod	1	4	8	2	1		**451.48**
single pod lacking YscK		4	8	2	1		**427.53**
YscK-(Q(Qc2))4 (delta-YscL)	1	4	8				**353.91**
Bernal pod ("leg") version 1		2	4	2	1		**262.55**
Bernal pod ("leg") version 2		2	4	2			**214.84**
Bernal pod ("leg") version 3		1	2	2	1		**180.06**
stable Q(Qc)2 complex		1	2				**82.49**
delta YscN	1	4	8	2			**403.77**
typical effector-chaperone complex						1	**82.22**
PAmCherry alone							**26.8**
dYscQ YscL				2	1		**151.17**
with effectors:							
complete sorting platform	6	24	48	12	6	24	**4682.16**
single pod	1	4	8	2	1	4	**780.36**
single pod lacking YscK		4	8	2	1	4	**756.41**
YscK-(Q(Qc2))4 (delta-YscL)	1	4	8			4	**682.79**
Bernal pod ("leg") version 1		2	4	2	1	2	**426.99**
Bernal pod ("leg") version 2		2	4	2		2	**379.28**
Bernal pod ("leg") version 3		1	2	2	1	1	**262.28**
stable Q(Qc)2 complex		1	2			1	**164.71**
delta YscN	1	4	8	2		4	**732.65**

Supplemental table 5 calculated MJD in nM of Sorting platform subcomplexes .

mit MW berechnet			
		Meßungenauigkeit	
		40	
		Eingabe MJD (OE)	
	single pod OE	270	
			MJD in nm
single pod ME	1.200103847		240.7413
YscQ pYV	0.567441283		350.1001
single pod YscK	0.981995188		266.1352
leg 1	0.834688639		288.6642
leg 2	0.780714435		298.4754
leg 3	0.736082077		307.3909
leg 1 ME	0.817913861		258.3903
leg 2 ME	0.786239721		263.5433
leg 3 ME	0.695275178		280.2528
Complete sorting platfrom	1.817120593		195.6502
Complete sorting platfrom_I	1.817120593		173.3644
dYscL	0.922043561		274.6506
dYscL_ME	0.956453918		238.9461
dYscQYscL	0.694398913		316.4822

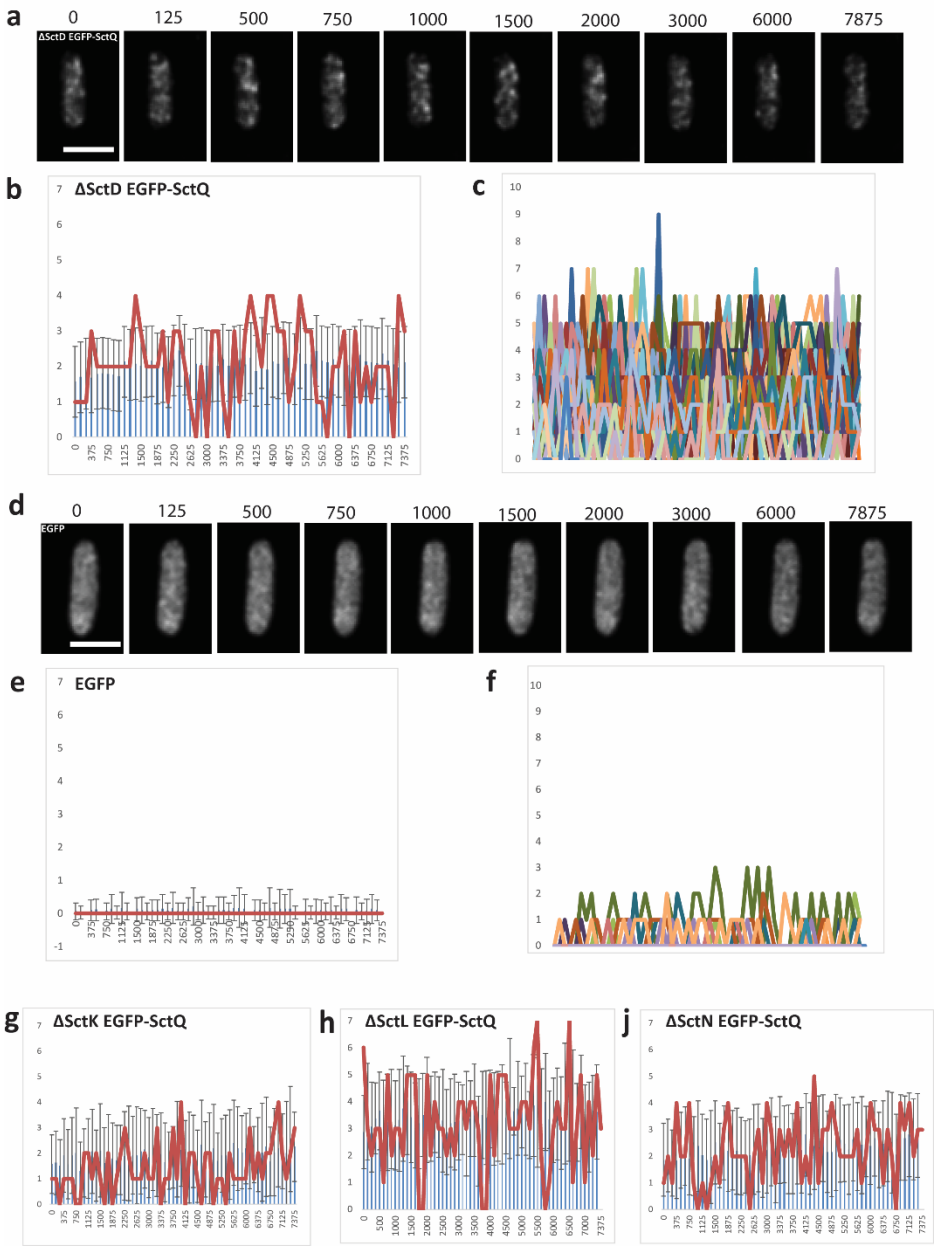

Supplemental Figure 11 Fluorescent foci can be detected in the bacterial cytosol.
(a) Single cell time lapse micrograph of a cell expressing EGFP-SctQ from the native locus in a ΔSctD background. (Numbers on top indicate time in ms. **(b)** Quantification of foci number detected with BiofilmQ over time of whole field, 49-58 cells, as shown in (a). **(c)** line graphs of all cells analyzed for (b), every color represents one cell. Total average number of foci detected: 128.6. **(d)** Single cell time lapse micrograph with cytosolic GFP expressed from a pBAD plasmid induced with 0.2% L-arabinose in an effector-less strain background. Due to a higher expression, that strain was not adjusted in brightness and contrast to the levels of the other strains. Quantification of foci number over time of whole field with BiofilmQ, 27-29 cells, as shown in (d). (**f**) Line graphs of all cells analyzed for **(e)** line graphs of all cells analyzed for (e). Total average number of foci detected: 5.5 **(F) (g)** Quantification of foci number of EGFP-SctQ in ΔSctK background over time. Total average number of foci detected: 117.3. **(h)** Quantification of foci number of EGFP-SctQ in ΔSctL background over time. Total average number of foci detected: 206.3. EGFP-SctQ foci quantification in ΔSctN stain background. Total average number of foci detected: 138.6. **Blue bars** represent the average number of foci. **Red lines** one randomly chosen single cell. Error bars denote standard deviation. Analyzed for this have been one set of micrographs out of two representative experiments with different conditions.

9 Material and methods

9.1 Materials

9.1.1 Reagents and equipment and tools used in this study

The following paragraph holds all the tools and equipment together with their supplier that are used in this study. Table 1 *Chemicals and reagents used in this study*is a list of chemicals, holds materials frequently used while Table 2 gives information about enzymes and kits used for this study. Table 3 lists devices and machinery critical for this study and Table 4 lists Software applications online tools.

Table 1 Chemicals and reagents used in this study

Reagents	Manufacturer
Chemicals	Roth (Karlsruhe), Merck (Darmstadt), Sigma-Aldrich (Taufkirchen)
Agarose NEEP Ultra-Quality	Carl Roth GmbH + Co KG (Karlsruhe)
Low Melting agarose	Sigma-Aldrich (Taufkirchen)
LB bacterial growth medium	Carl Roth GmbH + Co KG (Karlsruhe)
BHI bacterial growth medium	VWR International Leuven
Antibiotics	Roth (Karlsruhe)
L- arabinose	Carl Roth GmbH + Co KG (Karlsruhe)
Glucose	Carl Roth GmbH + Co KG (Karlsruhe)
Sucrose	Carl Roth GmbH + Co KG (Karlsruhe)
D(+) Saccharose	Carl Roth GmbH + Co KG (Karlsruhe)
Bacto Yeast Extract	Carl Roth GmbH + Co KG (Karlsruhe)
Ethidium bromide	Carl Roth GmbH + Co KG (Karlsruhe)
Gel Red	Sigma-Aldrich (Steinheim)
Ethidium bromide	Carl Roth GmbH + Co KG (Karlsruhe)
Gel loading dye purple 6X	New England Biolabs (NEB) (Frankfurt a.M.)
Protein Ladder	New England Biolabs (NEB) (Frankfurt a.M.)
Bromphenol blue, sodium salt	
SDS (Sodium Lauryl Sulfate)	Carl Roth GmbH + Co KG (Karlsruhe)
Glycerol	Carl Roth GmbH + Co KG (Karlsruhe)

Reagents	Manufacturer
Tris Base	Carl Roth GmbH + Co KG (Karlsruhe)
Anti-rabbit IgG	DAKO, Glostrup, Denmark
	Sigma-Aldrich, Munich, Germany
Anti-mouse IgG	Amersham, Freiburg, Germany
Anti-GFP monoclonal antibody	Proteintech, St. Leon-Rot, Germany
Anti-mCHerry	Thermo Fisher Scientific (Frankfurt a. M.)
Anti-Flag	Rockland, Limerick, Pennsylvania, USA
RFP-Trap Magnetic Agarose	ChromoTek GmbH, Planegg-Martinsried
Nitrocellulose membrane	GE Healthcare Europe GmbH (Freiburg)
Oligonucleotides	Eurofins MWG Operon (Ebersberg) Sigma
Roti-Mix-PCR3	Carl Roth GmbH + Co KG (Karlsruhe)
diaminopimelic acid	Carl Roth GmbH + Co KG (Karlsruhe)

Table 2 Enzymes and kits used in this study

Enzymes and Kits	Manufacturer
Restriction Enzymes	New England Biolabs (Frankfurt a. M.)
Phusion High-Fidelity DNA Polymerase	New England Biolabs (Frankfurt a. M.)
Q5® Hot Start High-Fidelity DNA Polymerase	New England Biolabs (Frankfurt a. M.)
Taq DNA Polymerase	New England Biolabs (Frankfurt a. M.)
Phire Hot Start II DNA Polymerase	Thermo Fisher Scientific (Frankfurt a. M.)
Antarctic Phosphatase	New England Biolabs (Frankfurt a. M.)
T4 DNA Ligase	Fermentas (St. Leon-Rot)
NucleoSpin® Gel and PCR Clean-up Kit	Macherey-Nagel (Düren)
NucleoSpin® Plasmid Kit	Macherey-Nagel (Düren
Genomic DNA mini Kit	Invitrogen™ Carlsbad

Table 3 Dives used in this study with applications

Application	Device	Manufacturer
Microscope	Deltavision elite deconvolution microscope	Applied Precision
PCR	Mastercycler personal Mastercycler nexus Mastercycler nexus gradient Mastercycler nexus X2	Eppendorf (Hamburg)
Thermomixer	Thermomixer compact Thermomixer comfort	Eppendorf (Hamburg)
	Dry block AccuBlock™	Labnet Wertheim
DNA illumination	E-BOX VX 2 Geldokumentation	Peqlab (Erlangen)
Nano Drop	DeNovix DS-11+Spectrometer	DeNovix Inc. (Wilmington)
OD_{600} Photometer	DeNovix DS-11+Spectrometer	DeNovix Inc. (Wilmington)
UV table	UVT_20 LE UV table	Herolab (Wiesloch)
Electroporator	MicroPulser Electroporator	BioRad (Feldkirchen)
Ultrasonicator	Sonopuls mini20	Bandelin (Berlin)
	UP200st Ultrasonic Processor	Hielscher (Teltow)
Protein electrophoresis	Mini-PROTEAN® Tetra Cell	Bio-Rad (München)
Western blotting	TransBlot®TurboTM ,	Bio-Rad (München)
Chemiluminescence detection	Luminescent image analyzer LAS-4000	Fujifilm (Düsseldorf)
Plate reader for absorbance measurements	Infinite M200 Pro	Tecan (Crailsheim)
Mass spectrometry	Q Exactive Plus Hybrid Quadrupole Orbitrap Mass Spectrometer	Thermo Scientific (Dreieeich)
Speed vacuum concentrator	Sovant SPD131DDA	Thermo Scientific (Dreieeich)

Table 4 Software applications online tools used in this study

Software applications and online tools	Source/Reference	URL
Serial cloner 2.6.1		http://serialbasics.free.fr/Serial_Cloner.html
SeqBuilder v12.3.1	DNASTAR Software for Life Scientists (Madison, WI)	
SeqMan Pro v12.3.1	DNASTAR Software for Life Scientists (Madison, WI)	
ImageJ-Fiji	(Schindelin *et al.*, 2012)	
BLAST ®		https://blast.ncbi.nlm.nih.gov/Blast.cgi
Uniprot	(Leinonen *et al.*, 2004)	https://www.uniprot.org/
STRING-known and predicted proteinprotein interactions	(Taboada et al., 2010)	https://string-db.org/
Phyre: Protein Homology/an Recognition Engine V 2.0	(Kelley and Sternberg, 2009)	http://www.sbg.bio.ic.ac.uk/phyre/html/
Oligo Calc: Oligonucleotide Properties Calculator	(Kibbe, 2007)	http://biotools.nubic.northwestern.edu/OligoCalc.html
NEB Webcolner	© Copyright 2020 New England Biolabs	http://nebcloner.neb.com/#!/
Webcutter2.0	(Maarek, 1997)	http://heimanlab.com/cut2.html
Perseus Computational platform	(Tyanova *et al.*, 2016)	
Scaffold v4.8.9	Proteome Software (Oregon, USA)	
Matlab R2020A	(MATLAB, 2020)	
Spyder Python 3.8	(Spyder, 2018)	
BiofilmQ	(Hartmann *et al.*, 2020)	https://drescherlab.org/data/biofilmQ/docs/

9.2 Microbial methods

9.2.1 Bacterial growth media used in this study

Unless otherwise state, *E. coli* and *P. aeruginosa* were grown in LB-Medium (Table 5) with the needed additive (Table 9) and antibiotics (Table 10) for the corresponding strain used. For the cultivation of *S. flexneri* and *Y. enterocolitica*, BHI media (Table 7) was used. For growth on plates,1.5% of agarose (Table *1*) was added to the media to create solid surface agar plates. All bacteria used in this study were grown on LB-agar plates. In case of *Y. enterocolitica* those contained a low salt LB medium (Table 6). In rare cases BHI plates were used to shorten growth periods of *Y. enterocolitica*.

Table 5 LB medium composition

Medium Composition LB	**(per Liter)**
Trypton	10g
Yeast extract	5g
NaCL	10g
In case of agar plates:	15g agar

Table 6 Low salt LB medium composition

Medium Composition LB	**(per Liter)**
Trypton	10g
Yeast extract	5g
NaCL	3g
In case of agar plates:	15g agar

Table 7 BHI medium composition

Medium Composition BHI	**(per Liter)**
Brain Heart infusion solids	17.5g
Peptones	10.0g
Glucose	2.0g
Sodium chloride	5.0g
Disodium Hydrogen Phosphate	2.5g
In case of agar plates:	15g agar

Table 8 Minimal medium for microscopy composition. Casamino acids were only added for long time experiments or selected experiments evolving secretion. For the majority of the experiments they were not used since they add a lot autofluoresces to the medium.

Medium Composition minimal Medium	**(per Liter)**
HEPES pH 7.2	100 mM
$(NH_4)_2SO_4$, ammonium sulfate	5 mM
NaCl	100 mM
Sodium glutamate	20 mM
$MgCl_2$	10 mM
K_2SO_4	5 mM
MES	50mM
Glycin	50mM
Casamino acids (only for long experiemnts)	0.5%

Table 9 Additives used for different media

Additives	Final concentration	Manufacturer
Diaminopimelic acid	60µg/ml	Carl Roth GmbH + Co KG (Karlsruhe)
$MgCl_2$	20mM	Carl Roth GmbH + Co KG (Karlsruhe)
EGTA	5mM	Carl Roth GmbH + Co KG (Karlsruhe)
Ca^{2+}	5mM	Carl Roth GmbH + Co KG (Karlsruhe)
Glycerol	0.4% v/v	Carl Roth GmbH + Co KG (Karlsruhe)
NaCl	200mM	Carl Roth GmbH + Co KG (Karlsruhe)

Table 10 Antibiotics used for strain and plasmid selection

Antibiotics	Final concentration	Manufacturer
Nalidixic acid	35µg/ml	Carl Roth GmbH + Co KG (Karlsruhe)
Ampicillin	20µg/ml	Carl Roth GmbH + Co KG (Karlsruhe)
Carbenicillin	20µg/ml	Carl Roth GmbH + Co KG (Karlsruhe)
Streptomycin	5µg/ml	Carl Roth GmbH + Co KG (Karlsruhe)
Kanamycin	5µg/ml	Carl Roth GmbH + Co KG (Karlsruhe)

9.2.2 Bacterial strain generation and genetic constructs

A list of strains used in this study can be found in (Table 11). The *Y. enterocolitica* strains used in this study are based on the *Y. enterocolitica* wild-type strain MRS40 (effector strain) (Sory *et al.*, 1995), and the strain IML421asd (ΔHOPEMTasd, effector-less strain), in which all major virulence effector proteins (YopH,O,P,E,M,T) are deleted (Kudryashev *et al.*, 2013). Furthermore, this strain harbors a deletion of the aspartate-beta-semialdehyde dehydrogenase gene which render the strain auxotrophic for diaminopimelic acid (DAP) (Table 9).

Unless stated otherwise, all fusion proteins used were expressed as endogenous fusions from their native location on the pYV virulence plasmid, which were introduced by two step homologous recombination with a *sucB (*pKNG) Pasmid based system (Kaniga *et al.*, 1991). Ectopical expression of single proteins or overexpression was done by expression from the pBad plasmid (incusible) or pACYC plasmid (constitutive) (Table 13).

For cloning and conjugation the *E. coli* strains Top10 and SM10λpir were used, respectively. All constructs were confirmed by sequencing (Eurofins Scientific and Microsynth Seqlab). Constructs with single amino acid substitutions in e.g. SctD or SctF were created by overlapping PCR using Phusion polymerase (New England Biolabs), and expressed from an arabinose controlled expression vector (pBAD). After confirmation of the sequence, the expression plasmids were prepped from the *E. coli* Top10 and electroporated into the corresponding *Y. enterocolitica* strain.

Table 11 Strains used in this study

Strain	Genotype	Reference
MRS40	Wild-type pYV *Y. enterocolitica* E40 Δ*blaA*	(Sory *et al.*, 1995)
IML421*asd* (HOPEMTasd)	MRS40 $yopO_{\Delta 12\text{-}427}$ $yopE_{21}$ $yopH\Delta_{11\text{-}352}$ $yopM_{23}$ $yopP_{23}$ $yopT_{135}$ Δ*asd*	(Kudryashev *et al.*, 2013)
AD4016	MRS40 *egfp-sctQ*	(Diepold *et al.*, 2010)
AD4085	IML421*asd egfp-sctQ*	(Kudryashev *et al.*, 2013)
AD4175	IML421*asd sctV-egfp* (mutated with pAD208)	This work
AD4306	IML421*asd egfp-sctD*	(Diepold *et al.*, 2015)
AD4411	IML421*asd egfp-sctQ ΔsctD*	(Diepold *et al.*, 2017)
AD4439	IML421*asd pamcherry1-sctD* (mutated with pAD439)	This work
AD4474	IML421*asd efgp-sctK*	(Diepold *et al.*, 2017)
ADTM4514	IML421*asd egfp-sctN*	(Diepold *et al.*, 2017)
ADTM4520	IML421*asd egfp-sctL*	(Diepold *et al.*, 2017)
ADTM4521	IML421*asd mcherry-sctL*	(Diepold *et al.*, 2017)
ADTM4525	IML421*asd halo-sctL*	(Diepold *et al.*, 2017)
ADMH4536	IML421*asd halo-sctL ΔsctF*	This work
DL001	*P. aeruginosa* PAO1 *egfp-sctQ*	(Lampaki *et al.*, 2020)
S. flexneri gfp-sctN	*S. flexneri* serotype 2a 2457T *gfp-sctN(spa47)*	(Burgess *et al.*, 2020)

9.2.3 Preparation of electro competent *E. coli*

This protocol has been provided by Andreas Diepold and is established and available in the lab. To prepare electro competent *E. coli strain* an overnight culture of the respective strain was inoculated from its storage at -80°C into a fresh LB medium with the strain specific antibiotics added and incubated over night at 37°C shaking 150 rpm. On the next day, a fresh 300 ml LB+antibiocita culture, in an 1000ml Colum, was inoculated to from the overnight culture, to an OD_{600} 0.1 and grown (~2h) at 37°C shaking to an OD_{600} of 0.6 -0.8. Next the cells were incubated on ice for 30 min. Subsequently, the culture was spilled up into 50 ml falcon tubes and centrifuged 3000 rpm/g 4°C for 15 min. The supernatant was discarded, resuspended in 20 ml ice-cold water and two tubes were pooled. After an additional centrifugation step, 3000 rpm/g 4°C for 15 min cells were resuspended in 15 ml/tube of ice-cold 10 % glycerol. In the final step, cells were pelleted again and taken up in 500µl ice-cold 10 % glycerol and aliquots of 50-100µl were snap frozen in liquid nitrogen and stored at -80 until usage.

9.2.4 Preparation of electrocompetent *Y. enterocolitica*

The protocol for the preparation of *Y. enterocolitica* has been provided by Andreas Diepold and is established and available in the lab. It is adapted from a protocol by C. Pfaff 2005. In the first step a fresh 100 ml culture of BHI media, in a 500ml flask, supplemented with Nal and Dap was inoculated to an OD_{600} 0.1 from an overnight culture. It was grown at 28°C to an OD_{600} of 0.45-0.6 (~3h). The flask was incubated on ice for 30 min and decanted into 50 ml falcon tubes. Next cells were collected by centrifugation, 2000 x g, 15 min at 4°C. After the supernatant was discarded the two pellets were collected in 40 m ice-cold water. Now cells were centrifuged again and resuspended in 20 ml ice-cold 10% glycerol. In the last step, cells were centrifuged, collected in 800 µl of ice-cold 10% glycerol and distributed in 100µl aliquots. Those were snap frozen stored at -80 until usage.

9.2.5 4.2.5 Transformation of electrocompetent cells

To transform prepped plasmids into electrocompetent *E. coli* cells or *Y. enterocolitica* cells, 1-2µl of plasmid, were mix with defrosted eletrocompetent cells (Preparation of electro *competent E. coli*and incubated on Ice for 15 minutes. In a next step, cells and plasmid were transferred into a precooled 2 mm electroporation cuvette and pulsed with the “Ec2” program in the electroporator (Table 3). Now 800µl of blank medium (LB/BHI+Dap) was added and cells were transferred into a fresh 1.5ml cup. After

90-120 min at 37/28°C 50µl and 50µl of a 1:100 dilution were plated on LB agar plates with the strain and plasmid corresponding antibiotics. Plates were incubated at 37/28°C for one or two days. For long-term storage an overnight culture of a single colony was inoculated and a glycerol stock was stored at -80°C.

9.2.6 Conjugation protocol for *Y. enterocolitica*

To mate and transfer the pKNG plasmid for a SM10λpir into a *Y. enterocolitica* strain, 1ml of acceptor and mutator strain were pletted, 2 min 10,000 rpm and washed once in 1 ml LB+Dap to remove traces of the antibiotics. Cells were pelleted again and taken up again in 100µl LB+Dap. Next, 20µl of acceptor and mutator strain were carefully mixed and 20µl were spotted on an LB+Dap agar plate. After 4h of incubation, all bacteria were removed with an inoculation loop and transferred into 1 ml of LB+Dap. After mixing carefully 20 µl have been plated on an LB+ Nal+Dap+Strep plate and incubated for 3 days (usually from Friday to Monday) at 28°C. When single colonies were visible, 4-6 of them have been used to inoculate 1ml of BHI+Nal+Dap+Strep cultures in 13 ml cultivation tubes (RRK1) and incubated overnight at 28°C shaking. This steps ensured to loop in of the pKNG Plasmid and kills of potentially left over *E. coli*. On the next day the 2µl of RRK1 cultures were used to inoculate 1-1.5 ml of BHI+Nal+Dap and grown in 13 ml culturing tube for 8 h to give the bacteria time for the loop outstep. At this point, a 15-20 µl of culture have been plated on LB+Nal+Dap+Suc plates to select for loop out conjugants again. Plates were incubated overnight at 28°C and colonies screened by colony PCR with flanking gene primers for positive insertion of deletion of the gene of interested. By confirmation of a positive clone it was inoculated into a LB+Nal+Dap+/-Strep culture to ensure that the pKNG Plasmid is truly looped out and the strain is correct. Afterwards the strain was stored as 20% Glycerolstock.

In the original protocol, 1.5µl of RRK1 was used to inoculate an RRK2 overnight. At the next day an RRK3 was inoculated and only plated after 4-5h of incubation. Those steps were to give more time for the loop out process and create nice single colonies on the agar plates. They turned out to not be needed.

9.2.7 Bacterial storage conditions

For long-term storage, Glycerol stocks have been prepared. For this, an overnight culture of the respective bacterial strain has been mixed 1:2 with a 40% glycerol solution, to create a stock with 20% (v/v) glycerol. The tubes have been snap-frozen with liquid nitrogen, documented in the strain collection list and stored at -80/-70°C.

9.2.8 Bacterial cultivation, in vitro secretion assays and fluorescence microscopy

Y. enterocolitica day cultures were inoculated from stationary overnight cultures to an OD_{600} of 0.15 and 0.12 for secreting and non-secreting conditions, respectively, in BHI medium (Suppl. Table 4) supplemented with nalidixic acid (35 mg/ml), diaminopimelic acid (80 mg/ml), glycerol (0.4%) and $MgCl_2$ (20 mM). Where required, ampicillin was added (0.2 mg/ml) to select for pBAD-based plasmids. For secreting conditions, cultures were additionally supplemented with 5 mM EGTA; for non-secreting conditions, cultures were additionally supplemented with 5 mM $CaCl_2$ and filtered through a 0.45 µm filter. Cultures were incubated at 28°C for 90 minutes. At this time point, expression of the *yop* regulon was induced by a rapid temperature shift to 37°C in a water bath and expression of proteins *in trans* was induced by addition of 0.2-1.0% arabinose, as indicated.

For effector visualization or total cell analysis, bacteria were incubated at 37°C between 1-3 hours, as indicated. 2 ml of the culture were collected at 21,000 *g* for 10 min. The supernatant was separated from the total cell fraction and precipitated with trichloroacetic acid (TCA) for 1-8 h at 4°C; proteins were collected by centrifugation for 15-20 min at 21,000 *g* and 4°C, washed once with ice cold acetone and then resuspended and normalized in SDS-PAGE loading buffer. Total cell samples were normalized to $2.5x10^8$ bacteria and supernatant samples to the equivalent of $3x10^8$ bacteria per SDS-PAGE gel lane. Samples were incubated for 5 minutes at 99°C, separated on 12-20% SDS-PAGE gels, using BlueClassic Prestained Marker (Jena Biosciences) as size standard, and stained with InstantBlue (Expedeon) (Table 1). Immunoblots were carried out using a primary rabbit antibody against *Y. enterocolitica* the respective protein of interssted (1:1000) in combination with a secondary antibody goat anti-rabbit, conjugated to horseradish peroxidase (Sigma A8275, 1:5000), and visualized using ECL chemiluminescent substrate (Pierce) on a LAS-4000 Luminescence Image Analyzer.

For fluorescence microscopy, bacteria were treated as described above. After 2-3 h at 37°C, 400 µl of bacterial culture were collected by centrifugation (2,400 *g*, 2 min) and resuspended in 200µl microscopy minimal medium (Suppl. Table 4). Cells were spotted on 1.5% low melting agarose pads (Sigma) in microscopy minimal medium in glass depression slides. Where required, 80 mg/ml DAP for IML421asd (ΔHOPEMTasd)-based strains, L-arabinose for induction of *in trans* expression, 5 mM Ca^{2+} for non-secreting conditions, or 5 mM EGTA for secreting conditions were added.

For the fluorescence microscopy experiment comparing different bacterial species, *Y. enterocolitica* were treated as above, except for the final resuspension for microscopy, which was done in BHI supplemented with 50 mM glycine, 50 mM MES, 50 mM HEPES, 80 mg/ml DAP and 5 mM EGTA and adjusted to the

indicated pH for all species. *P. aeruginosa o*vernight cultures were grown at 28°C. BHI medium (Suppl. Table 4) was supplemented with 20 mM $MgCl_2$, 200mM NaCl and 5 mM EGTA and inoculated to an OD_{600} of 0.15 and incubated for 2 h at 37°C. This culture was then used to inoculate a fresh culture containing the same supplements to an OD_{600} of 0.15. After 2 h, bacteria were collected and prepared for microscopy as described above for *Y. enterocolitica*. *S. flexneri* overnight cultures were inoculated from a fresh LB-agar plate or glycerol stocks into BHI broth supplemented with ampicillin (0.1 mg/ml) and kanamycin (0.05 mg/ml). On the next day, fresh BHI cultures were inoculated to an OD of 0.12 and grown to an OD of around 1 at 37°C (Burgess *et al.*, 2020). At this point, bacteria were collected and prepared for microscopy as described above for *Y. enterocolitica*. For the quantification of the fraction of injectisome - positive bacteria, 530-1143 bacteria in 21-25 fields of view from three independent experiments per strain and condition were classified independently by two blinded researches and the average numbers were used for the graphs.

9.2.9 Bacterial survival test

Wild-type *Y. enterocolitica* MRS40 were inoculated to an OD_{600} of 0.12 in non-secreting conditions and incubated for 1.5 h at 28°C to reach an exponential growth phase. Cells were collected by centrifugation at 2,400-3,000 *g* for 2-5 min. The supernatant was discarded and the collected bacteria were resuspended in a range of pH-adjusted media buffered with 50 mM glycine, 50 mM HEPES and 50 mM MES. Cultures were then placed in a 37°C shaking water bath and incubated at the indicated pH for 30 min. A dilution series in 1:10 steps was performed. 4 µl of the bacterial dilution were plated on a LB agar plate supplemented with nalidixic acid (35 mg/ml). Droplets were dried for 15 minutes before incubation of the plate overnight at 28°C.

9.2.10 Growth curve assays

Wild-type *Y. enterocolitica* MRS40 were inoculated to an OD_{600} of 0.12 in secreting conditions and incubated for 90 min at 28°C. At this point, cells were collected by centrifugation (2,400 *g*, 2 min), and resuspended in 37°C fresh pre-warmed secreting medium buffered with 50 mM glycine, 50 mM HEPES and adjusted to the indicated pH. After 90 min, one batch of cells incubated at pH 4 were collected again and resuspended in fresh buffered secretion medium at pH 7. All strains were incubated for further 90 min. During the experiment, the OD_{600} was measured every 30 min in technical duplicates, which were averaged; the figure displays the single data points for three independent biological replicates.

9.2.11 *Y. enterocolitica* YadA and cellular adhesion assays

To measure YadA adhesion to collagen at different pH values, an ELISA-like binding assay was performed (Leo *et al.*, 2008; Leo *et al.*, 2010; Saragliadis and Linke, 2019). Clear 96 well plates (Sarstedt, Ref. 82.1581) were coated with 100 µl of calf collagen type I (10 µg/ml, ThermoFisher A1064401) in H_2O with 0.01 M acetic acid for 1h at room temperature (RT). The supernatant was discarded and the wells were blocked with 1% BSA in PBS and afterwards washed three times with 0.1% BSA in PBS. Afterwards, 100 µL of purified YadA head domains with a C-terminal His_6-tag at a concentration of 10 µg/mL were incubated in the wells. In order to test binding at different pH, the YadA heads were diluted in acetic acid/sodium acetate at pH 4.0 or pH 5.0 and in PBS for higher pH values. Binding was allowed for 1h at RT. Afterwards, the plate was emptied and washed three times with 0.1% BSA in PBS. The wells were blocked with 1.0% BSA in PBS for 1h at RT. For detection, Ni-HRP conjugates (HisProbe-HRP, Thermo Fisher Scientific, Ref. 15165) were diluted in 0.1% BSA in PBS and 100 µl per well were incubated for 1 h at RT. The Ni-HRP conjugate solution was discarded and the wells washed three times with PBS. Detection was performed using ABTS substrate (Thermo Scientific. Ref. 34026). Development was allowed for 30 min. Absorption was measured at 405 nm on a plate reader (Biotek Synergy H1).

Glass binding assays for live *Y. enterocolitica* were performed in a flow cell. Bacteria were treated as mentioned above, resuspended in microscopy medium at the indicated pH value, and added to the flow cell as described above. Bacteria were tracked visually for 10 min afterwards.

9.3 Molecular biology methods

9.3.1 Oligonucleotides and plasmids used in this study

In Table 12 all the Oligonucleotides with there purpose and Primer AD number used in this study can be found. Table 13 displays all the plasmids that were used during this work.

Table 12 Oligonucleotides used in this study

Primer number	Purpose	Sequence (5`-3`)
AD439	pBAD_seq_fwd	ATGCCATAGCATTTTTATCC
AD340	pBAD_seq_rev	GCGTTCTGATTTAATCTGTATCAGG
AD341	sequencing, pKNG101	TATTAATTGATCTGCATCAACTTAACG
AD342	sequencing, pKNG101	GACTATACTAGTATACTCCGTCTACTGTACG
AD605	pHluorin-CW	GATCACATGTCCAAAGGAGAAGAACTTTTCACTGGAG
AD606	pHluorin-CCW	GATCGAATTCTTATTTGTATAGTTCATCCATGCCATG
AD647	pBad::YopH$_{1-17}$-EGFP-fwd	GACTTC**ATG**AACTTATCATTAAGCGATCTTCATCGTCAGGTATCT CGATTGGTGCAGAGCAAGGGCGAGGAGCTGTT
AD648	pBad::YopH$_{1-17}$-EGFP-rev	GACTGAATTC*TTA*CTTGTACAGCTCGTCCATGCC
AD649	pBAD-YopH1-17-sfGFP-fwd	GACTTC**ATG**AACTTATCATTAAGCGATCTTCATCGTCAGGTATCT CGATTGGTGCAGAGCAAAGGAGAAGAACTTTTCAC
AD650	pBAD-YopH$_{1-17}$-sfGFP-rev	GACTGAATTC*TTA*TTTGTAGAGCTCATCCATGCCATGT
AD652	pBAD-YopH$_{1-17}$-PAmCh -fwd	GACTTC**ATG**AACTTATCATTAAGCGATCTTCATCGTCAGGTATCT CGATTGGTGCAGAGCAAGGGCGAGGAGGATA
AD422	pBAD-YopH$_{1-17}$-PAmCh -rev	GACTGAATTCACCAGCGCCCTTGTACAGCTCGTCCATGC
AD681	pKNG101-SycH-preFP-fwd1	GACTGGGCCCTTGGGGTAGCATCTGGGAAG
AD682	pKNG101-SycH-preFP-rev1	TTTATAGAATTACAATTGAGATCTACCACCAGAGCCGCCCGAACC CCCAACCAGTAAATGAGATGATGA
AD683	pKNG101-SycH-preFP-fwd2	TCTGGTGGTAGATCTCAATTGTAATTCTATAAAAGAAAAACGTAC GGTATC
AD684	pKNG101-SycH-preFP-rev2	GACTTCTAGAAAGCAAAGGAAGTTCAGCGG
AD713	pKNG YscW-prePF-fwd1	GACTGGGCCCCTCGCACAGCACACATTGAT
AD714	pKNG YscW-prePF-rev1	TACAATTGAGTCAGATCTACCACCAGAGCCGCCCGAACCCCCTCT GGTATTAGGTGACTGGC
AD715	pKNG YscW-prePF-fwd2	GGTGGTAGATCTGACTCAATTGTAGAATTGCCAGTCACCTAATAC CA
AD716	pKNG YscW-prePF-fwd2	GACTTCTAGATGACTGCTGTTCTGCCATGA
AD797	pBAD::yscD-fwd	GACTTCATGAGTTGGGTCTGTCGTTTTT
AD798	pBAD::yscD- rev	GACTAGATCTTCATCGAGGTTTACCTCCATTG
AD799	pBAD::yscC-fwd	GACTCCATGGCTTTTTCGCTACATTCTTTTTTCAAG
AD800	pBAD::yscC-ref	GACTGAATTCTCACAATACGCCACGCTTAGG
AD801	pBAD::yscR-fwd	GACTTCATGATCCAGTTACCGGATGAAATTAATC
AD802	pBAD::yscC-rev	GACTGAATTCTCACCCTCCGTAACTAATCAC
AD862	pBAD::YscD$_{E212K}$ fwd	CCATGCTGC GCAG ATG AAGCCGGAATGGAATGCCATG
AD863	pBAD::YscD$_{E212K}$ rev	TCCATTCCGGCTT CAT CTGCGCAGCATGGAAGAACT
AD864	pBAD::YscD$_{E294Q}$ fwd	CAGACCAAATTG CTG AAG TAA TGC ATC AAG CCG CTT G
AD864	pBAD::YscD$_{E294Q}$ rev	GAT GCA TTA CTT CAG CAATTTGGTCTGGATTCAGATTTC
AD866	pBAD::YscD$_{H353Y}$ fwd	ATTCAATTCATCATACTGGGGTTGCCCCCCG
AD867	pBAD::YscD$_{H353Y}$ rev	GGGCAACCCCAGTATGATGAATTGAATTTTGAGGTGCAAG
AD915	pBad::YscD$_{E212Q}$ fwd	CCATGCTGCGCAGTTGAAGCCGGAATGGAATGCCATG

Primer number	Purpose	Sequence (5`-3`)
AD916	pBad::YscD$_{E212Q}$ rev	TTCCATTCCGGCTTCAACTGCGCAGCATGGAAGAACT
AD984	pBad::PamCh1-fwd	GACTGGTCTCCCATGGTGAGCAAGGGCGAGGAG
AD985	pBad::PamCh1-rev	GACTGAATTCTTACTTGTACAGCTCGTCCATGC
AD990	YscD$_{H193A}$_int_rev	GTGACAAGCGGGCAGCATTATCCTGGATATAACCAGTTAATAACCA
AD991	YscD$_{H193A}$_int_fwd	GTTATATCCAGGATAATGCTGCCCGCTTGTCACTGCAAAA
AD992	YscD$_{H205S}$_int_rev	GAATGGAATGCCAGAGCTCTCAAGAAAATTTTGCAGTGAC
AD993	YscD$_{H205S}$_int_fwd	AATTTTCTTGAGAGCTCTGGCATTCCATTCCGGCTT
AD994	YscD$_{H376G}$_int_rev	TGGATAGCGTTGACCATTGTCGAGTACCACATAAGGCA
AD995	YscD$_{H376G}$_int_fwd	GTACTCGACAATGGTCAACGCTATCCAGAAGGTGC
AD990	YscD$_{H193A}$_int_rev	GTGACAAGCGGGCAGCATTATCCTGGATATAACCAGTTAATAACCA
AD991	YscD$_{H193A}$_int_fwd	GTTATATCCAGGATAATGCTGCCCGCTTGTCACTGCAAAA
AD1039	pBad::sycO-yopO-fwd	GACTGGTCTCCCATGATTAACACCACCTTTACTGAGCTA
AD931	pBad::sycO-yopO-rev	GACTTTCGAATTAGAATTCACCAGATCTTCCCTTATCATCGTCGTCCTTGTAGTCACCCCATTCCCGCTCCAACCG
AD928	pBad::yopO-fwd	GACTGGTCTCCCATGAAAATCATGGGAACTATGCC
AD1040	pACYC-pamCh1-YscQ-full-fwd	GACTGGATCCTTGACTGAATGAGTTTGAGATCTGGTGCAG
AD1047	pACYC-pamCh1-YscQ-full-rev	GACTGTCGACTCATGAAATCGTAACCTCTGTCA
AD1046	pBad::pamCh1-YscQ-full-fwd	GACTACATGTCTTTGAGATCTGGTGCAG
AD87	YscQ rev	GACTGAATTC*TCA*TGAAATCGTAACCTCTGTCA
AD1111	pBad::pscD fwd (*P.aeruginosa*)	GACTCCATGGCCTGGAAGATCCGCTTCTAC
AD1112	pBad::pscD rev (*P aeruginosa*)	GACTAGATCTTCAGCGACCGACAGTCGC
AD1136	pBad::pscF fwd (*P.aeruginosa*))	GACTCCATGGCGCAGATATTCAACCCCAAC
AD1137	pBad::pscF rev (*P.aeruginosa*)	GACTGAATTCTCAGATCTTCTGCAGGATGCC
AD1138	pBad::pscF$_{N6C}$fwd(*P.aeruginosa)*	GACTCCATGGCGCAGATATTCTGCCCCAA
AD1139	pBad::ExsB fwd (*P.aeruginosa*)	GACTACATGTTATTGCCGCTGGCGTTGCTG
AD1140	pBad::ExsB rev (*P.aeruginosa*	GACTGAATTCTCAATCGTTGCCAGATCTTTCTT

Table 13 Strains and plasmids used in this study.

Plasmids	Genotype	Reference
pBAD-His B	pBR322-derived expression vector	Invitrogen
pKNG101	*oriR6K sacBR+ oriTRK2 strAB+* (suicide vector)	(Kaniga *et al.*, 1991)
pAD208	*pKNG101-sctV-egfp*	(Diepold *et al.*, 2017)
pAD439	*pKNG101-pamcherry1-sctD*	This work
pAD141	*pBAD::sctJ*	This work
pAD476	*pBAD::egfp*	(Diepold *et al.*, 2017)
pAD477	*pBAD::mCherry*	(Diepold *et al.*, 2017)
pAD603	*pBAD::sctV*	This work
pAD638	*pBAD::sctF*$_{S5C}$	This work
pEE010	*pBAD::sctD*$_{H193A,H205S,R214H,H353Y,H376G}$	This work
pISO85	*pKNG101-ΔsctF*	(Diepold *et al.*, 2010)
pSW001	*pBAD::pHluorin*	This work
pSW022	*pBAD::sctD*	This work
pSW023	*pBAD::sctC*	This work
pSW044	*pBAD::*pa*sctD*	This work
pSW039	*pBAD::pamch1*	This work
pSW043	*pBAD::pamch1-sctQ*	This work
pSW042	*pACYC184::pamCh1-sctQ*	This work
pSW040	*pBad::sycO-yopO*	This work
pSW041	*pBad::yopO*	This work

9.3.2 Generation of fluorescent fusions and inframe gene deletion

To create a seamless in frame deletion gene or insert a fluorescent protein+linkter the PKNG101 vector was used. Homologues regions, ~500bp upstream and downstream of the gene of interstate were selected to create homologues recombination sits. For fusion proteins the sequence of the tag protein and a linker were included preferably on the N-terminus but if needed also C-terminal (SctC, SctV). If there was any indication for the it might be needed to have different tag versions of the protein of interested

so call PreFP vectors have been designed. Those hold the flanking regions already and a tag can be included via restitution digestions in a way that you create a full fusion protein with start and stop codon and the linker in between. To do the Insilco work, serial cloner and DNA star have been used (**Table 4**).

Table 14 Linker to use for cloning.

	fwd:	rev.compl:
GFP:	GGT GCT GGC	ACC TGC CCC
YPet:	GGT GCT GGG	ACC TGC GCC
CyPet:	GGT GCA GGG	ACC AGC CCC
mCherry:	GGT GCA GGC	ACC AGC GCC

In case of overexpression of cross complication, a pBAD (inducible) or pACYC184 (constitutive) have been used. To construct those, the genes of interest were, were applicable combined with the chosen tag protein and linker by overlapping PCR. In the next step the generated insert was inserted into the plasmid backbone via restriction digestion. Generally final plasmids which include a PCR step, were mini prepped and sequence to confirm it accuracy. For detailed information how plasmids single plasmids were constructed and plasmid maps check: Q:\Sequences\Vectors\Stephan or H:\My Documents\Science Data\Clonings.

9.3.3 DNA isolation from *Y. enterocolitica*

Depending on the downstream use of the DNA two different methods were used to purify DNA. For PCR 100µl of bacterial overnight culture were heated up in a thermomixer (Table 3) to 99°C for 10 minutes to open up the cells. Afterwards leftover cells and cell debris were centrifuged down 10,000g for 10 minutes and DNA was stored at – 20°C for further use.

In cases where big amounts of high purity DNA were needed the Genomic DNA mini Kit (Table 3) was used according to manufacturing protocol. Afterwards DNA was stored at – 20°C for further use.

To pre the pYV plasmid that harbors the injectisome genes a miniprep was performed with the miniprep kit according to the manufacturing protocol (Table 3). After the DNA elution, DNA was stored at – 20°C for further use. For cloning purposes up to 1 µl of prepped DNA was used in PCR reactions.

9.3.4 Preparation of plasmids

For the preparation of plasmids, a fresh overnight culture (usually *E. coli* or *Y. enterocolitica*) harboring the plasmid of interest was used. Up to 5 ml of culture went into the prepping process and ia miniprep was performed with the miniprep kit according to the manufacturing protocol (Table 3). Plasmid elution was performed with prewarmed elution buffer at 55°C.

9.3.1 Preparation of gene fragments

To purify gene fragments for further downstream applications out of agarose gel of a digestion reaction, the DNA cleanup kit was used. The DNA sample was mix with the NTI buffer in a volume ratio of 1:2 and agarose was melted at 55°C Afterwards preparation was performed according to the protocol of the manufacturer. DNA elution was performed with prewarmed elution buffer at 55°C. If not used immediately, DNA was stored at -20°C until use.

9.3.2 Polymerase chain reaction (PCR)

Polymerase chain reaction (PCR) was used to amplify gene fragments of interest. For this two flanking primers at start and end of the gene were designed. Usually linker, restriction sites and a generic ATGC site were included at the start of the primer. The gene annealing, gene-specific sequence was chosen in a way that it was not shorter than 22 bp and with a predicted annealing temperature around 60°C (Salt Adjusted) in OligoClac (**Table 4**). For the PCR reaction single components H_2O, polymerase buffer, dNTP-mix, template DNA, forward and revers primer as well as the polymerase were combined in a Premix. In individual cases DMSO, MgCl or GC-enhancer were added. The polymerase enzyme was chosen based on its properties and adjusted to the task. TAC- and Phusion polymerase for cloning. Phusion, Q5 and Phire polymerase for cloning. Prosperities of the Premix were adjusted according to the manufacturing protocol of the specific polymerase used. Example: **Figure 43.** To confirm size and success of the polymerase an agarose gel was run to visualize the DNA.

In case of colony PCR which was used to confirm the presence or absence of a plasmid or gene a colony was picket with a 20µl pipet tip. Transferred on a Master-agarose plate with the respective antibiotic included for storage and then transfer into the aliquoted PCR mix (25µl) by pipetting up and down 2-3 times with the same tip as used before. To open up the cells, a 6 minutes step at 98°C was included in the PCR program which makes the DNA assessable for the amplification.

Number of tubes:	**1**	2x		98°	6 min
Volume per tube (ul):	**50**			98°	**10 sec**
Used Polymerase:	**Phu HM**			**55°**	**20 sec**
				72°	**XX min**
	Per tube	Premix		No of cycles:	**34**
Sample	**0.00**			72°	5 min
ddH20	33.8	38.9		4°/10°C	Pause
5x Phusion Buffer ***HF***	10.0	11.5			
dNTP-Mix (10 mM each)	1.0	1.2			
DNA if needed	1.0	1.2		**AD339/340**	
fwd Primer (10 uM)	2.0	2.3			
rev Primer (10 uM)	2.0	2.3			
Polymerase	0.2	0.2			
Sample:					
Control(s):					

Figure 43 Premix protocol for Phusion polymerase mix.

9.3.3 Agarose gel electrophoresis

Agarose Gel electrophoresis was performed to visualize gene fragments and separate them by size. Therefore, a 1% agarose solution was prepared and mix with ethidium bromide, later Gel red (0.1 µl/10 ml). A comb to create pockets was included and the gel was stored at room temperature to polymerize for around 20 min. Afterwards the gel was placed into a gel chamber filled with running buffer, sample and DNA Ladder (New England Biolabs) (Table 1) were loaded and the gel was run at 135 volts 500W and 150mA for 30 minutes. A gel documentation station (Peqlab) and UV table were used to examine the gels and document them.

9.3.4 Restriction digestion and ligation

To perform restriction digestion the manufacture enzyme and combination specific conditions were evaluated with the NEB online tool (**Table 4**) and the most favorable was chosen. In contrast to what the protocol suggested digestions were usually incubated 1 hour per enzyme, meaning a double digest for around 2h at the indicated temperature. After the digest time plasmid backbones were dephosphorylated with Antarctic phosphatase (**Table 2**) for up to 30 min. In a next step the products were purified with the respective kid. For the ligation backbone plasmid and insert were mix in a 1:3 equal molar ratio and ligated optimally overnight at 16°C. If that was not possible according to manufacturer protocol. After ligation plasmids were electroporated into the respective *E.coli* strain prepped from there again sequenced and then moved for long-term storage in a glycerol stock to –80°C.

9.3.5 Preparation of electrocompetent cells and electroporation

Electroporation was used as method to transfer cycler DNA into *E.coli* or *Y. enterocolitica* cells. For this electrocompetent cells were prepared in a first step. A 50-100ml culture was inoculated to an OD_{600} of 0.1 grown from a fresh overnight culture and grown to an of 04-06 (~3h). Next cell were stored on ice for 40 min while a centrifuge cooled down. Cells were harvested (2000 x g for *Y. enterocolitica*, 6000 for *E. coli* 15 min at 4°C) a resuspended in successively 20 ml (amounts for 50 ml initial culture) of ice-cold water, 10 ml ice-cold 10% glycerol and taken up in the end in 400µl of ice-cold glycerol. Those were dispensed in 100µl aliquots, shock frozen in liquid nitrogen and stored at -80°C until use.

For electroporation cell were thrown on ice transferred in a 2 mm electroporation cuvette, mixed with the plasmid of choice an incubated on ice on ice for 15 minutes. Next the cells electroporated (**Table 3**) and quickly recovered in 800µl of pre warmed growth media (BHI+Dap/LB) without antibiotics and grown for 90-120 minutes shanking at 28/37°C. Afterwards 50µl and 50µl of a 1:100 dilution were plated on LB plates supplemented with the respective supplements and antibiotics and incubated overnight at 28/37°C. Use of low salt LB agar or BHI agar can reduce the incubation time for *Y. enterocolitica* from two days down to one until single colony are visible.

9.4 Biochemical methods

9.4.1 SDS- polyacrylamide gel electrophoresis (SDS Page)

For effector visualization or total cell analysis, bacteria were incubated at 37°C between 1-3 hours, as indicated. 2 ml of the culture were collected at 21,000 *g* for 10 min. The supernatant was separated from the total cell fraction and precipitated with trichloroacetic acid (TCA) for 1-8 h at 4°C; proteins were collected by centrifugation for 15-20 min at 21,000 *g* and 4°C, washed once with ice cold acetone and then resuspended and normalized in SDS-PAGE loading buffer (SDS (2%w/v), TRIS-HCL (0.1 M), glycerol (10% w/v), DTT (0.05 M, pH = 6.8). Total cell samples were normalized to $2.5x10^8$ bacteria and supernatant samples to the equivalent of $3x10^8$ bacteria per SDS-PAGE gel lane (compositions SDS Gel **Table *15*-Table *18***). Samples were incubated for 5 minutes at 99°C, separated on 12-20% SDS-PAGE gels, using BlueClassic Prestained Marker (Jena Biosciences) as size standard, and stained with InstantBlue overnight (Expedeon).

Table 15 SDS upper buffer

Upper/stacking gel Buffer	
Tris base (1.5), pH 6.8 with HCL	60.5g
SDS	4.0g (0.4%)
ddH_2O	To one liter
	Sterile filter and store at 4°C

Table 16 SDS lower buffer.

Lower/separation gel Buffer	
Tris base (1.5), pH 8.8 with HCL	187g
SDS	4.0g (0.4%)
ddH_2O	To one liter
	Sterile filter and store at 4°C

Table 17 Resolving SDS gel composition

Resolving gel	**amount in 10 ml buffer enough for 2 11% gels**
ddH_2O	3.8 ml
Resolving buffer	2.5 ml
30% acrylamide	3.7 ml
10% APS	80µl
TEMED	6 µl
	Takes around 20 min to polymerize

Table 18 Stacking SDS gel composition

Stacking gel	**amount in 5 ml buffer enough for 2 11% gels**
ddH_2O	2.8 ml
Stacking buffer	1250 µl
30% acrylamide	825 µl
10% APS	50 µl
TEMED	3.75 µl
	Takes around 20 min to polymerize

9.4.2 Immunoblot (Western) analysis

Immunoblots were carried out to detect specific proteins using a primary rabbit antibody against *Y. enterocolitica* injectisome genes. For size separation a SDS was run (**9.4.1**). Proteins from the unstained gel were transferred on a nitrocellulose membrane by Turbo Blot (Bio-Rad) (**Table 3**). To block the membrane, the blot as incubated with 5% milk desolved in 1x PBS-0.2%-Tween PBS-T for one hour at room temperature. The blot was then washed 3-time with PBS-T before adding the primary antibody diluted in 10 ml 2 % Milk-PBS-T (e.g. SctD (MIPA232, 1:1000)). The blot was then incubated overnight at 4°C (or longer). After incubation the antibody dilution was stored at -20°C until further use and the blot was again 3 times with PBS-T. At this point the second antibody was applied again in 10 ml 2 % Milk-PBS-T dilution and incubated for 1h. Depending on the first antibody second was goat anti-rabbit/mouse antibody, conjugated to horseradish peroxidase (Sigma A8275, 1:5000), The secondary antibody was discarded the bot washed 3 time times with PBS-T and subsequently visualized by using ECL chemiluminescent substrate (Pierce) on a LAS-4000 Luminescence Image Analyzer.

9.4.3 pHluorin purification

The protocol described by Nakamura et al. (Nakamura *et al.*, 2009) was adapted for bench top purification. Expression of ratiometric GST-pHluorin$_{M153R}$ in *E. coli* DH5αZI was induced in a 500 ml culture with 1 mM IPTG, followed by 4 h incubation at 28°C. Cells were harvested and stored for further processing at -80°C. Next, cells were thawed on ice, resuspended in lysis buffer and disrupted by two passages through a French Press. The lysate was centrifuged (25,000 rpm, 60 min, 4°C) and the supernatant was gently mixed with the previously equilibrated glutathione agarose at 4°C for 1.5 h in a small spinning wheel. The agarose was collected by centrifugation (500 *g*, 5 min) and washed with PBS three times. A thrombin digest was performed in 2 ml PBS while incubating for 60 min on a roll mill. Agarose was removed by centrifugation (500 *g*, 5 min) and the protein was stored at -80°C for further use.

9.5 Microscopy based methods

9.5.1 Wide field fluorescence microscopy

Microscopy was performed on a Deltavision Elite Optical Sectioning Microscope (Applied Precision), equipped with a UApo N 100x/1.49 oil TIRF UIS2 objective (Olympus) and a UPlanSApo 100x/1.40 oil objective (Olympus), using an Evolve EMCCD Camera (Photometrics). Samples were illuminated for 0.1 s with a 488 nm laser with a TIRF depth setting of 3440 (TIRF) or for 0.2 s with green LED light (standard oil objective). Excitation and emission filter sets used were 475/28 and 525/48 nm (green), 575/25 and 625/45 nm (red), or 632/22 and 679/34 nm (Cy5). The micrographs where deconvolved using softWoRx 7.0.0 (standard "conservative" settings). Images were then further processed with ImageJ-Fiji. Where necessary, drift correction was performed with the StackReg Plugin. For figures, representative fields of view were selected, and brightness and contrast of the micrographs was adjusted identically within compared images.

Sample sizes and number of replicates for wide field microscopy and all other experiments were determined prior to the experiments, based on experimental feasibility and their potential to draw clear conclusions. These numbers were not changed based on the experimental outcome.

9.5.2 Flow cell based TIRF microscopy

A microscopy flow cell was manufactured based on (Berg and Block, 1984). Formation of injectisomes was induced under non-secreting conditions. After formation of the injectisomes, bacteria were collected and resuspended in approximately 0.5 volumes of microscopy medium (Suppl. Table 4) supplemented with 80 mg/ml DAP and 5mM EGTA. The flow cell was pre-incubated with microscopy medium and a bottom coverslip (25 mm No. 1.5; VWR) was attached to the cell. Bacteria were spotted on the coverslip and incubated for 1 min to allow attachment to the glass surface. The cover slip was covered with 60 µl of minimal medium and sealed from the top with an additional cover slip. The flow cell was mounted on the microscopy stage and gravity-driven buffer flow in the chamber was induced using a 1 ml syringe. To exchange the buffer in the flow cell, the tube was quickly relocated to a new reservoir. Complete buffer exchange in the flow cell was determined to take 39 $\pm$ 5 s (n = 7).

9.5.3 Maleimide based needle staining

To visualize the injectisome needles, expression of $SctF_{S5C}$ (Milne-Davies *et al.*, 2019) was induced from plasmid. Protein expression was induced with 0.4-1.0% L-arabinose at the temperature shift. After 2-3 h,

bacteria were collected and resuspended in 0.2 volumes of microscopy medium supplemented with 5 µM of CF 488A/568/633 maleimide dye (Sigma-Aldrich, USA) for 5 min in 100 µl of minimal medium at 37°C. After staining, cells were washed once with 500-1500 µl of minimal medium and spotted on 1.5% agarose pads in the same medium or analyzed in a flow cell as described above.

9.5.4 Halo staining with Janelia fluorescent dyes

To stain and visualize a defined pool of injectisome proteins, Halo-labeled proteins were visualized using Janelia Fluor 549-NHS ester or Janelia Fluor 646-NHS ester. 500 µl of bacterial culture were collected by centrifugation (2,400 *g*, 2 min) and resuspended in 100 µl microscopy medium. Bacteria were stained with 0.2 µM Janelia Fluor JF 646/JF 549 dyes at 37°C for 30 min in a tabletop shaker. Afterwards, bacteria were washed twice in 500 µl minimal medium and then visualized in a flow cell or on 1.5% agarose pads in the same medium.

9.5.5 Detection and quantification of fluorescent foci

Detection and quantification of foci was performed by first segmenting the images using the software BiofilmQ (Hartmann *et al.*, 2020). After segmentation, fluorescent foci were detected using a customized script within BiofilmQ. Foci were identified by finding local maxima within the bacterial cells prior to filtering by their quality, which was defined to be their brightness above the cell´s background intensity given by subtracting a smoothed image, divided by the overall mean fluorescence intensity of bacterial cells.

9.5.6 Quantification of fluorescent foci upon change of external pH

Bacteria were prepared for microscopy under secretion conditions as described above. After 2.5 h at 37°C, bacteria were loaded into the flow cell and buffer exchanges from pH 7 to pH4 and *vice versa* was performed. Cells were tracked by TIRF microscopy. Micrographs were acquired every 10s and quantification of foci was performed with BiofilmQ as described above.

Equilibration of cytosolic and external pH

2,4-dinitrophenol (DNP) was diluted in methanol and used at a final concentration of 2 mM in microscopy minimal medium. Cells were grown as described above, and resuspended in DNP containing medium immediately before being spotted on 1.5% agarose pads in the same medium containing DNP.

9.5.7 pHluorin calibration

The calibration was performed on a Deltavision Elite microscope. 5 µl of purified pHluorin protein were spotted on a KOH-cleaned microscopy slide in an enclosed compartment (Thermo Fisher Scientific GeneFrame, AB-0577) and incubated for 5 min to ensure attachment to the glass surface. Then, 10 µl of pH-adjusted PBS buffered with 200 mM glycine, 200 mM HEPES, and 200 mM MES were added. Ratiometric pHluorin fluorescence was determined using the DAPI excitation filter (390/18nm) or GFP excitation filter (475/28nm) at 32% illumination intensity, in combination with a GFP emission filter set (525/48nm) with 0.3 s exposure time. The overall fluorescence of the images before deconvolution was determined and corrected for background fluorescence levels, which were measured with an empty slide filled with PBS. The ratio of DAPI/Green vs Green/Green fluorescence was determined for a pH range from pH 8 – pH 5 in 0.5 pH steps.

9.5.8 Single particle tracking photoactivated localization microscopy (sptPALM)

Bacteria were cultivated under non-secreting conditions as described above. After 2.5 h of incubation at 37°C, the media was changed to pre-warmed (37°C) minimal microscopy medium containing the same supplements as the BHI before. Cells were incubated for 30 min and then washed four times in 5 volumes of pre-warmed (37°C) EZ medium (Suppl. Table 4) supplemented with DAP and 5 mM $CaCl_2$. Bacteria were concentrated 2x after the last wash and spotted on a 1.5% agarose pad in EZ medium supplemented with DAP and 5 mM $CaCl_2$ on a KOH-cleaned microscopy slide in an enclosed compartment (Thermo Fisher Scientific GeneFrame, AB-0577). Imaging was performed on a custom build setup based on an automated Nikon Ti Eclipse microscope equipped with appropriate dichroic and filters (ET DAPI/FITC/Cy3 dichroic, ZT405/488/561rpc rejection filter, ET610/75 bandpass, Chroma), and a CFI Apo TIRF 100x oil objective (NA 1.49, Nikon). All lasers (405 nm OBIS, 561 nm OBIS; all Coherent Inc. USA) were modulated via an acousto-optical tunable filter (AOTF) (Gooch and Housego, USA). Fluorescence was detected by an EMCCD camera (iXON Ultra 888, Andor, UK) in frame transfer mode and read-out parameter settings of EM-gain 300, pre-amp gain 2 and 30 MHz read-out speed. The z-focus was controlled using a commercial perfect focus system (Nikon). Acquisitions were controlled by a customized version of Micro-Manager (Edelstein *et al.*, 2010). Live cell sptPALM experiments were performed on a customized heating stage at 25°C. Live *Y. enterocolitica* PAmCherry-SctD cells were imaged in HILO illumination mode (Tokunaga *et al.*, 2008). Applied laser intensities measured after objective were 35 W/cm^2 (405 nm) and 800 W/cm^2 (561 nm). Prior to recording each new region of interest (ROI), a pre-bleaching step of 561 nm illumination was applied for 30 seconds to reduce autofluorescence. Videos were then recorded for 2000 frames pulsing

the 405 nm laser every 20th imaging frame at 5 Hz with an exposure time of 200 ms per frame. After sptPALM imaging, a bright light snapshot of all illuminated regions was recorded to obtain the bacterial cell shapes.

Single molecule localizations were obtained using *rapidSTORM* 3.3.1 (Wolter *et al.*, 2012) and single cells were manually segmented in *Fiji (ImageJ 1.51f)* (Schindelin *et al.*, 2012). sptPALM data was tracked, visualized and filtered using a customized tracking software written in C++ (***swift***, unpublished software, RG Endesfelder). Trajectories were allowed to have a maximum of 5 frames of gap time (e.g. caused by fluorophore blinking). Trajectories were assigned to their diffusive states (static and mobile) on the basis of the experimental localization precision of about 25 nm (determined by the NeNA method (Endesfelder *et al.*, 2014). For trajectories with more than 6 one-frame jumps, the mean jump distance (MJD) was calculated (jumps spanning several frames due to dark times were not used in MJD calculations). The obtained MJDs were weighted by the number of jumps and displayed in a histogram using OriginPro 9.4 (Origin LAB Corporation, USA). To estimate the diffusion coefficient D from the MJDs (M) at the frame rate τ=200 ms and the localization precision σ_m=25 nm, the equation $D=M^2\pi^{-1}-\sigma_m^2\tau^{-1}$ was used.

9.6 Mass Spectrometry based methods

9.6.1 Co-immunoprecipitation

For the CoIP, 100 ml of the respective cultures, were inoculated to a OD_{600} of 0.15 and incubated shaking 180rpm, 28°C, for 90min. After that cultures were shifted in a water bath to 37°C, incurable plasmids were induced with 0.5% L-arabinose and the cultures were incubated for 3 more hours. Now the samples were normalized to an OD_{600} of 1.0 and a total cell sample of 2 ml cultures was collected as first control sample. Next cells were washed with 10 ml Ice-cold PBS and then resuspended in HNN lysis buffer (50mM HEPES pH7.5, NaCl 150mM, 50mM NaF). Now 1% Triton 100, 1 pill of protease inhibitors and lysozyme 0.8mg/ml were added and this point 50µl of samples was taken as a control. Cells were incubated at 4°C on a rotator for 30 min. After that they were sonicated 12 pulses for 30 seconds and inverted after every 5 pulses. This was followed by an additional incubation on a rotator 30 min at 4°C and then again sonification (12 pulses, 30 seconds). After a third incubation on the rotator for 30 min at 4°C, unbroken cells were removed by centrifugation: 20 000g, 20min 4°C. At this step a control sample (50µl) was taken again. And cell pellets were stored at -20°C. The supernatant was now mixed with 20µl Chromotec RFP magnetic beats and incubated on and rotator for one hour at 4°C. Afterward samples were taken again as a process control. Now beats were separated with a magnetic rack and the supernatant was discarded after taking again

50µl as a control sample. Beats were subsequently washed tow times by the addition of 1 ml HHN buffer and mixed by pipetting up and down. For the elution beats were resuspended in 200µl 5% SDS without any blue dye and sored at -20°C until transfer to the proteomics facility. In case of low elution, a separate elusion based on pH was performed in addition and the sample was pooled afterwards.

9.6.2 Total cell analysis

For total cell MS analysis, the following protocol was performed in triplicates from independent overnight cultures. The bacterial cultures were brought to an exponential growth path phase and the injectisome assembly was triggered by a shift temperature upshift to 37°C. After 3h of incubation, samples were normalized based on their OD_{600} in a final volume of 2 ml. Cells were collated by centrifugation 5/10 min 20.000g at 4°C washed 3 times with Ice-cold PBS. The cell pellet was then resuspended in 300µl 2% SDC 10mABC provided by the proteomics facility and incubated for 10 minutes at 90°C. Samples were stored at -20°C until processing at the proteomics facility. From there on, the samples were processed by Jörg Kahnt, Witold Szymanski and Timo Glatter.The first results were usually summarized in from of a Scaffold file with peptide counts. Supernated samples were processed in a similar way.

10 List of abbreviations

ABC	Ammonium bicarbonate
BHI	Brain heart infusion medium
Ca^{2+}	Calcium Chloride
CoIP	Co-immunoprecipitation
CryoET	Electron cryotomography
CryoEM	cryoto electron Microscopy
DAP	Diaminopimelic acid
DIC	Differential interference contrast
DMSO	Dimethylsulfoxid
DNA	Deoxyribonucleic acid
E. col	*Escherichia coli*
EGTA	Egtazic acid
FRAP	Fluoresces recovery after photo bleaching
FRET	Förster resonance energy transfer
Fwd.	Forward primer
g	gravitational acceleration constant
GFP	Green fluorescent protein
h	hours
Kb	Kilobases
kDA	Kilo Dalton
LB	Luria-Bertani medium
min	Minutes

MOI	Multiplicity of infection
MS	Mass spectrometry
ms	milli seconds
MW	Molecular weight
Nal	Nalidixic acid
n.s.	not significant
NS	non-secreting condtions/medium
OD_{600}	Optical density at 600 nm
P. aeruginosa	Pseudomonas aeruginosa
PAGE	Polyacrylamide gel electrophoresis
PAmCh	photo aktivatible mcherry
PBS	Phosphate bufferd saline
PBS	Phosphate bufferd saline with 2% Tween
PCR	Polymerase chain reaction
pYV	Plasmid of *Yerinia* virulence
rev.	Reverse primer
RT	Room temperature
S	Secreting conditons/medium
sec	seconds
S. enterica	*Salmonella enterica*
S. flexneri	*Shigella flexneri*
sfGFP	superfolder Green fluorescent protein
SDS	Sodium dodecyl sulfate

SLS	Sodum lauryl sulfate
SPI-1	*Salmonella* pathogenicity island 1
SPI-2	*Salmonella* pathogenicity island 1
spp.	Species
sptPALM	Single-Particle Tracking Photoactivated
t	time
T3SS/TXSS	Type III secretion system/ Type X secretion system
WT	Wild type
TCA	Trichloroacetic acid
TRIS	Tris(hydroxymethylamiomethane)
TIRF	Total internal reflection fluorescence microscope
Y. enterocolitica	*Yersinia enterocolitica*
Y. pestis	*Yersinia pestis*
Y. pseudotuberculosis	*Yersinia pseudotuberculosis*
Yop	*Yersinia* outer membrane proteins

11 Sources

Abby, S.S., Rocha, E.P.C., Mead, D., Hackstadt, T., and Rey, S. (2012) The Non-Flagellar Type III Secretion System Evolved from the Bacterial Flagellum and Diversified into Host-Cell Adapted Systems. *PLoS Genet* **8**: e1002983.

Aberg, C., and Duderstadt, K.E. (2016) Stability versus exchange : a paradox in DNA replication Stability versus exchange : a paradox in DNA replication. .

Abrusci, P., McDowell, M.A., Lea, S.M., and Johnson, S. (2014) Building a secreting nanomachine: A structural overview of the T3SS. *Curr Opin Struct Biol* **25**: 111–117.

Abrusci, P., Vergara-Irigaray, M., Johnson, S., Beeby, M.D., Hendrixson, D.R., Roversi, P., *et al.* (2012) Architecture of the major component of the type III secretion system export apparatus. *Nat Struct Mol Biol* .

Akeda, Y., and Galán, J.E. (2005) Chaperone release and unfolding of substrates in type III secretion. *Nature* **437**: 911–915.

Al-Eryani, Y., Ib Rasmussen, M., Kjellström, S., Højrup, P., Emanuelsson, C., and Wachenfeldt, C. von (2016) Exploring structure and interactions of the bacterial adaptor protein YjbH by crosslinking mass spectrometry. *Proteins Struct Funct Bioinforma* .

Almawi, A.W., Matthews, L.A., and Guarné, A. (2017) FHA domains: Phosphopeptide binding and beyond. *Prog Biophys Mol Biol* **127**: 105–110.

Arai, S., Saijo, S., Suzuki, K., Mizutani, K., Kakinuma, Y., Ishizuka-Katsura, Y., *et al.* (2013) Rotation mechanism of Enterococcus hirae v 1-ATPase based on asymmetric crystal structures. *Nature* .

Armentrout, E.I., and Rietsch, A. (2016) The Type III Secretion Translocation Pore Senses Host Cell Contact. *PLOS Pathog* **12**: e1005530.

Ashkenazi, S., Levy, I., Kazaronovski, V., and Samra, Z. (2003) Growing antimicrobial resistance of Shigella isolates. *J Antimicrob Chemother* .

Bai, F., Morimoto, Y. V, Yoshimura, S.D.J., Hara, N., Kami-Ike, N., Namba, K., and Minamino, T. (2014) Assembly dynamics and the roles of FliI ATPase of the bacterial flagellar export apparatus. *Sci Rep* **4**: 6528.

Beeby, M., Ferreira, J.L., Tripp, P., Albers, S.V., and Mitchell, D.R. (2020) *Propulsive nanomachines: the convergent evolution of archaella, flagella and cilia*. Oxford University Press, .

Beeckman, D.S.A., and Vanrompay, D.C.G. (2010) Bacterial secretion systems with an emphasis on the chlamydial Type III secretion system. *Curr Issues Mol Biol* **12**: 17–41.

Berg, H.C., and Block, S.M. (1984) A Miniature Flow Cell Designed for Rapid Exchange of Media Under High-power Microscope Objectives. *Microbiology* **130**: 2915–2920.

Berger, C., Ravelli, R.B.G., López-iglesias, C., Diepold, A., and Peters, P.J. (2021) Structure of the *Yersinia* injectisome in intracellular host cell phagosomes revealed by cryo FIB electron tomography. *J Struct Biol* 107701.

Bergeron, J.R.C., Worrall, L.J., De, S., Sgourakis, N.G., Cheung, A.H., Lameignere, E., *et al.* (2015) The modular structure of the inner-membrane ring component PrgK facilitates assembly of the type III

secretion system basal body. *Structure* .

Bergeron, J.R.C., Worrall, L.J., Sgourakis, N.G., DiMaio, F., Pfuetzner, R.A., Felise, H.B., *et al.* (2013) A refined model of the prototypical Salmonella SPI-1 T3SS basal body reveals the molecular basis for its assembly. *PLoS Pathog* **9**: e1003307.

Bernal, I., Börnicke, J., Heidemann, J., Svergun, D., Horstmann, J.A., Erhardt, M., *et al.* (2019) Molecular Organization of Soluble Type III Secretion System Sorting Platform Complexes. *J Mol Biol* **431**: 3787–3803.

Bhoite, S., Gerven, N. van, Chapman, M.R., and Remaut, H. (2019) Curli Biogenesis: Bacterial Amyloid Assembly by the Type VIII Secretion Pathway. In *Protein Secretion in Bacteria*. .

Bibel, D.J., and Chen, T.H. (1976) Diagnosis of plague: an analysis of the Yersin Kitasato controversy. *Bacteriol Rev* **40**: 633–651.

Bitter, W., Houben, E.N.G., Bottai, D., Brodin, P., Brown, E.J., Cox, J.S., *et al.* (2009) Systematic genetic nomenclature for type VII secretion systems. *PLoS Pathog* .

Black, R.E., Jackson, R.J., Tsai, T., Medvesky, M., Shayegani, M., Feeley, J.C., *et al.* (1978) Epidemic *Yersinia enterocolitica* Infection Due to Contaminated Chocolate Milk. *N Engl J Med* .

Blaylock, B., Riordan, K.E., Missiakas, D.M., and Schneewind, O. (2006) Characterization of the *Yersinia enterocolitica* type III secretion ATPase YscN and its regulator, YscL. *J Bacteriol* **188**: 3525–34.

Block, S.M., and Berg, H.C. (1984) Successive incorporation of force-generating units in the bacterial rotary motor. *Nature* **309**: 470–472.

Blocker, A.J., Deane, J.E., Veenendaal, A.K.J., Roversi, P., Hodgkinson, J., Johnson, S., and Lea, S.M. (2008) What's the point of the type III secretion system needle? *Proc Natl Acad Sci U S A* **105**: 6507–6513.

Bohn, E., Sonnabend, M., Klein, K., and Autenrieth, I.B. (2019) Bacterial adhesion and host cell factors leading to effector protein injection by type III secretion system. *Int J Med Microbiol* **309**: 344–350.

Bolin, I., Portnoy, D.A., and Wolf-Watz, H. (1985) Expression of the temperature-inducible outer membrane proteins of Yersiniae. .

Bottone, E.J. (1997) *Yersinia enterocolitica*: The charisma continues. *Clin Microbiol Rev* **10**: 257–276.

Bottone, E.J., and Mollaret, H.-H. (1977) *Yersinia Enterocolitica* : A Panoramic View of a Charismatic Microorganism. *CRC Crit Rev Microbiol* **5**: 211–241.

Boucher, R.C. (2004) New concepts of the pathogenesis of cystic fibrosis lung disease. *Eur Respir J* **23**: 146–158.

Braig, K., Menz, R.I., Montgomery, M.G., Leslie, A.G., and Walker, J.E. (2000) Structure of bovine mitochondrial F1-ATPase inhibited by Mg2+ADP and aluminium fluoride. *Structure* .

Brossollet, J., and Mollaret, H.H. (1994) Pourquoi la peste ?: le rat, la puce et le bubon. 160.

Brotcke Zumsteg, A., Goosmann, C., Brinkmann, V., Morona, R., and Zychlinsky, A. (2014) IcsA is a *Shigella flexneri* adhesion regulated by the type III secretion system and required for pathogenesis. *Cell Host Microbe* .

Broz, P., Mueller, C.A., Müller, S.A., Philippsen, A., Sorg, I., Engel, A., and Cornelis, G.R. (2007) Function and molecular architecture of the *Yersinia* injectisome tip complex. *Mol Microbiol* .

Burgess, J.L., Case, H.B., Burgess, R.A., and Dickenson, N.E. (2020) Dominant negative effects by inactive Spa47 mutants inhibit T3SS function and *Shigella* virulence. *PLoS One* **15**: 1–19.

Burghout, P., Beckers, F., Wit, E. de, Boxtel, R. van, Cornelis, G.R., Tommassen, J., and Koster, M. (2004) Role of the pilot protein YscW in the biogenesis of the YscC secretin in *Yersinia enterocolitica*. *J Bacteriol* **186**: 5366–75.

Burkinshaw, B.J., and Strynadka, N.C.J. (2014) Assembly and structure of the T3SS. *Biochim Biophys Acta - Mol Cell Res* .

Butan, C., Lara-Tejero, M., Li, W., Liu, J., and Galán, J.E. (2019) High-resolution view of the type III secretion export apparatus in situ reveals membrane remodeling and a secretion pathway. *Proc Natl Acad Sci U S A* **116**: 24786–24795.

Büttner, D. (2012) Protein export according to schedule: architecture, assembly, and regulation of type III secretion systems from plant- and animal-pathogenic bacteria. *Microbiol Mol Biol Rev* **76**: 262–310.

Bzymek, K.P., Hamaoka, B.Y., and Ghosh, P. (2012) Two Translation Products of *Yersinia yscQ* Assemble To Form a Complex Essential to Type III Secretion. *Biochemistry* **51**: 1669–1677.

Carter, P.B., Zahorchak, R.J., and Brubaker, R.R. (1980) Plague virulence antigens from *Yersinia enterocolitica. Infect Immun* **28**: 638–640.

Cascales, E., and Christie, P.J. (2003) The versatile bacterial type IV secretion systems. *Nat Rev Microbiol* .

Case, H.B., and Dickenson, N.E. (2018) MxiN Differentially Regulates Monomeric and Oligomeric Species of the *Shigella* Type Three Secretion System ATPase Spa47. *Biochemistry* .

Chaban, B., Hughes, H.V., and Beeby, M. (2015) The flagellum in bacterial pathogens: For motility and a whole lot more. *Semin Cell Dev Biol* **46**: 91–103.

Chagnot, C., Zorgani, M.A., Astruc, T., and Desvaux, M. (2013) Proteinaceous determinants of surface colonization in bacteria: bacterial adhesion and biofilm formation from a protein secretion perspective. *Front Microbiol* **4**.

Chakravortty, D., Rohde, M., Jäger, L., Deiwick, J., and Hensel, M. (2005) Formation of a novel surface structure encoded by *Salmonella* Pathogenicity Island 2. *EMBO J* **24**: 2043–2052.

Chatterjee, P., Sass, G., Swietnicki, W., and Stevens, D.A. (2020) Review of potential pseudomonas weaponry, relevant to the pseudomonas–aspergillus interplay, for the mycology community. *J Fungi* **6**: 1–22.

Chen, L., Zou, Y., Kronfl, A.A., and Wu, Y. (2020) Type VI secretion system of *Pseudomonas aeruginosa* is associated with biofilm formation but not environmental adaptation. *Microbiologyopen* .

Chen, S., Thompson, K.M., and Francis, M.S. (2016) Environmental Regulation of *Yersinia* Pathophysiology. *Front Cell Infect Microbiol* **6**: 25.

Cheng, S., Liu, Y., Crowley, C.S., Yeates, T.O., and Bobik, T.A. (2008) Bacterial microcompartments: Their properties and paradoxes. *BioEssays* .

Clerc, P., Baudry, B., and Sansonetti, P.J. (1986) Plasmid-mediated contact haemolytic activity in *Shigella* species: correlation with penetration into HeLa cells. *Ann Inst Pasteur Microbiol* **137A**: 267–78.

Coburn, B., Sekirov, I., and Finlay, B.B. (2007a) Type III secretion systems and disease. *Clin Microbiol Rev*

20: 535–49.

Coburn, B.A., Grassl, G.A., and Finlay, B.B. (2007b) Salmonella , the host and disease: a brief review. *Immunol Cell Biol* **85**: 112–118.

Cornelis, G. (2006) The type III secretion injectisome. *Nat Rev Microbiol* **4**: 811–825.

Cornelis, G., Sluiters, C., Lambert de Rouvroit, C., and Michiels, T. (1989) Homology between virF, the transcriptional activator of the Yersinia virulence regulon, and AraC, the Escherichia coli arabinose operon regulator. *J Bacteriol* .

Cornelis, G., Vanootegem, J.C., and Sluiters, C. (1987) Transcription of the yop regulon from *Y. enterocolitica* requires trans acting pYV and chromosomal genes. *Microb Pathog* **2**: 367–379.

Cornelis, G.R. (2002) *Yersinia* type III secretion: Send in the effectors. *J Cell Biol* **158**: 401–408.

Cover, T.L., and Aber, R.C. (1989) *Yersinia Enterocolitica*. *N Engl J Med* **321**: 16–24.

Damen, X.M.P.M., Phan, T.H., Ummels, R., Rubio-Canalejas, A., Bitter, W., and Houben, X.E.N.G. (2020) Modification of a pe/ppe substrate pair reroutes an esx substrate pair from the mycobacterial esx-1 type VII secretion system to the esx-5 system. *J Biol Chem* **295**: 5960–5969.

Davis, A.J., and Mecsas, J. (2007) Mutations in the *Yersinia pseudotuberculosis* type III secretion system needle protein, YscF, that specifically abrogate effector translocation into host cells. *J Bacteriol* .

Dawson, J.E., Seckute, J., De, S., Schueler, S.A., Oswald, A.B., and Nicholson, L.K. (2009) Elucidation of a pH-folding switch in the Pseudomonas syringae effector protein AvrPto. *Proc Natl Acad Sci U S A* **106**: 8543–8.

Deane, J.E., Roversi, P., Cordes, F.S., Johnson, S., Kenjale, R., Daniell, S., *et al.* (2006) Molecular model of a type III secretion system needle: Implications for host-cell sensing. *Proc Natl Acad Sci U S A* **103**: 12529–12533.

Dechant, R., Binda, M., Lee, S.S., Pelet, S., Winderickx, J., and Peter, M. (2010) Cytosolic pH is a second messenger for glucose and regulates the PKA pathway through V-ATPase. *EMBO J* **29**: 2515–26.

Delepelaire, P. (2004) Type I secretion in gram-negative bacteria. *Biochim Biophys Acta - Mol Cell Res* .

Deng, W., Marshall, N.C., Rowland, J.L., McCoy, J.M., Worrall, L.J., Santos, A.S., *et al.* (2017) Assembly, structure, function and regulation of type III secretion systems. *Nat Rev Microbiol* **15**: 323–337.

Desvaux, M., Hébraud, M., Talon, R., and Henderson, I.R. (2009) Secretion and subcellular localizations of bacterial proteins: a semantic awareness issue. *Trends Microbiol* .

Diepold, A. (2020) Assembly and post-assembly turnover and dynamics in the type III secretion system. *Curr Top Microbiol Immunol* **427**: 35–66.

Diepold, A., Amstutz, M., Abel, S., Sorg, I., Jenal, U., and Cornelis, G.R. (2010) Deciphering the assembly of the *Yersinia* type III secretion injectisome. *EMBO J* **29**: 1928–1940.

Diepold, A., and Armitage, J.P. (2015) Type III secretion systems: the bacterial flagellum and the injectisome. *Philos Trans R Soc London B Biol Sci* **370**.

Diepold, A., Kudryashev, M., Delalez, N.J., Berry, R.M., and Armitage, J.P. (2015) Composition, Formation, and Regulation of the Cytosolic C-ring, a Dynamic Component of the Type III Secretion Injectisome. *PLOS*

Biol **13**: e1002039.

Diepold, A., Sezgin, E., Huseyin, M., Mortimer, T., Eggeling, C., and Armitage, J.P. (2017) A dynamic and adaptive network of cytosolic interactions governs protein export by the T3SS injectisome. *Nat Commun* **8**: 15940.

Diepold, A., Wagner, S., J, W., C, V., J, V., W, R., *et al.* (2014) Assembly of the bacterial type III secretion machinery. *FEMS Microbiol Rev* **38**: 802–822.

Diepold, A., Wiesand, U., Amstutz, M., and Cornelis, G.R. (2012) Assembly of the *Yersinia* injectisome: the missing pieces. *Mol Microbiol* **85**: 878–92.

Diepold, A., Wiesand, U., and Cornelis, G.R. (2011) The assembly of the export apparatus (YscR,S,T,U,V) of the *Yersinia* type III secretion apparatus occurs independently of other structural components and involves the formation of an YscV oligomer. *Mol Microbiol* **82**: 502–514.

Dietsche, T., Tesfazgi Mebrhatu, M., Brunner, M.J., Abrusci, P., Yan, J., Franz-Wachtel, M., *et al.* (2016) Structural and Functional Characterization of the Bacterial Type III Secretion Export Apparatus. *PLOS Pathog* **12**: e1006071.

Doherty, G.P., Bailey, K., and Lewis, P.J. (2010) Stage-specific fluorescence intensity of GFP and mCherry during sporulation In Bacillus Subtilis. *BMC Res Notes* **3**: 303.

Edelstein, A., Amodaj, N., Hoover, K., Vale, R., and Stuurman, N. (2010) Computer control of microscopes using μManager. *Curr Protoc Mol Biol* **Chapter 14**: Unit14.20.

Endesfelder, U., Malkusch, S., Fricke, F., and Heilemann, M. (2014) A simple method to estimate the average localization precision of a single-molecule localization microscopy experiment. *Histochem Cell Biol* **141**: 629–38.

Engel, J., and Balachandran, P. (2009) Role of *Pseudomonas aeruginosa* type III effectors in disease. *Curr Opin Microbiol* **12**: 61–66.

Engel, J.N. (2003) Molecular Pathogenesis of Acute *Pseudomonas Aeruginosa* Infections. Springer, Boston, MA, pp. 201–229.

Enninga, J., Mounier, J., Sansonetti, P., and Nhieu, G.T. Van (2005) Secretion of type III effectors into host cells in real time. *Nat Methods* **2**: 959–966.

Enninga, J., and Rosenshine, I. (2009) Imaging the assembly, structure and activity of type III secretion systems. *Cell Microbiol* **11**: 1462–1470.

Erhardt, M., Mertens, M.E., Fabiani, F.D., and Hughes, K.T. (2014) ATPase-Independent Type-III Protein Secretion in *Salmonella enterica*. *PLoS Genet* **10**: e1004800.

Espenhain, L., Riess, M., Müller, L., Colombe, S., Ethelberg, S., Litrup, E., *et al.* (2019) Cross-border outbreak of *yersinia enterocolitica* O3 associated with imported fresh spinach, Sweden and Denmark, march 2019. *Eurosurveillance* **24**: 1–5.

Evans, D.F., Pye, G., Bramley, R., Clark, A.G., Dyson, T.J., and Hardcastle, J.D. (1988) Measurement of gastrointestinal pH profiles in normal ambulant human subjects. *Gut* **29**: 1035–41.

Filloux, A., Hachani, A., and Bleves, S. (2008) The bacterial type VI secretion machine: Yet another player for protein transport across membranes. *Microbiology* .

Formal, S.B. (1989) Inoculum Size in Shigellosis and Implications For Expected Mode of Transmission. *J Infect Dis* .

Foster, J.W. (2004) *Escherichia coli* acid resistance: tales of an amateur acidophile. *Nat Rev Microbiol* **2**: 898–907.

Fowler, J.M., and Brubaker, R.R. (1994) Physiological basis of the low calcium response in *Yersinia pestis*. *Infect Immun* .

Fredriksson-Ahomaa, M., Stolle, A., and Korkeala, H. (2006) Molecular epidemiology of *Yersinia enterocolitica* infections. *FEMS Immunol Med Microbiol* **47**: 315–329.

Freudl, R. (2013) Leaving home ain't easy: Protein export systems in Gram-positive bacteria. *Res Microbiol* .

Fukuoka, H., Sowa, Y., Kojima, S., Ishijima, A., and Homma, M. (2007) Visualization of functional rotor proteins of the bacterial flagellar motor in the cell membrane. *J Mol Biol* **367**: 692–701.

Galán, J.E. (2009) Common Themes in the Design and Function of Bacterial Effectors. *Cell Host Microbe* **5**: 571–579.

Gayraud, M., Scavizzi, M.R., Mollaret, H.H., Guillevin, L., and Hornstein, M.J. (1993) Antibiotic Treatment of *Yersinia enterocolitica* Septicemia: A Retrospective Review of 43 Cases. *Clin Infect Dis* **17**: 405–410.

Ghoul, M., Pommepuy, M., Moillo-Batt, A., and Cormier, M. (1989) Effect of carbonyl cyanide m-chlorophenylhydrazone on *Escherichia coli* halotolerance. *Appl Environ Microbiol* **55**: 1040–1043.

Ghuman, A., Zhou, Y., Liu, Y., Mao, L., and Ramasamy, R.P. (2018) Bacteriophage-Assisted Magnetic Separation and Electrochemical Detection of Pathogenic Bacteria from Food Matrix. *ECS Trans* **85**: 1475–1480.

Gorasia, D.G., Veith, P.D., Hanssen, E.G., Glew, M.D., Sato, K., Yukitake, H., *et al.* (2016) Structural Insights into the PorK and PorN Components of the Porphyromonas gingivalis Type IX Secretion System. *PLoS Pathog* .

Green, E.R., and Mecsas, J. (2016) Bacterial Secretion Systems: An Overview. *Microbiol Spectr* **4**.

Greening, C., and Lithgow, T. (2020) Formation and function of bacterial organelles. *Nat Rev Microbiol* .

Grimm, J.B., Brown, T.A., English, B.P., Lionnet, T., and Lavis, L.D. (2017) Synthesis of Janelia Fluor HaloTag and SNAP-Tag Ligands and Their Use in Cellular Imaging Experiments. *Methods Mol Biol* **1663**: 179–188.

Grosdent, N., Maridonneau-Parini, I., Sory, M.-P., and Cornelis, G.R. (2002) Role of Yops and adhesins in resistance of *Yersinia enterocolitica* to phagocytosis. *Infect Immun* **70**: 4165–76.

Guo, E.Z., Desrosiers, D.C., Zalesak, J., Tolchard, J., Berbon, M., Habenstein, B., *et al.* (2019) A polymorphic helix of a *Salmonella* needle protein relays signals defining distinct steps in type III secretion. *PLOS Biol* .

Gurung, J.M., Amer, A.A.A., Francis, M.K., Costa, T.R.D., Chen, S., Zavialov, A. V., and Francis, M.S. (2018) Heterologous complementation studies with the YscX and YscY protein families reveals a specificity for *Yersinia pseudotuberculosis* type III secretion. *Front Cell Infect Microbiol* **8**: 1–16.

Håkansson, S., Schesser, K., Persson, C., Galyov, E.E., Rosqvist, R., Homblé, F., and Wolf-Watz, H. (1996) The YopB protein of Yersinia pseudotuberculosis is essential for the translocation of Yop effector proteins across the target cell plasma membrane and displays a contact-dependent membrane disrupting activity.

EMBO J **15**: 5812–5823.

Han, Y.W., and Miller, V.L. (1997) Reevaluation of the virulence phenotype of the inv yada double mutants of *Yersinia pseudotuberculosis*. *Infect Immun* **65**: 327–330.

Haneburger, I., Eichinger, A., Skerra, A., and Jung, K. (2011) New insights into the signaling mechanism of the pH-responsive, membrane-integrated transcriptional activator CadC of *Escherichia coli*. *J Biol Chem* **286**: 10681–9.

Hartmann, R., Jeckel, H., Jelli, E., Singh, P.K., Vaidya, S., Bayer, M., *et al.* (2020) Quantiative image analysis of microbial communitites with BiofilmQ. *Nat Microbiol* in print.

Hauser, A.R., Cobb, E., Bodí, M., Mariscal, D., Vallés, J., Engel, J.N., and Rello, J. (2002) Type III protein secretion is associated with poor clinical outcomes in patients with ventilator-associated pneumonia caused by *Pseudomonas aeruginosa*. *Crit Care Med* **30**: 521–528.

Hawgood, B.J. (2008) Alexandre Yersin (1863-1943): discoverer of the plague bacillus, explorer and agronomist. *J Med Biogr* **16**: 167–172.

Helenius, A., Kartenbeck, J., Simons, K., and Fries, E. (1980) On the entry of Semliki forest virus into BHK-21 cells. *J Cell Biol* **84**: 404–20.

Heroven, A.K., and Dersch, P. (2014) Coregulation of host-adapted metabolism and virulence by pathogenic *yersiniae*. *Front Cell Infect Microbiol* **4**: 146.

Hodgkinson, J.L., Horsley, A., Stabat, D., Simon, M., Johnson, S., Fonseca, P.C.A. Da, *et al.* (2009) Three-dimensional reconstruction of the *Shigella* T3SS transmembrane regions reveals 12-fold symmetry and novel features throughout. *Nat Struct Mol Biol* .

Hoe, N.P., and Goguen, J.D. (1993) Temperature sensing in *Yersinia pestis*: Translation of the LcrF activator protein is thermally regulated. .

Hong, J., Hunt, A.G., Masters, P.S., and Lieberman, M.A. (1979) Requirement of acetyl phosphate for the binding protein-dependent transport systems in *Escherichia coli. Proc Natl Acad Sci U S A* **76**: 1213–1217.

Houben, D., Demangel, C., Ingen, J. van, Perez, J., Baldeón, L., Abdallah, A.M., *et al.* (2012) ESX-1-mediated translocation to the cytosol controls virulence of mycobacteria. *Cell Microbiol* .

Hu, Bo; Lara-Tejero, Maria; Kong, Qingke; Galán, Jorge. E; Liu1, J. (2017) In situ molecular archi- tecture of the *Salmonella* type III secretion machine. *Physiol Behav* **176**: 139–148.

Hu, B., Lara-Tejero, M., Kong, Q., Galán, J.E., and Liu, J. (2017) In Situ Molecular Architecture of the *Salmonella* Type III Secretion Machine. *Cell* **168**: 1065-1074.e10.

Hu, B., Morado, D.R., Margolin, W., Rohde, J.R., Arizmendi, O., Picking, W.L., *et al.* (2015) Visualization of the type III secretion sorting platform of *Shigella flexneri*. *Proc Natl Acad Sci* **112**: 1047–1052.

Hu, J., Worrall, L.J., Hong, C., Vuckovic, M., Atkinson, C.E., Caveney, N., *et al.* (2018) Cryo-EM analysis of the T3S injectisome reveals the structure of the needle and open secretin. *Nat Commun* **9**.

Hu, Y., Lu, P., Wang, Y., Ding, L., Atkinson, S., and Chen, S. (2009) OmpR positively regulates urease expression to enhance acid survival of *Yersinia pseudotuberculosis*. *Microbiology* **155**: 2522–2531.

Hu, Y., Lu, P., Zhang, Y., Li, L., and Chen, S. (2010) Characterization of an aspartate-dependent acid survival system in *Yersinia pseudotuberculosis*. *FEBS Lett* **584**: 2311–2314.

Hueck, C.J. (1998) Type III protein secretion systems in bacterial pathogens of animals and plants. *Microbiol Mol Biol Rev* **62**: 379–433.

Hüsing, S., Look, U. van, Guse, A., Gálvez, E.J.C., Charpentier, E., Blair, D.F., *et al.* (2020) Controlling membrane barrier during bacterial type-III protein secretion. *bioRxiv* .

Ibuki, T., Imada, K., Minamino, T., Kato, T., Miyata, T., and Namba, K. (2011) Common architecture of the flagellar type III protein export apparatus and F- and V-type ATPases. *Nat Struct Mol Biol* .

Inoue, Y., Ogawa, Y., Kinoshita, M., Terahara, N., Shimada, M., Kodera, N., *et al.* (2019) Structural Insights into the Substrate Specificity Switch Mechanism of the Type III Protein Export Apparatus. *Structure* **27**: 965-976.e6.

Iriarte, M., and Cornelis, G.R. (1998) YopT, a new Yersinia Yop effector protein, affects the cytoskeleton of host cells. *Mol Microbiol* **29**: 915–929.

Jackson, M.W., and Plano, G. V. (2000) Interactions between type III secretion apparatus components from *Yersinia pestis* detected using the yeast two-hybrid system. *FEMS Microbiol Lett* **186**: 85–90.

Jain, M., Bar-Meir, M., McColley, S., Cullina, J., Potter, E., Powers, C., *et al.* (2008) Evolution of *Pseudomonas aeruginosa* type III secretion in cystic fibrosis: a paradigm of chronic infection. *Transl Res* .

Jennison, A. V., and Verma, N.K. (2004) *Shigella flexneri* infection: Pathogenesis and vaccine development. *FEMS Microbiol Rev* **28**: 43–58.

Jensen, J.L., Yamini, S., Rietsch, A., and Spiller, B.W. (2020) The structure of the type III secretion system export gate with CdsO, an ATPase lever arm. *PLoS Pathog* **16**: 1–18.

Johnson, S., and Blocker, A. (2008) Characterization of soluble complexes of the *Shigella flexneri* type III secretion system ATPase. *FEMS Microbiol Lett* **286**: 274–278.

Jong, M.F. de, and Alto, N.M. (2018) Cooperative immune suppression by *Escherichia coli* and *Shigella* effector proteins. *Infect Immun* .

Jouihri, N., Sory, M.P., Page, A.L., Gounon, P., Parsot, C., and Allaoui, A. (2003) MxiK and MxiN interact with the Spa47 ATPase and are required for transit of the needle components MxiH and MxiI, but not of Ipa proteins, through the type III secretion apparatus of Shigella flexneri. *Mol Microbiol* **49**: 755–767.

Journet, L., Agrain, C., Broz, P., Cornelis, G.R., and Galán, J.E. (2003) The Needle Length of Bacterial Injectisomes Is Determined by a Molecular Ruler. *Science (80-)* **302**: 1757–1760.

Kadari, M., Lakhloufi, D., Delforge, V., Imbault, V., Communi, D., Smeesters, P., and Botteaux, A. (2019) Multiple proteins arising from a single gene: The role of the Spa33 variants in *Shigella* T3SS regulation. *Microbiologyopen* 1–19.

Käll, L., Krogh, A., and Sonnhammer, E.L.L. (2007) Advantages of combined transmembrane topology and signal peptide prediction--the Phobius web server. *Nucleic Acids Res* **35**: W429-32.

Kaniga, K., Delor, I., and Cornelis, G.R. (1991) A wide-host-range suicide vector for improving reverse genetics in Gram-negative bacteria: inactivation of the blaA gene of *Yersinia enterocolitica*. *Gene* **109**: 137–41.

Kapatral, V., and Minnich, S.A. (1995) Co-ordinate, temperature-sensitive regulation of the three *Yersinia enterocolitica* flagellin genes. *Mol Microbiol* **17**: 49–56.

Keet, E.E. (1974) *Yersinia enterocolitica* septicemia. Source of infection and incubation period identified. *N Y State J Med* .

Keller, B., Mühlenkamp, M., Deuschle, E., Siegfried, A., Mössner, S., Schade, J., *et al.* (2015) *Yersinia enterocolitica* exploits different pathways to accomplish adhesion and toxin injection into host cells. *Cell Microbiol* **17**: 1179–1204.

Kelley, L.A., and Sternberg, M.J.E. (2009) Protein structure prediction on the web: A case study using the phyre server. *Nat Protoc* .

Kenjale, R., Wilson, J., Zenk, S.F., Saurya, S., Picking, W.L., Picking, W.D., and Blocker, A. (2005) The needle component of the type III secreton of *Shigella* regulates the activity of the secretion apparatus. *J Biol Chem* .

Kerfeld, C.A., and Erbilgin, O. (2015) Bacterial microcompartments and the modular construction of microbial metabolism. *Trends Microbiol* .

Kibbe, W.A. (2007) OligoCalc: An online oligonucleotide properties calculator. *Nucleic Acids Res* .

Kimbrough, T.G., and Miller, S.I. (2000) Contribution of Salmonella typhimurium type III secretion components to needle complex formation. *Proc Natl Acad Sci U S A* **97**: 11008–11013.

Kimbrough, T.G., and Miller, S.I. (2002) Assembly of the type III secretion needle complex of Salmonella typhimurium. *Microbes Infect* **4**: 75–82.

Kooger, R., Szwedziak, P., Böck, D., and Pilhofer, M. (2018) CryoEM of bacterial secretion systems. *Curr Opin Struct Biol* **52**: 64–70.

Koornhof, H.J., Smego, R.A., and Nicol, M. (1999) Yersiniosis II: The pathogenesis of *Yersinia* infections. *Eur J Clin Microbiol Infect Dis* **18**: 87–112.

Koraimann, G. (2003) Lytic transglycosylases in macromolecular transport systems of Gram-negative bacteria. *Cell Mol Life Sci* **60**: 2371–2388.

Korotkov, K. V., Sandkvist, M., and Hol, W.G.J. (2012) The type II secretion system: Biogenesis, molecular architecture and mechanism. *Nat Rev Microbiol* .

Kostakioti, M., Newman, C.L., Thanassi, D.G., and Stathopoulos, C. (2005) Mechanisms of protein export across the bacterial outer membrane. *J Bacteriol* .

Kotloff, K.L., Winickoff, J.P., Ivanoff, B., Clemens, J.D., Swerdlow, D.L., Sansonetti, P.J., *et al.* (1999) Global burden of *Shigella* infections: Implications for vaccine development and implementation of control strategies. *Bull World Health Organ* **77**: 651–666.

Kowal, J., Chami, M., Ringler, P., Müller, S.A., Kudryashev, M., Castaño-Díez, D., *et al.* (2013a) Structure of the dodecameric *Yersinia enterocolitica* secretin YscC and its trypsin-resistant core. *Structure* **21**: 2152–2161.

Kowal, J., Chami, M., Ringler, P., Müller, S.A., Kudryashev, M., Castaño-Díez, D., *et al.* (2013b) Structure of the dodecameric *Yersinia enterocolitica* secretin YscC and its trypsin-resistant core. *Structure* **21**: 2152–2161.

Koziolek, M., Grimm, M., Becker, D., Iordanov, V., Zou, H., Shimizu, J., *et al.* (2015) Investigation of pH and Temperature Profiles in the GI Tract of Fasted Human Subjects Using the Intellicap® System. *J Pharm Sci*

104: 2855–2863.

Krulwich, T.A., Sachs, G., and Padan, E. (2011) Molecular aspects of bacterial pH sensing and homeostasis. *Nat Rev Microbiol* **9**: 330–343.

Kudryashev, M., Diepold, A., Amstutz, M., Armitage, J.P., Stahlberg, H., and Cornelis, G.R. (2015) *Y ersinia enterocolitica* type III secretion injectisomes form regularly spaced clusters, which incorporate new machines upon activation. *Mol Microbiol* **95**: 875–884.

Kudryashev, M., Stenta, M., Schmelz, S., Amstutz, M., Wiesand, U., Castaño-Díez, D., *et al.* (2013) In situ structural analysis of the *Yersinia enterocolitica* injectisome. *Elife* **2**: e00792.

Kuhlen, L., Abrusci, P., Johnson, S., Gault, J., Deme, J., Caesar, J., *et al.* (2018) Structure of the core of the type III secretion system export apparatus. *Nat Struct Mol Biol* **25**: 583–590.

Kumar, M., Mommer, M.S., and Sourjik, V. (2010) Mobility of Cytoplasmic, Membrane, and DNA-Binding Proteins in Escherichia coli. *Biophys J* **98**: 552–559.

Kusmierek, M., Hoßmann, J., Witte, R., Opitz, W., Vollmer, I., Volk, M., *et al.* (2019) A bacterial secreted translocator hijacks riboregulators to control type III secretion in response to host cell contact. *PLOS Pathog* **15**: e1007813.

Lambert, P.A. (2002) Mechanisms of antibiotic resistance in Pseudomonas aeruginosa. In *Journal of the Royal Society of Medicine, Supplement*. Royal Society of Medicine Press, pp. 22–26.

Lambert, T.J. (2019) FPbase: a community-editable fluorescent protein database. *Nat Methods* .

Lampaki, D., Diepold, A., and Glatter, T. (2020) A Serial Sample Processing Strategy with Improved Performance for in-Depth Quantitative Analysis of Type III Secretion Events in *Pseudomonas aeruginosa*. *J Proteome Res* **19**: 543–553.

Lara-Tejero, M. (2020) The type III secretion system sorting platform. In *Current Topics in Microbiology and Immunology*. pp. 133–142.

Lara-Tejero, M., Kato, J., Wagner, S., Liu, X., and Galán, J.E. (2011) A Sorting Platform Determines the Order of Protein Secretion in Bacterial Type III Systems. *Science (80-)* **331**.

Lasica, A.M., Ksiazek, M., Madej, M., and Potempa, J. (2017) The Type IX Secretion System (T9SS): Highlights and Recent Insights into Its Structure and Function. *Front Cell Infect Microbiol* **7**.

Lau, G.W., Hassett, D.J., and Britigan, B.E. (2005) Modulation of lung epithelial functions by *Pseudomonas aeruginosa*. *Trends Microbiol* .

Lauber, F., Deme, J.C., Lea, S.M., and Berks, B.C. (2018) Type 9 secretion system structures reveal a new protein transport mechanism. *Nature* **564**: 77–82.

Leake, M.C., Chandler, J., Wadhams, G.H., Bai, F., Berry, R.M., and Armitage, J.P. (2006) Stoichiometry and turnover in single, functioning membrane protein complexes. *Nature* **443**: 355–358.

Lee, P.-C., Zmina, S.E., Stopford, C.M., Toska, J., and Rietsch, A. (2014) Control of type III secretion activity and substrate specificity by the cytoplasmic regulator PcrG. *Proc Natl Acad Sci U S A* **111**: E2027-36.

Leinonen, R., Garcia Diez, F., Binns, D., Fleischmann, W., Lopez, R., and Apweiler, R. (2004) UniProt archive. *Bioinformatics* .

Lenn, T., Leake, M.C., and Mullineaux, C.W. (2008) Clustering and dynamics of cytochrome bd-I complexes in the *Escherichia coli* plasma membrane in vivo. *Mol Microbiol* **70**: 1397–1407.

Leo, J.C., Elovaara, H., Bihan, D., Pugh, N., Kilpinen, S.K., Raynal, N., *et al.* (2010) First analysis of a bacterial collagen-binding protein with collagen toolkits: Promiscuous binding of YadA to collagens may explain how YadA interferes with host processes. *Infect Immun* **78**: 3226–3236.

Leo, J.C., Elovaara, H., Brodsky, B., Skurnik, M., and Goldman, A. (2008) The *Yersinia* adhesin YadA binds to a collagenous triple-helical conformation but without sequence specificity. *Protein Eng Des Sel* **21**: 475–484.

Leo, J.C., Oberhettinger, P., Schütz, M., and Linke, D. (2015) The inverse autotransporter family: intimin, invasin and related proteins. *Int J Med Microbiol* **305**: 276–82.

Leslie, T., Whitehouse, C.A., Yingst, S., Baldwin, C., Kakar, F., Mofleh, J., *et al.* (2011) Outbreak of gastroenteritis caused by *Yersinia pestis* in Afghanistan. *Epidemiol Infect* **139**: 728–735.

Letzelter, M., Sorg, I., Mota, L.J., Meyer, S., Stalder, J., Feldman, M., *et al.* (2006) The discovery of SycO highlights a new function for type III secretion effector chaperones. *EMBO J* **25**: 3223–3233.

Leyton, D.L., Rossiter, A.E., and Henderson, I.R. (2012) From self sufficiency to dependence: Mechanisms and factors important for autotransporter biogenesis. *Nat Rev Microbiol* .

Lindner, F., Milne-Davies, B., Langenfeld, K., Stiewe, T., and Diepold, A. (2020) LITESEC-T3SS - Light-controlled protein delivery into eukaryotic cells with high spatial and temporal resolution. *Nat Commun* **7**: 354–356.

Lippa, A.M., and Goulian, M. (2012) Perturbation of the Oxidizing Environment of the Periplasm Stimulates the PhoQ / PhoP System in Escherichia coli. 1457–1463.

Lombardi, C., Tolchard, J., Bouillot, S., Signor, L., Gebus, C., Liebl, D., *et al.* (2019) Structural and Functional Characterization of the Type Three Secretion System (T3SS) Needle of Pseudomonas aeruginosa. *Front Microbiol* **10**: 573.

Lyons, B.J.E., Atkinson, C.E., Deng, W., Serapio-Palacios, A., Finlay, B.B., and Strynadka, N.C.J. (2021) Cryo-EM structure of the EspA filament from enteropathogenic *Escherichia coli*: revealing the mechanism of effector translocation in the T3SS. *Structure* 1–9.

Ma, Q., Zhai, Y., Schneider, J.C., Ramseier, T.M., and Saier, M.H. (2003) Protein secretion systems of *Pseudomonas aeruginosa* and *P. fluorescens*. *Biochim Biophys Acta - Biomembr* .

Maarek, Y.S. (1997) WebCutter: A system for dynamic and tailorable site mapping. *Comput Networks* .

Majewski, D.D., Worrall, L.J., Hong, C., Atkinson, C.E., Vuckovic, M., Watanabe, N., *et al.* (2019) Cryo-EM structure of the homohexameric T3SS ATPase-central stalk complex reveals rotary ATPase-like asymmetry. *Nat Commun* **10**: 626.

Marteyn, B.S., Gazi, A.D., and Sansonetti, P.J. (2012) Shigella: A model of virulence regulation in vivo. *Gut Microbes* .

Marteyn, B.S., West, N.P., Browning, D.F., Cole, J.A., Shaw, J.G., Palm, F., *et al.* (2010) Modulation of *Shigella* virulence in response to available oxygen in vivo. *Nature* **465**: 355–8.

Martinez-Argudo, I., and Blocker, A.J. (2010) The Shigella T3SS needle transmits a signal for MxiC release,

which controls secretion of effectors. *Mol Microbiol* **78**: 1365–1378.

Masi, M., and Wandersman, C. (2010) Multiple signals direct the assembly and function of a type 1 secretion system. *J Bacteriol* .

MATLAB (2020) MATLAB (R2020a). *www.mathworks.com/products/matlab* .

Mauracher, C.A., Gillam, S., Shukin, R., and Tingle, A.J. (1991) pH-dependent solubility shift of rubella virus capsid protein. *Virology* **181**: 773–777.

McClements, D.J., and Li, Y. (2010) Review of in vitro digestion models for rapid screening of emulsion-based systems. *Food Funct* **1**: 32.

McCormick, T.H.A., Siber, A.M., and Maurelli, A.T. (1998) Requirement of the *Shigella flexneri* virulence plasmid in the ability to induce trafficking of neutrophils across polarized monolayers of the intestinal epithelium. *Infect Immun* .

McDowell, M.A., Marcoux, J., McVicker, G., Johnson, S., Fong, Y.H., Stevens, R., *et al.* (2016) Characterisation of *Shigella* Spa33 and *Thermotoga* FliM/N reveals a new model for C-ring assembly in T3SS. *Mol Microbiol* **99**: 749–766.

Meuskens, I., Saragliadis, A., Leo, J.C.C., and Linke, D. (2019) Type V Secretion Systems: An Overview of Passenger Domain Functions. *Front Microbiol* **10**: 1–19.

Miesenböck, G., Angelis, D.A. De, and Rothman, J.E. (1998) Visualizing secretion and synaptic transmission with pH-sensitive green fluorescent proteins. *Nature* **394**: 192–5.

Mika, J.T., Schavemaker, P.E., Krasnikov, V., and Poolman, B. (2014) Impact of osmotic stress on protein diffusion in Lactococcus lactis. *Mol Microbiol* **94**: 857–870.

Miki, T., Iguchi, M., Akiba, K., Hosono, M., Sobue, T., Danbara, H., and Okada, N. (2010) Chromobacterium pathogenicity island 1 type III secretion system is a major virulence determinant for Chromobacterium violaceum-induced cell death in hepatocytes. *Mol Microbiol* .

Mikula, K.M., Kolodziejczyk, R., and Goldman, A. (2013) Yersinia infection tools—characterization of structure and function of adhesins. *Front Cell Infect Microbiol* **2**: 169.

Miletic, S., Fahrenkamp, D., Goessweiner-Mohr, Wald, J., Pantel, M., Vesper, O., *et al.* (2020a) Substrate-engaged type III secretion system structures reveal gating mechanism for unfolded protein translocation. *bioRxiv preprin* 1–39.

Miletic, S., Goessweiner-Mohr, N., and Marlovits, T.C. (2020b) The structure of the type III secretion system needle complex. *Curr Top Microbiol Immunol* **427**: 67–90.

Mills, E., Baruch, K., Charpentier, X., Kobi, S., and Rosenshine, I. (2008) Real-time analysis of effector translocation by the type III secretion system of enteropathogenic *Escherichia coli. Cell Host Microbe* **3**: 104–13.

Milne-Davies, B., Wimmi, S., and Diepold, A. (2020) Adaptivity and dynamics in type III secretion systems. *Mol Microbiol* .

Milne-Davies, B.A., Helbig, C., Wimmi, S., and Diepold, A. (2019) Life after secretion – *Yersinia enterocolitica* rapidly toggles effector secretion and can resume cell division in response to changing external conditions. *Front Microbiol* **10**: 2128.

Minamino, T., and Macnab, R.M. (2000) FliH, a soluble component of the type III flagellar export apparatus of Salmonella, forms a complex with FliI and inhibits its ATPase activity. *Mol Microbiol* .

Minamino, T., and Namba, K. (2008) Distinct roles of the FliI ATPase and proton motive force in bacterial flagellar protein export. *Nature* **451**: 485–488.

Morimoto, Y. V., Kojima, S., Namba, K., Minamino, T., and Iino, T. (2011) M153R Mutation in a pH-Sensitive Green Fluorescent Protein Stabilizes Its Fusion Proteins. *PLoS One* **6**: e19598.

Mota, L.J., Journet, L., Sorg, I., Agrain, C., and Cornelis, G.R. (2005) Bacterial injectisomes: needle length does matter. *Science (80-)* **307**: 2005.

Mouton, J.B. (1975) Les hommes et la peste en France et dans les pays européens et méditerranéens. Tome I: la peste dans l'histoire. *pascal-francis.inist.fr* .

Mueller, C.A., Broz, P., Müller, S.A., Ringler, P., Erne-Brand, F., Sorg, I., *et al.* (2005) The V-antigen of Yersinia forms a distinct structure at the tip of injectisome needles. *Science (80-)* **310**: 674–676.

Mueller, S.H., Spenkelink, L.M., and Oijen, A.M. van (2019) When proteins play tag: the dynamic nature of the replisome. *Biophys Rev* **11**: 641–651.

Mühlenkamp, M., Oberhettinger, P., Leo, J.C.C., Linke, D., and Schütz, M.S.S. (2015) *Yersinia* adhesin A (YadA) - Beauty & beast. *Int J Med Microbiol* **305**: 252–258.

Müller, S.A., Pozidis, C., Stone, R., Meesters, C., Chami, M., Engel, A., *et al.* (2006) Double hexameric ring assembly of the type III protein translocase ATPase HrcN. *Mol Microbiol* .

Muthuramalingam, M., Whittier, S.K., Lovell, S., and Battaile, K.P. (2020) The Structures of SctK and SctD from *Pseudomonas aeruginosa* Reveal the Interface of the Type III Secretion System Basal Body and Sorting Platform. 1–42.

Nakamura, S., Kami-ike, N., Yokota, J.P., Kudo, S., Minamino, T., and Namba, K. (2009) Effect of Intracellular pH on the Torque?Speed Relationship of Bacterial Proton-Driven Flagellar Motor. *J Mol Biol* **386**: 332–338.

Natale, P., Brüser, T., and Driessen, A.J.M. (2008) Sec- and Tat-mediated protein secretion across the bacterial cytoplasmic membrane-Distinct translocases and mechanisms. *Biochim Biophys Acta - Biomembr* .

Nauth, T., Huschka, F., Schweizer, M., Bosse, J.B., Diepold, A., Failla, A.V., *et al.* (2018) Visualization of translocons in Yersinia type III protein secretion machines during host cell infection. *PLOS Pathog* **14**: e1007527.

Navarro, L., Alto, N.M., and Dixon, J.E. (2005) Functions of the Yersinia effector proteins in inhibiting host immune responses. *Curr Opin Microbiol* .

Nisco, N.J. De, Rivera-Cancel, G., and Orth, K. (2018) The Biochemistry of Sensing: Enteric Pathogens Regulate Type III Secretion in Response to Environmental and Host Cues. *MBio* **9**: e02122-17.

Notti, R.Q., and Stebbins, C.E. (2016) The Structure and Function of Type III Secretion Systems. In *Virulence Mechanisms of Bacterial Pathogens, Fifth Edition*. American Society of Microbiology, pp. 241–264.

Nuorti, J.P., Niskanen, T., Hallanvuo, S., Mikkola, J., Kela, E., Hatakka, M., *et al.* (2004) A Widespread Outbreak of *Yersinia pseudotuberculosis* O:3 Infection from Iceberg Lettuce . *J Infect Dis* **189**: 766–774.

Pan, S.Q., Charles, T., Jin, S., Wu, Z.L., and Nester, E.W. (1993) Preformed dimeric state of the sensor protein VirA is involved in plant-Agrobacterium signal transduction. *Proc Natl Acad Sci U S A* .

Papanikou, E., Karamanou, S., and Economou, A. (2007) Bacterial protein secretion through the translocase nanomachine. *Nat Rev Microbiol* .

Parry, B.R., Surovtsev, I. V., Cabeen, M.T., O'Hern, C.S., Dufresne, E.R., and Jacobs-Wagner, C. (2014) The bacterial cytoplasm has glass-like properties and is fluidized by metabolic activity. *Cell* **156**: 183–194.

Parsot, C., Hamiaux, C., and Page, A.L. (2003) The various and varying roles of specific chaperones in type III secretion systems. *Curr Opin Microbiol* **6**: 7–14.

Pastur., A.Y.-A.I., and 1894, undefined La peste bubonique à Hong-Kong. *ci.nii.ac.jp* .

Pathogenicity Islands and Other Mobile Virulence Elements (1999) .

Patterson, G.H., Knobel, S.M., Sharif, W.D., Kain, S.R., and Piston, D.W. (1997) Use of the green fluorescent protein and its mutants in quantitative fluorescence microscopy. *Biophys J* **73**: 2782–2790.

Paul, K., Erhardt, M., Hirano, T., Blair, D.F., and Hughes, K.T. (2008) Energy source of flagellar type III secretion. *Nature* **451**: 489–492.

Pédelacq, J.D., Cabantous, S., Tran, T., Terwilliger, T.C., and Waldo, G.S. (2006) Engineering and characterization of a superfolder green fluorescent protein. *Nat Biotechnol* .

Pepe, J.C., Badger, J.L., and Miller, V.L. (1994) Growth phase and low pH affect the thermal regulation of the *Yersinia enterocolitica* inv gene. *Mol Microbiol* **11**: 123–135.

Pepe, J.C., and Miller, V.L. (1993) *Yersinia enterocolitica* invasin: A primary role in the initiation of infection. *Proc Natl Acad Sci U S A* **90**: 6473–6477.

Pepe, J.C., Wachtel, M.R., Wagar, E., and Miller, V.L. (1995) Pathogenesis of defined invasion mutants of *Yersinia enterocolitica* in a BALB/c mouse model of infection. *Infect Immun* **63**: 4837–4848.

Perdomo, J.J., Gounon, P., and Sansonetti, P.J. (1994) Polymorphonuclear leukocyte transmigration promotes invasion of colonic epithelial monolayer by *Shigella flexneri*. *J Clin Invest* .

Perry, R.D., and Fetherston, J.D. (1997) Yersinia pestis - Etiologic agent of plague. *Clin Microbiol Rev* **10**: 35–66.

Petrovska, I., Nüske, E., Munder, M.C., Kulasegaran, G., Malinovska, L., Kroschwald, S., *et al.* (2014) Filament formation by metabolic enzymes is a specific adaptation to an advanced state of cellular starvation. *Elife* **3**.

Pettersson, J., Nordfelth, R., Dubinina, E., Bergman, T., Gustafsson, M., Magnusson, K.E., and Wolf-Watz, H. (1996) Modulation of Virulence Factor Expression by Pathogen Target Cell Contact. *Science (80-)* **273**: 1231–1233.

Pha, K. (2016) Yersinia type III effectors perturb host innate immune responses . *World J Biol Chem* .

Philpott, D.J., Edgeworth, J.D., and Sansonetti, P.J. (2000) The pathogenesis of *Shigella flexneri* infection: Lessons from in vitro and in vivo studies. *Philos Trans R Soc B Biol Sci* .

Pohlner, J., Halter, R., Beyreuther, K., and Meyer, T.F. (1987) Gene structure and extracellular secretion of *Neisseria* gonorrhoeae IgA protease. *Nature* .

Portnoy, D.A., Wolf-Watz, H., Bolin, I., Beeder, A.B., and Falkow, S. (1984) Characterization of common virulence plasmids in *Yersinia* species and their role in the expression of outer membrane proteins. *Infect Immun* **43**: 108–114.

Pozidis, C., Chalkiadaki, A., Gomez-Serrano, A., Stahlberg, H., Brown, I., Tampakaki, A.P., *et al.* (2003) Type III protein translocase. HrcN is a peripheral membrane ATPase that is activated by oligomerization. *J Biol Chem* .

Puhar, A., and Sansonetti, P.J. (2014) Type III secretion system. *Curr Biol* .

Pukatzki, S., Ma, A.T., Revel, A.T., Sturtevant, D., and Mekalanos, J.J. (2007) Type VI secretion system translocates a phage tail spike-like protein into target cells where it cross-links actin. *Proc Natl Acad Sci U S A* .

Radics, J., Königsmaier, L., and Marlovits, T.C. (2014) Structure of a pathogenic type 3 secretion system in action. *Nat Struct Mol Biol* **21**: 82–87.

Rajashekar, R., Liebl, D., Chikkaballi, D., Liss, V., and Hensel, M. (2014) Live Cell imaging reveals novel functions of *Salmonella enterica* SPI2-T3SS effector proteins in remodeling of the host cell endosomal system. *PLoS One* .

Rapoza, M.P., and Webster, R.E. (1993) The filamentous bacteriophage assembly proteins require the bacterial SecA protein for correct localization to the membrane. *J Bacteriol* **175**: 1856–1859.

Rappl, C., Deiwick, J., and Hensel, M. (2003) Acidic pH is required for the functional assembly of the type III secretion system encoded by *Salmonella* pathogenicity island 2. *FEMS Microbiol Lett* **226**: 363–372.

Rimpilainen, M., Forsberg, A., and Wolf-Watz, H. (1992) A novel protein, LcrQ, involved in the low-calcium response of *Yersinia pseudotuberculosis* shows extensive homology to YopH. *J Bacteriol* .

Robinson, C., and Bolhuis, A. (2004) Tat-dependent protein targeting in prokaryotes and chloroplasts. *Biochim Biophys Acta - Mol Cell Res* .

Rocha, J.M., Richardson, C.J., Zhang, M., Darch, C.M., Cai, E., Diepold, A., and Gahlmann, A. (2018) Single-molecule tracking in live Yersinia enterocolitica reveals distinct cytosolic complexes of injectisome subunits. *Integr Biol* **10**: 502–515.

Roehrich, A.D., Guillossou, E., Blocker, A.J., and Martinez-Argudo, I. (2013) *Shigella* IpaD has a dual role: signal transduction from the type III secretion system needle tip and intracellular secretion regulation. *Mol Microbiol* **87**: 690–706.

Roggenkamp, A., Ackermann, N., Jacobi, C.A., Truelzsch, K., Hoffmann, H., and Heesemann, J. (2003) Molecular analysis of transport and oligomerization of the *Yersinia enterocolitica* adhesin YadA. *J Bacteriol* .

Rohde, J.R., Fox, J.M., and Minnich, S.A. (1994) Thermoregulation in *Yersinia enterocolitica* is coincident with changes in DNA supercoiling. *Mol Microbiol* **12**: 187–199.

Rohde, J.R., Luan, X.S., Rohde, H., Fox, J.M., and Minnich, S.A. (1999) The *Yersinia enterocolitica* pYV virulence plasmid contains multiple intrinsic DNA bends which melt at 37°C. *J Bacteriol* **181**: 4198–4204.

Ross, J.A., and Plano, G. V. (2011) A C-terminal region of Yersinia pestis YscD binds the outer membrane secretin YscC. *J Bacteriol* **193**: 2276–2289.

Russell, A.B., Hood, R.D., Bui, N.K., Leroux, M., Vollmer, W., and Mougous, J.D. (2011) Type VI secretion delivers bacteriolytic effectors to target cells. *Nature* .

Russell, A.B., Peterson, S.B., and Mougous, J.D. (2014) Type VI secretion system effectors: Poisons with a purpose. *Nat Rev Microbiol* .

Sabina, Y., Rahman, A., Ray, R.C., and Montet, D. (2011) *Yersinia enterocolitica* : Mode of Transmission, Molecular Insights of Virulence, and Pathogenesis of Infection. *J Pathog* **2011**: 1–10.

Sakaguchi, T., Köhler, H., Gu, X., McCormick, B.A., and Reinecker, H.C. (2002) Shigella flexneri regulates tight junction-associated proteins in human intestinal epithelial cells. *Cell Microbiol* .

Saragliadis, A., and Linke, D. (2019) Assay development for the discovery of small-molecule inhibitors of YadA adhesion to collagen. *Cell Surf* **5**: 100025.

Schiffrin, B., Brockwell, D.J., and Radford, S.E. (2017) Outer membrane protein folding from an energy landscape perspective. *BMC Biol* .

Schindelin, J., Arganda-Carreras, I., Frise, E., Kaynig, V., Longair, M., Pietzsch, T., *et al.* (2012) Fiji: An open-source platform for biological-image analysis. *Nat Methods* **9**: 676–682.

Schlumberger, M.C., Müller, A.J., Ehrbar, K., Winnen, B., Duss, I., Stecher, B., and Hardt, W.-D. (2005) Real-time imaging of type III secretion: *Salmonella* SipA injection into host cells. *Proc Natl Acad Sci U S A* **102**: 12548–53.

Schraidt, O., Lefebre, M.D., Brunner, M.J., Schmied, W.H., Schmidt, A., Radics, J., *et al.* (2010) Topology and organization of the *Salmonella* typhimurium type III secretion needle complex components. *PLoS Pathog* **6**: 1–12.

Schraidt, O., and Marlovits, T.C. (2011) Three-dimensional model of *Salmonella*'s needle complex at subnanometer resolution. *Science (80-)* **331**: 1192–5.

Shaulov, L., Gershberg, J., Deng, W., Finlay, B.B., and Sal-Man, N. (2017) The Ruler Protein EscP of the Enteropathogenic *Escherichia coli* Type III Secretion System Is Involved in Calcium Sensing and Secretion Hierarchy Regulation by Interacting with the Gatekeeper Protein SepL. *MBio* **8**: e01733-16.

Shoaib, M., Shehzad, A., Raza, H., Niazi, S., Khan, I.M., Akhtar, W., *et al.* (2019) A comprehensive review on the prevalence, pathogenesis and detection of: *Yersinia enterocolitica*. *RSC Adv* **9**: 41010–41021.

Silva, Y.R. de O., Contreras-Martel, C., Macheboeuf, P., and Dessen, A. (2020a) Bacterial secretins: Mechanisms of assembly and membrane targeting. *Protein Sci* .

Silva, Y.R. de O., Contreras-Martel, C., Macheboeuf, P., and Dessen, A. (2020b) Bacterial secretins: Mechanisms of assembly and membrane targeting. *Protein Sci* **29**: 893–904.

Slonczewski, J.L., Rosen, B.P., Alger, J.R., and Macnab, R.M. (1981) pH homeostasis in Escherichia coli: measurement by 31P nuclear magnetic resonance of methylphosphonate and phosphate. *Proc Natl Acad Sci U S A* **78**: 6271–5.

Small, P., Blankenhorn, D., Welty, D., Zinser, E., and Slonczewski, J.L. (1994) Acid and base resistance in *Escherichia coli* and *Shigella flexneri*: Role of rpoS and growth pH. *J Bacteriol* **176**: 1729–1737.

Smego, R.A., Frean, J., and Koornhof, H.J. (1999) Yersiniosis I: Microbiological and clinicoepidemiological aspects of plague and non-plague *Yersinia* infections. *Eur J Clin Microbiol Infect Dis* **18**: 1–15.

Sory, M.-P., Boland, A., Lambermont, I., and Cornelis, G.R. (1995) Identification of the YopE and YopH domains required for secretion and internalization into the cytosol of macrophages, using the cyaA gene fusion approach. *Proc Natl Acad Sci U S A* **92**: 11998–12002.

Soto, E., Espinosa, N., Díaz-Guerrero, M., Gaytán, M.O., puente, J.L., and González-Pedrajo, B. (2017) Functional Characterization of EscK(Orf4), a Sorting Platform Component ofthe *EnteropathogenicEscherichia* coliInjectisome. **199**: 1–19.

Sourjik, V., and Wingreen, N.S. (2012) Responding to chemical gradients: Bacterial chemotaxis. *Curr Opin Cell Biol* **24**: 262–268.

Souza Santos, M. de, and Orth, K. (2019) The Role of the Type III Secretion System in the Intracellular Lifestyle of Enteric Pathogens. In *Bacteria and Intracellularity*. pp. 215–225.

Spaeth, K., Chen, Y.-S., and Valdivia, R. (2009) The Chlamydia type III secretion system C-ring engages a chaperone-effector protein complex. *PLoS Pathog* **5**: e1000579.

Spreter, T., Yip, C.K., Sanowar, S., André, I., Kimbrough, T.G., Vuckovic, M., *et al.* (2009) A conserved structural motif mediates formation of the periplasmic rings in the type III secretion system. *Nat Struct Mol Biol* **16**: 468–76.

Spyder (2018) SPYDER IDE. *Spyder Proj* .

Stainier, I., Iriarte, M., and Cornelis, G.R. (1997) YscM1 and YscM2, two *Yersinia enterocolitica* proteins causing downregulation of yop transcription. *Mol Microbiol* **26**: 833–843.

Stanley, S.A., Raghavan, S., Hwang, W.W., and Cox, J.S. (2003) Acute infection and macrophage subversion by Mycobacterium tuberculosis require a specialized secretion system. *Proc Natl Acad Sci U S A* .

Stebbins, C.E., and Galán, J.E. (2001) Maintenance of an unfolded polypeptide by a cognate chaperone in bacterial type III secretion. *Nature* **414**: 77–81.

Stenhouse, M., and Milner, L. (1982) Yersinia enterocolitica. A hazard in blood transfusion. *Transfusion* **22**: 396–398.

Stingl, K., and Reuse, H. De (2005) Staying alive overdosed: How does *Helicobacter pylori* control urease activity? *Int J Med Microbiol* **295**: 307–315.

Straley, S.C., Skrzypek, E., Plano, G. V., and Bliska, J.B. (1993) Yops of *Yersinia* spp. pathogenic for humans. *Infect Immun* **61**: 3105–3110.

Surovtsev, I. V, and Jacobs-wagner, C. (2018) Review Subcellular Organization : A Critical Feature of Bacterial Cell Replication. *Cell* **172**: 1271–1293.

Symmons, M.F., Bokma, E., Koronakis, E., Hughes, C., and Koronakis, V. (2009) The assembled structure of a complete tripartite bacterial multidrug efflux pump. *Proc Natl Acad Sci U S A* .

Tacconelli, E., and Magrini, N. (2017) Global priority list of antibiotic-resistant bacteria to guide research, discovery, and development of new antibiotics. .

Tachiyama, S., Chang, Y., Muthuramalingam, M., Hu, B., Barta, M.L., Picking, W.L., *et al.* (2019) The cytoplasmic domain of MxiG interacts with MxiK and directs assembly of the sorting platform in the *Shigella* type III secretion system. *J Biol Chem* jbc.RA119.009125.

Taylor, D.J., Krishna, N.K., Canady, M.A., Schneemann, A., and Johnson, J.E. (2002) Large-scale, pH-

dependent, quaternary structure changes in an RNA virus capsid are reversible in the absence of subunit autoproteolysis. *J Virol* **76**: 9972–80.

Terahara, N., Inoue, Y., Kodera, N., Morimoto, Y. V., Uchihashi, T., Imada, K., *et al.* (2018) Insight into structural remodeling of the FlhA ring responsible for bacterial flagellar type III protein export. *Sci Adv* **4**: eaao7054.

Tertti, R., Skurnik, M., Vartio, T., and Kuusela, P. (1992) Adhesion protein YadA of *Yersinia* species mediates binding of bacteria to fibronectin. *Infect Immun* **60**: 3021–3024.

Thomas, D., Morgan, D.G., and DeRosier, D.J. (2001) Structures of bacterial flagellar motors from two FliF-FliG gene fusion mutants. *J Bacteriol* .

Tinaztepe, E., Wei, J.R., Raynowska, J., Portal-Celhay, C., Thompson, V., and Philipsa, J.A. (2016) Role of metal-dependent regulation of ESX-3 secretion in intracellular survival of *Mycobacterium tuberculosis*. *Infect Immun* .

Tokunaga, M., Imamoto, N., and Sakata-Sogawa, K. (2008) Highly inclined thin illumination enables clear single-molecule imaging in cells. *Nat Methods* **5**: 159–61.

Torruellas, J., Jackson, M.W., Pennock, J.W., and Plano, G. V. (2005) The *Yersinia pestis* type III secretion needle plays a role in the regulation of Yop secretion. *Mol Microbiol* **57**: 1719–1733.

Treuner-Lange, A., and Søgaard-Andersen, L. (2014) Regulation of cell polarity in bacteria. *J Cell Biol* **206**: 7–17.

Tusk, S.E., Delalez, N.J., and Berry, R.M. (2018) Subunit Exchange in Protein Complexes. *J Mol Biol* **430**: 4557–4579.

Tyanova, S., Temu, T., Sinitcyn, P., Carlson, A., Hein, M.Y., Geiger, T., *et al.* (2016) The Perseus computational platform for comprehensive analysis of (prote)omics data. *Nat Methods* .

Uliczka, F., Pisano, F., Schaake, J., Stolz, T., Rohde, M., Fruth, A., *et al.* (2011) Unique cell adhesion and invasion properties of *yersinia enterocolitica* O:3, the most frequent cause of human yersiniosis. *PLoS Pathog* **7**.

Veenendaal, A.K.J., Hodgkinson, J., Schwarzer, L., Stabat, D., Zenk, S., and Blocker, A.J. (2007) The type III secretion system needle tip complex mediates host cell sensing and translocon insertion. *Mol Microbiol* **63**: 1719–1730.

Wadhams, G.H., and Armitage, J.P. (2004) Making sense of it all: bacterial chemotaxis. *Nat Rev Mol Cell Biol* **5**: 1024–1037.

Wagner, S., Grin, I., Malmsheimer, S., Singh, N., Torres-Vargas, C.E., and Westerhausen, S. (2018) Bacterial type III secretion systems: A complex device for the delivery of bacterial effector proteins into eukaryotic host cells. *FEMS Microbiol Lett* **365**: 1–13.

Wagner, S., Königsmaier, L., Lara-Tejero, M., Lefebre, M.D., Marlovits, T.C., and Galán, J.E. (2010a) Organization and coordinated assembly of the type III secretion export apparatus. *Proc Natl Acad Sci U S A* **107**: 17745–50.

Wagner, S., Stenta, M., Metzger, L.C., Dal Peraro, M., and Cornelis, G.R. (2010b) Length control of the injectisome needle requires only one molecule of Yop secretion protein P (YscP). *Proc Natl Acad Sci U S A* .

Wang, H., Avican, K., Fahlgren, A., Erttmann, S.F., Nuss, A.M., Dersch, P., *et al.* (2016) Increased plasmid copy number is essential for *Yersinia* T3SS function and virulence. *Science* **353**: 492–5.

Wieser, S., and Schütz, G.J. (2008) Tracking single molecules in the live cell plasma membrane-Do's and Don't's. *Methods* **46**: 131–140.

Wilharm, G., and Heider, C. (2014) Interrelationship between type three secretion system and metabolism in pathogenic bacteria. *Front Cell Infect Microbiol* **4**: 150.

Wilharm, G., Lehmann, V., Krauss, K., Lehnert, B., Richter, S., Ruckdeschel, K., *et al.* (2004) *Yersinia enterocolitica* Type III Secretion Depends on the Proton Motive Force but Not on the Flagellar Motor Components MotA and MotB. *Infect Immun* **72**: 4004–4009.

Wolter, S., Löschberger, A., Holm, T., Aufmkolk, S., Dabauvalle, M.-C., Linde, S. van de, and Sauer, M. (2012) rapidSTORM: accurate, fast open-source software for localization microscopy. *Nat Methods* **9**: 1040–1.

Worrall, L.J., Hong, C., Vuckovic, M., Deng, W., Bergeron, J.R.C., Majewski, D.D., *et al.* (2016) Near-atomic-resolution cryo-EM analysis of the *Salmonella* T3S injectisome basal body. *Nature* **540**: 597–601.

Xing, Q., Shi, K., Portaliou, A., Rossi, P., Economou, A., and Kalodimos, C.G. (2018) Structures of chaperone-substrate complexes docked onto the export gate in a type III secretion system. *Nat Commun* **9**: 1773.

Yerushalmi, H., Lebendiker, M., and Schuldiner, S. (1995) EmrE, an Escherichia coli 12-kDa multidrug transporter, exchanges toxic cations and H+ and is soluble in organic solvents. *J Biol Chem* **270**: 6856–6863.

Yip, C.K., Kimbrough, T.G., Felise, H.B., Vuckovic, M., Thomas, N.A., Pfuetzner, R.A., *et al.* (2005) Structural characterization of the molecular platform for type III secretion system assembly. *Nature* .

Young, G.M., Amid, D., and Miller, V.L. (1996) A bifunctional urease enhances survival of pathogenic *Yersinia enterocolitica* and Morganella morganii at low pH. *J Bacteriol* **178**: 6487–95.

Yu, X.-J., Grabe, G.J., Liu, M., Mota, L.J., and Holden, D.W. (2018) SsaV Interacts with SsaL to Control the Translocon-to-Effector Switch in the *Salmonella* SPI-2 Type Three Secretion System. *MBio* **9**.

Yu, X.-J., Liu, M., Matthews, S., and Holden, D.W. (2011) Tandem translation generates a chaperone for the *Salmonella* type III secretion system protein SsaQ. *J Biol Chem* **286**: 36098–107.

Yu, X.-J., McGourty, K., Liu, M., Unsworth, K.E., and Holden, D.W. (2010) pH sensing by intracellular *Salmonella* induces effector translocation. *Science* **328**: 1040–3.

Zhang, Y., Lara-Tejero, M., Bewersdorf, J., and Galán, J.E. (2017) Visualization and characterization of individual type III protein secretion machines in live bacteria. *Proc Natl Acad Sci U S A* **114**: 6098–6103.

Zilkenat, S., Franz-Wachtel, M., Stierhof, Y.D., Galán, J.E., Macek, B., and Wagner, S. (2016) Determination of the stoichiometry of the complete bacterial type III secretion needle complex using a combined quantitative proteomic approach. *Mol Cell Proteomics* **15**: 1598–1609.

Zurawski, D. V., Mumy, K.L., Faherty, C.S., McCormick, B.A., and Maurelli, A.T. (2009) *Shigella flexneri* type III secretion system effectors OspB and OspF target the nucleus to downregulate the host inflammatory response via interactions with retinoblastoma protein. *Mol Microbiol* .

12 Acknowledgments

At first, I want to thank my supervisor and mentor during the last four years, Andreas Diepold. Thank you for giving me the opportunity to start the lab with you, for the trust and support you put in me, your always positive, excited and curious way in which you guided me through the adventures of my Ph.D. and my project. I also want to thank the members of my Thesis Advisory Committee, Martin Thanbichler and Ulrike Endesfelder. The meeting with you and discussions about my project were always helpful to see where I am right now and which further directions need to be explored. Thank you as well for the nice atmosphere during our meetings and the curiosity you had for my project, I always looked forward to those meetings and highly enjoyed it to discuss my science with you. Additionally, I want to thank Simon Ringgaard and Lotte Søgaard-Andersen for the opportunity to do first my Masters and now my Ph.D. within your Lab and the Department of Ecophysiology.

I want to thank all past and present members of the Diepold lab: Katja, Bailey, Hend, Flo, Dimi, Lisa and Carlos, Kerstin and Moritz, Vera, Saskia and Anna-Lena, Ivan, as well as our summer students, Dorothy, Emma and Maya. Thanks for all the support, help, discussions, coffees as well as all the happy and sad moments we encountered together. Especially I want to thank you Bailey for coming to Germany, it was a pleasure to the Ph.D. side by side with you in the Diepold Lab.

Thank you as well to the A2 floor, Ringgard lab: Preta, Jan, Shankar, Carolina, Ale, Sam, Eric, Sara, Barbara, Caro, Marco and Leo which continued to support me even after I left the group to do my Ph.D. in the Diephold lab next door and were nice neighbors droning the last years. Thank you as well to our new neighbors for the Søgaard-Andersen lab: Maria, Luis, Johannes and Michael, it is really nice to have you up here on A2 and brings our two groups closer together. Thank you as well to all the past and present members of the entire Department of Ecophysiology. All of you contributed and continue to do so to our nice working atmosphere and I always felt welcome and well placed within our department. Especially I want to thank Sofya, for looking out for me, for all the fun as well shared food, coffee and long days spent together in the institute.

I would also like to thank all my collaborators for their work on this project: Ulrike, Alex, Bartosz, Hannah, Knut, Ina, Dirk, Timo Jörg and Witold. I highly value your contributions, enthusiasm and discussions with you and without you, this Ph.D. would have not been possible.

Last but not least I want to thank all my friends and colleagues within the institute, from the PhD Reps, the IMPRS, the MPI, within my falt and in Marburg and everyone that I did not mention now. You welcomed me and supported me, throughout this time. Thank you all for all the kind words you found, cheerfulness and encouragement and the great time we had together throughout the years at the MPI and in Marburg. The last years here shaped who I am today as a scientist and as a person and I always felt very welcomed and valued here. Without all of you, it would not have been the same.

13 Erklärung

Hiermit versichere ich, dass ich die Vorliegende Dissatertion

“Molecular function and regulation of bacterial injectisome”

selbstständig verfasst, keine anderen als die Text angegebenen Hilfsmittel verwendet und an sämtliche Stellen, die im Wortlaut oder dem Sinn nach anderen Werken entnommen sind, mit Quellenangaben kenntlich gemacht habe.

Die Dissertation wurde in der jetzigen oder einer ähnlichen From noch bei keiner anderen Hochschule eingereicht und hat noch keinen sonstigen Prüfungszwecken gedient

Marburg den ___.___._____ _____

Stephan Wimmi

14 Einverständniserklärung

Ich erkläre mich dam einverstanden, dass die vorliegende Dissertation

„ Molecular function and regulation of the bacterial injectisome “

in Bibliotheken allgemein zugänglich gemacht wird. Dazu gehört, dass sie

- von der Bibliothek der Einrichtung, in der ich meine Arbeit anfertig habe, zur Benutzung in ihren Räumen bereitgehalten wird;

- in konventionellen und maschinenlesbaren Katalogen, Verzeichnissen und Datenbanken verzeichnet wird;

- im Rahmen der urheberrechtichen Bestimmungen für Kopierzwecke genutzt werden kann.

Marburg, den ___.___.2021

_____

Stephan Wimmi

_____

Dr. Andreas Diepold